Polymers of Intrinsic Microporosity and Poly(ionic liquid)s: Synthesis, Characterization and Gas Permeation Studies

Thesis Submitted to AcSIR

For the Award of the Degree of

DOCTOR OF PHILOSOPHY

In

CHEMICAL SCIENCES

By

Bharat Shrimant

(AcSIR Reg. No: 10CC12A26049)

Under the Guidance of

Dr. Prakash P. Wadgaonkar (Supervisor)

Dr. Ulhas K. Kharul (Co- Supervisor)

Polymer Science and Engineering Division,

CSIR-National Chemical Laboratory,

Pune-411008, India

2018

Dedicated

To

My Beloved Parents

For their Love, Support and Encouragement….

सीएसआईआर - राष्ट्रीय रासायनिक प्रयोगशाला
(वैज्ञानिक तथा औद्योगिक अनुसंधान परिषद)
डॉ. होमी भाभा मार्ग, पुणे - 411 008, भारत
CSIR - NATIONAL CHEMICAL LABORATORY
(Council of Scientific & Industrial Research)
Dr. Homi Bhabha Road, Pune - 411 008, India

CERTIFICATE

This is to certify that the work incorporated in this Ph.D. thesis entitled **"Polymers of Intrinsic Microporosity and Poly(ionic liquid)s: Synthesis, Characterization and Gas Permeation Studies"** submitted by **Mr. Bharat Shrimant** to Academy of Scientific and Innovative Research (AcSIR) in fulfillment of the requirements for the award of the Degree of **Doctor of Philosophy in Chemical Sciences**, embodies original research work carried out under my supervision. I further certify that this work has not been submitted to any other University or Institution in part or full for the award of any degree or diploma. Research material obtained from other sources has been duly acknowledged in the thesis. Any text, illustration, tables, etc., used in the thesis from other sources, have been duly cited and acknowledged.

Bharat Shrimant
(Student)

Dr. Prakash P. Wadgaonkar
(Supervisor)

Dr. Ulhas K. Kharul
(Co-Supervisor)

Communication Channels
NCL Level DID : 2590
NCL Board No. : +91-20-25902000
EPABX : +91-20-25893300
: +91-20-25893400
FAX
Director's Office : +91-20-25902601
COA's Office : +91-20-25902660
SPO's Office : +91-20-25902664
WEBSITE
www.ncl-india.org

DECLARATION

I hereby declare that the original research work embodied in the thesis entitled, "**Polymers of Intrinsic Microporosity and Poly(ionic liquid)s: Synthesis, Characterization and Gas Permeation Studies"** submitted to Academy of Scientific and Innovative Research (AcSIR) for the award of degree of Doctor of Philosophy (Ph.D.) is the outcome of experimental investigations carried out by me under the supervision of Dr. Prakash P. Wadgaonkar and Dr. Ulhas K. Kharul at CSIR-National Chemical Laboratory, Pune. I further affirm that to the best of my knowledge, the work incorporated is original and has not been submitted any other Academy, Institute and University for the award of any degree.

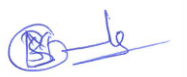

March, 2018

CSIR-National chemical Laboratory

Pune-411008

Bharat Shrimant

(Research Student)

ACKNOWLEDGEMENT

It is my great pleasure to acknowledge the people whose contributions made my academic journey successful, although mentioning is not sufficient to thank them in right way.

It gives me an immense pleasure and pride to express my sincere gratitude and respect for my research supervisor ***Dr. Prakash P. Wadgaonkar*** *for believing in my abilities and providing me an incredible opportunity to pursue my career as a Ph. D. student. I would aslo like to thank my research co-supervisor* ***Dr. Ulhas K. Kharul*** *whose advice especially in the gas permeation studies has been valuable during the course of this study. I thank both of them for their excellent guidance, constant encouragement, sincere advice, understanding and support during the tenure of my doctoral research. I consider myself very fortunate for my association with them, which has given a significant boost in my career.*

I wish to express my sincere thanks to the Doctoral Advisory Committee members ***Dr. Ashish Orpe, Dr. M. V. Badiger*** *and* ***Dr. C. V. Avadhani*** *for the regular assessment of my research work, suggestions and valuable advice. I am grateful to* ***Prof. Ashwinikumar Nangia****, Director, CSIR-NCL,* ***Dr. Vijayamohanan K. Pillai*** *and* ***Dr. Sourav Pal*** *(Former Directors, CSIR-NCL),* ***Dr. Ulhas K. Kharul,*** *Chair, Polymer Science and Engineering, Division, CSIR-NCL and* ***Dr. Ashish Lele*** *(Former Chair, Polymer Science and Engineering, Division, CSIR-NCL) for providing all necessary infrastructure and facilities.*

I would like to thank Dr. A. V. Ambade, Dr. S. K. Asha, Dr. Samir Chikkali, Dr. Rahul Banerjee and all other scientists of NCL for their motivation, constant encouragement and support. I would like to thank Mr. Shamal K. Menon, Dr. Neelima, Mrs. Dhoble, Mrs. Sangita, Mr. Arun Torris and Mrs. Poorvi for their guidance in characterization techniques. I would like to extend my thanks to Dr. Rajamohanan, Dr. Ajithkumar, Amol and Dinesh for their timely help with recording of NMR spectra. Yuvraj Dangat for DFT measurements, Arjun, Divya and Apurva for the BET surface area measurements, Mrs. Shantakumari for HRMS facility and Dr. Asha's group for IR facility.

I would like to express special thanks to Dr. U. P. Mulik, (C-MET, Pune), Prof. S. V. Lonikar, (Solapur University, Solapur), Prof. Vaishali Shinde (Savirtibai Phule Pune University, Pune), Prof. N. M. Gaudgaon, Prof. Biradar, Prof. M. B. Halli, Prof. Anand Saudandane and Prof. K. Siddappa (Gulbarga University, Gulbarga), Dr. B. S. Sasidhar (CSIR-NIIST), Dr. Yogesh Mane and Dr. Dayanand Jadhav (Sri Chhatrapati Shivaji College, Omerga) for valuable guidance from time to time.

I would like to mention gratitude towards to my seniors Dr. Bhausaheb Tawade, Dr. Pandurang Honkhambe, Dr. Ankush Mane, Dr. Rahul Shingte, Dr. Arvind More, Dr. Arun Kulkarni, Dr. Anjana Sarkar, Dr. Snehalata Bapat, Dr. Nilakshi Sadavarte, Dr. Dnyaneshwar Palaskar, Dr. Prakash Sane, Dr. Sharad Pasale, Dr. Savita Kumari, Dr. Parimal Naik, Dr. Aarti Shedge, Dr. Prakash Babu and Dr. Deelip Raut for devoting their precious time and for valuable suggestions during my Ph.D. tenure.

I was very fortunate to work with a fantastic group of colleagues in the PPW's and Membrane group. I want to give special thanks to my lab mates Dr. Sachin P., Dr. Shradhha, Dr. Ravindra P., Dr. Sayali, Dr. Nagnath, Dr. Nagendra, Dr. Rupesh, Dr. Anita, Dr. Anand, Dr. Bishnu, Deepshikha, Indravadan, Vikas, Amol, Harshal, Sachin K. Samadhan, Nitin V., Durgaprasad, Abhijeet, Rupali, Ketan, Deepak, Kavita, Geethika, Namdev, Ashwini, Clement Ravet, Shakeeb, Yogesh, Sachin B., Nitin B., Uday, Sagar, Rohit, Kiran, Shebeeb, Nishina, Bhavana and Supriya. I thank all of them individually from the bottom of my heart.

No words can suffice to acknowledge my prized friends in and out of NCL who have helped me at various stages of my work in NCL. I wish to thank Dr. Nagesh More, Dr. Sachin B., Venkannababu, Shravan, Suryakant, Kishan, Shatru, Basavaraj N., Gurunath, Sharanappa K., Ajit, Manoj, Krishna, Jyotiba, Ambaji, Shrikant, Manik, Pradnya, Ravindr and Arun N., Trimbak, Goudappa Patil, Anil H., Dhammaraj, Dr. Priyadarshini, Dr. Sumati, Dr. Kalpana and Dr. Prabhakar for helping me in various aspects of life as well as work.

I would like to thank all my teachers in my entire academic journey from Govt. Primary School, Jogewadi (Mahadevpur) to Gulbarga University, Gulbarga for imbibing good morals and knowledge in me.

Without the funding I received, this Ph.D would not have been possible and I would like to express my sincere appreciation to University Grants Commission (UGC), New Delhi for awarding JRF and SRF.

Finally, I dedicate this thesis to the people who mean the most to me, my father ***Sri. Shrimant Ganapati*** *and mother* ***Smt. Vimalabai Shrimant.*** *Their patience and sacrifices are always a main source of my inspiration and will remain throughout my life, motivating me to pursue still higher goals. I would like to thank my sisters Anuradha and Sandhya, my brother Lahu, Aruna Vahini and Vithal Mama for their love, prayer, constant support and encouragement. I wish to thank my nephews Poonam, Prithviraj and Aditi whose presence in my life is always refreshing, making me feel relaxed and comfortable.*

I wish to thank great scientific community whose achievements are constant source of inspiration for me.

Finally, I am grateful to the God for continuous source of inspiration and giving me a beautiful and healthy life.

Bharat Shrimant

List of Abbreviations

BET	Brunauer–Emmett–Teller
BPADA	4,4'-(4,4'-Isopropylidenediphenoxy)bis(phthalic anhydride)
BTDA	3,3',4,4'-Benzophenonetetracarboxylic dianhydride
$CHCl_3$	Chloroform
DFT	Density functional theory
DMAc	*N*,*N*-Dimethylacetamide
DMF	*N*,*N*-Dimethylformamide
DSC	Differential scanning calorimetry
6-FDA	4,4′-Hexafluoroisopropylidene(diphthalic anhydride)
GPC	Gel permeation chromatography
HR-MS	High resolution mass spectroscopy
η_{inh}	Inherent viscosity
K_2CO_3	Potassium carbonate
M_n	Number average molecular weight
M_w	Weight average molecular weight
NMP	*N*-Methyl-2-pyrrolidone
ODPA	4,4′-Oxydiphthalic anhydride
PI	Polyimide
PILs	Poly(ionic liquid)s
PIMs	Polymers of Intrinsic Microporosity
PMDA	1,2,4,5-Benzenetetracarboxylic dianhydride
TGA	Thermogravimetric analysis
T_g	Glass transition temperature
THF	Tetrahydrofuran
TLC	Thin layer chromatography
T_{10}	10 % weight loss temperature
T_{Max}	Maximum degradation temperature
WAXD	Wide angle X-ray diffraction

TABLE OF CONTENTS

Chapter 1: Introduction and Literature Survey

Chapter 2: Scope and Objectives

Chapter 3: Materials, Characterization and Techniques

Chapter 4: Synthesis, Characterization and Gas Permeation Properties of Adamantane-Containing Polymers of Intrinsic Microporosity

Chapter 6: Synthesis and Gas Permeation Properties of Spirofluoroxanthene-Containing Polymers of Intrinsic Microporosity

List of Schemes

List of Figures

List of Tables

Chapter 1

Introduction and Literature Survey

Gas separation is an expanding technology with a rapidly developing market comprised of applications such as oxygen or nitrogen enrichment from air, acid gas removal from natural gas, hydrogen separation, hydrocarbon recovery from natural gas streams, etc. This chapter presents the fundamental scientific principles of gas separations, various methods for gas separations, solution-diffusion model and structure/property- relationships. The current challenges viz., trade-off relationship between permeability and selectivity, plasticization and physical aging associated with the development of superior membranes are discussed herein in brief. Synthesis and structure-property relationship of next generation polymers such as thermally rearranged (TR) polymers, polymers of intrinsic microporosity (PIMs) and poly(ionic liquid)s (PILs) are discussed with a focus on work published in the last two decades.

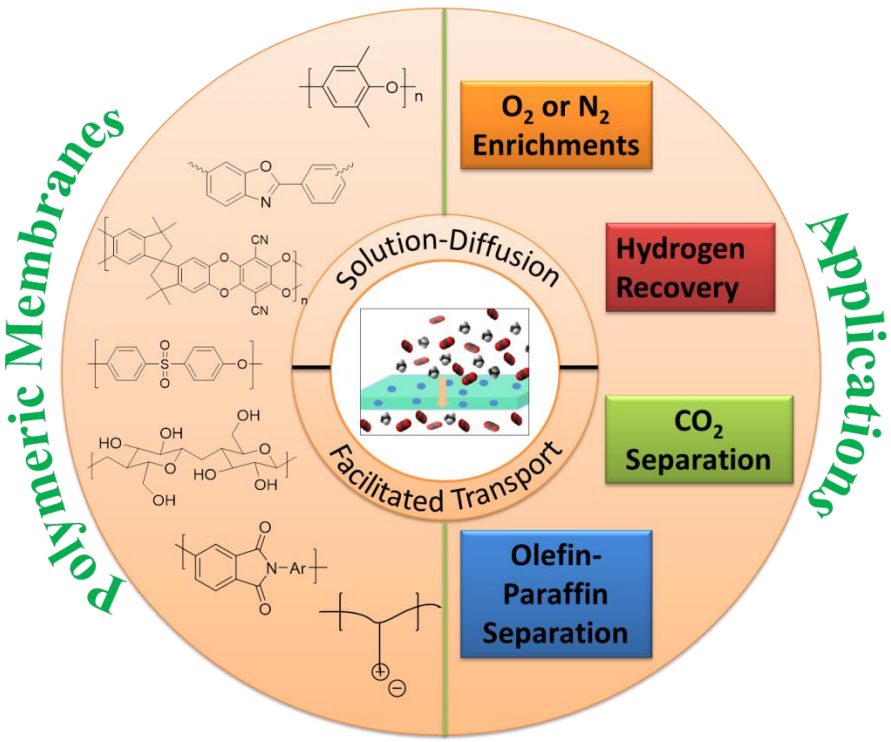

In the recent years, gas separations have been of great interest to both industry and academia. The market for gas separation membrane grew significantly since its beginnings in the 1970s and continued growth is expected in the coming years as technology improves and applications expand.[1] In 1960, Sidney Loeb and Sirivasan Sourirajan created the first asymmetric reverse osmosis membrane for water purification.[2,3] This breakthrough made desalination by reverse osmosis potentially economical. It took another 10 years to develop membrane technology to fabricate the membranes on a large scale. The time was then ready to apply membrane technology in the field of gas separation. The first commercially available membrane (Prism membrane) was developed by Air Products for hydrogen separation from nitrogen.[4] An early application of membrane technology was for separation of hydrogen gas from nitrogen in Haber process and argon and methane from ammonia plant.[4,5] Next, the efforts were directed towards hydrogen separation from light hydrocarbon mixtures in refineries and carbon monoxide ratio adjustment in syn gas plants.

In the 1990s, a number of other applications of membranes were developed and the four commercial applications are listed in **Table 1.1**. These are the largest market segments of gas separation membrane industry (80-90 %).[6] Recently, some new applications such as air and natural gas dehydration have shown some commercial success.[7] The bulk of today's membrane technology market need is served by the same polymers used for these applications in 1990s. Over the past 25 years, the gas separation application market has expanded significantly. The current market for membrane technology is in the range of $1.0−1.5 billion/yr and is expected to continue to grow in the coming years.[8]

Table 1.1: Current commercial gas separation membrane applications[6]

Sr. No.	Application	Separation performed	Polymer	Approximate market (2015)
1	**Hydrogen recovery**	H_2/N_2, H_2/CH_4, H_2/CO	Polysulfones, polyimides	$200 million/year
2	**N_2 Enrichment**	O_2/N_2	Polyimides, polysulfones, poly(phenylene oxide)s, polycarbonates	$800 million/year
3	**Natural gas treatment**	CO_2/CH_4, H_2S/CH_4, He/CH_4	Cellulose acetates, polyimides	$300 million/year
4	**Vapour recovery**	C_3H_6/N_2, C_2H_4/N_2, C_2H_4/Ar, CH_4/N_2, gasoline/air	Silicone rubber	$100 million/year

Several review articles have reported overall progress in the field.[7–11] The applications of gas separation include hydrogen recovery from ammonia plant, O_2 or N_2 enrichments, natural gas purification, helium recovery, flue gas separation, H_2 separation from hydrocarbons, refinery gas purification, syngas ratio adjustment, etc.[11,12] Of these, the most important gas separation applications are discussed in the following sections.

1.1 APPLICATIONS OF GAS SEPARATION

1.1.1 Hydrogen Recovery

An initial target of gas separation applications was hydrogen separation from their mixtures such as methane and nitrogen. Due to smaller size, hydrogen is much more permeable than other gases, such as nitrogen, methane, and carbon monoxide, leading to high selectivity for hydrogen in gas mixtures for many polymers.[4,5] The most important separations of hydrogen are: 1) Hydrogen recovery from ammonia synthesis and 2) Adjusting syngas (H_2/CO) ratios.

In Haber process, ammonia is synthesized by reacting nitrogen with hydrogen over a catalyst at high pressure and temperature.[4,5] Hydrogen is produced from methane reforming. However, methane remains in small quantities. To achieve higher conversion a recycle is needed. Monsanto in 1979, offered polysulfone-based hollow fiber (Prism membrane) membrane for recycling process and achieved 95 % recovery of H_2.[13]

Syngas consists of H_2 and CO, which is produced from natural gas steam reforming and oxidation of heavy oils. The separation of H_2 is easy from CO with gas separation membranes because the size of H_2 is smaller than that of CO.

1.1.2 Air Separation

Today, the enrichment of N_2 from the air is gaining interest industrially in various applications such as refrigeration, inerting, food packaging, etc.[14] The nitrogen is separated from air by three industrial processes viz., cryogenic distillation, pressure swing adsorption (PSA), and membrane technology. The largest market for membrane-based separation is nitrogen enrichment. The commercially available N_2 purification membranes are poly(4-methyl-1-pentene) and tetrabromo substituted bisphenol-based polycarbonates by Generon membranes (TPX), polyimides by Praxair and polyimide and aromatic polyamide membranes by Medal.[15]

1.1.3 Natural Gas Purification

Generally, natural gas consists of methane, carbon dioxide, ethane, higher hydrocarbons, hydrogen sulphide, and inert gases.[16] As CO_2 and H_2S are acidic, it is necessary to separate

them from natural gas to avoid corrosion of pipeline and equipments.[17] Natural gas is purified by various methods which include solvent absorption, cryogenic distillation and membrane-based separation. The worldwide market for natural gas separation is approximately $5 billion/yr, and membrane technology currently accounts for approximately 5% of this market share and it is anticipated to grow to $220 million/yr by 2020.[2,18] National Energy Technology Laboratory (NETL, US) reported that separation of CO_2 from natural gas by methanolamine technology requires cost of around $40–100/ton of CO_2 whereas membrane technology requires cost of around $23/ton of CO_2 which indicates that membrane technology is attractive in terms of its lower cost.[8] Cellulose acetate-based hollow-fiber membrane was the first membrane used by Separex and Cynara for natural gas purification. Over the last decades, polyimides have gained attention for purification of nitrogen gas.[2]

1.2 TECHNOLOGIES FOR GAS SEPARATION

1.2.1 Solvent Absorption

Solvent absorption deals with the absorption of CO_2 or H_2S with liquid amine solvent. Currently, the primary process to remove CO_2 from natural gas and power plant flue gas is solvent absorption. Solvents used in this process are monoethanolamine (MEA), diethanolamine (DEA), methyldiethanolamine (MDEA), diisopropanolamine (DIPA), and aminoethoxyethanol (diglycolamine) (DGA).[19] The flue gas from fossil fuel power plant is passed through a column in which amine solvent preferentially absorbs CO_2 gas than other components of the flue gas stream. This method involves the reaction of amine with CO_2 and formation of carbamic acid. At moderate temperature (>100 °C), carbamic acid decomposes to the corresponding amine and carbon dioxide.[19] However, this method has limitations including high cost due to the regeneration of solvents and corrosive nature of amine solvents.[20]

1.2.2 Cryogenic Distillation

This method includes separation of gas from their mixtures by stages involving compression, liquification and then distillation according to their differences in boiling temperatures. This is a physical process that separates CO_2 under low temperature (critical temperature of CO_2 = 31.1 °C). This method has advantages over other separation processes because of easy transportation of the liquid product.[21] The high-energy consumption and high costs associated with gas compression and cooling are the limitations of the method.[22]

1.2.3 Membrane Technology

Gas separation technologies using polymeric membrane materials have attracted much attention recently due to potential energy savings and growing industrial demand than other commercial technologies.[23]

The advantages of membrane-based separations over other conventional methods are:

- Lower energy consumption and cost-effectiveness
- No regeneration of solvent
- Moving parts are not required
- Easy scale-up
- Low capital area
- The operational simplicity

The various polymer families such as polyimides, polyamides, polysulfones, polycarbonates, cellulose acetate, poly(phenylene oxide), polybenzimidazole, poly(dimethylsiloxane), etc have been widely investigated for gas separation applications.[6,24] The only equipments necessary for membrane separation are the membrane and compressor. Having advantages, there are some limitations of membrane-based separation such as plasticization, physical aging and permeability-selectivity trade-off relation, wherein more permeable membrane materials are generally less selective and vice-versa.[25]

In the past 30 years, several polymers have been evaluated as potential membrane materials for separation applications. However, even today no better polymer for commercial exploitation has been made available than the polymers that were practiced commercially in the 1990s. An overall theme of development work in the past decades has been to improve polymer structure-property-performance relationships by systematic structral variations. This idea has given useful empirical rules and correlations.

For commercial applications, the membrane should be robust, thermally and chemically stable and should not undergo physical aging in the film form.

1.3 GAS TRANSPORT THROUGH MEMBRANES

The membrane is a selective barrier and is able to separate selectively one gas from their mixture. Pressure is the driving force for the gas to permeate through the membrane.[25–27] Transport of gases through membrane depends on properties of gases and membrane (morphology and functionality). There are three mechanisms such as Knudsen diffusion,

molecular sieving and solution-diffusion by which gas transport through the membrane can take place (**Figure 1.1**).[13]

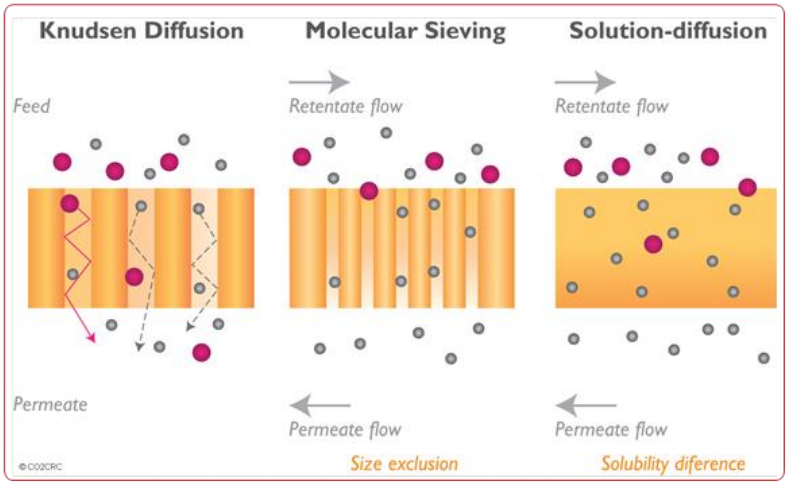

Figure 1.1: Mechanism for membrane-based gas separations.

Knudsen diffusion is based on the molecular mass of gas and inversely proportional to the square root of the molecular mass of diffusing species.[13] This separation is followed by macroporous and mesoporous membranes.[28] Molecular sieving mechanism depends on the size of the penetrant molecules. Generally, small size molecules readily permeate through the membrane while larger molecules do not permeate.[25] The transport of gas molecules through dense, nanoporous membranes is based on solution-diffusion mechanism. Solution-diffusion mechanism consists of three main steps: (i) sorption of the gases at upstream side, (ii) diffusion of gas across the membrane and (iii) desorption at the downstream side.[25,29]

1.4 METHODS FOR DETERMINATION OF GAS PERMEABILITY

Separation properties such as sorption and diffusion through the dense membrane depend on properties of the polymer as well as gas molecules.[25,30] There are two types of polymeric membranes , viz., rubbery (operational temperature is higher than their Tg) or glassy (operational temperature is lower than their Tg) in nature.[26] Generally, permeability P is considered as the product of diffusivity and solubility and is given by:

$$P = D \times S$$

Permeability is usually expressed in Barrer (10^{-10} cm^3(STP)cm/s.cm.cmHg).

Gas diffusion D is related to the free volume in polymers and the size of penetrating gases, whereas gas solubility S is related to the chemical affinity between gas molecules and the polymer. Thus, selectivity is considered as the ratio of permeability coefficients of gas pairs.

$\alpha = Pi/Pj = Di\ Dj \times Si\ Sj$

The permeability can be determined by

a) Time-lag or variable pressure method or

b) Variable volume method

1.4.1 Time-Lag or Variable-Pressure Method

Generally, both permeability and diffusivity are measured by single measurement through this method. Constant gas pressure is applied on the upstream side of the membrane and then increase in pressure at the downstream side of the membrane is measured. Initially, the pressure is increased nonlinearly at the downstream side and then linearly as a function of time. Permeation coefficient can be calculated by using the slope of the curve.[30,31]

1.4.2 Variable-Volume Method

According to this method, the pressure is applied on one side of the membrane and the gas is allowed to expand on the opposite side, which is usually maintained at atmospheric pressure. The change in the volume of the permeate is then measured as a function of time with the displacement of a short column of mercury in a capillary.[30]

1.5 MEMBRANE MATERIALS FOR GAS SEPARATION APPLICATIONS

The design of a membrane material for a gas separation application is based on specific physical and chemical properties. Moreover, robust, thermally and mechanically stable materials are required to be applied in a membrane gas separation process. The properties of membranes depend upon the material, membrane structure, thickness and membrane configuration (e.g., flat, hollow fiber).[24,28]

Inorganic, metallic and polymeric membranes have been reported for gas separations. However, each of these are associated with some advantages and disadvantages. Currently, much research efforts have been devoted towards designing membranes that would provide high permeability as well as selectivity.[2] Inorganic membranes (e.g., silica, zeolites, etc.) and carbon-based molecular sieves are particularly interesting because they can withstand aggressive conditions as well as high temperatures. However, they have some limitations such as high cost, modest reproducibility, brittleness and low permeability.[2,32] Metallic membranes are used mostly for hydrogen separation and are associated with high cost and scalability issues. Currently, polymeric membranes have attracted increasing interest in the field of gas separation due to their easy processability and easy tunability.

1.6 FACTORS AFFECTING GAS SEPARATION PERFORMANCE

Gas permeability and selectivity of membranes depend on gas as well as polymer properties and these aspects are discussed in the following sections.

1.6.1 Physical Properties of Polymer

1.6.1.1 Chain packing density

Diffusion of gas through polymeric membranes depends on the polymer chain packing and free volume present in the polymer. Glassy polymers are usually affected by the diffusion selectivity as the gas diffuses through the free space between polymer chains so-called free volume.[33,34] The gas permeability increases with increasing free volume by disturbing polymer chain packing.[35] Fractional free volume (V_f) can be estimated using semi-empirical Bondi's method by the following equation.[36,37]

$$V_f = V\text{-}V_w/V$$

where, V is specific volume and V_w is Van der volume.

1.6.1.2 Chain and subgroup mobility

Gas permeability and selectivity of polymer membranes is also influenced by the polymer chain rigidity.[38] The incorporation of flexible linkages such as -O-, -CH_2-, etc into the polymer backbone increases chain mobility which results into increase in free volume and consequently increase in gas diffusivity is observed.[39] The introduction of rigid groups either in the backbone or as pendant groups brings about restricted rotation of polymer chains and thereby increase in selectivity is attained.[33,40]

1.6.1.3 Polarity

Polarity is related to an inexact distribution of electrons about atoms, functional groups or molecules. Polarity can be measured by cohesive energy density in the polymer.[41,42] The introduction of polar groups such as nitrogen-containing ring, imidazole, pyridine, Troger's base and hydroxyl groups into the polymers increases the solubility of acidic gases such as CO_2 and H_2S by Lewis acid-base interaction.[43,44]

1.6.1.4 Crosslinking

It has been reported that nature of cross linking agent and the degree of cross-linking affect the gas transport properties.[45] Generally, cross-linking helps to decrease plasticization and increase resistivity towards chemicals.[46] Polymer segmental mobility is reduced by crosslinking and thus increase in selectivity is reported at the cost of reduction in permeability.[46]

1.6.2 Properties of Gas

1.6.2.1 Condensability of gas molecules

It has been observed that increasing condensability of a gas results in increase in its solubility into the polymer.[47] Gas critical temperature (Tc) correlates well with the solubility coefficient of a range of penetrants in a polymer.[48] For example, in most polymers, CO_2 (Tc = 31 °C) is more soluble than CH_4 (Tc = -82.1°C) and O_2 (Tc = -118.4 °C) is more soluble than N_2 (Tc = - 147 °C). With increase in solubility of gases into polymers, increase in permeability and decrease in selectivity has been reported.[33]

1.6.2.2 Size and shape of gas molecules

The diffusion of gas through polymer depends on size and shape of gas molecules as characterized by the Van der Waals volume or kinetic diameter. Generally, glassy polymers exhibit higher diffusion coefficient with small penetrant size.[33,49] The diffusivity of gas molecules is also dependent on the their shape. Diffusivity of linear CO_2 is higher than spherical CH_4 molecules of equivalent molecular volume. The Vander Waals volumes of CO_2 and CH_4 are predicted to be 17.5 and 17.2 cm^3 / mol. Thus, the kinetic diameter is frequently used to characterize the penetrant size.[33]

1.6.3 Effects of Operating Parameters

1.6.3.1 Temperature

The gas diffusivity increases significantly at elevated temperature as the segmental motions of polymer chains increase with temperature and consequently increase in permeability is observed.[33,44] The solubility coefficient of a given gas decreases with temperature. Nevertheless, this decrease is overcome by the substantial increase in the diffusion coefficient resulting in a net increase in the permeability coefficient.[33]

1.6.3.2 Pressure

The diffusivity, solubility and, in turn, permeability may vary considerably as the pressure of gas changes.[33,50] It is observed that low sorbing penetrants such as H_2, He, N_2, and O_2 show insignificant pressure dependence on the permeability of rubbery or glassy polymers. Usually, decrease in permeability with increasing pressure is explained by the dual-mode model due to plasticization effect. This behavior is typically observed in the case of glassy polymers for more soluble penetrants such as CO_2.[51,52]

1.6.4 Effects of Membrane Preparation Parameters

The gas separation performance of dense membranes varies with membrane fabrication method, solvent used for casting and casting temperature.[53] Generally, solution casting method is used for the preparation of dense membranes. Khulbe and co-workers observed increase in permeability and decrease in selectivity foe O_2/N_2 and CO_2/CH_4 gas pairs with increase in boiling points of the casting solvent.[54] In gas separation, membrane morphology depends upon properties of the solvent used in preparing polymer solution, solution concentration and surface (glass, steel, Teflon, etc.) on which the membrane is cast. The casting techniques such as drop casting, blade casting etc., affect gas permeation properties.[53] The gas permeation properties of poly(vinyltrimethyl silane) (PVTMS) and poly(trimethylsilyl-norbornene) (PTMSNB) were demonstrated to be dependant on the hydrocarbon solvent used for casting the films.[55] Huang *et al*. correlated the effect of film thickness on aging time and observed rate of the aging effect was higher in the thinner films for gas permeation properties of polysulfone, PPO and Matrimid.[56] By lowering the film thickness, diffusion coefficients decreased for all the gases. Recently, McKeown and co-workers also reported that gas separation properties of PIMs were affected by the solvents used for casting the films.[57]

1.7 COMMERCIALLY AVAILABLE POLYMERS FOR GAS SEPARATION APPLICATIONS

Various polymeric materials have been employed for gas separation applications such as cellulose acetate, polyethersulfone, polyamide, polyimide, cross-linked poly(2,6 dimethylphenylene oxide), etc. For industrial applications, membrane should possess

- High permeability and selectivity over other gases,
- Thermal and chemical robustness,
- Resistance to plasticization and aging,
- Cost-effectiveness and
- Manufactured into different membrane forms such as flat sheet or hollow fibers with low cost.[58]

The following section will highlight some commercial polymers such as polyethersulfone, cellulose acetate (CA), poly(2,6-dimethyl-1,4-phenylene oxide) (PPO) and polyimides (PIs) investigated as membrane materials for gas permeation properties.[29,58]

1.7.1 Cellulose Acetate (CA)

The first generation commercial polymeric membrane used for natural gas purification is cellulose acetate (CA). CA and its derivatives (**Figure 1.2**) have been in use since then in gas

separations for removal of acid gases from natural gas.[59] The permeability of CA varied with the degree of acetylation. It was reported that by increasing the degree of acetylation from 1.75 to 2.85, CO_2 permeability increased from 1.84 to 6.56 Barrer.[19] The enhancement of permeability is due to the replacement of hydroxyl groups with acetate groups.[59] CA-based membranes are cost-effective as the raw material-cellulose- is abundantly available and is a renewable resource. However, CA-based membranes get plasticized in the presence of CO_2 which limits their widespread applications.

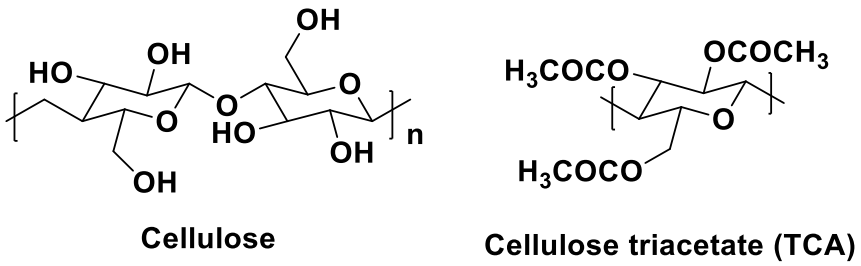

Figure 1.2: Structures of cellulose acetate and cellulose triacetate

1.7.2 Polyethersulfones

Monsanto Co. in the 1970s developed the first large-scale membrane for gas separation process, by utilizing asymmetric hollow fiber membrane of polyethersulfone based on bisphenol-A.[60] The commercially available polyethersulfones (Victrex PES, Udel, PSF and Radel R) are shown in **Figure 1.3**. Polyethersulfones have gained significant attention due to their excellent thermo-mechanical properties and ease of fabrication of membranes in a wide variety of configurations and modules.[19,61,62] The substitutions such as methyl groups on the phenyl rings significantly increase the gas permeability.[63] The enhancement of permeability was observed by replacing isopropylidene ($-(CH_3)_2C-$) bridging moiety with bulky hexafluoroisopropylidene ($-(CF_3)_2C-$) moiety mainly due to the increased free volume .[63,64] Recently, Tawade et al. reported polyethersulfone containing pendant pentadecyl chains and observed an increase in permeability for carbon dioxide due to the internal plasticization effect.[65]

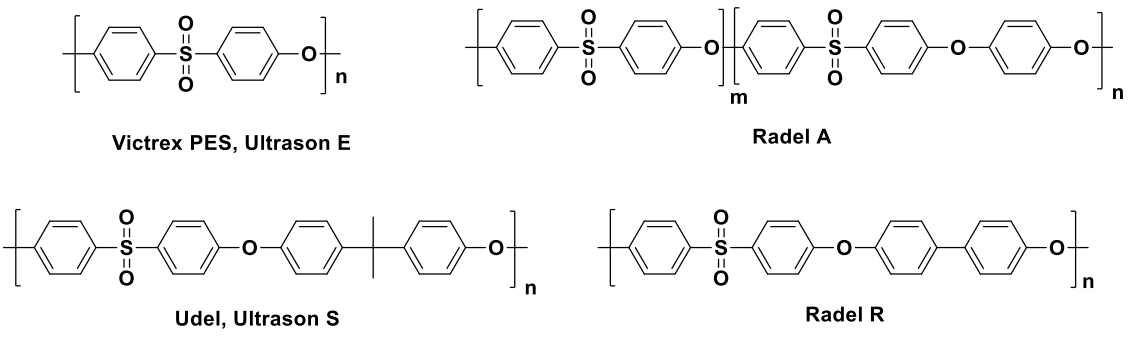

Figure 1.3: Representative examples of commercially available polyethersulfones

1.7.3 Poly(2,6-dimethyl-1,4-phenylene oxide) (PPO)

PPO is a high-performance polymer with good mechanical and thermo-chemical stability. PPO was discovered by Hay and coworkers and it was commercialized by General Electric (now SABIC) (**Figure 1.4**).[66] The permeability of PPO was found to vary with the extent of bromination.[67,68] PPO exhibited relatively high permeability to light gases due to ease of rotation of the phenyl rings about the ether linkages with moderate selectivity. Currently, most of the research on PPO is being focused on its chemical modification.[56,69]

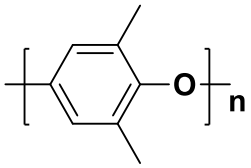

Figure 1.4: Structure of PPO

1.7.4 Polyimides (PIs)

Polyimides (PIs) are the most studied polymers for gas separation applications due to their excellent thermal and mechanical stability and structural tunability. The commercially available PIs are Matrimid (Air Liquide), Upilex (Ube), polyetherimide (SABIC), etc (**Figure 1.5)**. Generally, PIs exhibited low permeability and high selectivity. However, the gas separation properties of polyimides can be varied by changing dianhydride and diamine moieties or a substituent on them. By restricting both chain mobility and chain packing in PIs, increase in both permeability and selectivity was achieved.[29,70] PIs containing hexafluoroisopropylidine (–$(CF_3)_2$–) linkages have attracted much attention because they are more selective towards CO_2 relative to CH_4. The incorporation of hexafluoro groups in the polymer *via* dianhydride namely hexafluoro isopropylidenediphthalic anhydride (6FDA) increases the stiffness of polymer chains and disturbed chain packing due to the steric hindrance of CF_3 groups.[71] The "*First Generation Polyimides*" contains 6FDA-based polymers used by Air Liquide, Praxair, Parker-Hannifin, and Ube for various gas separation applications.

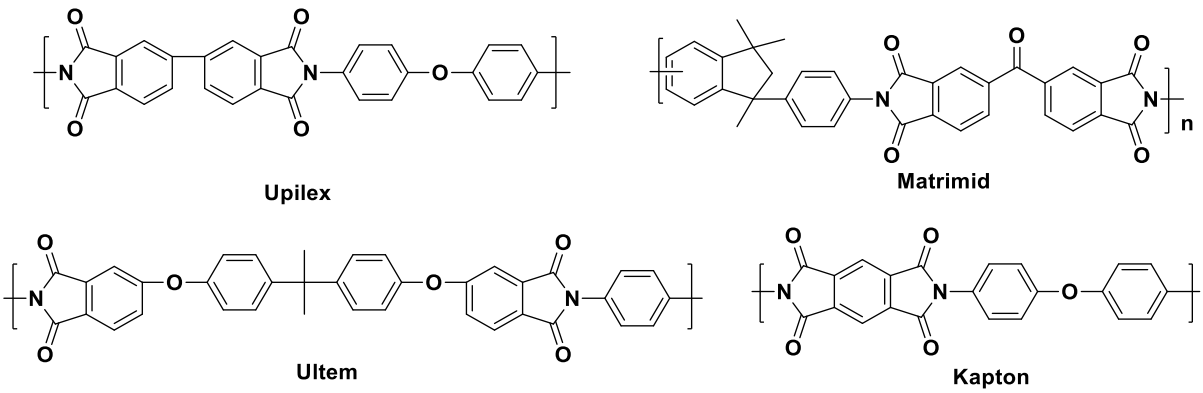

Figure 1.5: Representative examples of commercially available polyimides

1.8 CHALLENGES IN POLYMERIC MEMBRANE MATERIALS FOR GAS SEPARATION APPLICATIONS

The performance of the polymeric membranes described above is limited by several factors such as plasticization, physical aging and permeability/selectivity trade-off which are discussed below.

1.8.1 Plasticization

Plasticization occurs when the membrane is exposed to highly soluble gases that produce significant swelling in the polymer matrix. Due to this, polymer chain mobility and free volume increases which results into increased permeability and decreased selectivity.[72,73] Among various gases, CO_2 is a more soluble gas and the plasticization by CO_2 has been widely studied.[19] The pure and mixed-gas CO_2 and CH_4 permeability was studied by Donohue et al., for CA-based membranes and they reported an increase in methane mixed-gas permeability compared to pure CH_4. As a consequence, a severe loss in CO_2/CH_4 selectivity was observed during mixed gas permeation.

1.8.2 Physical aging

Physical aging is another frequently encountered issue that impacts on the performance of the polymeric membrane. Generally, glassy polymer chains pack loosely, creating excess free volume in the polymer matrix.[19] The polymer chains gradually get closer with time to fill this excess free volume which ultimately results in the reduction in the free volume.[74] Due to this, a decrease in permeability is generally accompanied by an increase in selectivity. This decay in membrane permeability is due to the relaxation of the non-equilibrium free volume and subsequently re-ordering of polymer chains.[74] The permeability of PIM-1 thin films was decreased by 67%, as compared to 53% decrease for thick films at 45 days of aging due to the higher aging rates in thin films.[75]

1.8.3 Permeability/selectivity trade-off (Robeson upper bound)

The key parameters to judge the performance of polymers for gas separation applications are the permeability and selectivity. Generally, polymeric materials exhibit high permeability and low selectivity or vice versa as recognized by Robeson. Later, Freeman provided a theoretical basis to trade-off relationship between permeability and selectivity.[76] Generally, glassy polymers that contain twisted and rigid structures offer the best combinations of selectivity and permeability due to poor chain packing.[77] Robeson plot (**Figure 1.6**) is widely used to judge the relative performance of new membrane materials.[77] Recently, a large number of examples of polymeric membranes have been reported which exceed the empirical upper

bound.[7,10,11] Currently, the research efforts have been directed towards synthesis of new membrane materials with improved separation performance.

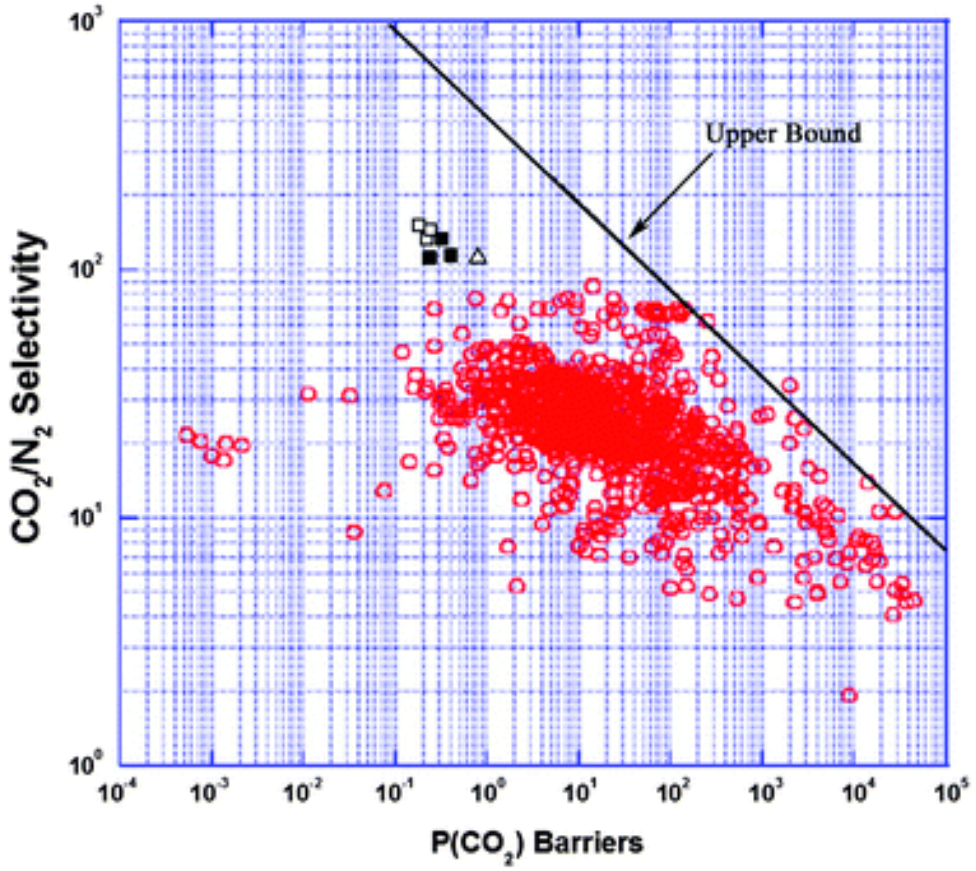

Figure 1.6: Robeson upper bound

1.9 EMERGING POLYMERIC MEMBRANE MATERIALS

Over the past three decades, polymeric gas separation membranes have been widely used for a variety of industrial gas separations applications.[58] Generally, commercial polymers exhibit low permeability and high selectivity. In this context, new generation membranes with improved gas separation performance are gaining interest.[10,11] Recently, new polymeric materials are being developed to address demands of process economics in terms of not only the enhanced intrinsic permeability and selectivity; but also better physical properties.[19] The classes of new generation materials include polymers of intrinsic microporosity (PIMs), thermally rearranged (TR) polymers, polyimides (PIs), poly(ionic liquids) (PI-PILs), etc.[10,19] The highlighting features of these polymeric materials are discussed below in brief.

1.9.1 Polymers of Intrinsic Microporosity (PIMs)

PIMs contain interconnected pores with pore size less than 2 nm. The intrinsic microporosity is defined as a continuous network of interconnected intermolecular microcavities. The origin of intrinsic microporosity is a consequence of shape and rigidity of polymer structure which

is responsible for frustrating of polymer chain packing.[78] Generally, polymers pack space efficiently because the macromolecules can bend and twist to maximize intermolecular interactions.[79] There are a few examples of "ultra-high free-volume" polymers, best represented by the much studied polyacetylene derivative *viz*., poly(1-trimethylsilyl-1-propyne) (PTMSP) and the fluoropolymer Teflon AF 2400 (a copolymer of 4,5-difluoro-2,2-bis(trifluoromethyl)-1,3-dioxole and tetrafluoroethylene).[80,81] These polymers have been classified as "microporous" on the basis of exceptionally high gas permeability which is 2–3 orders of magnitude higher than that of conventional polymers.[82]

PIMs have been of great interest for many potential applications in fields such as catalysis, sensors, gas storage and gas separation due to their extraordinarily high porosity and surface area.[10] These materials also exhibit good solubility in organic solvents and self-standing films can be fabricated *via* solution-casting. The microporosity of these polymers is referred to as "intrinsic" since it arises directly from their structure instead of the processing protocol. Budd and McKeown in 2004 reported new ladder-like polymer namely PIM-1 with high BET surface area (**Figure 1.7**).[83] Since then, PIM-1 has been widely studied with respect to its microporosity characteristics and properties such as sorption and diffusion.[84,85] The gas permeability of PIM-1 is nearly 100 fold higher than that of conventional glassy polymers used for gas separation..[10]

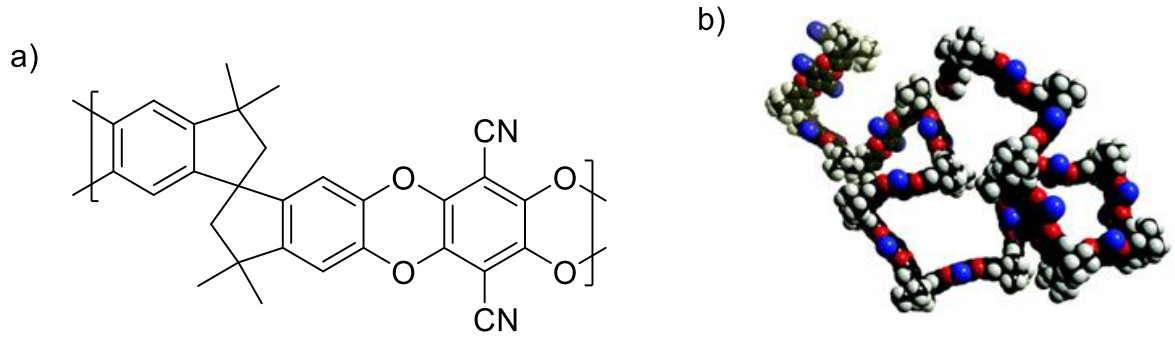

Figure 1.7: a) Chemical and b) contorted structure of PIM-1

1.9.1.1 Synthesis of PIMs

McKeown and Budd exploited a unique polycondensation reaction of 5,5,6,6-tetrahydroxy-3,3,3,3-tetramethyl-1,1-spirobisindane and tetrafluoroterephthalonitrile *via* double aromatic nucleophilic substitution to form polymer containing dibenzodioxane ring as depicted in **Scheme 1.1**. The reaction involves double nucleophilic attack of phenoxide ion to the activated carbon of halo compounds. Reaction accelerates if the halide-containing monomer is activated by an electron-withdrawing substituent such as –CN.[83] PIMs can be synthesized by two methods and are discussed in the following sections

1. Low temperature method
2. High temperature method

1.9.1.1.1 Low Temperature Method

In this method, polymerization reaction is carried out with equimolar quantities of monomers in DMF using potassium carbonate as a base at 60-70 °C for 24-80 h (**Scheme 1.1**). The advantage of this method is to provide polymer in high molar mass with easy to control molecular weight. The concentration of the monomers is an important parameter because at very high and low concentrations there exists a possibility of formation of insoluble cross-linked materials or cyclic oligomers, respectively. [86,87] For particular monomer combinations, the reaction conditions, concentration and temperature are required to be optimized.

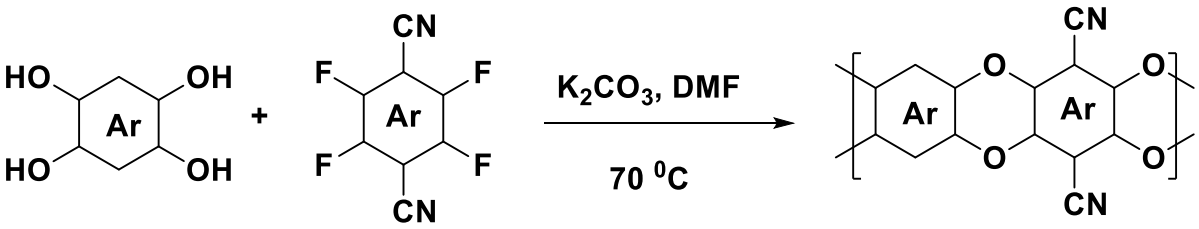

Scheme 1.1: Synthesis of PIMs by low-temperature method.

1.9.1.1.2 High Temperature Method

This method was developed by Michael Guiver's group at the Canadian NRC laboratories.[88] The polymerization involves reaction of stoichiometric quantities of monomers with high speed stirring in DMAc at 150 ℃ for 5-30 minutes using potassium carbonate as a base (**Scheme 1.2**). The high molecular mass can be achieved to provide mechanically robust solvent cast films.[87,89]

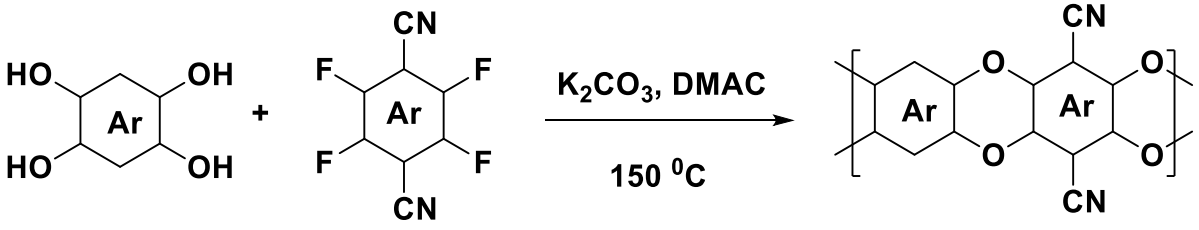

Scheme 1.2: Synthesis of PIMs by high temperature method

1.9.1.2 Structure-Property Relationship in PIMs

PIMs are non-network materials containing interconnected pores and possess high surface area. There is growing interest in PIMs for potential applications such as gas storage, sensors, CO_2 capture, and gas separation.[90] Since the publication of the first report on polymers of intrinsic microporosity (PIM-1), several PIMs have been reported.[78,83] PIM-7 showed high selectivity for O_2/N_2 gas pair with extraordinary O_2 permeability and the gas permeability data was located above 1991 Robeson upper bound. These results could be attributed to their fused ring structures which satisfied the chain rigidity and hindered the rotation of polymer chains. PIM-7 also demonstrated high CO_2 permeability and selectivity for CO_2/N_2 and CO_2/CH_4 gas pairs, which surpassed Robeson upper bound.[91,92] To improve the selectivity, a new series of copolymers containing trifluoromethyl-phenylsufone was synthesized by polycondensation.[91] These PIMs exhibited higher selectivity for CO_2/N_2 and O_2/N_2 that PIM-1.[93] This could be due to the presence of pendant $–SO_2Ph$ groups which decrease free volume and hinder the diffusion of gases resulting into decrease in permeability and increase in selectivity. Subsequently, it was inferred from molecular modeling studies that there is some degree of conformational flexibility about the spiro centre of the spirobisindane unit and dibenzodioxin ring.[94] Consequently, recent studies on PIMs have been conducted to improve their rigidity by incorportion of rigid units into polymers. To reduce the flexibility, McKeown and coworkers synthesized spirobifluorene-based PIM (SBF-PIM) and reported increase in gas permeability as well as selectivity. SBF-PIM exhibited CO_2 permeability of 13900 and CO_2/N_2 selectivity of 17.7.[95] To date, several examples of PIMs containing various units such as triptycene,[96,97] spirobisindane,[91,92] Tröger's base,[98–100] spirobischromane,[101] spirobifluorene,[102] hexaphenylbenzene,[57] binaphthalene,[103] tetraphenylethylene,[104] phthalimide,[105] tribenzotriquinacene[106], cardo PIMs, etc.[107] have been synthesized and evaluated as membrane materials for gas separation (**Figure 1.8** and **Table 1.2)**. These PIMs exhibited high gas separation performance due to their microporous nature. Recently, McKeown and co-workers reported the highest permeability to date by preparing 2D ultrapermeable PIMs (**Table 1.2**). These PIMs exhibited highest gas separation performance compared to other polymeric membrane materials used for gas separation applications. For example, PIM-TMN-Trip and PIM-TMN-SBI exhibited CO_2 permeability of 33,300 and 17,500 Barrer, respectively.[108]

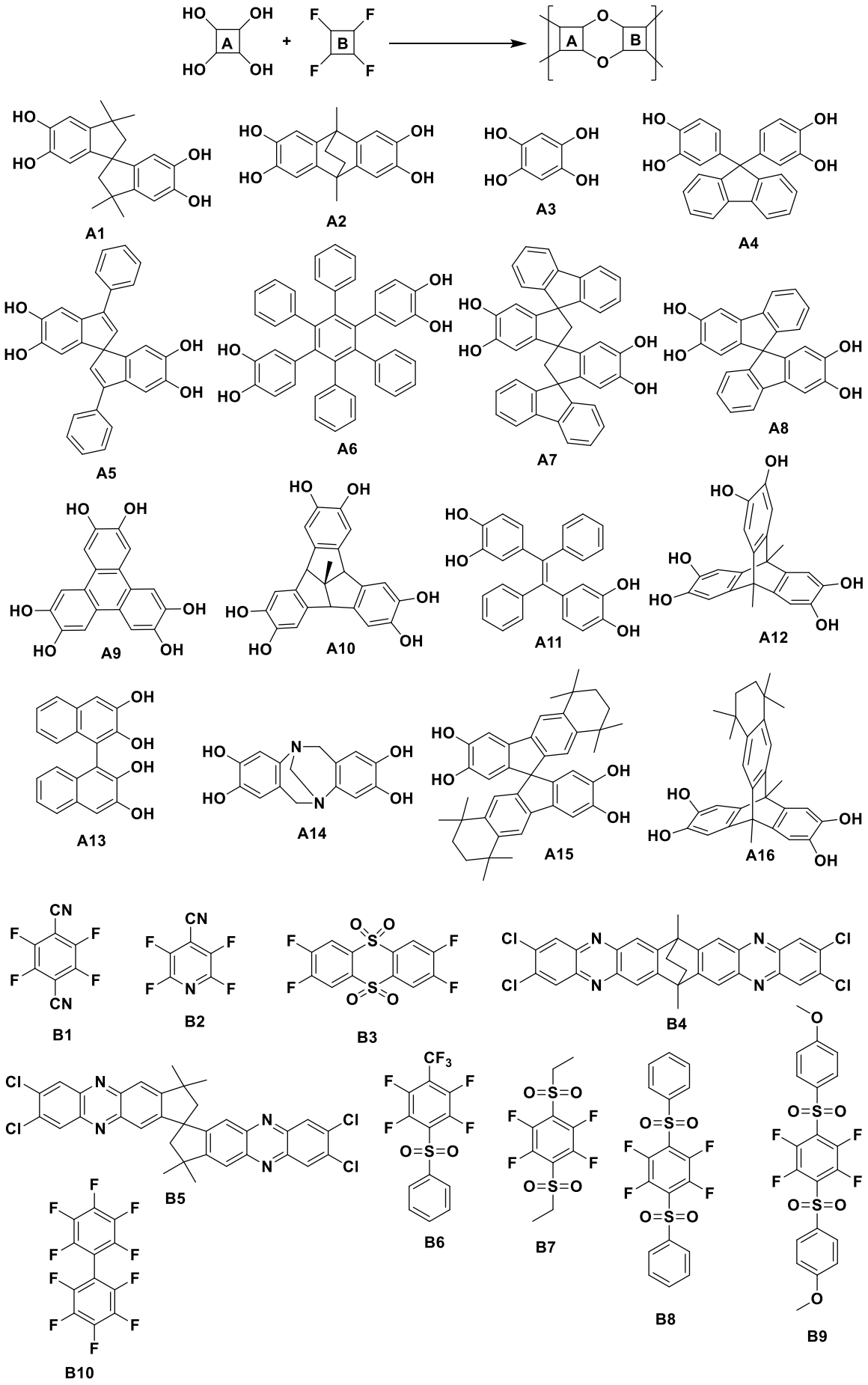

Figure 1.8: Representative bis(catechol)s (A) and tetrahalo (B) monomers used for the synthesis of PIMs

Table 1.2: Gas permeability and selectivity of reported PIMs

Code	Monomers	Permeability					Selectivity				Ref.
		H_2	N_2	O_2	CH_4	CO_2	H_2/N_2	O_2/N_2	CO_2/N_2	CO_2/CH_4	
PIM-1	A1+B1	1300	92	370	125	2300	14	4	25	18	83
	A1+B1	5010	823	2270	1360	13600	6.1	2.8	16.6	10	95
Cardo-PIM-1	A4+B5	3580	727	1790	-	8310	4.9	2.5	11	-	109
PIM-7	A1+B5	1100	42	190	62	860	2.6	4.5	21	14	
PIM-SBF	A8+B1	6320	786	2640	1100	13,900	8	3.4	18	13	95
PIM-CO-100	A2+B1 (NS)	-	-	-	-	-	-	-	-	-	10
PIM-6	A3+B9	-	-	-	-	-	-		-	-	
Polymer from 6	A5+B1	-	-	-	-	-	-	-	-	-	
HBP-PIM	A6+B1	1413	190	534	361	3800	7.44	2.81	20	10.5	57
Polymer from 7	A7+B1	-	-	-	-	-	-	-	-	-	10
	A9+B1	-	-	-	-	-	-	-	-	-	
TBTQ-PIM-1	A10+B1	-	-	-	-	-	-	-	-	-	
TPE-PIM	A11+B1	604	33.4	138	41	862	18	4.2	25.8	20.9	104
Tri-PIM	A12+B1 (NS)	-	-	-	-	-	-	-	-	-	10
DNPIM-33	A13(1)+ A1(2)+B1(3)	2347	242	907	-	4646	9.7	3.75	19.2	-	101,103
TB-PIM-23	A14+A1 +B1	-	240	864	353	4353	-	3.6	18.1	12.3	110
TB-PIM-25	A14+A1 +B1	-	262	917	375	4441	-	3.5	17.0	11.8	
TOTPIM-100	A1+B3	1368	190	642	-	3056	7.2	3.40	16.1	-	101
DSPIM1-100	A1+B8 (NS)	-	-	-	-	-	-	-	-	-	
PSTFPIM1	A1+B6	-	33	156	-	731	-	4.7	22	-	
PIM-2	A1+B10	-	-	-	-	-	-	-	-	-	10
PIM-TMN-SBI	A15+B1	7,190	1,080	3,200	-	17,500	6.65	2.96	16.2	-	108
PIM-TMN-Trip	A16+B1	16,900	2,230	7,470	-	33,300	7.78	3.5	14.9	-	

Continued…..

Table 1.2 (Continued)

TFMPS-PIM1	A1+B6	-	33	156	-	731	-	4.7	22	-	93
TFMPS-PIM2	A1+B(2) +B6(1)	-	75	308	-	1476	-	4.1	20	-	
TFMPS-PIM3	A1+B1(1) +B6(1)	-	158	561	-	2841	-	3.6	18	-	
TFMPS-PIM4	A1+B1(1) +B6(2)	-	217	737	-	3616	-	3.4	17	-	
DS-PIM1-33	A1+B1(2) +B8(1)	-	88	322	-	1408	-	3.7	16	-	91
DS-PIM2-33	A1+B1(2) +B7(1)	-	52	216	-	1077	-	4.2	21	-	
DS-PIM3-33	A1+B1(2) +B9(1)	-	93	369	-	2154	-	3.9	23	-	

1.9.2 Thermally Rearranged (TR) Polymers

Park and co-workers firstly reported thermally rearranged (TR) polymers based on polybenzoxazoles (PBOs).[111,112] TR polymers are derived from functionalized polyimides by post-thermal conversion process so-called thermally rearranged (TR) polymers.[113,114] TR polymers demonstrated extraordinary gas permeability and selectivity. The microporosity is generated in TR polymers as a result of evolution of CO_2 due to thermal rearrangement and consequently the gas permeability of TR polymer membranes is improved as compared to corresponding precursor polyimide.[10] TR polymers by virtue of their microporous nature are potentially useful in applications such as pervaporation and nanofiltration.[115,116]

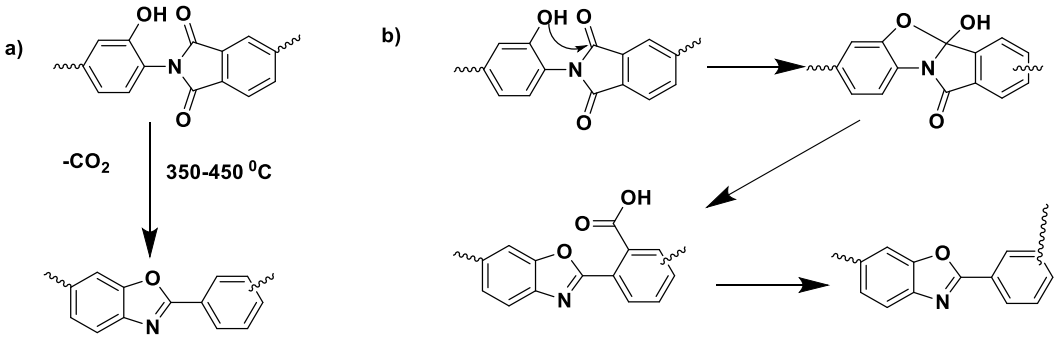

Scheme 1.3: a) Synthesis of TR polymers and b) mechanism for the synthesis of TR polymers

1.9.2.1 Synthesis of TR Polymers

TR polymer is obtained by thermal rearrangement of hydroxyl-containing polyimides. The imidization method of precursors plays an important role in the physical properties of TR-

PBOs, thermal rearrangement or conversion ratio as a function of treatment temperature affects the chemical structures of precursor polyimides and free volume of the resulting TR polymers (**Scheme 1.3a**).[113,117] In thermal cyclization mechanism, hydroxyl group attacks on strongly electrophilic carbonyl group which results into the opening of the ring to form carboxy-benzoxazole, followed by decarboxylation at temperatures of 350 to 450 °C to form benzoxazole with elimination of CO_2 (**Scheme 1.3b**).[7]

1.9.2.2 Structure-Property Relationship in TR Polymers

Since the discovery of TR polymers in 2007, several TR polymers have been developed and their structure-property relationship has been investigated (**Figure 1.9** and **Table 1.3**).[10,111,113] TR polymers have many benefits such as; i) enhanced chain rigidity and ii) disrupted inter-chain spacing due to very rigid and microporous nature.[113,118] TR polymers exhibited slightly lower permeability but higher selectivity than PIMs as a result of the different polymer spatial arrangements. Combining PIM and TR simultaneously enhanced both gas permeability and selectivity. The gas permeability is dependent on the chemical structure of precursors and resulting TR polymer membranes. Gas transport properties of TR polymers are also dependent on the degree of thermal rearrangement, which can be controlled by reaction time and conditions. Polymer chain packing density and chain mobility influence gas permeability and selectivity of TR polymers. Polymers containing bulky hexafluoro group showed high gas permeability with low packing density and high selectivity.[117,119]

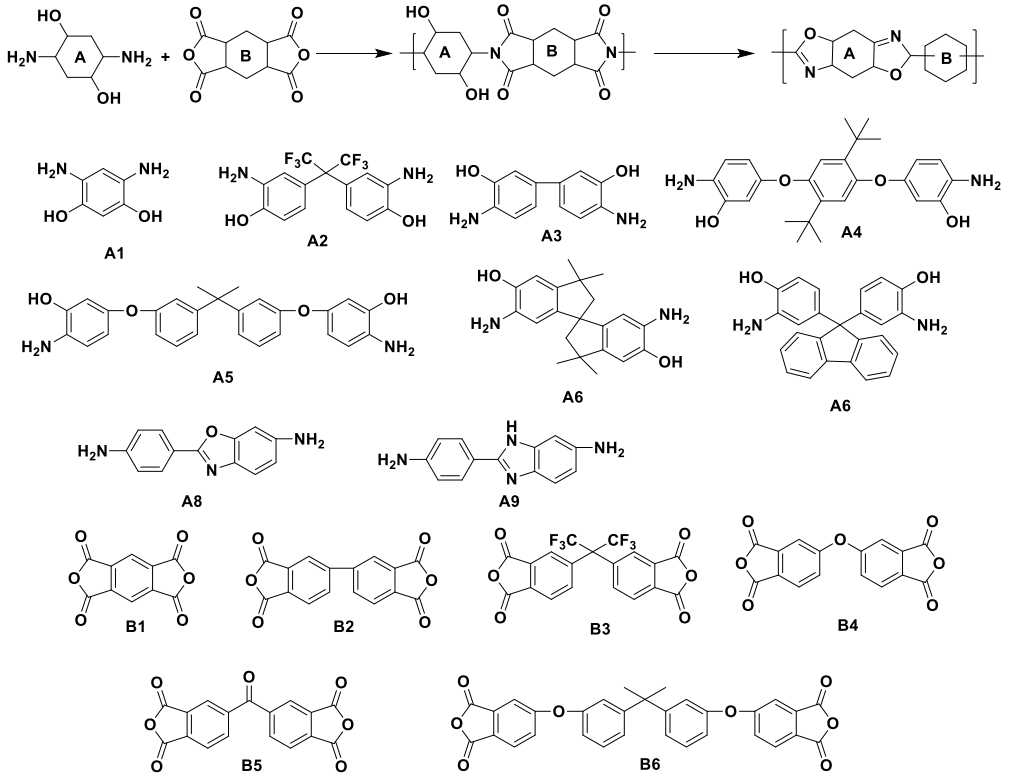

Figure 1.9: Representative hydroxyl-functionalized diamine (A) and dianhydride (B) monomers used for the synthesis of TR polymers

The most widely studied TR polymer is TR-PBO obtained by thermal rearrangement of hydroxyl polyimides (HPI) and showed CO_2 permeability of 5000 Barrers and selectivity for CO_2/N_2 and CO_2/CH_4 of 35 and 55, respectively.[117] Comesana-Gándara et al. introduced 3,3'-diamino-4,4'-dihydroxybiphenyl (mHAB) into TR polymers by condensation reaction of mHAB with 4,4'-hexafluoroisopropylidenediphthalic anhydride (6FDA) and their corresponding TR-PBO demonstrated an improvement in both gas permeability and selectivity. For example, TR-PBO membrane exhibited a CO_2 permeability of 720 Barrers and selectivity for CO_2/N_2 and CO_2/CH_4 gas pairs of 21 and 23, respectively.[113] Since then, various polymers have been investigated and reported as membrane materials for gas separations (**Figure 1.9** and **Table 1.3**).[120–124]

Table 1.3: Gas permeability and selectivity of reported TR-polymers

Code	Monomers	Permeability					Selectivity				Ref.
		H_2	N_2	O_2	CH_4	CO_2	H_2/N_2	O_2/N_2	CO_2/N_2	CO_2/CH_4	
HAB-6FDA-TR-400	A3+B3	155	4.5	21	3.03	95	34.4	4.7	21.1	31.4	113
6FAP-BisADA–TR400	A2+B6	34	0.54	3.1	0.39	13	62.9	5.7	24.1	33.3	
6FAP-6FDA-PBO	A2+B3	4194	284	1092	151	4201	14.8	3.8	15	28	117
TR-PEBO	A5+B3	439	20	88	17	486	22.0	4.4	24.3	28.6	121
CPBO	A6+B3	371	11.8	54.2	9.2	255	31.4	4.6	21.6	27.7	123
spiroTR-6FDA	A6+B3	429	30	120	34	675	14.3	3.9	22	20	124
spiroTR-6PMDA	A6+B1	261	11	48	15	263	23.7	4.4	24	18	
spiroTR-BPDA	A6+B2	43	5.2	20	5.7	87	5.2	3.9	17	15	
spiroTR-BPADA	A6+B6	19	0.45	2.1	0.53	8.8	42.2	4.7	22	19	
R-TR-PBOIa	A2+A8+B3	191	5.0	25	2.70	114	38	5.0	23	42	125
R-TR-PBOIa	A2+A9+B3	135	2.6	14	1.20	66	51	5.4	25	56	

1.9.3 Polyimides

Polyimide was invented by Bogert and Renshaw in 1908.[39] However, the commercialization of polyimide was done in 1955 by DuPont as Kapton.[8] Since then, various polyimides containing different units have been reported and applied in various fields such as gas separation, microelectronics, aircraft and the space industry, memory devices, etc. due to their outstanding thermo-oxidative stability, unique electrical properties and solvent

resistance, and high mechanical strength.[126,127] In addition, polyimides find applications in electronics industry for flexible cables, as an insulating film on the magnetic wire and for medical tubing. Examples of commercial polyimide films include Apical®, Kapton®, UPILEX®, VTEC PI®, Norton TH® and Kaptrex®.[39,127] However, their applications are limited in many fields because of limited solubility in common organic solvents and high glass transition or melting temperatures, which preclude their melt processability by injection moulding or extrusion. Accordingly, great efforts have been made to improve the processing characteristics of intractable polyimides.

1.9.3.1 Synthesis of Polyimides

In general, polyimides are synthesized by polycondensation of monomer pairs such as diamines with dianhydrides, diester-acids with diamines, tetracarboxylic acids with diamines, diisocyanates with dianhydrides, diamines with dithioanhydrides, and silylated diamines with dianhydrides.[39] Of these, polycondensation of aromatic diamine with dianhydride is the most popular method and is discussed in the following sections.

1.9.3.1.1 One-Step High Temperature Solution Polymerization

This process involves reacting stoichiometric quantities of dianhydride and diamine monomers in a high boiling solvent (**Scheme 1.4**). The commonly used solvents are *m*-cresol and chlorophenols. The imidization proceeds *via* the amic acid route although the concentration of polyamic acid at any time is very less. The polyamic acid rapidly converts to polyimide. This method is performed in the presence of catalysts such as isoquinoline and tertiary amines. The advantages of this method are that there is absence of "defect sites," of either amic acid or isoimide type in the resulting polymers and formation of high molecular weight polyimides even from sterically hindered diamine monomers.[128]

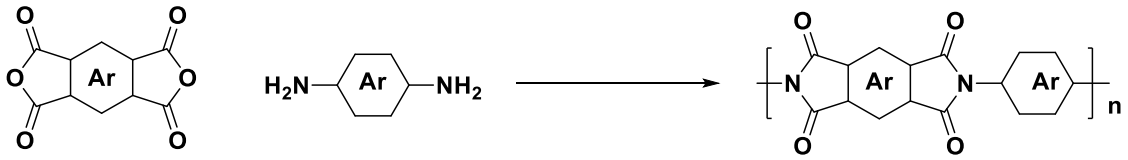

Scheme 1.4: Synthesis of polyimides

1.9.4 Polyimides of Intrinsic Microporosity (PIM-PIs)

Polyimides with a ladder-like and contorted structure have attracted much attention for gas separation applications.[10,129] In PIM-PIs, high permeability and selectivity is observed due to highly contorted structure and the presence of rigid imide rings. PIM-PIs exhibited good thermo-chemical stability as well as good solubility in most polar aprotic solvents, which facilitates solution-processibility needed for membrane fabrication.[88,130] The first report on PIM-PIs was published by Thomas and coworkers in 2007.[131] Subsequently, Budd and co-

workers in 2008 reported spirobisindane-based PIM-PIs for gas separation applications. They observed that PIM-PIs membranes showed O_2 permeability of 490 Barrers with an O_2/N_2 selectivity of 3.5 and thus the gas permeability data was located above 1991 Robeson upper bound.[132] Another approach to prepare PIM-PI involved use of hydroxyl-functionalized spirobisindane monomer. Hydroxyl groups in the polymer backbone could enhance CO_2 solubility by Lewis acid-base interaction and consequently improved CO_2 permeability. For instance, PIM-PI-OH showed CO_2 permeability of 263 Barrer and CO_2/CH_4 selectivity of 29.[133] The use of iptycene-containing monomers was also explored for the synthesis of PIM-PIs and the resulting polymers exhibited excellent gas permeation properties.[97] Inspired by the gas permeation performance of the TB-containing PIMs, research efforts were directed to design a new class of PIM-PIs containing TB units.[134] PIM-TB-PIs exceeded Robeson upper bound for most of the gas pairs.[135] Ethanoanthracene-based (EA) polyimide (PIM-PI-EA) was synthesized and evaluated as membrane material for gas separation applications. The permeability data of PIM-PI-EA was located above 2008 Robeson upper bound for important gas pairs such as CO_2/CH_4 and CO_2/N_2. This significant enhancement in gas performance could be attributed to the presence of rigid ethanoanthracene units.[136] To date, various units such as triptycene, Troger's base, spirobisindane, spirobifluorene, spirobichroman, etc., have been incorporated into PIM-PIs with an objective to improve the permeability and selectivity of PIM-PIs (**Figure 1.10** and **Table 1.4**).[118,137–140] These studies suggest that combination of PIs with PIMs leading to create microporosity are of great interest for obtaining high permeability and selectivity.[132] Recently, Pinnau and co-workers synthesized carbocyclic PIM-PIs by polymerization of carbocyclic unit containing dianhydrides with aromatic diamines which exhibited excellent gas separation performance.[136]

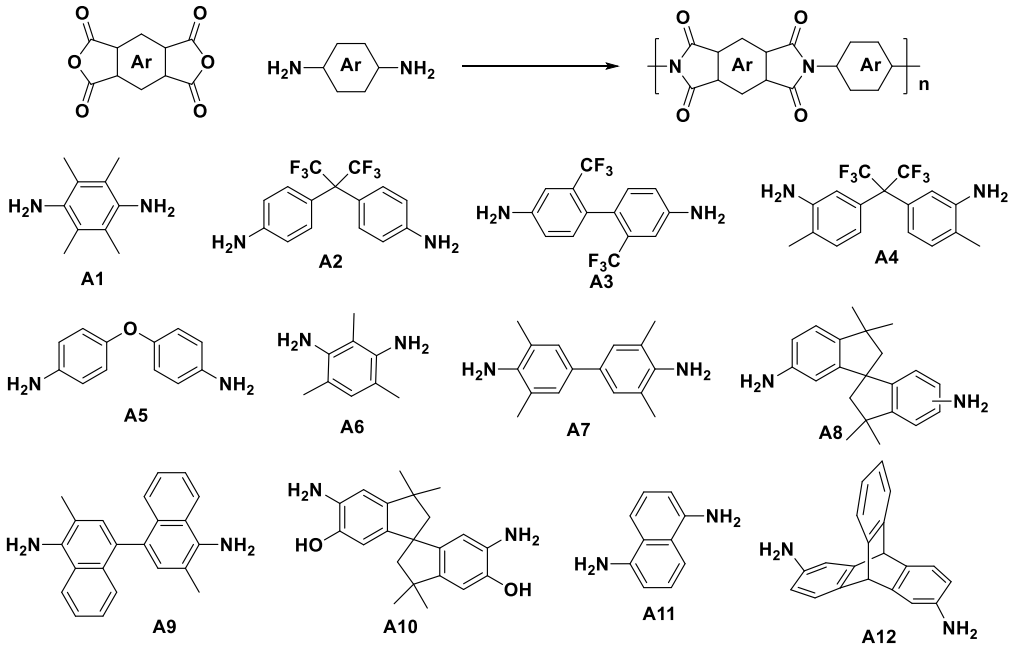

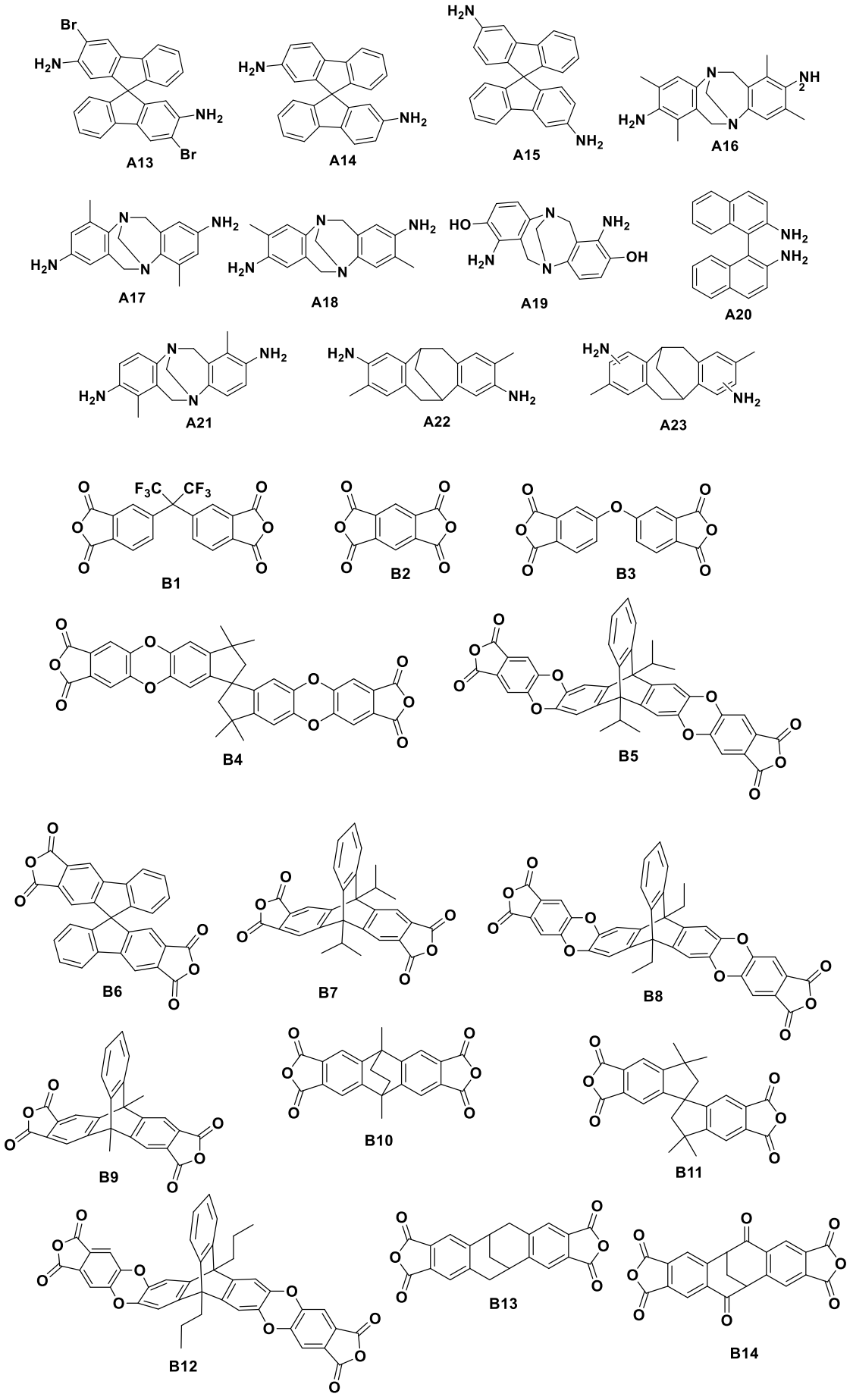

Figure 1.10: Representative diamine (A) and dianhydride (B) monomers used for the synthesis of PI-PIMs

Table 1.4: Gas permeability and selectivity of reported PIM-PIs

Code	Monomers	Permeability					Selectivity				Ref.
		H_2	N_2	O_2	CH_4	CO_2	H_2/N_2	O_2/N_2	CO_2/N_2	CO_2/CH_4	
BINAM-PMDA	A20+B2	-	-	-	-	-	-	-	-	-	131
PIM-PI-1	A1+B4	530	47	150	77	1100	11	3.2	23	14	132
PIM-PI-2	A2+B4	220	9	39	9	210	24	4.3	23	13	
PIM-PI-3	A4+B4	360	23	85	27	520	16	3.7	23	19	
PIM-PI-4	A3+B4	300	16	64	20	420	18	4.0	26	21	
PIM-PI-7	A11+B4	350	19	77	27	510	17	4.1	27	19	91
PIM-PI-8	A9+B4	1600	160	545	260	3700	10	3.4	23	14	
PIM-PI-9	A1+B11	840	94	295	170	2180	8.9	3.1	23	13	
PIM-PI-10	A9+B11	670	84	270	168	2154	8.0	3.2	26	13	
PIM-PI-11	A8+B11	625	65	208	129	1523	9.6	3.2	23	12	
6FDA-SBF	A14+B1	234	7.8	35.1	6.4	182	30.0	4.5	23.3	27.3	138
PMDA-SBF	A14+B2	230	8.5	35.5	9.1	197	27.1	4.2	23.2	21.6	
SPDA-SBF	A14+B4	501	28.6	111	41.1	614	17.5	3.9	21.5	14.9	
6FDA-BSBF	A13+B1	531	27.0	107	24.9	580	19.7	4.0	21.5	23.3	
PMDA-BSBF	A13+B2	560	28.8	116	36.5	693	19.4	4.0	24.1	19.0	
SPDA-BSBF	A13+B4	919	69.0	243	102	1340	13.3	3.5	19.4	13.1	
TBDA1-SBI-PI	A17+B4	398	35	190	45	895	27	5.4	25.6	19.7	135
TBDA2-SBI-PI	A18+B4	530	49	240	65	1213	24	4.9	24.8	18.7	
TDA1-DMN	A9+B9	3050	182	783	216	3700	16.7	4.3	20.3	17.1	99
TDAi3-DMN	A9+B7	2233	160	594	211	3154	14.0	3.7	19.7	14.9	
PIM-6FDA-OH	A10+B1	259	10.8	45.2	9.1	263	24	4.2	24	29	133
PIM-PMDA-OH	A10+B2	190	6.9	30.5	7.7	198	28	4.4	29	26	
KAUST-PI-1	A1+B5	3983	107	627	105	2389	37	5.9	33	23	97
KAUST-PI-2	A7+B5	2368	98	490	101	2071	24	5.0	21	21	
KAUST-PI-3	A6+B5	1625	43	238	43	916	38	5.5	21	21	
KAUST-PI-4	A5+B5	302	10.6	48	10.7	286	29	4.5	27	27	
KAUST-PI-5	A2+B5	1558	87	356	77	1552	18	4.1	18	20	
KAUST-PI-6	A4+B5	409	14.4	64.8	11	322	28	4.5	22	29	
KAUST-PI-7	A9+B5	3198	225	842	354	4391	14	3.7	20	12	
KAUST-PI-1'	A1+B12	560	32	123	33	645	17.5	3.8	20.1	19.5	
KAUST-PI-5'	A2+B12	546	18	90	20	406	30.3	5.0	22.5	20.3	
KAUST-PI-5"	A2+B8	712	32	126	30	679	22.2	3.9	21.2	22.6	

Continued…..

Table 1.4 (Continued)

TBDA1-6FDA-PI	A17+B1	253	6.5	28	3.3	155	35.1	3.9	23.8	46.9	134
TBDA1-ODPA-PI	A17+B3	36.4	0.5	2.5	0.37	13.4	71.4	5.0	26.8	36.2	
TBDA2-6FDA-PI	A18+B1	390	12	47	8	285	32.5	4.0	23.8	35.6	
TBDA2-6FDA-PI	A18+B1	159	3.8	16.2	2.2	106	41.8	4.3	27.9	48.2	
4MTBPA-6FDA	A16+B1	1446	133	408	116	1672	10.37	3.1	12.6	14.41	135
4MTBPA-PMDA	A16+B2	3300	290	1080	390	4460	11.4	3.72	15.4	11.44	
4MTBPA-SBIDA	A16+B11	3200	373	1132	591	5140	8.6	3.03	13.8	8.70	
4MTBPA-SBFDA	A16+B6	2901	264	941	371	4476	11	3.56	17.0	12.06	
PIM-PI-EA	A9+B10	4230	369	1380	457	7340	11.5	3.7	19.9	16.1	136
CTB1-DMN	A9+B13	1295	76.2	320	95.7	1661	17.0	4.2	21.8	17.4	141
CTB2-DMN	A9+B14	1150	39.9	206	40.4	948	28.8	5.2	23.7	23.5	
6FDA-HTB	A19+B1	167	2.26	13.6	0.92	67	73.9	6.0	29.6	73	142
SBI-HTB	A19+B1	467	16.6	75.7	16.3	466	28.1	4.6	28.1	29	
6FDA-TBDA	A21+B1	262	7.6	35	5.2	174	34.5	4.6	22.9	33	
6FDA-CTBDA	A22+B1	375	14.8	56	11.6	291	25.3	3.8	19.6	25	
6FDA-iCTBDA	A23+B1	313	12.2	49	8.9	230	26.7	3.9	18.9	25	
Matrimid		18	0.32	2.1	0.28	10	56	6.6	31	36	143

1.9.5 Polymeric Ionic Liquids (PILs)

Poly(ionic liquid)s (PILs) are the new class of polymer electrolytes which contain ionic groups either in the backbone or as a pendant.[144] Recently, PILs have attracted considerable attention due to their unique properties such as ionic conductivity and electrochemical stablity.[145]

There are two pathways to incorporate ionic groups into polymers.

1. Synthesis of PILs from ionic group containing monomers
2. Post-modification of polymers

1.9.5.1 Synthesis of PILs

1.9.5.1.1 Synthesis of polymers from ionic group containing monomers

Most of the polymers containing pendant ionic liquid groups are synthesized by chain polymerization of ionic group containing monomers to form homopolymers or copolymers. The polymerization of ionic group monomers is simple, straightforward, and widely adopted strategy to prepare PILs[146,147] The advantage of this method is that the obtained polymers have a well-defined structure.[145,148]

Examples of difunctional monomers containing ionic liquid groups are known in the literature particularly for the synthesis of aliphatic polymers such as polyesters, polyurethanes, etc.[144,149–153] Polyimide-based PILs (PI-PILs) were synthesized by polycondensation of dianhydrides and ionic group containing diamines and were evaluated as membrane materials for gas separation applications.[147]

1.9.5.1.2 Post-modification of polymers

This method involves *N*-quaternization of polymers *via* *N*-quaternization of nitrogen containing ring with alkyl or benzyl halides. The advantage of this method is that the obtained polymers have predetermined molecular weights as well as possibility to tune the degree of *N*-quaternization.[145,154] Shaplov, et al.[155] reported for the first time post-modification of polyimides into PILs by *N*-quaternization followed by metathesis and demonstrated improved gas permeation properties of PI-PILs especially for CO_2.

1.9.5.2 Structure-Property Relationship in PILs

It is a challenging task for both industry and scientific communities to separate CO_2 from nitrogen or methane because such separation process requires membrane with high CO_2 permeability and selectivity.[145,156,157] The major obstacle of most of the reported PILs is that they are brittle in nature and thus they could not be used at higher pressure. To overcome this limitation, researchers have aimed to improve the mechanical strength of PILs. It is reported that mechanical stability can be improved by tuning polymer structure. The mechanically stable PILs were reported in 2006 by Hu and co-workers by grafting polyethylene glycol (PEG) on to PILs. It was observed that PILs exhibited good separation performances for CO_2/N_2 gas pair at 40 psi upstream pressure.[31] Styrene and acrylate containing imidazolium-based PILs were also developed by Nobel's group with changing *N*-alkyl substituents by polymerization of IL monomer in the presence of cross-linker on the porous polymer support.[158] They observed that with increasing length of *N*-alkyl substituent, the gas permeability of PILs was increased. PILs containing bulky anion (Tf_2N^-) were developed by Carlisle et. al. and observed an improvement in gas separation of CO_2.[159] Mechanical stability

and high CO_2 permeability of 101.4 Barrer was reported for vinyl imidazolium-based PILs by Li et al. using the addition of crosslinking.[160,161] Film-forming pyrrolidinium-based PILs were reported by Tome et. al. and observed increase in CO_2-based performance.[162] Li and coworkers were the first to report synthesis of PI-PILs.[147] The synthesis was carried out by condensation of IL-based diamines with 6FDA. The gas permeation of these copolyimides (IL content upto 25 mol%) was recorded at 10 atm upstream pressure, while homopolyimide failed to form a film. The authors reported that with increasing IL content in copolyimide decrease in permeability and increased selectivity due to reduction in free volume.[147] The post-modification of polyimides was first reported by Shaplov and coworkers.[155] They post-modified polyimides containing imidazole and quinuclidine moieties with alkyl halides into PI-PILs and reported CO_2 permeability of 85 barrer. The gas permeability and selectivity data of representative reported polymers are collected in **Figure 1.11-1.17** and **Table 1.5**.

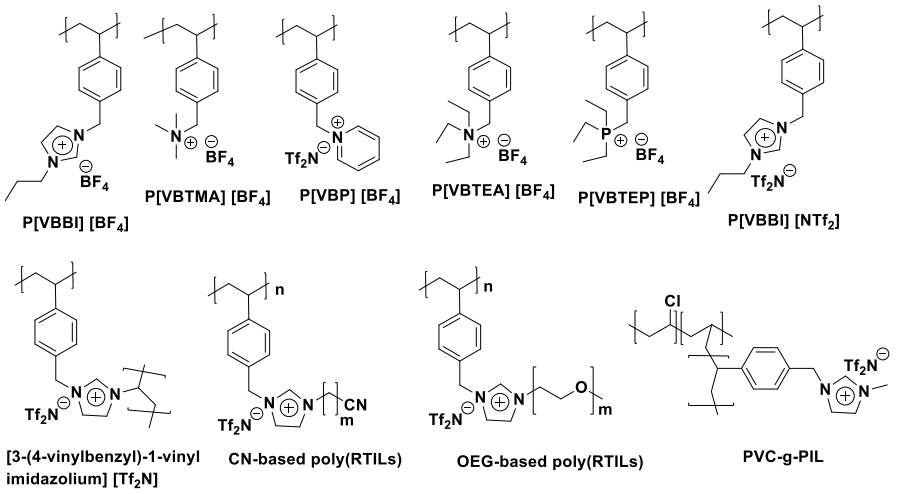

Figure 1.11: Polystyrene-based PILs

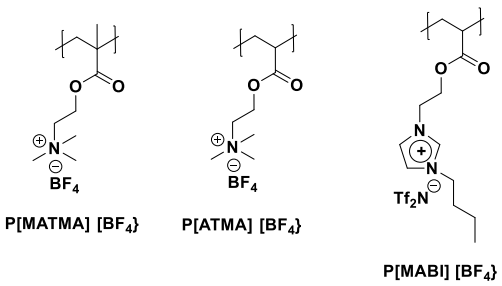

Figure 1.12: Polyacrylic-based PILs

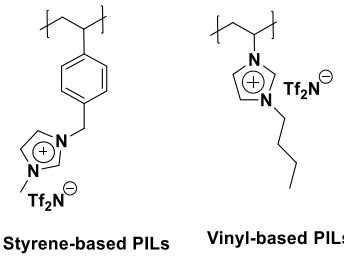

Figure 1.13: Film-forming styrene and vinyl-based PILs

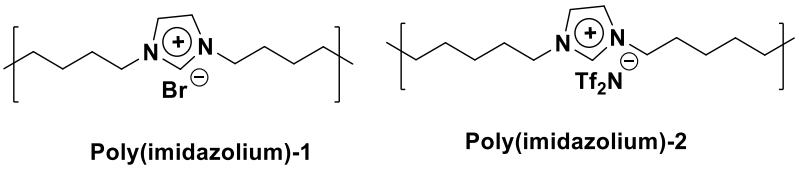

Figure 1.14: Polyimidazolium-based PILs

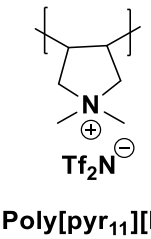

Figure 1.15: Polypyrrole-based PILs

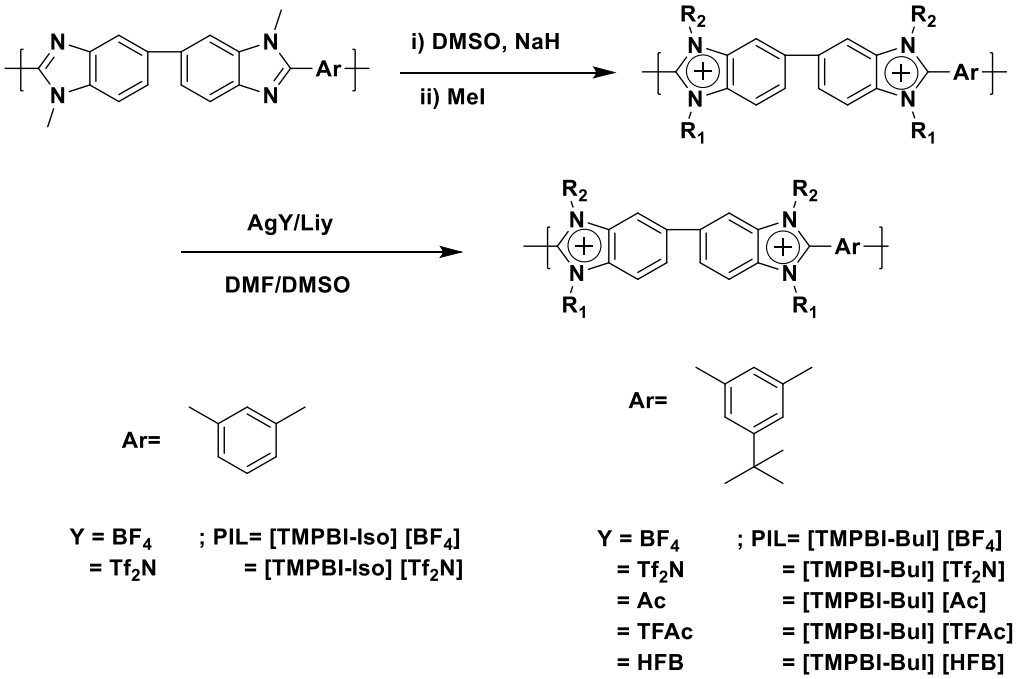

Figure 1.16: Polybenzimadazole-based PILs

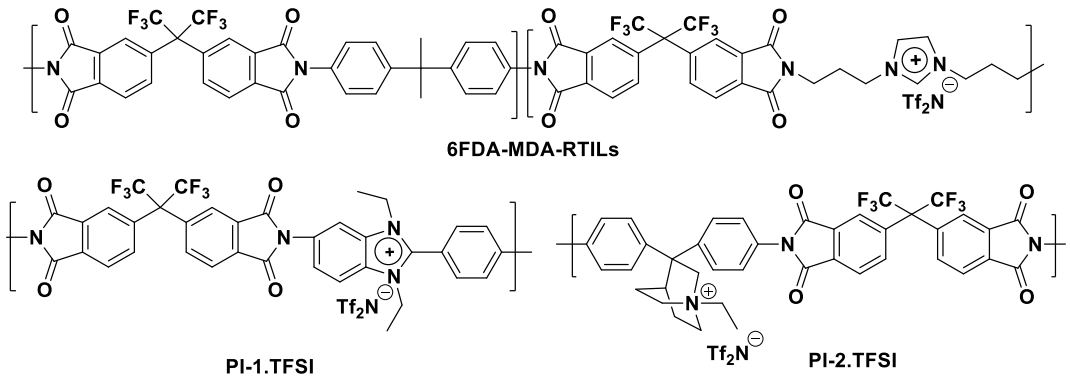

Figure 1.17: Polyimide-based PILs

Table 1.5: Gas permeability and selectivity of reported PILs

Code	Permeability	Selectivity		Ref.
	CO_2	CO_2/N_2	CO_2/CH_4	
P[VBBI] [BF4]	-	-	-	154,163–166
P[VBTMA] [BF4]	-	-	-	
P[VBP] [BF4]	-	-	-	
P[VBTEA] [BF4]	-	-	-	
P[VBTEP] [BF4]	-	-	-	
P[VBBI] [Tf2N]	-	-	-	
P[MATMA] [BF4]	-	-	-	
P[ATMA] [BF4]	-	-	-	
P[MABI] [BF4]	-	-	-	
Styrene based PIL	9.2	32	39	20
Vinyl based PIL	67.3	14.5	10.6	
P[VBVI] [TF2N]	101	20.6	12.9	145,167
CN-based poly(RTILs)	8.2	40	30	156,168–170
OEG-based poly(RTILs)	22	44	29	
PVC-g-PIL	17.9	24.7	-	171
Poly(imidazolium)-1	0.13	-	-	157
Poly(imidazolium)-2	5.2	24	20	
[TMPBI-Iso] [BF4]	1.02	21	78	172,173
[TMPBI-Iso] [Tf2N]	8.2	23	59	
[TMPBI-BuI] [BF4]	4.8	24	48	
[TMPBI- BuI] [Tf2N]	17.9	23	43	
[TMPBI- BuI] [Ac]	-	-	-	
[TMPBI- BuI] [TFAc]	2.16	17	43	
[TMPBI- BuI] [HFB]	6.52	13	31	
6FDA-MDA-RTILs (25%)	9.2	21.9	61.5	146
PI-1.TFSI	103	18.4	19.07	155
PI-2.TFSI	38	15.2	15.8	
Poly[pyr11][NTf_2]	5.09	22.2	28.6	162

1.10 SUMMARY

Membrane technologies have been in the use on industrial scale for various important gas separations such as natural gas purification (CO_2/CH_4), purification of flue gas (CO_2/N_2), purification of oxygen (O_2/N_2), etc. Membrane gas separation is a mature and expanding technology. Since the discovery of the first gas separation unit based on polysulfone hollow fiber membrane built by Monsanto, hundreds of new polymeric materials have been synthesized in the academic laboratories. Over the period of time, spectacular advancements

were made in terms of material synthesis and empirical rules were framed. However, industry still uses polymeric membranes which were developed in the 1990s. The present day commercial polymeric membranes face challenges such as physical aging, plasticization and trade-off relationship between permeability and selectivity wherein high permeability is gained by sacrificing selectivity and vice-versa. As a consequence, next generation membranes based on PIMs, PILs and TR polymers have gained significant attention in the recent years as potential candidates for improved gas separation performance in practical applications. TR polymers and PIMs have demonstrated good combination of permeability and selectivity and some of the candidates belonging to these classes of polymers are located above 2008 Robeson upper bound. In particular, PILs showed good combination of permeability/selectivity for CO_2 separation and hence are of continued interest. Thus, TR polymers, PIMs and PILs hold promise and are being intensely researched.

1.11 REFERENCES

1. Lonsdale, H. K. *J. Membr. Sci.*, 1982, **10**, 81–181.
2. Baker, R. W., Lokhandwala, K., Baker, R. W., Lokhandwala, K. *Ind. Eng. Chem. Res.*, 2008, **47**, 2109–2121.
3. Spillman, R. In *Membrane Separations Technology. Principles and Applications* 1995; pp. 589–667.
4. Lu K, Song C, S. V. Hydrogen and syngas production and purification technologies. Hoboken, NJ: John Wiley & Sons, Inc.; 2010.
5. Null, I. H. R., Coeur, C., Balmer, F. L. *US Pat.*, 1979.
6. Pandey, P., Chauhan, R. S. *Prog. Polym. Sci.*, 2001, **26**, 853–893.
7. Galizia, M., Chi, W. S., Smith, Z. P., Merkel, T. C., Baker, R. W., Freeman, B. D. *Macromolecules*, 2017, **50**, 7809−7843.
8. Sanders, D. F., Smith, Z. P., Guo, R., Robeson, L. M., McGrath, J. E., Paul, D. R., Freeman, B. D. *Polymer*, 2013, 54, 4729–4761.
9. Ma, C., Urban, J. J. *Proc. Nat. Res. Soc.*, 2018, **2**, 2002.
10. Kim, S., Lee, Y. M. *Prog. Polym. Sci.*, 2015, **43**, 1–32.
11. Jue, M. L., Lively, R. P. *React. Funct. Polym.*, 2015, **86**, 40–43.
12. Galizia, M., Chi, W. S., Smith, Z. P., Merkel, T. C., Baker, R. W., Freeman, B. D. *Macromolecules*, 2017, **50**, 7809–7843.
13. George, S. C., Thomas, S. *Prog. Polym. Sci.*, 2001, **26**, 985–1017.
14. K., S. Handbook of industrial membranes. 1st ed. Oxford, UK: Elsevier 1995., Science Publishers Ltd.;, 1995.
15. Edgar S. Sanders, Jr., Daniel 0. Clark; John A. Jensvold, Henry N. Beck; G. Glenn Lipscomb, F. L. C. *US Pat.*, 1989, 1–30.
16. Allam, R. J., Bredesen, R., Drioli, E. *Carbon Dioxide Recover. Util.*, 2003, 53–120.
17. Cooley, T. E., Coady, A. B. *US Pat.*, 1978, 1–10.
18. Cui, X., Bustin, R. M., Dipple, G. *Fuel*, 2004, **83**, 293–303.
19. Sanders, D. F., Smith, Z. P., Guo, R., Robeson, L. M., McGrath, J. E., Paul, D. R., Freeman, B. D. *Polymer*, 2013, 54, 4729–4761.
20. Li, P., Paul, D. R., Chung, T.-S. *Green Chem.*, 2012, **14**, 1052.
21. Smith, A. R., Klosek, J. *Fuel Proc. Techn.*, 2001, **70**, 115–134.
22. Kaaeid A. Lokhandwala, R. W. B. *US Pat.*, 1998, 1–16.
23. Aaron, D., Tsouris, C. *Sep. Purif. Techn.*, 2005, **40**, 321–348.
24. Bernardo, P., Drioli, E., Golemme, G. *Ind. Eng. Chem. Res.*, 2009, **48**, 4638–4663.
25. Shao, L., Low, B. T., Chung, T.-S., Greenberg, A. R. *J. Membr. Sci.*, 2009, **327**, 18–31.
26. Koros, W. J., G. k. F. *J. Membr. Sci.*, 1993, **83**, 1–80.
27. Koros, W. J., Mahajan, R. *J. Membr. Sci.*, 2001, **181**, 141.
28. Javaid, A. *Chem. Eng.J.*, 2005, **112**, 219–226.
29. Stern, S. A., Mi, Y., Yamamoto, H., Al, S. E. T. *J. Polym. Sci. Part B Polym. Phys.*, 1989, **27**, 1887–1909.
30. Stern, S. A., Gareis, P. J., Sinclair, T. F., Mohr, P. H. *J. Appl. Polym. Sci.*, 1963, **7**, 2035–2051.
31. Hu, X., Tang, J., Blasig, A., Shen, Y., Radosz, M. *J. Membr. Sci.*, 2006, **281**, 130–138.
32. Baker, R. W. *Ind. Eng. Chem. Res.*, 2002, **41**, 1393–1411.
33. Ghosal, K., Freeman, B. D. *Polym. Adv. Technol.*, 1994, **5**, 673–697.
34. Karadkar, P. B., Kharul, U. K., Bhole, Y. S., Badhe, Y. P., Tambe, S. S., Kulkarni, B. D. *J. Membr. Sci.*, 2007, **303**, 244–251.
35. Hellums, M. W., Koros, W. J., Husk, G. R., Paul, D. R. *J. Membr. Sci.*, 1989, **46**, 93–112.
36. Hu C-C, Chang C-S, Ruaan R-C, Lai J-Y *J. Membr. Sci.*, 2003, **226**, 51–61.
37. Bondi, A. *J. Phys. Chem.*, 1965, **68**, 441–451.

38. Coleman, M. R., Koros, W. J. *J. Membr. Sci.*, 1990, **50**, 285–297.
39. Liaw, D. J., Wang, K. L., Huang, Y. C., Lee, K. R., Lai, J. Y., Ha, C. S. *Prog. Polym. Sci.*, 2012, **37**, 907–974.
40. Calle, M., Lozano, A. E., de Abajo, J., de la Campa, J. G., Álvarez, C. *J. Membr. Sci.*, 2010, **365**, 145–153.
41. Nataraj, S. K., Sridhar, S., Shaikha, I. N., Reddy, D. S., Aminabhavi, T. M. *Sep. Purif. Techn.*, 2007, **57**, 185–192.
42. Mulder, M. Basic Principles of Membrane Technology, 1996.
43. Hirayama, Y., Kase, Y., Tanihara, N., Sumiyama, Y., Kusuki, Y., Haraya, K. *J. Membr. Sci.*, 1999, **160**, 87–99.
44. Costello, L. M., Koros, W. J. *J. Polym. Sci. Part B Polym. Phys.*, 1994, **32**, 701–713.
45. Powell, C. E., Qiao, G. G. *J. Membr. Sci.*, 2006, **279**, 1–49.
46. Liu, Y., Pan, C., Ding, M., Xu, J. *J. Appl. Polym. Sci.*, 1999, **73**, 521–526.
47. Kanehashi, S., Nagai, K. *J. Membr. Sci.*, 2005, **253**, 117–138.
48. Pixton, M. R., Paul, D. R. *Polymer*, 1995, 8277–8286.
49. Sadeghi, M., Semsarzadeh, M. A., Moadel, H. *J. Membr. Sci.*, 2009, **331**, 21–30.
50. Lin, W. H., Chung, T. S. *J. Membr. Sci.*, 2001, **186**, 183–193.
51. Ghosal, K., Chern, R. T., Freeman, B. D. *Macromolecules*, 1996, **29**, 4360–4369.
52. Stern, S. A., Mauze, G. R., Frisch, H. L. *J. Polym. Sci. Part B Polym. Phys.*, 1983, **21**, 1275–1298.
53. Hacarlioglu, P., Toppare, L., Yilmaz, L. *J. Appl. Polym. Sci.*, 2003, **90**, 776–785.
54. Khulbe, K. C., Matsuura, T., Lamarche, G., Kim, H. J. *J. Membr. Sci.*, 1997, **135**, 211–223.
55. Malakhov, A. O., Dibrov, G. A., Litvinova, E. G., Novitsky, E. G. *Pet. Chem.*, 2015, **55**, 803–809.
56. Huang, Y., Paul, D. R. *J. Polym. Sci. Part B Polym. Phys.*, 2007, **45**, 1390–1398.
57. Carta, M., Bernardo, P., Clarizia, G., Jansen, J. C., McKeown, N. B. *Macromolecules*, 2014, **47**, 8320–8327.
58. Brunetti, A., Scura, F., Barbieri, G., Drioli, E. *J. Membr. Sci.*, 2010, **359**, 115–125.
59. Puleo, A. C., Paul, D. R., Kelley, S. S. *J. Membr. Sci.*, 1989, **47**, 301–332.
60. Paul, D. R. *Polymer*, 1995, **36**, 3165–3172.
61. Babari, T. A., Koros, W. J., Paul, D. R. *J. Membr. Sci.*, 1989, **42**, 303–314.
62. Aguilar-Vega, M., Paul, D. R. *J. Polym. Sci. Part B Polym. Phys.*, 1993, **31**, 1599–1610.
63. McHattie, J. S., Koros, W. J., Paul, D. R. *Polymer*, 1991, **32**, 840–850.
64. H, J. S. M., Koros, W. J., Paul, D. R. *Polymer*, 1992, **33**, 1701–1711.
65. Tawade, B. V., Shaligram, S. V., Valsange, N. G., Kharul, U. K., Wadgaonkar, P. P. *Polym. Int.*, 2016, **65**, 567–576.
66. Hay A.S., Blanchard H.S., Endres G. F., E. J. W. *J. Am. Chem. Soc.*, 1959, **2**.
67. Schmitkons, A. E. E., Mitchell, T., Corporation, M. O., York, N. *Patent*, 1981, 2–5.
68. Science, M., V, E. S. P. B., Chern, R. T., Sheu, F. R., Jia, L., Stannett, V. T., Hopfenberg, H. B. *J. Membr. Sci.*, 1987, **35**, 103–115.
69. Khulbe, K. C., Hamad, F., Feng, C., Matsuura, T., Gumi, T., Palet, C. *Sep. Purif. Techn.*, 2004, **36**, 53–62.
70. Kim, T. H., Koros, W. J., Husk, G. R., O'Brien, K. C. *J. Membr. Sci.*, 1988, **37**, 45–62.
71. Xiao, Y., Low, B. T., Hosseini, S. S., Chung, T. S., Paul, D. R. *Prog. Polym. Sci.*, 2009, **34**, 561–580.
72. Xia, J., Chung, T. S., Li, P., Horn, N. R., Paul, D. R. *Polymer*, 2012, **53**, 2099–2108.
73. Psaume, R., Aptel, P., Aurelle, Y., Mora, J. C., Bersillon, J. L. *J. Membr. Sci.*, 1988, **36**, 373–384.
74. Rowe, B. W., Freeman, B. D., Paul, D. R. *R. Soc. Chem.*, 2011, **1**, 58–83.
75. Tiwari, R. R., Jin, J., Freeman, B. D., Paul, D. R. *J. Membr. Sci.*, 2017, **537**, 362–371.
76. Robeson, L. M. *J. Membr. Sci.*, 1991, **62**, 165–185.
77. Robeson, L. M. *J. Membr. Sci.*, 2008, **320**, 390–400.

78. McKeown, N. B. *ISRN Mater. Sci.*, 2012, **2012**, 1–16.
79. Wu, D., Xu, F., Sun, B., Fu, R., He, H., Matyjaszewski, K. *Chem. Rev.*, 2012, **112**, 3959–4015.
80. Srinivasan, R., Auvil, S. R. *J. Membr. Sci.*, 1994, **86**, 67–86.
81. A.Yu. Alentiev, Yu.R Yampolskii, V.P. Shantarovich, S.M. Nemser, N. A. P. *J. Membr. Sci.*, 1997, **126**, 123–132.
82. Masuda, T., Isobe, E., Higashimura, T., Takada, K. *J. Am. Chem. Soc.*, 1983, **105**, 7473–7474.
83. Budd, P. M., Elabas, E. S., Ghanem, B. S., Makhseed, S., McKeown, N. B., Msayib, K. J., Tattershall, C. E., Wang, D. *Adv. Mater.*, 2004, **16**, 456–459.
84. Budd, P. M., McKeown, N. B., Ghanem, B. S., Msayib, K. J., Fritsch, D., Starannikova, L., Belov, N., Sanfirova, O., Yampolskii, Y., Shantarovich, V. *J. Membr. Sci.*, 2008, **325**, 851–860.
85. Vopička, O., De Angelis, M. G., Du, N., Li, N., Guiver, M. D., Sarti, G. C. *J. Membr. Sci.*, 2014, **459**, 264–276.
86. Song, J., Du, N., Dai, Y., Robertson, G. P., Guiver, M. D., Thomas, S., Pinnau, I. *Macromolecules*, 2008, **41**, 7411–7417.
87. Naiying, D., Jingshe, S., Robertson, G. P., Pinnau, I., Guiver, M. D. *Macromol. Rapid Commun.*, 2008, **29**, 783–788.
88. McKeown, N. B. *ISRN Mater. Sci.*, 2012, **2012**, 1–16.
89. Ghanem, B. S. *Polym. Chem.*, 2012, **3**, 96–98.
90. McKeown, N. B., Budd, P. M. *Chem. Soc. Rev.*, 2006, **35**, 675–683.
91. Ghanem, B. S., McKeown, N. B., Budd, P. M., Al-Harbi, N. M., Fritsch, D., Heinrich, K., Starannikova, L., Tokarev, A., Yampolskii, Y. *Macromolecules*, 2009, **42**, 7881–7888.
92. Ghanem, B. S., McKeown, N. B., Budd, P. M., Selbie, J. D., Fritsch, D. *Adv. Mater.*, 2008, **20**, 2766–2771.
93. Du, N., Robertson, G. P., Song, J., Pinnau, I., Thomas, S., Guiver, M. D. *Macromolecules*, 2008, **41**, 9656–9662.
94. Heuchel, M., Fritsch, D., Budd, P. M., McKeown, N. B., Hofmann, D. *J. Membr. Sci.*, 2008, **318**, 84–99.
95. Bezzu, C. G., Carta, M., Tonkins, A., Jansen, J. C., Bernardo, P., Bazzarelli, F., Mckeown, N. B., Bezzu, B. C. G., Carta, M., Tonkins, A., Jansen, J. C., Bazzarelli, F., McKeown, N. B. *Adv. Mater.*, 2012, **24**, 5930–5933.
96. Luo, S., Wiegand, J. R., Kazanowska, B., Doherty, C. M., Konstas, K., Hill, A. J., Guo, R. *Macromolecules*, 2016, **49**, 3395–3405.
97. Swaidan, R., Al-Saeedi, M., Ghanem, B., Litwiller, E., Pinnau, I. *Macromolecules*, 2014, **47**, 5104–5114.
98. Wang, Z. G., Wang, D., Zhang, F., Jin, J., Liu, X., Wang, D., Jin, J., Ma, X., Swaidan, R., Belmabkhout, Y., Zhu, Y., Litwiller, E., Jouiad, M., Pinnau, I., Han, Y. *Macromolecules*, 2014, **45**, 3841–3849.
99. Zhuang, Y., Seong, J. G., Do, Y. S., Lee, W. H., Lee, M. J., Cui, Z., Lozano, A. E., Guiver, M. D., Lee, Y. M. *Chem. Commun.*, 2016, **52**, 3817–3820.
100. Zhao, Y., Wang, T., Zhang, L., Cui, Y., Han, B. *Polym. Chem.*, 2015, **6**, 748–753.
101. Fritsch, D., Bengtson, G., Carta, M., McKeown, N. B. *Macromol. Chem. Phys.*, 2011, **212**, 1137–1146.
102. Bezzu, C. G., Carta, M., Tonkins, A., Jansen, J. C., Bernardo, P., Bazzarelli, F., McKeown, N. B. *Adv. Mater.*, 2012, **24**, 5930–5933.
103. Du, N., Robertson, G. P., Pinnau, I., Guiver, M. D. *Macromolecules*, 2010, **43**, 8580–8587.
104. Ma, X., Pinnau, I. *Polym. Chem.*, 2016, **7**, 1244–1248.
105. Makhseed, S., Ibrahim, F., Samuel, J. *Polymer*, 2012, **53**, 2964–2972.
106. Short, R., Carta, M., Bezzu, C. G., Fritsch, D., Kariuki, B. M., McKeown, N. B. *Polym. Chem.*, 2011, **47**, 6822–6824.

107. Carta, M., Croad, M., Jansen, J. C., Bernardo, P., Clarizia, G., McKeown, N. B. *Polym. Chem.*, 2014, **5**, 5255–5261.
108. Rose, I., Bezzu, C. G., Carta, M., Comesaña-Gándara, B., Lasseuguette, E., Ferrari, M. C., Bernardo, P., Clarizia, G., Fuoco, A., Jansen, J. C., Hart, K. E., Liyana-Arachchi, T. P., Colina, C. M., McKeown, N. B. *Nat. Mater.*, 2017, **16**, 932–938.
109. Ghanem, B. S., McKeown, N. B., Budd, P. M., Fritsch, D. *Macromolecules*, 2008, **2**, 1640–1646.
110. Wang, Z. G., Liu, X., Wang, D., Jin, J. *Polym. Chem.*, 2014, **5**, 2793.
111. Schieber, J., Southard, J., Thaisen, K., Sorby, H. C. *Science*, 2007, **318**, 254–259.
112. Park, H. B., Han, S. H., Jung, C. H., Lee, Y. M., Hill, A. J. *J. Membr. Sci.*, 2010, **359**, 11–24.
113. Dong, G., Lee, Y. M. *J. Mater. Chem. A*, 2017, **5**, 13294–13319.
114. Kim, S., Lee, Y. M. *Nanotechnol. Sustain. Dev. First Ed.*, 2014, **14**, 265–276.
115. Ong, Y. K., Wang, H., Chung, T. S. *Chem. Eng. Sci.*, 2012, **79**, 41–53.
116. Ribeiro, C. P., Freeman, B. D., Kalika, D. S., Kalakkunnath, S. *J. Membr. Sci.*, 2012, **390**–**391**, 182–193.
117. Han, S. H., Misdan, N., Kim, S., Doherty, C. M., Hill, A. J., Lee, Y. M. *Macromolecules*, 2010, **43**, 7657–7667.
118. Du, N., Park, H. B., Dal-Cin, M. M., Guiver, M. D. *Energy Environ. Sci.*, 2012, **5**, 7306–7322.
119. Calle, M., Lozano, A. E., Lee, Y. M. *Eur. Polym. J.*, 2012, **48**, 1313–1322.
120. Guo, R., Sanders, D. F., Smith, Z. P., Freeman, B. D., Paul, D. R., McGrath, J. E. *J. Mater. Chem. A*, 2013, **1**, 6063.
121. Calle, M., Lee, Y. M. *Macromolecules*, 2011, **44**, 1156–1165.
122. Jung, C. H., Lee, J. E., Han, S. H., Park, H. B., Lee, Y. M. *J. Membr. Sci.*, 2010, **350**, 301–309.
123. Yeong, Y. F., Wang, H., Pallathadka P., K., Chung, T. S. *J. Membr. Sci.*, 2012, **397**–**398**, 51–65.
124. Li, S., Jo, H. J., Han, S. H., Park, C. H., Kim, S., Budd, P. M., Lee, Y. M. *J. Membr. Sci.*, 2013, **434**, 137–147.
125. Zhuang, Y., Seong, J. G., Lee, W. H., Do, Y. S., Lee, M. J., Wang, G., Guiver, M. D., Lee, Y. M. *Macromolecules*, 2015, **48**, 5286–5299.
126. Zachmann, H. G. Advances in Polymer Science, 1976, vol. 99.
127. Dhara, M. G., Banerjee, S. *Prog. Polym. Sci.*, 2010, **35**, 1022–1077.
128. Vinogradova, S. V., Vygodskii, Y. S., Korshak, V. V. *Polym. Sci. U.S.S.R.*, 1970, **12**, 2254–2262.
129. Xu, Y., Jin, S., Xu, H., Nagai, A., Jiang, D. *Chem. Soc. Rev.*, 2013, **42**, 8012.
130. Kim, S., Lee, Y. M. *Prog. Polym. Sci.*, 2015, **43**, 1–32.
131. Weber, J., Su, Q., Antonietti, M., Thomas, A. *Macromol. Rapid Commun.*, 2007, **28**, 1871–1876.
132. Ghanem, B. S., McKeown, N. B., Budd, P. M., Selbie, J. D., Fritsch, D. *Adv. Mater.*, 2008, **20**, 2766–2771.
133. Ma, X., Swaidan, R., Belmabkhout, Y., Zhu, Y., Litwiller, E., Jouiad, M., Pinnau, I., Han, Y. *Macromolecules*, 2012, **45**, 3841–3849.
134. Wang, Z. G., Wang, D., Zhang, F., Jin, J. *ACS Macro Lett.*, 2014, **45**, 3841–3849.
135. Lee, M., Bezzu, C. G., Carta, M., Bernardo, P., Clarizia, G., Jansen, J. C., McKeown, N. B. *Macromolecules*, 2016, **49**, 4147–4154.
136. Rogan, Y., Malpass-Evans, R., Carta, M., Lee, M., Jansen, J. C., Bernardo, P., Clarizia, G., Tocci, E., Friess, K., Lanč, M., McKeown, N. B. *J. Mater. Chem. A*, 2014, **2**, 4874–4877.
137. Ghanem, B. S., Swaidan, R., Litwiller, E., Pinnau, I. *Adv. Mater.*, 2014, **26**, 3688–3692.
138. Ma, X., Salinas, O., Litwiller, E., Pinnau, I. *Macromolecules*, 2013, **46**, 9618–9624.
139. Rogan, Y., Malpass-Evans, R., Carta, M., Lee, M., Jansen, J. C., Bernardo, P.,

Clarizia, G., Tocci, E., Friess, K., Lanč, M., McKeown, N. B. *J. Mater. Chem. A*, 2014, **2**, 4874–4877.
140. Rogan, Y., Starannikova, L., Ryzhikh, V., Yampolskii, Y., Bernardo, P., Bazzarelli, F., Jansen, J. C., McKeown, N. B. *Polym. Chem.*, 2013, **4**, 3813–3820.
141. Ma, X., Abdulhamid, M. A., Pinnau, I. *Macromolecules*, 2017, **50**, 5850–5857.
142. Abdulhamid, M. A., Ma, X., Miao, X., Pinnau, I. *Polymer*, 2017, **130**, 182–190.
143. Guiver, M. D., Robertson, G. P., Dai, Y., Bilodeau, F., Kang, Y. S., Lee, K. J., Jho, J. Y., Won, J. *J. Polym. Sci. Part A Polym. Chem.*, 2002, **40**, 4193–4204.
144. Yuan, J., Mecerreyes, D., Antonietti, M. *Prog. Polym. Sci.*, 2013, **38**, 1009–1036.
145. Mecerreyes, D. *Prog. Polym. Sci.*, 2011, **36**, 1629–1648.
146. Li, P., Zhao, Q., Anderson, J. L., Varanasi, S., Coleman, M. R. *J. Polym. Sci. Part A Polym. Chem.*, 2010, **48**, 4036–4046.
147. Li, P., Coleman, M. R. *Eur. Polym. J.*, 2013, **49**, 482–491.
148. Yuan, J., Antonietti, M. *Polymer*, 2011, **52**, 1469–1482.
149. Gao, R., Zhang, M., Wang, S. W., Moore, R. B., Colby, R. H., Long, T. E. *Macromol. Chem. Phys.*, 2013, **214**, 1027–1036.
150. Shaplov, A. S., Lozinskaya, E. I., Losada, R., Wandrey, C., Zdvizhkov, A. T., Korlyukov, A. A., Lyssenko, K. A., Malyshkina, I. A., Vygodskii, Y. S. *Polym. Adv. Technol.*, 2011, **22**, 448–457.
151. Cowan, M. G., Gin, D. L., Noble, R. D. *Acc. Chem. Res.*, 2016, **49**, 724–732.
152. Tome, L. C., Marrucho, I. M. *Chem. Soc. Rev.*, 2016, **45**, 2785–2824.
153. Du, N., Park, H. B., Dal-Cin, M. M., Guiver, M. D. *Energy Environ. Sci.*, 2012, **5**, 7306–7322.
154. Lu, J., Yan, F., Texter, J. *Prog. Polym. Sci.*, 2009, **34**, 431–448.
155. Shaplov, A. S., Morozova, S. M., Lozinskaya, E. I., Vlasov, P. S., Gouveia, A. S. L., Tomé, L. C., Marrucho, I. M., Vygodskii, Y. S. *Polym. Chem.*, 2016, **7**, 580–591.
156. Bara, J. E., Carlisle, T. K., Gabriel, C. J., Camper, D., Finotello, A., Gin, D. L., Noble, R. D. *Ind. Eng. Chem. Res.*, 2009, **48**, 2739–2751.
157. Carlisle, T. K., Wiesenauer, E. F., Nicodemus, G. D., Gin, D. L., Noble, R. D. *Ind. Eng. Chem. Res.*, 2013, **52**, 1023–1032.
158. Bara, J. E., Gabriel, C. J., Lessmann, S., Carlisle, T. K., Finotello, A., Gin, D. L., Noble, R. D. *Ind. Eng. Chem. Res.*, 2007, **46**, 5380–5386.
159. Carlisle, T. K., Bara, J. E., Lafrate, A. L., Gin, D. L., Noble, R. D. *J. Membr. Sci.*, 2010, **359**, 37–43.
160. Li, P., Pramoda, K. P., Chung, T.-S. *Ind. Eng. Chem. Res.*, 2011, **50**, 9344–9353.
161. Tome, L. C., Patinha, D. J. S., Freire, C. S. R., Rebelo, L. P. N., Marrucho, I. M. *RSC Adv.*, 2013, **3**, 12220–12229.
162. Tomé, L. C., Mecerreyes, D., Freire, C. S. R., Rebelo, L. P. N., Marrucho, I. M. *J. Membr. Sci.*, 2013, **428**, 260–266.
163. Bara, J. E., Camper, D. E., Gin, D. L., Noble, R. D. *Acc. Chem. Res.*, 2010, **43**, 152–159.
164. Hallett, J. P., Welton, T. *Chem. Rev.*, 2011, **111**, 3508–3576.
165. Privalova, E. I., Karjalainen, E., Nurmi, M., Mäki-Arvela, P., Eränen, K., Tenhu, H., Murzin, D. Y., Mikkola, J. P. *Chem. Sus. Chem*, 2013, **6**, 1500–1509.
166. MacFarlane, D. R., Tachikawa, N., Forsyth, M., Pringle, J. M., Howlett, P. C., Elliott, G. D., Davis, J. H., Watanabe, M., Simon, P., Angell, C. a *Energy Environ. Sci.*, 2014, **7**, 232–250.
167. Hao, L., Li, P., Yang, T., Chung, T. S. *J. Membr. Sci.*, 2013, **436**, 221–231.
168. Bara, J. E., Lessmann, S., Gabriel, C. J., Hatakeyama, E. S., Noble, R. D., Gin, D. L. *Ind. Eng. Chem. Res.*, 2007, **46**, 5397–5404.
169. Bara, J. E., Gin, D. L., Noble, R. D. *Ind. Eng. Chem. Res.*, 2008, **47**, 9919–9924.
170. Bara, J. E., Noble, R. D., Gin, D. L. *Ind. Eng. Chem. Res.*, 2009, **48**, 4607–4610.
171. Chi, W. S., Hong, S. U., Jung, B., Kang, S. W., Kang, Y. S., Kim, J. H. *J. Membr. Sci.*, 2013, **443**, 54–61.

172. Bhavsar, R. S. Kumbharkar S. C. Rewar, A. S. and Kharul, U. K. *Polym. Chem.*, 2014, **5**, 4083–4096.
173. Bhavsar, R. S., Kumbharkar, S. C., Kharul, U. K. *J. Membr. Sci.*, 2014, **470**, 494–503.

Chapter 2

Scope and Objectives

Polymeric materials to be used for applications in gas separations should exhibit high permeability and selectivity to decrease capital area and product purity. Most of the commercially available polymers such as Matrimid, polysulfone, PPO, etc., generally exhibit low permeability and high selectivity. Therefore, there is a need to design and synthesize new polymers with improved gas separation performance *via* judicious choice of monomers. This chapter outlines scope of the present work and the specific objectives.

2.1 SCOPE AND OBJECTIVES

Over the past few decades, gas separation membranes have attracted great attention for industrial gas separation applications such as hydrogen recovery, natural gas purification, nitrogen/oxygen enrichment and separation of carbon dioxide from flue gas.[1] Generally, commercially available polymeric membranes exhibit low permeability and high selectivity. Due to this, existing commercial polymeric membranes are not competitive with other technologies for large-scale gas separations.[2] For commercial applications, polymeric membrane materials should exhibit high gas permeability in order to minimize the required membrane area and high selectivity for product purity.[3] However, there exists a trade-off relationship between gas permeability and selectivity for polymeric membranes as illustrated by Robeson; wherein highly permeable polymer membranes display low selectivity and vice versa.[45] It has been demonstrated that high performance over Robeson upper bound could be achieved by increasing both permeability and selectivity.[6] Permeability can be increased by increasing inter-chain distance *via* disturbing polymer chain packing and selectivity can be increased by increasing backbone rigidity and polymer-gas interactions.[7] To surpass the Robeson upper bound by preparing highly permeable and selective polymers has become the theme of current research in this field. Therefore, there is a need to prepare new polymeric materials with improved permeability and selectivity.

Recently, polymers of intrinsic microporosity (PIMs) have gained considerable attention for various applications such as gas adsorption and separation due to their rigid and contorted structure.[8] For gas separation applications, PIMs exhibited high gas permeability and moderate selectivity of one gas over other following Robeson trade-off relationship between permeability and selectivity.[9] PIM-1 is the firstly synthesized polymer in this class and was prepared by polycondensation of 5,5′,6,6′-tetrahydroxy-3,3,3′,3′-tetramethyl-1,1′-spirobisindane (TTSBI) with 2,3,5,6-tetrafluoroterephthalonitrile (TFTPN) *via* double aromatic nucleophilic substitution reaction. PIM-1 exhibited more than 100-fold higher gas permeability as compared to commercially available polymers such as Matrimid, polysulfone, etc.[10] Based on the attractive properties of PIM-1, many other ladder PIMs, modified PIM-1, and polyimides of intrinsic microporosity (PIM-PI) have been reported with excellent gas separation properties.[9,11] However, there is still a quest for novel designed building blocks to further improve the understanding of structure-property-performance relationships in PIMs.

Poly(ionic liquids) or polymeric ionic liquids (PILs) are a new class of polymer electrolytes and have attracted significant attention for gas separation applications due to their combination of unique properties of ionic liquids (ILs) and polymer architecture.[12,13] PILs showed appreciable gas permeability and selectivity especially for CO_2 due to the interaction

of CO_2 with ionic groups present in the polymers.[14] However, a limited number of film-forming PILs have been reported till date.[15] Therefore, it is of great interest to synthesize new film-forming PILs and establish the structure-property relationship.

Thus, overall objective of the present work was to tune the properties of polymeric membranes by structural variations and to develop understanding of gas permeation characteristics in PIMs and PILs. **Figure 2.1** suitably illustrates the theme of the thesis.

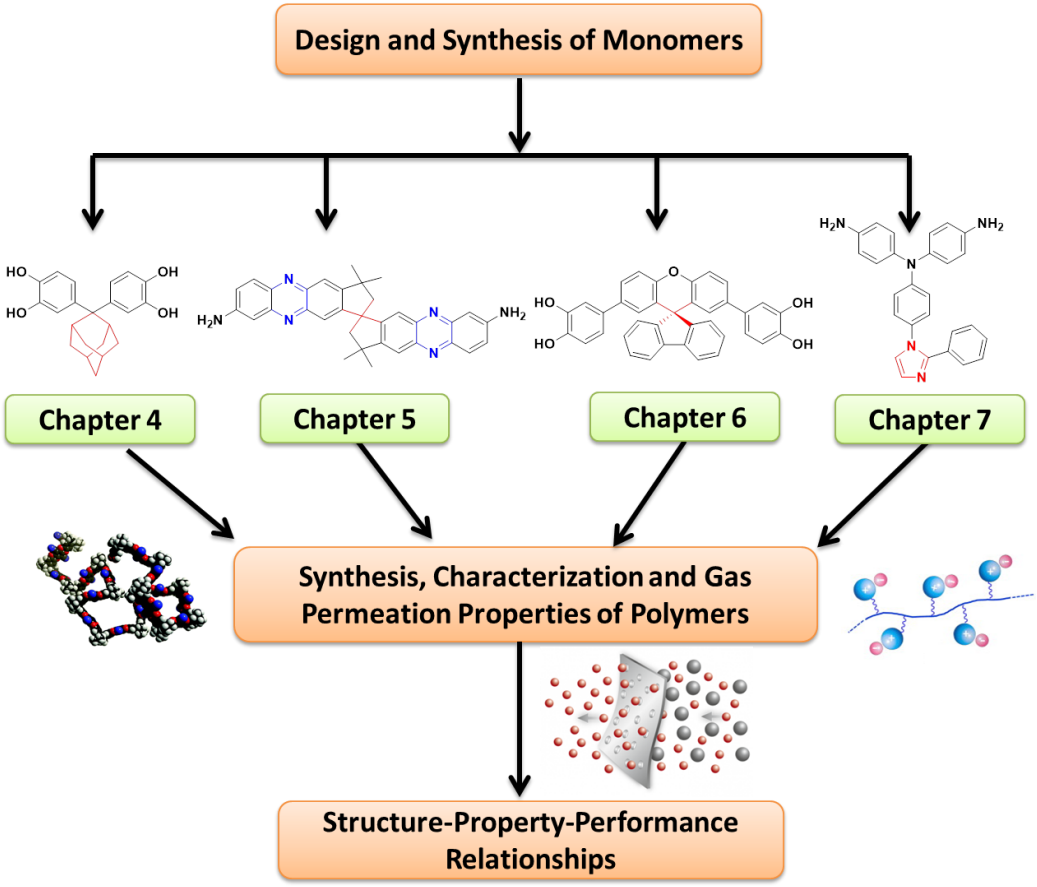

Figure 2.1: Theme of the thesis

a) Incorporation of adamantane unit into PIMs and investigations of the effects of adamantane units on physical and gas permeation properties

The presence of bulky group in the polymer backbone or as pendant is known to improve the gas separation properties by disturbing polymer chain packing *via* creating the free volume.[16] In this context, adamantane-containing polymers have gained significant attention due to their bulky and diamond-like structure which improves gas separation performance by increasing free volume *via* disturbance in polymer chain packing.[17] Taking into consideration the attractive property of adamantane unit, the objectives of present work were as follows:

1. Synthesis of adamantane-containing bis(catechol) namely, 4,4'-((1r,3r)-adamantane -2,2-diyl)bis(benzene-1,2diol) (THADM).

2. To synthesize homopolymer and copolymers of intrinsic microporosity (ADM-PIMs) containing adamantane units by polycondensation of THADM and various compositions of THADM and 5,5′,6,6′-tetrahydroxy-3,3,3′,3′-tetramethyl-1,1′-spirobisindane (TTSBI) with 2,3,5,6-tetrafluoroterephthalonitrile (TFTPN).
3. To determine the physical properties of PIMs such as crystallinity, microporosity and thermal properties.
4. To evaluate the gas permeation properties of adamantane-containing PIMs for He, H_2, N_2, O_2, CH_4 and CO_2 by variable-volume method.
5. To investigate the effects of adamantane units on physical and gas permeation properties.

b) Synthesis of polyimides of intrinsic microporosity (PIM-PIs) containing spirobisindane and phenazine units and investigation of influence of spirobisindane and phenazine units on their physical and gas permeation properties

It is reported that gas separation performance of polymers is improved by increasing both permeability and selectivity.[18] Recently spirobisindane-containing polymers have been extensively studied for gas separations due to improved gas permeability characteristics as they contains contorted structure. Phenazine is a heterocyclic ring and helps to improve thermal stability and gas separation performance. Inspired by the excellent properties of spirobisindane and phenazine units, the following objectives were chosen:

1. To synthesize diamine containing spirobisindane and phenazine unit namely, 3,3,3',3'-tetramethyl-2,2',3,3'-tetrahydro-1,1'-spirobi[cyclopenta [b]phenazine]-7,7'-diamine (TTSBIDA)
2. To synthesize a new series of PIM-PIs containing spirobisindane and phenazine units by polycondensation of TTSBIDA with aromatic dianhydrides *via* one-step high temperature method.
3. Determination of physical properties such as crystallinity, microporosity and thermal properties of PIM-PIs
5. Evaluation of gas permeation properties of PIM-PIs containing spirobisindane and phenazine units for He, H_2, N_2, O_2, CH_4 and CO_2 by variable-volume method.
6. To investigate the effects of spirobisindane and phenazine units on physical and gas permeation properties.

c) Incorporation of spiro[fluorene-9,9'-xanthene] (SFX) unit as new building block to induce microporosity into PIMs and investigations of the effects of SFX units on physical and gas permeation studies

Recently, spirocylic units containing polymers have gained considerable attention for gas separation applications due to their improved gas permeation characteristics.[19] Despite dozens of monomers reported till date to synthesize PIMs, only a few PIMs containing spirocyclic units such as spirobifluorene, spirobifluorene and spirobischromane are available in the literature.[20] This clearly suggests that there is a plenty of scope for preparation of PIMs containing spirocyclic unit as new building block to induce microporosity and investigate their gas separation to improve structure-property relationship. In continuation of investigations on synthesis of PIMs with new spirocyclic units, the specific objectives selected were as follows:

1. Synthesis of bis(catechol) containing SFX unit, namely, 4,4'-(spiro[fluorene-9,9'-xanthene]-2',7'-diyl)bis(benzene-1,2-diol) (THSFX).
2. To synthesize PIMs-containing SFX units by polycondensation of THSFX and varying compositions of THSFX and TTSBI with TFTPN
3. To determine the crystallinity, thermal properties and microporosity of PIMs
4. To evaluate gas permeation properties of SFX-based PIMs for He, H_2, N_2, O_2, CH_4 and CO_2 by variable-volume method.
5. To investigate the effects of SFX units on physical and gas permeation properties.

d) Synthesis of new film-forming polyimide-based PILs and investigation of the effects of anion groups on their physical and gas permeation studies

Ionic groups in the polymer backbone or as pendant are known to improve the CO_2-based separation by Lewis acid-base interaction.[21] In this context, PILs have gained significant attention as they contains ionic groups.[21] However, only a limited number of film-forming PILs have been reported till date.[12] Taking into consideration the attractive properties of PILs for CO_2 separation, the following specific objectives were chosen.

1. Synthesis of diamine containing triphenylamine and 2-phenylimidazole unit, namely, N^1-(4-aminophenyl)-N^1-(4-(2-phenyl-1H-imidazol-1-yl) phenyl)benzene-1,4-diamine (ImTPADA) and its polycondensation with aromatic dianhydrides to obtain the corresponding polyimides.
2. To synthesize PILs by *N*-quaternization of PI-6FDA with methyl iodide and anion exchange reaction with $LiTf_2N$
3. To evaluate the gas permeation properties of PIs and PI-PILs for He, H_2, N_2, O_2, CH_4 and CO_2 by variable-volume method.
4. To investigate the effects of hinge groups of dianhydrides and anion variation on physical and gas permeation properties.

2.2 REFERENCES

1. Sanders, D. F., Smith, Z. P., Guo, R., Robeson, L. M., McGrath, J. E., Paul, D. R., Freeman, B. D. *Polymer*, 2013, 54, 4729–4761.
2. Baker, R. W., Low, B. T. *Macromolecules*, 2014, **47**, 6999–7013.
3. Du, N., Park, H. B., Dal-Cin, M. M., Guiver, M. D. *Energy Environ. Sci.*, 2012, **5**, 7306–7322.
4. Robeson, L. M. *J. Membr. Sci.*, 1991, **62**, 165–185.
5. Robeson, L. M. *J. Membr. Sci.*, 2008, **320**, 390–400.
6. Koros, W. J., Mahajan, R. *J. Membr. Sci.*, 2001, **181**, 141.
7. Guiver, M. D., Lee, Y. M. *Science*, 2013, **339**, 284–285.
8. Dong, G., Lee, Y. M. *J. Mater. Chem. A*, 2017, **5**, 13294–13319.
9. Ma, C., Urban, J. J. *Proc. Nat. Res. Soc.*, 2018, **2**, 2002.
10. Budd, P. M., McKeown, N. B., Ghanem, B. S., Msayib, K. J., Fritsch, D., Starannikova, L., Belov, N., Sanfirova, O., Yampolskii, Y., Shantarovich, V. *J. Membr. Sci.*, 2008, **325**, 851–860.
11. Galizia, M., Chi, W. S., Smith, Z. P., Merkel, T. C., Baker, R. W., Freeman, B. D. *Macromolecules*, 2017, **50**, 7809–7843.
12. Yuan, J., Mecerreyes, D., Antonietti, M. *Prog. Polym. Sci.*, 2013, **38**, 1009–1036.
13. Jue, M. L., Lively, R. P. *React. Funct. Polym.*, 2015, **86**, 40–43.
14. Liu, J., Hou, X., Park, H. B., Lin, H. *Chem. Eur. J.*, 2016, **22**, 15980–15990.
15. Cowan, M. G., Gin, D. L., Noble, R. D. *Acc. Chem. Res.*, 2016, **49**, 724–732.
16. Xu, Z. K., Dannenberg, C., Springer, J., Banerjee, S., Maier, G. *Chem. Mater.*, 2002, **14**, 3271–3276.
17. Maya, E. M., García-Yoldi, I., Lozano, a. E., de la Campa, J. G., de Abajo, J. *Macromolecules*, 2011, **44**, 2780–2790.
18. Jue, M. L., Lively, R. P. *React. Funct. Polym.*, 2015, **86**, 40–43.
19. Kim, S., Lee, Y. M. *Prog. Polym. Sci.*, 2015, **43**, 1–32.
20. McKeown, N. B. *ISRN Mater. Sci.*, 2012, **2012**, 1–16.
21. Tome, L. C., Marrucho, I. M. *Chem. Soc. Rev.*, 2016, **45**, 2785–2824.

Chapter 3

Materials, Characterization and Techniques

3.1 MATERIALS

3.1.1 Chemicals

5,5′,6,6′-Tetrahydroxy-3,3,3′,3′-tetramethyl-1,1′-spirobisindane (TTSBI) (Aldrich), 4-nitro-1,2-phenylenediamine (Aldrich), 4-bromophenol (Aldrich), 9-fluorenone (Aldrich), 3,4-dimethoxyphenylboronic acid (Aldrich), 2,3,5,6-tetrafluoroterephthalonitrile (TFTPN, Aldrich), 2-phenylimidazole (Alfa Aesar), 1-fluoro 4-nitrobenzene (Aldrich), iodomethane (Aldrich) and bis(trifluoromethane) sulfonimide lithium salt **(**$LiTf_2N$, Aldrich) were purchased and used as received. 4,4′-(Hexafluoroisopropylidene) diphthalic anhydride (6-FDA), 4,4'-(4,4'-isopropylidene diphenoxy)bis(phthalicanhydride) (BPADA), 4,4′-oxydiphthalic anhydride (ODPA), 3,3',4,4'-benzophenonetetracarboxylic dianhydride (BTDA) and 1,2,4,5-benzenetetracarboxylic dianhydride (PMDA) were purchased from Aldrich and were sublimed prior to use. Boron tribromide (BBr_3) in dichloromethane (Aldrich), tetrakis(triphenylphosphine)palladium(0) **(**$Pd(PPh_3)_4$), 10 wt% Pd/C (Aldrich), sodium hydride (Alfa Aesar), potassium carbonate (Aldrich), hydrazine hydrate (Thomas Baker), isoquinoline (Aldrich), glacial acetic acid (Thomas Baker), methanesulfonic acid (Aldrich) and sulphuric acid (Thomas Baker) were purchased and were used as received.

3.1.2 Solvents

N,*N*-Dimethylacetamide (DMAc), *N*,*N*-dimethylformamide (DMF), *N*-methyl-2-pyrrolidone (NMP), dimethyl sulfoxide (DMSO), tetrahydrofuran (THF) and *m*-cresol were purchased from Aldrich and were distilled prior to use. Toluene, chloroform, dichloromethane, methanol, ethyl acetate, pet ether, and ethanol were procured from Alfa Aesar and were used as received.

3.2 CHARACTERIZATION AND TECHNIQUES

Different techniques were used for characterization of monomers and polymers and are listed below.

3.2.1 IR Spectroscopy

IR spectroscopy was used to analyse functional groups present in the monomers and polymers. IR spectra were recorded on Perkin Elmer spectrum GX spectrophotometer in the range 4000-400 cm^{-1} using either chloroform solvent or KBR pellets.

3.2.2 NMR Spectroscopy

^{1}H and ^{13}C NMR spectra of monomers and polymers were recorded using a Bruker-AV spectrometer at operating frequency of 200 MHz or 400 MHz in $CDCl_3$ or DMSO-d_6 with tetramethylsilane as an internal standard.

3.2.3 HR-MS Analysis

HR-MS analysis of monomers was carried out on Thermo Scientific Q-exacative with Accela 1250 Pump.

3.2.4 Solubility Tests

The solubility of polymers was tested at 3 wt % concentration in various organic solvents at room temperature.

3.2.5 Inherent Viscosity

Inherent viscosity of polymers was measured at 0.5 g/dL concentration using Ubbelohde suspended level viscometer at 35 ± 0.1 °C. Inherent viscosity was calculated by the following equation

$$\eta_{inh} = \ln \eta_r / C$$

$$\eta_r = t/t_o$$

Where, t is flow time of polymer solution and $t_o$is the flow time of pure solvent.

3.2.6 Gel Permeation Chromatography (GPC)

Molecular weights and dispersity values of polymers were determined from GPC measurements in chloroform or DMF with RI-150 detector using polystyrene as a standard. Number average molecular weight (M_n), weight average molecular weight (M_w) and dispersity (M_w/M_n) was determined using GPC measurements.

3.2.7 X-Ray Diffraction (XRD)

X-Ray diffractograms of polymers were obtained on Rigaku Dmax 2500 with a scanning rate of 2° / min. The *d*-spacing of polymers was calculated from peak maxima of XRD using Bragg's equation

$$n\lambda = 2d\sin\theta$$

Where, *d* is the *d*-spacing (inter-chain distance), n is a positive integer number, λ is the wavelength and θ is the scattering angle.

3.2.8 Thermogravemetric Analysis (TGA)

TGA of polymers was performed on Perkin Elmer TGA-7system at a heating rate of 10 °C / min under N_2 atmosphere from 30 to 900 °C.

3.2.9 Differential Scanning Calorimetry (DSC)

Differential scanning calorimetry (DSC) was performed with DSC Q10 at a heating rate of 10 °C/ min in N_2 atmosphere. DSC analysis was used to measure glass transition temperature (T_g) of polymers.

3.2.10 Mechanical Properties

Mechanical properties of polymers such as tensile strength, elongation at break and Young's modulus were measured on Rheometrics Scientifics (Model Mark IV) (UK) instrument at room temperature with strain rate of 1.5 mm/min. Six samples were measured for each polymer and data was averaged.

3.2.11 Density and Fractional Free Volume (FFV)

The density (ρ) of membranes was determined using specific gravity bottle in decalin at 35±0.1°C. The density measurements were carried out on three specimens and average value was taken.

The fractional free volume (FFV) of polymers was calculated from group contribution method (Bondi's method)[1,2] using the following equation

$$FFV = V_{sp} - V_w/V_{sp}$$

where, V_{sp} is the specific volume and V_w is the van der Waals volume of the polymer.

3.2.12 Nitrogen Adsorption Measurements

The BET surface area and N_2 adsorption/desorption of polymers were determined using Micrometrics ASAP 2.20 at 77 K. Pore size, pore volume and BET surface area was calculated. Before analysis, powder samples were degassed at 120 °C for 12 h.

3.2.13 Density Functional Theory (DFT)

3.2.13.1Energy Optimization

Density functional theory (DFT) calculations were carried out using Turbomole 6.0 suite of programs.[3] Geometry optimizations were performed using the dispersion corrected Perdew, Burke, and Erzenhoffunctionals (PBE).[4] The electronic configuration of the atoms was described by a triple-ζ basis set augmented by a polarization function (Turbomole basis set

TZVP).[5] The resolution of identity (ri),[6] along with the multipole accelerated resolution of identity (marij)[7] approximations were employed for an efficient treatment of electronic Coulomb term in the DFT calculations.

3.2.13.2DFT calculations

The dihedral were constrained and optimized at ten degree of increment starting from the DFT optimized structure. The structural rigidity parameter was calculated by fitting a harmonic model in the best approximation of $V_D=(\phi_{ijkl}-\phi_0)^2$ with k_{ijkl}as a spring constant. The spring constant of harmonic model is considered as a rigidity parameter.

3.2.14 Gas Permeation Study

Gas permeability of membranes was measured using the variable-volume method.[8] The permeability of gases was measured in the following order: He, H_2, N_2, O_2, CH_4, and CO_2. The schematic and photograph of permeation equipment is given in **Figure 3.1** and **3.2**, respectively. One end of the feed side of cell was connected through valve V1 to the feed gas cylinder and a pressure gauge (0-550 psi range) while the valve V2 (vent) was used to control the feed pressure. On the permeate side of the cell, a calibrated borosilicate glass capillary containing a small mercury slug (~ 4-6 mm in length) was connected. The membrane cell assembly was kept in a thermostat and the displacement of the mercury slug was measured with time. Three membrane samples prepared under identical conditions were analysed for each polymer and permeability values were averaged.

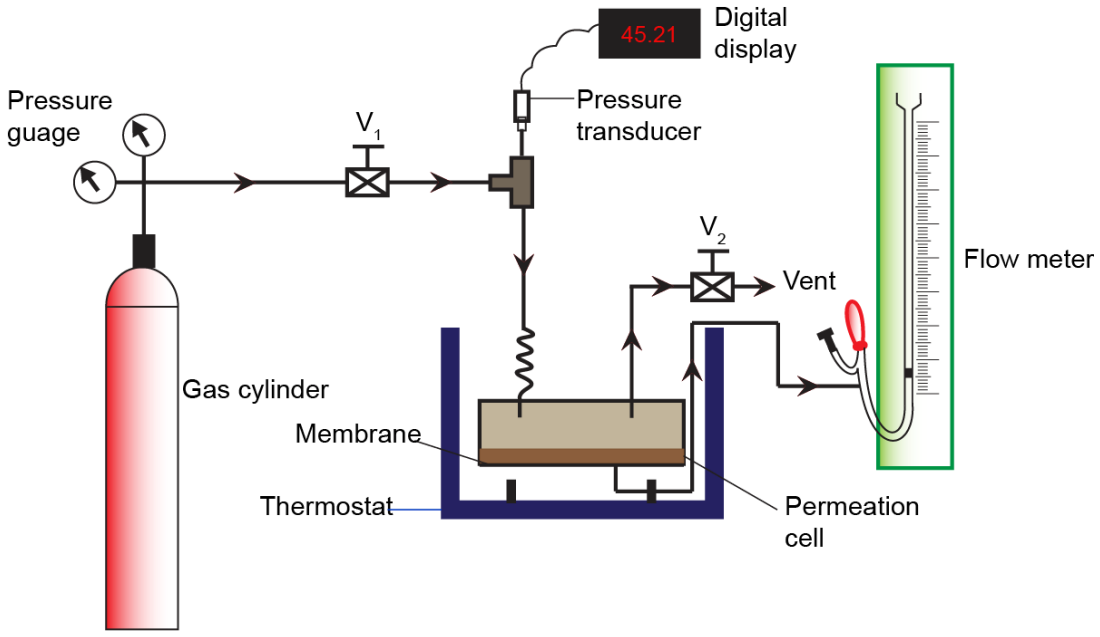

Figure 3.1 Schematic of gas permeation equipment

Figure 3.2 Photograph of gas permeation equipment

The permeability was calculated by using the following equation:

$$P = \frac{N \cdot l}{(p_1 - p_2)}$$

where, P is the permeability expressed in barrer (1 barrer = 10^{-10} cm^3 (STP) cm/(cm^2 s cm Hg)), N is the steady-state penetrate flux (cm^3 cm^{-2} s), l is the membrane thickness (cm), and p_1 and p_2 are the feed and permeate side pressures (cm Hg), respectively. Variations in the permeability from average data collected for 3 samples prepared under identical conditions was 1-13% depending upon the analysed gas.

3.3 REFERENCES

1. Bondi, A. *J. Phys. Chem.*, 1965, **68**, 441–451.
2. D.W. Van Krevelen, K. T. Nijenhuis, Properties of polymers; Elsevier, 2009.
3. Ahlrichs, R., Bar, M., Marco, H., Horn, H., Kolmel, C. *Chem. Phys. Lett.*, 1989, **162**, 165–169.
4. Perdew, J. P., Burke, K., Ernzerhof, M. *Phys. Rev. Lett.*, 1996, **77**, 3865–3868.
5. Schäfer, A., Huber, C., Ahlrichs, R., Schafer, A., Huber, C., Ahlrichs, R. *J. Chem. Phys.*, 1994, **8**, 5829–5835.
6. Eichkorn, K., Htiser, M., Ahlrichs, R., Eichkorn, K., Treutler, O., Marco, H., Ahlrichs, R. *Chem. Phys. Lett.*, 1995, **240**, 283–290.
7. Sierka, M., Hogekamp, A., Ahlrichs, R. *J. Chem. Phys.*, 2003, **20**, 9136–9148.
8. Kumbharkar, S. C., Karadkar, P. B., Kharul, U. K. *J. Membr. Sci.*, 2006, **286**, 161–169.

Chapter 4

Synthesis, Characterization and Gas Permeation Properties of Adamantane-Containing Polymers of Intrinsic Microporosity

A new bis(catechol) monomer, namely, 4,4'-((1r,3r)-adamantane-2,2-diyl)bis(benzene-1,2-diol) (THADM) was designed and synthesized. THADM was synthesized by condensation of 2-adamantanone with veratrole followed by demethylation of the formed (1r,3r)-2,2-bis(3,4 dimethoxyphenyl)adamantane. Polycondensation reactions of THADM and various compositions of THADM and 5,5,6',6'-tetrahydroxy-3,3,3',3'-tetramethylspirobisindane were performed with 2,3,5,6-tetrafluoroterephthalonitrile to obtain the homopolymer and copolymers of intrinsic microporosity. These polymers showed good solubility in organic solvents and could be cast into self-standing films from their solutions in chloroform. PIMs exhibited reasonably high molecular weights (38,100–61,700 g/mol), intrinsic microporosity with high BET surface area (703–741 m^2/g) and high thermal stability ($T_{10\%}$ = 513–518 °C). Gas permeability analysis demonstrated that PIMs exhibited high permeability and appreciable selectivity. For instance, THADM-based polymer of intrinsic microporosity (PIM) showed $P(CO_2)$=1080 and $\alpha(CO_2/N_2)$=26.7. The gas permeability data of PIMs were located close to 2008 Robeson upper bound for gas pairs such as CO_2/CH_4, CO_2/N_2, H_2/N_2, and O_2/N_2.

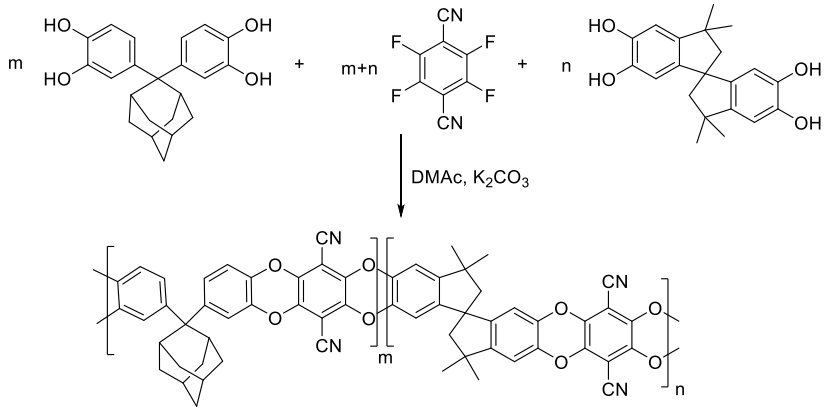

m/n = 100/0 (ADM-PIM); 75/25 (ADM-PIM-75); 50/50 (ADM-PIM-50); 25/75 (ADM-PIM-25); 0/100 (PIM-1)

J. Polym. Sci. Part A: Polym. Chem., **2018**, 56, 16-24

4.1 INTRODUCTION

Polymers of Intrinsic Microporosity (PIMs) are defined as polymers that contain interconnected pores of size less than 2 nm in diameter.[1–3] PIMs are of great interest for various gas separation applications such as H_2 recovery from ammonia production or hydrocarbon processing, natural gas purification, N_2 production from air, and CO_2 separation and capture.[2,4–6] Polymeric materials to be used for gas separation should possess high intrinsic permeability to decrease capital area and high selectivity to increase product purity.[7–11] However, membranes based on conventional polymers generally suffer from trade-off relationship between permeability and selectivity as described by the Robeson and theoretically verified by Freeman.[12,13] It has been demonstrated that high performance over Robeson upper bound could be achieved by increasing polymer backbone rigidity and increasing inter-chain spacing.[6,14–17]

Over the last few years, adamantane-containing polymers have attracted significant attention for gas separation and storage applications due to improved permeability characteristics.[18–20] Owing to the rigid, bulky and diamond-like structure of adamantane which consists of four cyclohexane rings fused in chair conformation, disturbance in polymer chain packing is observed which consequently leads to increase in free volume. Maya et. al., described the gas permeability of polyimide-containing pendant adamantane units and found that the gas permeability increased with incorporation of adamantane units into polyimides with slight decrease in selectivity.[21] Bera *et. al.*, reported polyamides containing pendant adamantane units and observed that performance of some of the polyamides surpassed 2008 Robeson upper bound for O_2/N_2 gas pair.[22] Recently, Carta et. al., synthesized Tröger's base-PIMs containing adamantane units and evaluated their gas separation performance.[23] The incorporation of adamantane and Tröger's base units in polymers imparted intrinsic microporosity and improved gas separation performance owing to the rigid and contorted structure.

In this work, a new adamantane-containing bis(catechol), namely, 4,4'-((1r,3r)-adamantane -2,2-diyl)bis(benzene-1,2diol) (THADM) was designed and synthesized. THADM was polycondensed with TFTPN *via* double aromatic nucleophilic substitution to form corresponding homopolymer. In addition, copolymers of intrinsic microporosity were synthesized by polycondensation of varying compositions of THADM and 3,3,3',3'-tetramethylspirobisindane-5,5',6,6'-tetraol (TTSBI) with 2,3,5,6-tetrafluoro terephthalonitrile (TFTPN). PIMs were characterized by IR, ^{1}H and ^{13}C NMR spectroscopy, X-ray diffraction analysis, TGA and N_2 adsorption measurements. Gas permeability characteristics of PIMs were evaluated for He, H_2,

N_2, O_2, CH_4 and CO_2 by variable-volume method. The effect of incorporation of adamantane units on physical properties such as *d*-spacing, BET surface area and gas permeability characteristics of PIMs were investigated.

4.2 EXPERIMENTAL

Details about materials used in the study and experimental techniques such as solubility study, IR, ^{1}H and ^{13}C NMR spectroscopy, TGA, DSC, XRD, DFT and gas permeability analysis are given in **Chapter 3**.

4.2.1 Preparations

4.2.1.1 Synthesis of (1r,3r)-2,2-bis(3,4-dimethoxyphenyl)adamantane (TMADM)

A 500 mL two-necked round-bottom flask equipped with a magnetic stirring bar and a nitrogen inlet was charged with glacial acetic acid (40 mL), sulphuric acid (20 mL) and 3-mercaptopropionic acid (0.5 mL). To the reaction mixture, 2-adamantanone (15.02 g, 100 mmol) and veratrole (32 mL, 250 mmol) were added and the temperature was maintained at 0 °C. The reaction mixture was stirred at same temperature for 2 h and then at room temperature for 6 days. Water (100 mL) was added into the reaction mixture, and extracted with ethyl acetate (200 mL). The ethyl acetate solution was washed with brine (3 x 50 mL), dried over sodium sulphate, filtered and the solvent was evaporated on a rotary evaporator. The crude product was purified by column chromatography on silica gel using pet ether: ethyl acetate (80:20, v/v) as eluent to obtain TMADM as a colourless solid.

Yield: 12 g, 29 %

Melting point: 152 °C

IR (KBr, cm^{-1}): 1215 (C-O-C).

^{1}HNMR (200 MHz, $CDCl_3$, δ/ppm): 6.95 (d, 4H, Ar-H), 6.75 (d, 2H, Ar-H), 3.85 (s, 6H, 2-OCH_3), 3.80 (s, 6H, 2-OCH_3), 3.15 (s, 2H, 2-CH), 2.07 (d, 4H, 2-CH_2). 1.82-1.73 (m, 8H, 4-CH and 2–CH_2)

^{13}C-NMR (50 MHz, $CDCl_3$, δ/ppm): 148.7, 146.1, 141.3, 117.9, 111.1, 109.5, 55.9, 55.6, 49.7, 37.9, 33.3, 32.3, 27.4.

HRMS (ESI): calcd. for $C_{26}H_{32}O_4$ ($[M+H]^+$): 408.2295; found: 408.2295.

4.2.1.2 Synthesis of 4,4'-((1r,3r)-adamantane-2,2-diyl)bis(benzene-1,2diol) (THADM)

A 250 mL two necked round-bottom flask equipped with a magnetic stirring bar, a nitrogen inlet and an addition funnel was charged with TMADM (10 g, 24.4 mmol) and dry dichloromethane

(30 mL). After cooling to 0 °C, BBr_3 (9.3 mL, 9.79 mmol) was added dropwise to the reaction mixture over a period of 30 minutes. The reaction mixture was stirred at the same temperature for 1 h and then at room temperature for 6 h. The reaction mixture was quenched by addition of ice-cold water (20 mL) and extracted with ethyl acetate (200 mL). The ethyl acetate solution was washed with brine (3 x 30 mL), dried over sodium sulphate, filtered and the solvent was then evaporated on a rotary evaporator. The crude product was purified by column chromatography on silica gel using pet ether: ethyl acetate (50:50, v/v) as eluent to obtain THADM as a colourless solid

Yield: 6 g, 69 %

Melting point: 158 °C

IR (KBr, cm^{-1}): 3416 (-OH).

^{1}H-NMR (200 MHz, DMSO-d_6, δ/ppm): 8.55 (s, 4H, 4-OH), 6.74 (s, 2H, Ar-H), 6.62 (d, 2H, Ar-H), 6.57 (d, 2H, Ar-H), 3.0 (s, 2H, 2-CH), 1.94 (d, 4H, 2-CH_2), 1.72-1.62 (m, 8H, 4-CH and 2–CH_2)

^{13}C-NMR (50 MHz, DMSO-d_6, δ/ppm): 144.8, 141.9, 140.1, 116.2, 115.3, 113.2, 48.6, 37.6, 33.0, 31.3, 26.9.

HRMS (ESI): calcd. for $C_{22}H_{23}O_4$ ($[M+H]^+$): 351.1590; found:351.1591

4.2.1.3 Synthesis of PIMs

A 100 mL three-necked round-bottom flask equipped with a magnetic stirring bar and a nitrogen inlet was charged with THADM (1.5 g, 4.26 mmol), TFTPN (0.85 g, 4.26 mmol) and DMAc (15 mL). The reaction mixture was heated to 120 °C for 5 minutes and then K_2CO_3 (3.5 g, 25.54 mmol) was added at once (the colour changed from orange-red to orange-yellow). The reaction mixture was heated at 150 °C for 5 minutes. Toluene (4 mL) was added and the reaction mixture was stirred at the same temperature until the reaction mixture became viscous. The reaction mixture was precipitated into methanol and yellow powder was collected by filtration. The polymer was purified by dissolving in chloroform and re-precipitating into methanol (500 mL). The solid polymer was separated and dried in vacuum oven at 120 °C for 2 days to obtain ADM-PIM as a yellowish powder.

IR ($CHCl_3$, cm^{-1}): 2237 (-CN stretching), 1264 (Ar-O-Ar).

^{1}H NMR (400 MHz, $CDCl_3$, δ/ppm): 7.01 (d, 4H, Ar-H), 6.88 (s, 2H, Ar-H), 3.02 (s, 2H, 2-CH), 1.94-1.57 (m, 12H, 4-CH and 4-CH_2).

Copolymers were synthesized by polycondensation of varying compositions of THADM and TTSBI with TFTPN using the similar procedure. PIMs were designated as ADM-PIM-75, ADM-PIM-50 and ADM-PIM-25 wherein the feed molar composition of THADM and TTSBI was 75:25, 50:50 and 25:75 mol%, respectively.

4.2.2 Preparation of Dense Membranes

The films of PIMs were prepared by casting of chloroform solution of polymers (~5 wt %,) onto a clean and levelled petri-dish. The solvent was slowly evaporated at room temperature. The obtained membranes were removed from petri-dish and were then dried at 100 °C for 3 days. The membrane thickness was measured by digital micrometer (80 ± 10 μm).

4.3 RESULTS AND DISCUSSION

4.3.1 Synthesis and Characterization of 4,4'-((1r,3r)-Adamantane-2,2-diyl)bis(benzene-1,2diol)

The two-step route for the synthesis of adamantane-containing bis(catechol) namely, 4,4'-((1r,3r)-adamantane-2,2-diyl)bis(benzene-1,2diol) (THADM) is depicted in **Scheme 4.1**. In the first step, condensation of commercially available 2-adamantanone with veratrole was carried out in the presence of acetic acid, sulfuric acid and 3-mercaptopropionic acid to obtain (1r,3r)-2,2-bis(3,4 dimethoxyphenyl) adamantane (TMADM). In the presence of acid, 2-adamantanone gets protonated. The reaction proceeds *via* attack of two molecules of veratrole on carbonyl carbon of protonated 2-adamantanone followed by elimination of water. The product was purified by column chromatography using mixture of pet ether and ethyl acetate as an eluent. The chemical structure of TMADM was confirmed by IR (**Figure SI 4.1**), ^{1}H (**Figure SI 4.2**) and ^{13}C NMR spectroscopy (**Figure SI 4.3**) and HRMS.

In the second step, TMADM was converted to THAMD *via* demethylation. The demethylation of TMADM was carried out using boron tribromide in dichloromethane at 0 °C to obtain THADM. BBr_3 was used as demethylation reagent, as it has been widely used to cleave ethers because the reaction proceeds under mild conditions.[24,25] It promotes C-O bond cleavage in ether by coordinating to ethereal oxygen to form alkyl bromide and the aryloxyborane. Aryloxyborane is hydrolysed to bis(catechol) during workup. The product was purified by column chromatography using mixture of pet ether and ethyl acetate as an eluent.

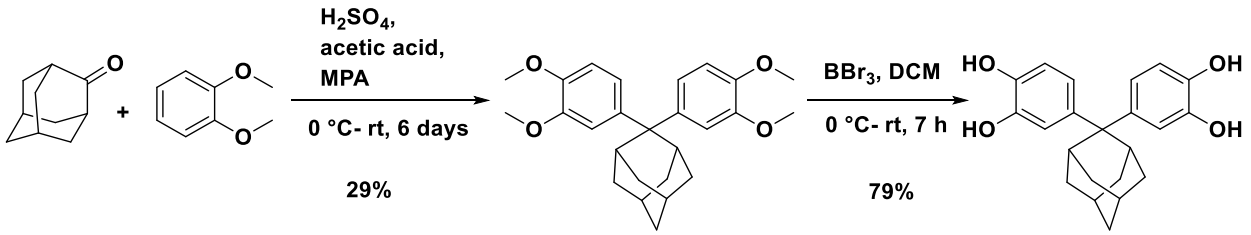

Scheme 4.1: Synthesis of 4,4'-((1r,3r)-adamantane-2,2-diyl)bis(benzene-1,2diol) (THADM).

The chemical structure of THADM was confirmed by IR, ^{1}H and ^{13}C NMR spectroscopy and HR-MS analysis.

IR spectrum of THADM is shown in **Figure 4.1.** The broad absorption band at 3416 cm^{-1} with a shoulder is due to stretching vibration of the phenolic group.

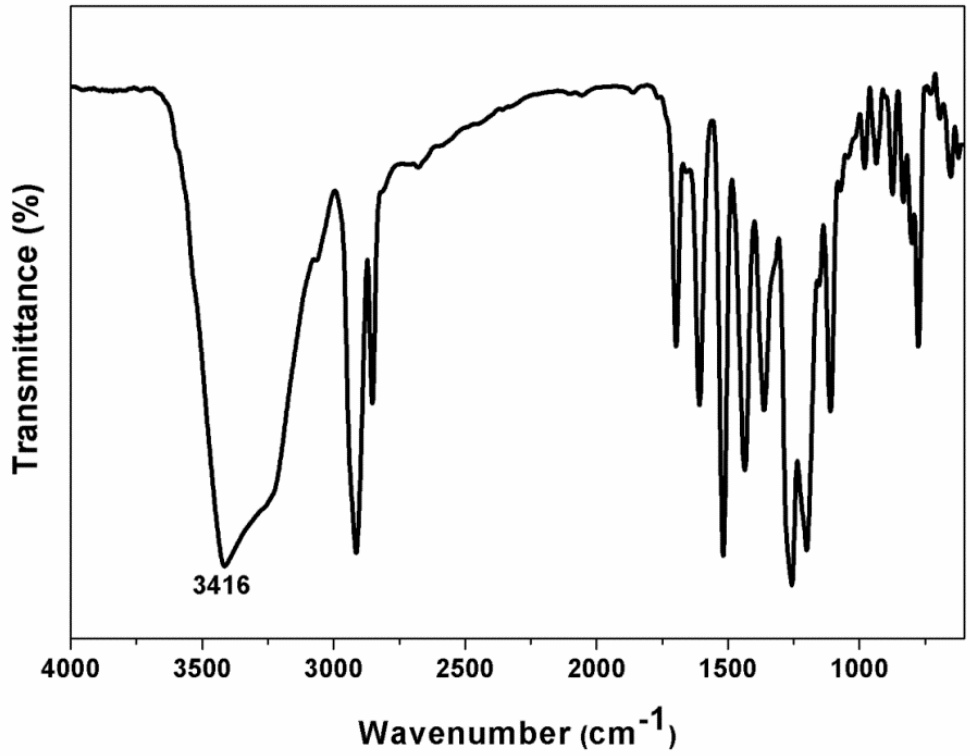

Figure 4.1: IR spectrum of 4,4-((1r,3r)-adamantane-2,2-diyl)bis(benzene-1,2 diol) (THADM)

^{1}H NMR spectrum of THADM is presented in **Figure 4.2.** The peak due to phenolic hydroxyl group was observed at δ = 8.55 ppm. The presence of adamantane unit protons was confirmed by the appearance of a singlet at δ = 3.0 ppm, a doublet at δ = 1.94 ppm and a multiplet in the range 1.72-1.62 ppm. The aromatic protons were observed as a singlet at δ = 6.74 ppm and two separate doublets at δ = 6.62 and 6.57 ppm.

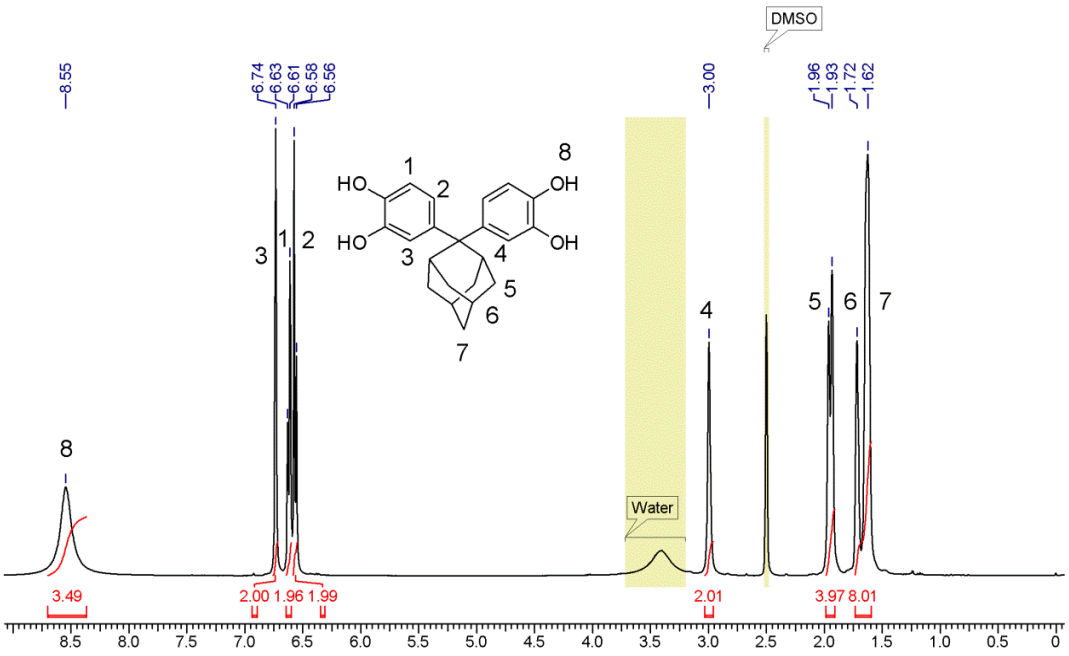

Figure 4.2: ^{1}H NMR spectrum (in DMSO-d_6) of 4,4'-((1r,3r)-adamantane-2,2-diyl)bis(benzene-1,2 diol) (THADM).

^{13}C NMR spectrum of THADM along with assignments is represented in **Figure 4.3**. The carbon attached to phenolic –OH group showed two signals at δ = 144.8 and 141.9 ppm in the downfield region due to inductive effect of hydroxyl group. The other aromatic carbons were observed in the range δ = 140.1-113.2 ppm. The peaks due to adamantane unit carbons appeared as 5 signals in the region δ = 48.6-26.9 ppm. The disappearance of methyl groups indicated complete conversion of TMADM to THADM.

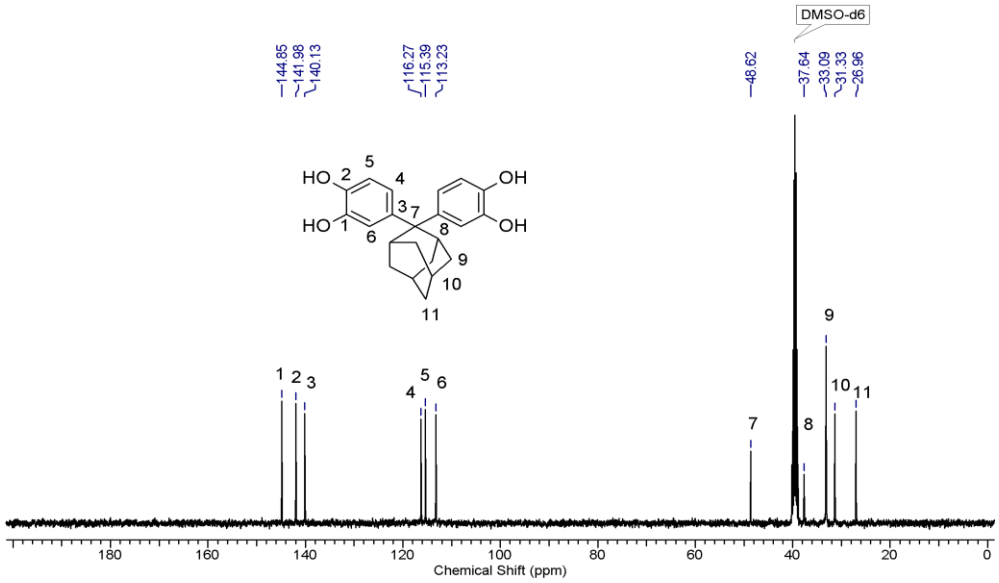

Figure 4.3: ^{13}C NMR spectrum (in DMSO-d_6) of 4,4'-((1r,3r)-adamantane-2,2-diyl)bis(benzene-1,2 diol) (THADM)

Structure of THADM was further supported by HRMS analysis (**Figure 4.4**). HRMS showed signal at 351.1590 corresponding to $[M+H]^+$ of THADM (calcd. $[M+H]^+$ for $C_{22}H_{23}O_4$ =351.1591).

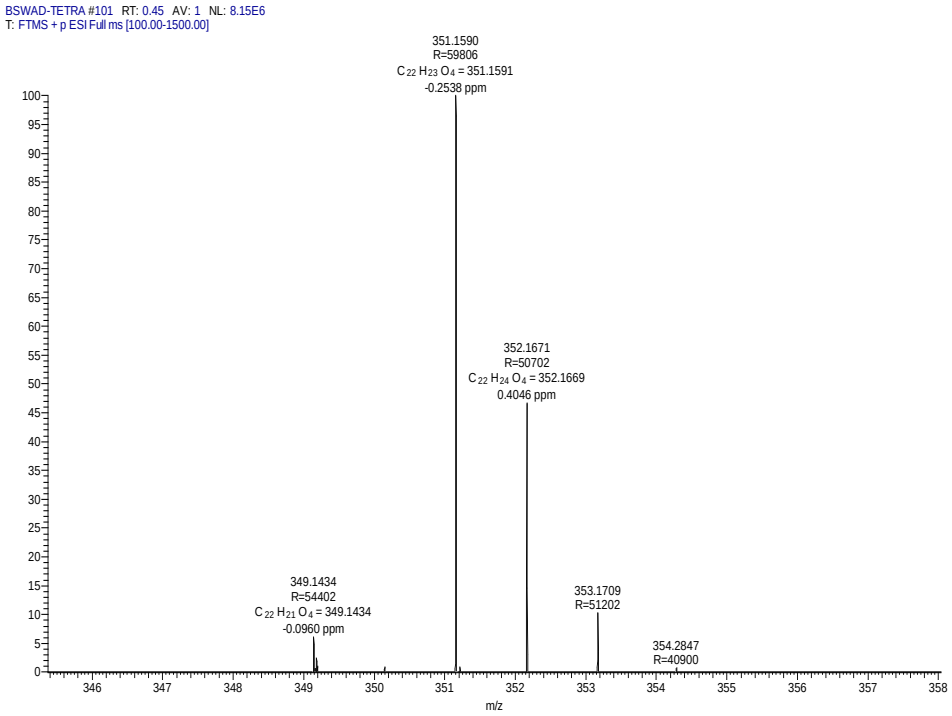

Figure 4.4: HR-MS of 4,4-((1r,3r)-adamantane-2,2-diyl)bis(benzene-1,2 diol) (THADM)

4.3.2 Synthesis and Characterization of PIMs Containing Adamantane Units

Homopolymer containing adamantane units was synthesized by polycondensation of THADAM with TFTPN in DMAc in the presence of K_2CO_3 as a base at high temperature (**Scheme 4.2**). Generally, aromatic nucleophilic substitution reaction is known to proceed readily if the halide-containing monomer is activated by an electron-withdrawing substituent such as -CN, CF_3, sulfone, etc.[10] The reaction proceeds *via* nuclophilic attack of phenoxide ion on to the activated carbon of halide containing monomer to form polymer with hydrogen fluoride as the by-product.[26] PIM-1 was synthesized as a reference polymer by polycondensation of 5,5,6',6'-tetrahydroxy-3,3,3',3'-tetramethylspirobisindane (TTSBI) with 2,3,5,6-tetrafluoroterephthalonitrile (TFTPN) for comparison. In addition, copolymers containing different contents of adamantane units such as 25, 50 and 75 mol % were prepared from varying compositions of THADM and TTSBI with TFTPN and which were referred to as ADM-PIM-25, ADM-PIM-50 and ADM-PIM-75, respectively. The formation of polymers was confirmed by IR, ^1H and ^{13}C NMR spectroscopy.

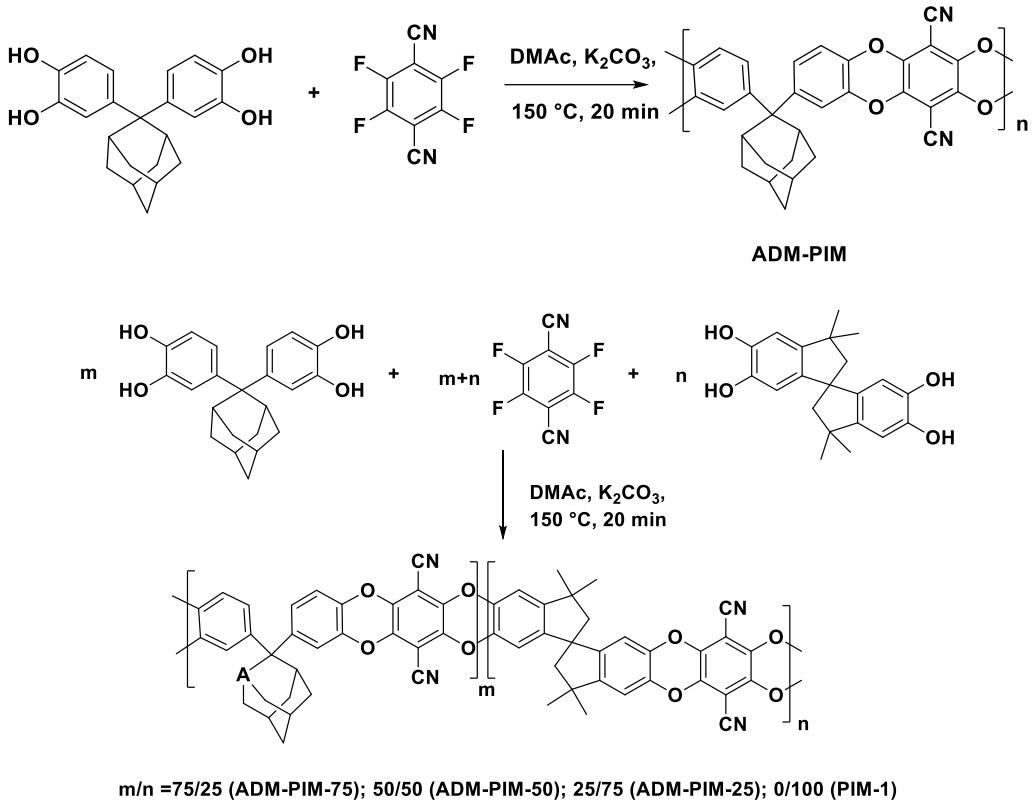

Scheme 4.2: Synthesis of homopolymer and copolymers containing adamantane units

IR spectrum **(Figure 4.5**) of ADM-PIM exhibited bands of -CN and Ar-O-Ar at 2237 cm^{-1} and 1264 cm^{-1}, respectively. IR spectra of other PIMs are shown in **Figure SI 4.4**.

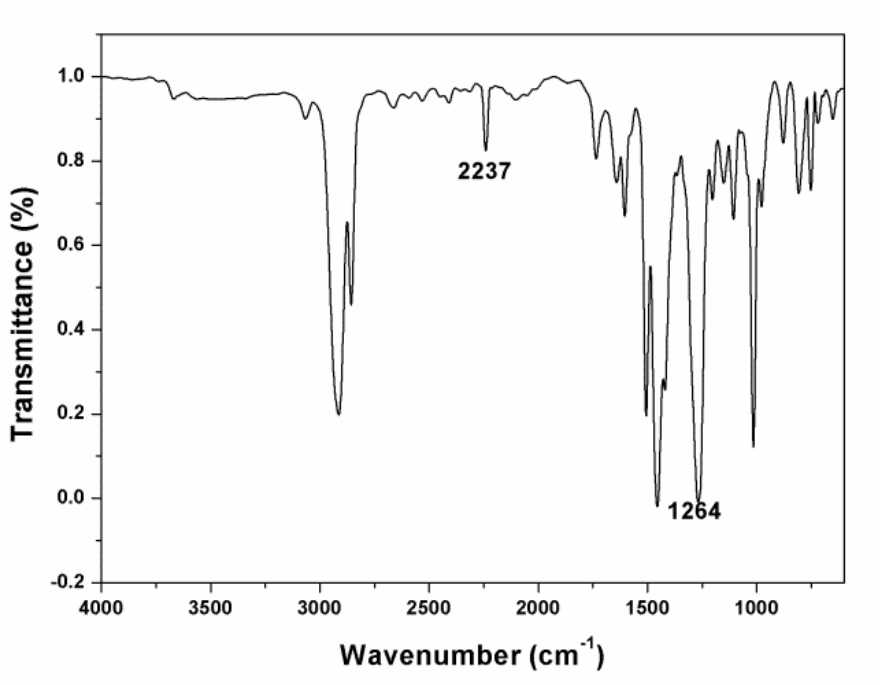

Figure 4.5: IR spectrum of ADM-PIM.

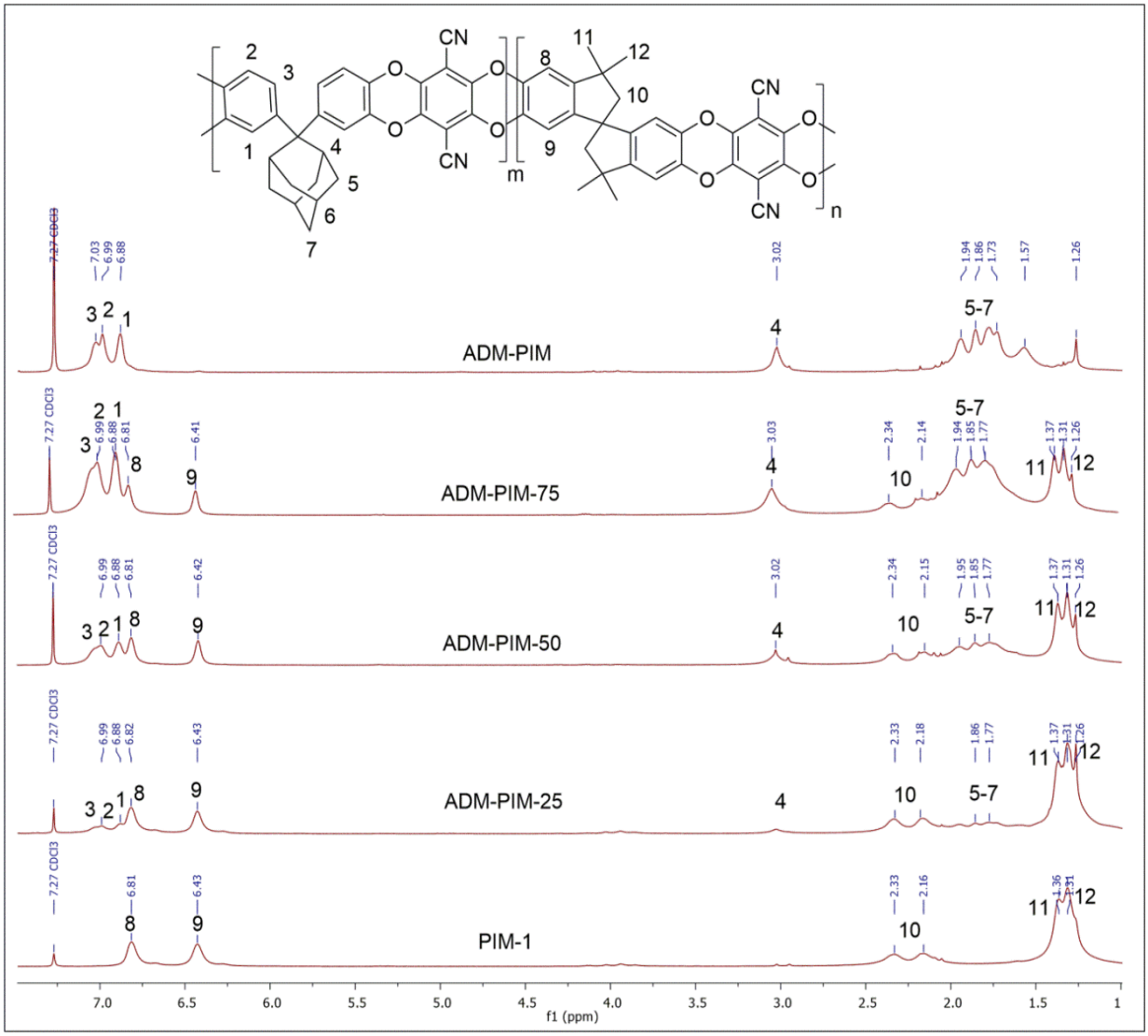

Figure 4.6: Stacked ^{1}H NMR spectra (in $CDCl_3$) of ADM-PIMs and PIM-1

In ^{1}H NMR spectrum of ADM-PIM (**Figure 4.6**), the peaks due to adamantane unit appeared at δ = 3.0 ppm and in the region δ = 1.84-1.58 ppm. The composition of copolymers was determined by ^{1}H NMR spectroscopy (**Table 4.1**). The stacked ^{1}H NMR spectra of ADM-PIM, ADM-PIM-75, ADM-PIM-50, ADM-PIM-25 and PIM-1 are depicted in **Figure 4.6**. For composition determination, the integrated intensity of aromatic proton (labeled as 9) of spirobisindane unit was compared with the aliphatic proton (labeled as '4') of adamantane unit which appeared at δ = 3.01 ppm. The composition determined by ^{1}H NMR spectroscopy was in excellent agreement with the feed composition (**Table 4.1**). ^{13}C NMR spectra of all PIMs are shown in **Figure SI 4.5-4.9**.

Table 4.1: Copolymer composition of PIMs from ^{1}H NMR spectra

Sr. No.	Polymer	Feed THADM (mol %)	Observed THADM (mol %)
1	**ADM-PIM-75**	75	74.2 ± 0.4
2	**ADM-PIM-50**	50	49.4 ± 0.4
3	**ADM-PIM-25**	25	24.3 ± 0.4

4.3.3 Solubility of PIMs

The solubility of PIMs (3 wt %) was tested at room temperature in various organic solvents and the results are collected **Table 4.2**. PIMs exhibited good solubility in organic solvents. PIMs were found to be soluble at room temperature in dichloromethane (DCM), chloroform ($CHCl_3$), tetrahydrofuran (THF) and *N*,*N*-dimethylacetamide (DMAc) and were partially soluble in dimethyl sulfoxide (DMSO) and toluene. The good solubility of PIMs could be attributed to the bulky adamantane and spirobisindane units present in the PIMs which allow penetration of the solvent molecules by disturbing packing of polymer chains. Due to good solubility of PIMs in organic solvents, the self-standing films could be cast from their solutions in chloroform as shown in **Figure 4.7**. These membranes were further used for gas permeability analysis.

Table 4.2: Solubility data of PIMs[a]

Sr. No.	Polymer	$CHCl_3$	DCM	THF	DMAc	DMSO	Toluene	Acetone	Ethanol
1	**ADM-PIM**	++	++	++	++	+-	+-	–	–
2	**ADM-PIM-75**	++	++	++	++	+-	+-	–	–
3	**ADM-PIM-50**	++	++	++	++	+-	+-	–	–
4	**ADM-PIM-25**	++	++	++	++	+-	+-	–	–
5	**PIM-1**	++	++	++	++	+-	+-	–	–

[a:] Solubility tests of PI-PIMs were carried out at 3 wt % (w/v) concentration at room temperature. ++: Soluble, +-: partially soluble, –insoluble

Figure 4.7: Films of a) PIM-1, b) ADM-PIM-25, c) ADM-PIM-50, d) ADM-PIM-75 and e) ADM-PIM

4.3.4 Molecular Weights of PIMs

Molecular weights of PIMs were determined by GPC measurements in chloroform using polystyrene as the standard. Number average molecular weights were in the range 38100-61700 g/mol (**Table 4.3**), indicating formation of reasonably high molecular weight polymers. As synthesized PIMs were film-forming, no special efforts were made in the present work to optimise molecular weights of PIMs synthesized by polycondensation route.

Table 4.3: Synthesis and properties of PIMs

Sr. No.	Polymer	M_n (g/mol)[a]	M_w (g/mol)[a]	Dispersity[b]	$T_{10\%}$ (°C)[c]	Char Yield (%)[d]
1	**ADM-PIM**	56200	130000	2.3	514	54
2	**ADM-PIM-75**	48100	114000	2.4	518	53
3	**ADM-PIM-50**	51200	117000	2.3	517	56
4	**ADM-PIM-25**	61700	141000	2.3	513	52
5	**PIM-1**	38100	90000	2.3	515	63

[a:] Molecular weights were determined from GPC in chloroform (polystyrene standard). [b:] Dispersity= M_w/M_n. [c:] Temperature at which 10% weight loss was recorded by TGA at a heating rate of 10 °C/min. under N_2 atmosphere. [d:] Percentage char yield under nitrogen atmosphere at 900 °C.

Table 4.4: Properties of PIMs

Sr. No.	Polymer	*d*-Spacing (Å)[a]	S_{BET} (m^2/g)[b]	Total pore volume (cc/g)[c]	Pore diameter (nm)[d]
1	**ADM-PIM**	6.32	703	0.57	0.62
2	**ADM-PIM-75**	6.41	707	0.62	0.62
3	**ADM-PIM-50**	6.50	713	0.65	0.62
4	**ADM-PIM-25**	6.60	715	0.67	0.71
5	**PIM-1**	6.70	741	0.69	0.74

[a:] *d*-Spacing was calculated from XRD patterns using Bragg's equation. [b:] BET surface area was calculated from N_2 adsorption method. [c:] Pore volume was calculated from nitrogen adsorption method at p/p_o = 0.98. [d:] Pore diameter was calculated from DFT method.

4.3.5 X-Ray Diffraction of PIMs

X-Ray diffraction study was carried out to determine the crystallinity of polymers. In XRD patterns (**Figure 4.8**), broad halo was observed at 2θ = 10-25° which indicated their amorphous nature. The amorphous nature could be attributed to the presence of bulky adamantane and spirobisindane units which disturbed polymer chain packing. The average *d*-spacing is the inter-

chain distance between polymer chains and was obtained from the peak maxima of XRD patterns using Bragg's equation. The *d*-spacing values of PIMs are given in **Table 4.4.** These PIMs showed high *d*-spacing values due to the presence of adamantane and spirobisindane units which disturb packing of polymer chains. In this series, the order of *d*-spacing is as follows: PIM-1 > ADM-PIM-25 > ADM-PIM-50 > ADM-PIM-75 > ADM-PIM. ADM-PIMs showed lower *d*-spacing than PIM-1 which could be due to spirobisindane unit is more effective than adamantane unit for disturbing polymer chain packing.

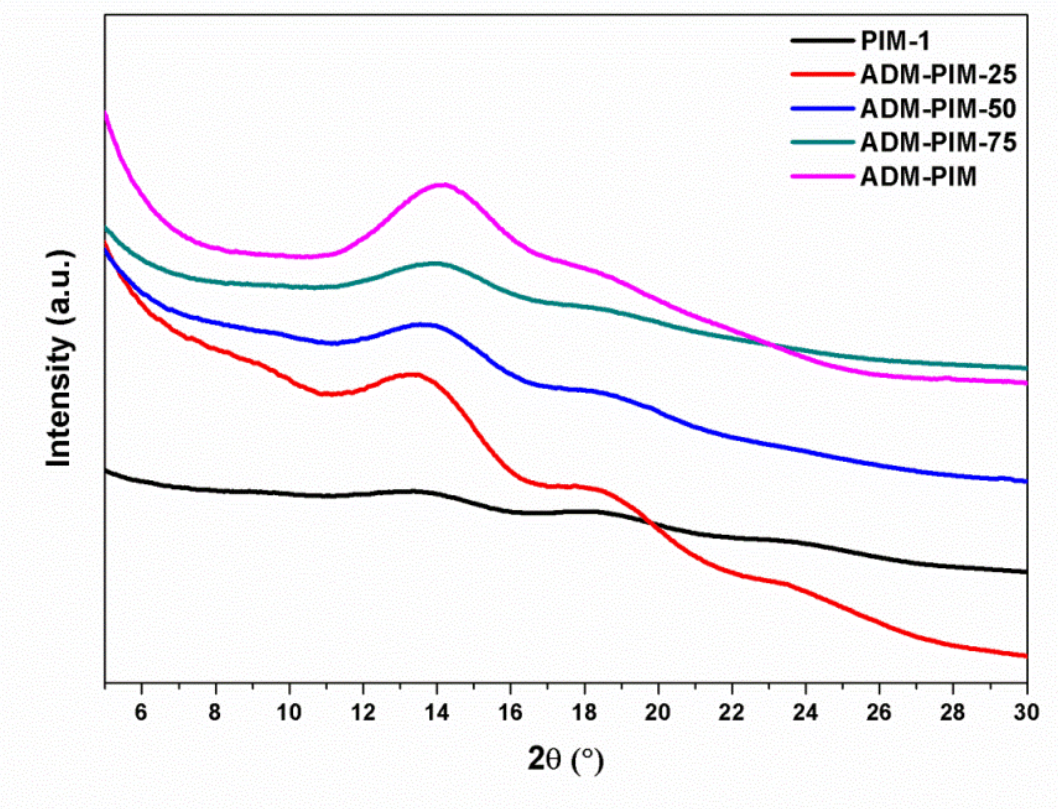

Figure 4.8: X-Ray diffractograms of PIM-1 and ADM-PIMs

4.3.6 Thermal Properties of PIMs

Thermogravimetric analysis was carried out to determine the thermal stability of PIMs. The analysis was performed under nitrogen at a heating rate of 10 °C / min and the results are summarized in **Table 4.3 and Figure 4.9**. T_{10} value, which is generally used as a parameter for comparison of relative thermal stability of polymers, was found in the range 513-518 °C. The excellent thermal stability could be attributed to the presence of rigid adamantane and spirobisindane units in the polymer backbone. DTG curves of ADM-PIMs and PIM-1 indicated single stage weight loss with maximum decomposition temperature (T_{max}) in the range 514-524 °C. The char yields of ADM-PIMs, obtained from TG curves, were in the narrow range of 52-56

%. The % char yields of ADM-PIMs were lower than that of PIM-1. This could be due to the presence of lower ratio of aromatic to aliphatic content in ADM-PIMs compared to PIM-1. However, systematic trend in percentage char yield as a function of content of aliphatic moieties was not observed in case of ADM-PIMs. DSC was used to detect the glass transition temperature (T_g) of PIMs. T_g was not detected in DSC analysis carried out upto 390 °C. Similar observations reported were by Pinnau and co-workers concerning T_g for tetraphenylethylene-based PIMs.[27]

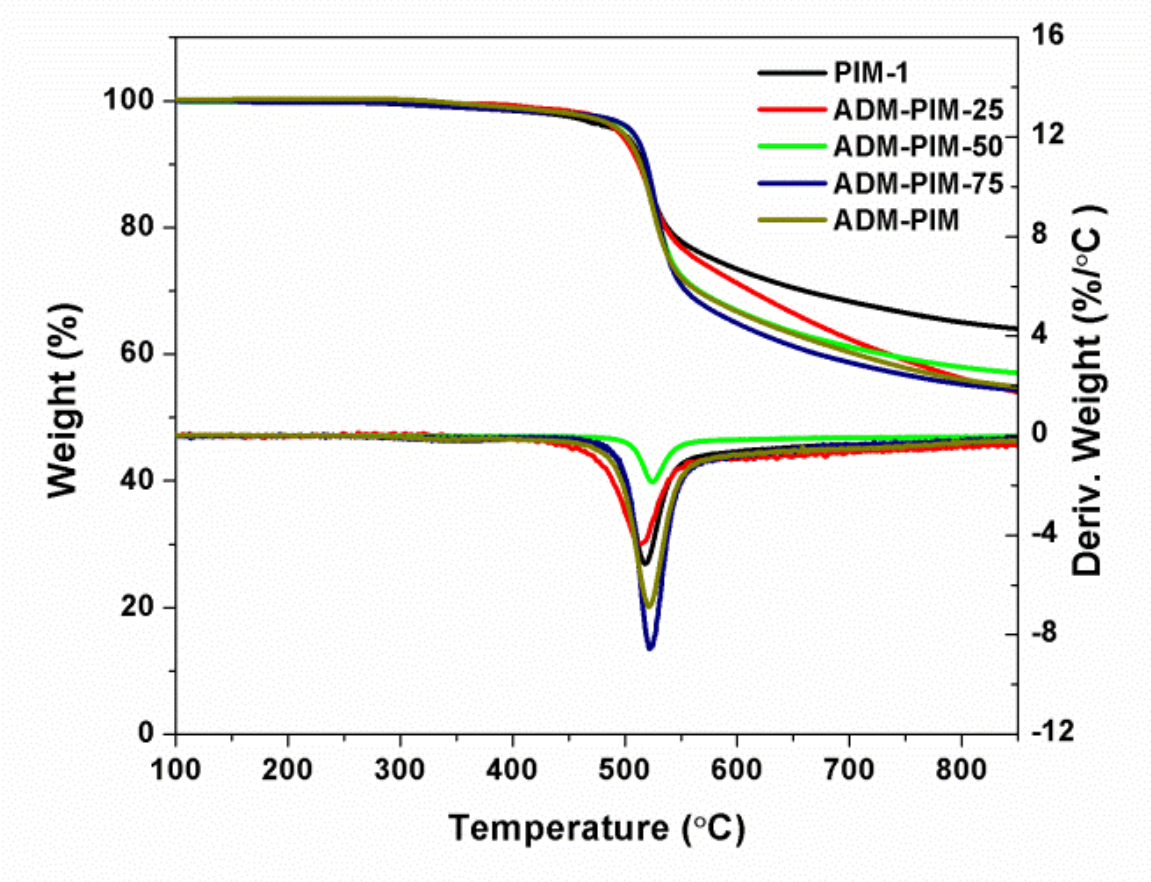

Figure 4.9: TG and DTG curves of PIMs.

4.3.7 Intrinsic Microporosity of PIMs

BET surface area and pore volume of PIMs was determined by N_2 adsorption/desorption measurements at 77 K as shown in **Figure 4.10.** Prior to measurements, all polymers were degassed at 120 °C for 12 h. The isotherms of PIMs were of Type-I which is the characteristic of microporous polymers. The pore diameters of PIMs were in the range 0.62-0.74 nm which further supports their microporous nature. PIMs exhibited high BET surface area (**Table 4.4**) in the range 703-715 m^2/g, indicating that PIMs possessed intrinsic microporosity. The microporosity in these polymers could be generated due to the presence of bulky adamantane and/or spirobisindane units. In this series, BET surface area decreased with increasing content of

adamantatane units and the order is as: ADM-PIM < ADM-PIM-75 < ADM-PIM-50 < ADM-PIM-25 < PIM-1. The results indicated that spirobisindane unit is more effective than adamantane unit in disturbing the chain packing due to the contorted nature of the former.

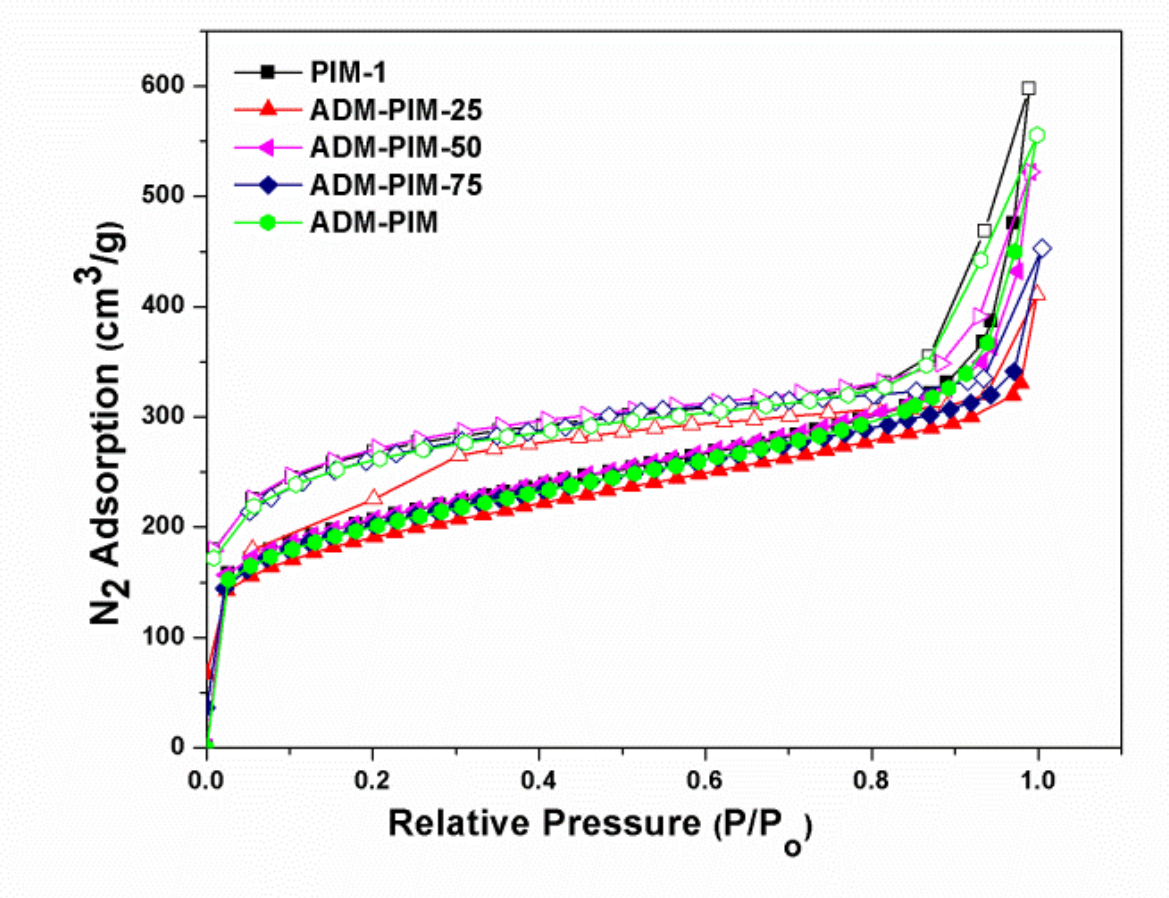

Figure 4.10: Nitrogen adsorption (filled circles) and desorption (empty circles) of PIMs.

4.3.8 Density Functional Theory (DFT) Analysis

Density functional theory (DFT) was used to determine the angle of twisted structure of PIM-1 and ADM-PIM. The energy minimized structures of two repeating units of ADM-PIM and PIM-1 were obtained by DFT. Both ADM-PIM and PIM-1 were zig-zag coiled structures as shown in **Figure 4.11**. The angle between twisted structure of ADM-PIM and PIM-1 were ~103° and ~114°, respectively. These results indicated that PIM-1 is more open than that of ADM-PIM due to higher angle. This result suggested that contorted spirobisindane units disturbed polymer chain packing more effectively than cardo adamantane units.

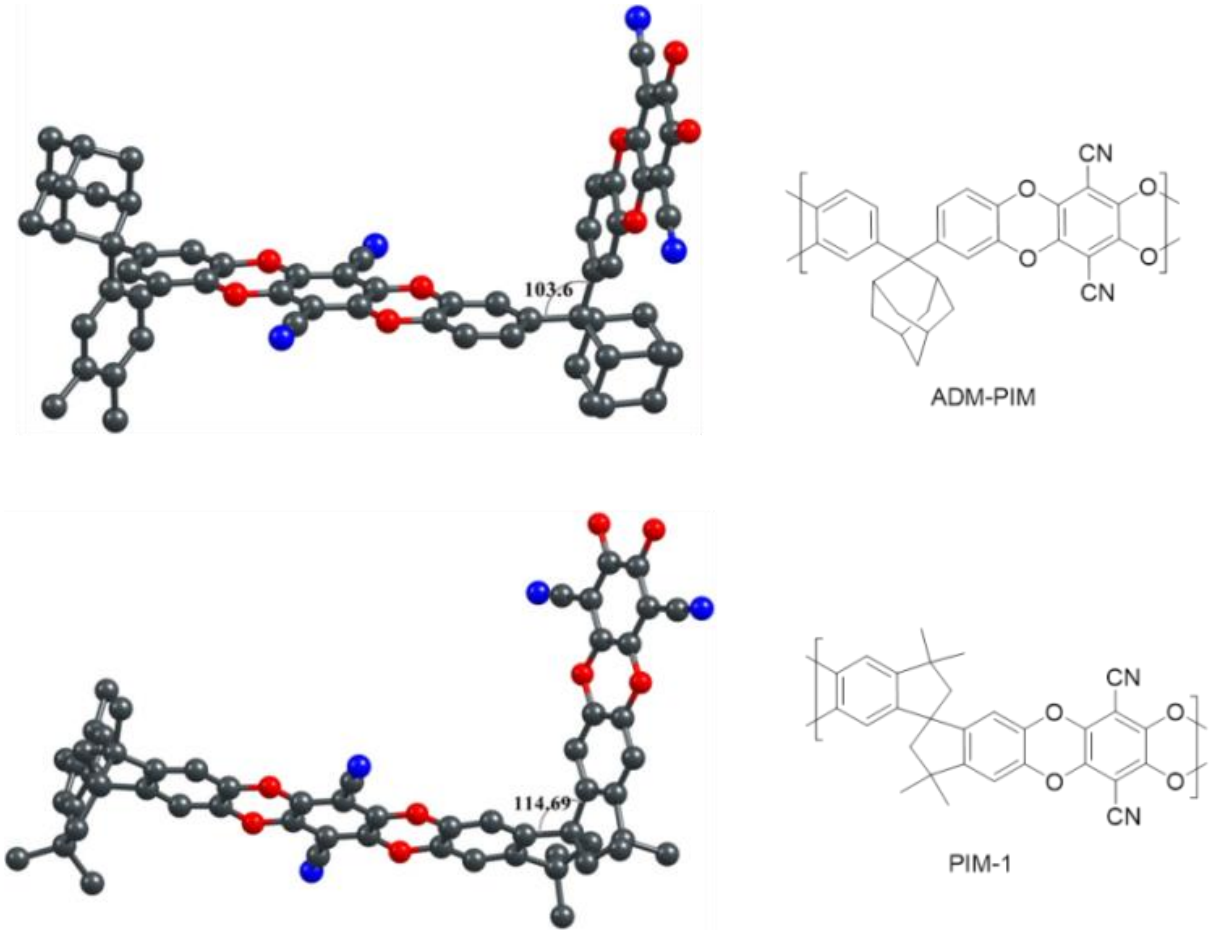

Figure 4.11: Energy minimized structures of two repeating units of ADM-PIM and PIM-1 (Red= oxygen, blue= nitrogen and black = carbon).

4.4 GAS PERMEABILITY

The pure gas permeability data of PIMs were determined by variable-volume method at 1 bar and at room temperature. The data on gas permeability and selectivity of PIMs are summarized in **Table 4.5 and 4.6**. For all PIMs, the order for gas permeability is: $CO_2 > H_2 > He > O_2 > CH_4 > N_2$. In general, PIMs exhibited high gas permeability with moderate selectivity. This is due to the presence of cardo adamantane and contorted spirobisindane units in PIMs which create microporosity by disturbing the chain packing. It could be seen that the gas permeability of PIMs varied with the variation of contents of adamantane units in PIMs, which is discussed in the following sections.

4.4.1 Effect of Adamantane Unit on Gas Permeation Properties

In order to understand the influence of adamantane unit on gas separation properties, the gas permeability data were compared with PIM-1 which was tested under similar conditions. The

higher gas permeability and lower selectivity of PIM-1 compared to ADM-PIM is attributed to higher pore diameter of PIM-1 (0.74 nm) compared to ADM-PIM (0.62 nm). For all the gases, permeability increased in the order: ADM-PIM < ADM-PIM-75 < ADM-PIM-50 < ADM-PIM-25 < PIM-1. For example, the CO_2 permeability of PIMs decreased from 2626 to 1080 whereas selectivity of CO_2/N_2 gas pair increased from 13.8 to 26.7 and for CO_2/CH_4 gas pair from 12.7 to 22.6. The selectivity for O_2/N_2 gas pair increased from 2.8 to 5.7 whereas permeability decreased from 452 to 232. The gas permeability analysis demonstrated that permeability decreased whereas the selectivity increased for all gases with increasing content of adamantane units. The effect of adamantane units on gas permeability could be clearly understood by correlating *d*-spacing and BET surface area of these PIMs with gas permeability. The high selectivity of ADM-PIMs could be explained by DFT. DFT indicated that ADM-PIM is relatively more compact than PIM-1, due to this ADM-PIMs are more selective and less permeable than PIM-1.

Table 4.5: Gas permeability of ADM-PIMs and reported adamantane-containing polymers

Sr No.	Polymer	Permeability (Barrer)[a,b,c]					
		He	**H_2**	**N_2**	**O_2**	**CH_4**	**CO_2**
1	**ADM-PIM**	440 (353)	763 (631)	41 (24)	232 (144)	48 (30)	1080 (720)
2	**ADM-PIM-75**	636 (445)	1092 (748)	68 (43)	285 (190)	82 (49)	1694 (1118)
3	**ADM-PIM-50**	760 (562)	1270 (871)	86 (56)	358 (241)	103 (68)	1793 (1226)
4	**ADM-PIM-25**	832 (591)	1540 (1216)	123 (88)	474 (344)	152 (112)	2110 (1524)
5	**PIM-1**	855 (742)	1674 (1360)	191 (126)	452 (392)	207 (164)	2626 (2150)
6	**PI-ADA-1**[21]	-	-	0.72	3.79	0.39	14.39
7	**PI-ADA-2**[21]	-	-	0.83	4.79	0.45	16.06
8	**PI-ADA-3**[21]	-	-	0.67	3.23	0.37	12.93
9	**TB-Ad-Me**[23] **(As cast)**	-	161.4	11.24	40.20	18.7	200.5
10	**TB-Ad-Me**[23] **(MeOH-treated)**	-	1800	121	437	162	1820

[a:] Units of permeability (P): 1 Barrer = 10^{-10} cm^3 (STP) cm /cm^2 s cm Hg. [b:] Gas permeability of aged films (150 days) of PIMs are given in parentheses. [c:] Gas permeability data taken from literature (entries 6-10) are marked in red.

Table 4.6: Gas selectivity of ADM-PIMs and reported adamantane-containing polymers

Sr No.	Polymer	Selectivity (α)[a,b,c]			
		H_2/N_2	O_2/N_2	CO_2/N_2	CO_2/CH_4
1	**ADM-PIM**	18.8 (26.3)	5.7 (6.0)	26.7 (30)	22.6 (24)
2	**ADM-PIM-75**	16.3 (17.4)	4.3 (4.4)	25.3 (26.0)	20.6 (22.8)
3	**ADM-PIM-50**	14.7 (15.5)	4.2 (4.3)	20.8 (21.9)	17.6 (18.0)
4	**ADM-PIM-25**	12.5 (13.8)	3.9 (3.9)	17.1 (17.3)	13.8 (13.6)
5	**PIM-1**	8.7 (10.8)	2.9 (3.1)	13.8 (17.0)	12.7 (13.1)
6	**PI-ADA-1 (28)**	-	5.3	20	36.8
7	**PI-ADA-2 (28)**	-	5.8	19.4	35.7
8	**PI-ADA-3 (28)**	-	4.8	19.3	34.9
9	**TB-Ad-Me**[23] **(As cast)**	19.7	4.9	24.4	10.8
10	**TB-Ad-Me**[23] **(MeOH-treated)**	14.9	3.6	15.1	11.3

[a:] Selectivity (α) = P_1/P_2. [b:] Gas selectivity of aged films (150 days) of PIMs are given in parentheses. [c:] Gas selectivity data taken from literature (entries 6-10) are marked in red.

4.4.2 Effect of Physical Aging on Gas Permeation Properties

Physical aging occurs in all PIMs despite their high intra-chain rigidity. In fact, the initially high free volume created by greater backbone rigidity and contorted nature serves as a driving force for faster physical aging.[27,28] Physical aging is a relaxation process in which polymer chains get closer resulting into decrease in free volume and consequently decrease in gas permeability.[29,30] The gas permeability measurements on PIM films aged for 150 days were carried out and the results are included in **Table 4.5 and 4.6**. After aging, there was significant decrease in gas permeability for all the gases *viz*. He, H_2, N_2, O_2, CH_4 and CO_2 and increase in selectivity for all gas pairs. For example, the CO_2 permeability of ADM-PIM decreased from 1080 to 720 Barrer with increase in selectivity of CO_2/N_2 and CO_2/CH_4 from 26.7 to 30 and 22.6 to 24, respectively. For O_2 separation, the gas permeability decreased from 232 to 144 Barrer whereas selectivity for O_2/N_2 gas pair increased from 5.7 to 6.0. It is worth to note that the gas permeability of aged membranes is still higher than the commercially available polymers such as Matrimid (CO_2 = 10 Barrer) and polysulfone (CO_2 = 5.6 Barrer). Similar observations have been documented in the literature concerning effect of physical aging on gas permeability characteristics of PIMs.[23,29]

4.4.3 Comparison of ADM-PIMs with Reported Adamantane-Containing Polymers

The gas permeability and selectivity of PIMs were compared with literature reported data of adamantane-containing polymers **(Sr. No. 6-10)** and the data are summarized in **Table 4.5 and 4.6**. For polymeric membranes there exists trade-off relationship between permeability and selectivity, wherein increase in permeability is at the cost of selectivity and vice-versa. This trade-off relationship was invented by Robeson and theoretically supported by Freeman by plotting gas permeability data of various polymers.[7,12] The more superior polymers demonstrated gas permeability data above well-defined upper bound. Robeson plots (**Figure 4.12**) were used to compare the performance of present PIMs with reported adamantane-containing polymers. The gas permeability data of present PIMs was found to be above 1991 Robeson upper bound and located close to 2008 Robeson upper bound for CO_2/CH_4, CO_2/N_2 and H_2/N_2 gas pairs. The data of ADM-PIM was located above 2008 Robeson upper bound for O_2/N_2 gas pair whereas data for ADM-PIM-50, ADM-PIM-75 and ADM-PIM-25 was close to 2008 Robeson upper bound.

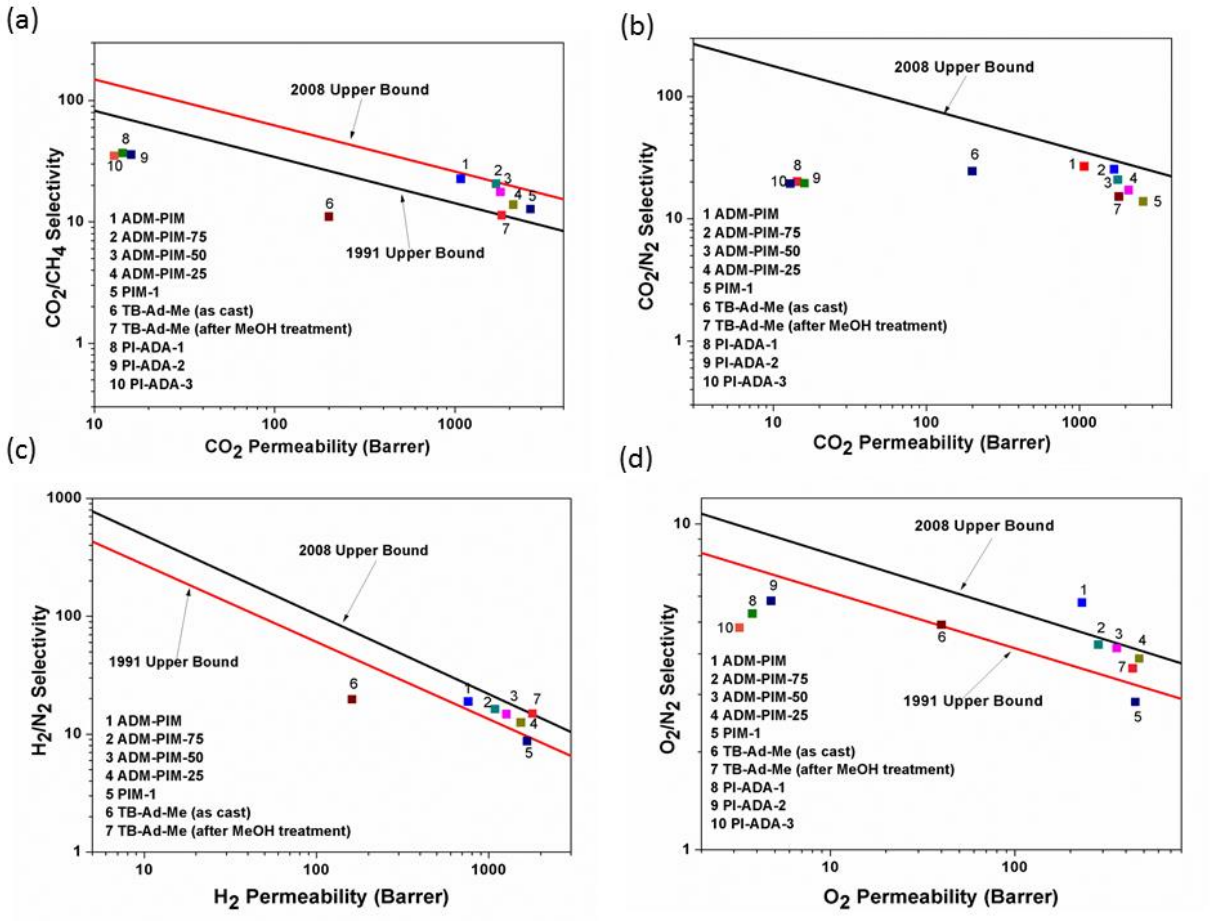

Figure 4.12: Robeson plots of PIMs for (a) CO_2/CH_4; (b) CO_2/N_2; (c) H_2/N_2 and (d) O_2/N_2 gas pairs.

In order to compare the relative performance of these PIMs, the gas permeability data was correlated with commercially available polymers and adamantane-containing polymers reported in the literature. The CO_2 permeability of the present PIMs is higher than Matrimid (10 barrer),[31] Kapton (3.51),[7] and polysulfone (5.6).[32] It can be seen from results in **Table 4.5 and 4.6 and Figure 4.12**, that the performance of present PIMs was above 2008 Robeson upper bound for CO_2/CH_4, CO_2/N_2 and O_2/N_2 compared to other reported adamantane-containing polymers. These results could be attributed to the incorporation of bulky adamantane and spirobisindane units in PIMs, which contribute to the stiffening of polymer chains and help to create microporosity.

4.5 CONCLUSIONS

A new adamantane-containing bis(catechol), namely, 4,4-((1r,3r)-adamantane-2,2-diyl)bis(benzene-1,2 diol) (THADM) was successfully synthesized starting from 2-adamantanone and veratrole. THADM and varying compositions of THADM and TTSBI were polycondensed with TFTPN by aromatic nucleophilic substitution reaction to obtain corresponding homo- and co-polymers. PIMs exhibited reasonably high molecular weights in the range 38100-62000 g/mol and good solubility in organic solvents and thus could be cast into self-standing films. X-Ray diffraction analysis showed that PIMs were amorphous in nature. The *d*-spacing of ADM-PIMs were in the range 6.31-6.70 Å. TGA showed that PIMs exhibited excellent thermal stability with T_{10} values in the range 514-518 °C. PIMs possessed intrinsic microporosity and displayed high BET surface area in the range 703-741 m^2/g. PIMs exhibited high gas permeability due to their microporous nature. The incorporation of adamantane units in PIMs resulted in increased gas selectivity with decreased permeability for different gas pairs. ADM-PIM demonstrated an excellent combination of gas permeability and selectivity for O_2/N_2 gas pair with gas permeability data located above 2008 Robeson upper bound. Overall, the incorporation of bulky adamantane and spirobisindane units in PIMs was demonstrated as an efficient strategy to tune their physical properties and consequently gas permeability characteristics.

4.6 REFERENCES

1. Kim, S., Lee, Y. M. *Prog. Polym. Sci.*, 2015, **43**, 1–32.
2. Wu, D., Xu, F., Sun, B., Fu, R., He, H., Matyjaszewski, K. *Chem. Rev.*, 2012, **112**, 3959–4015.
3. McKeown, N. B., Budd, P. M. *Chem. Soc. Rev.*, 2006, **35**, 675–683.
4. Thomas, C. J., Trend, J. E., Rakow, N. A., Wendland, M. S., Poirier, R. J., Paolucci, D. M. *Sensors*, 2011, **11**, 3267–3280.
5. Wang, Y., McKeown, N. B., Msayib, K. J., Turnbull, G. A., Samuel, I. D. W. *Sensors*, 2011, **11**, 2478–2487.
6. Du, N., Park, H. B., Dal-Cin, M. M., Guiver, M. D. *Energy Environ. Sci.*, 2012, **5**, 7306–7322.
7. Robeson, L. M. *J. Membr. Sci.*, 1991, **62**, 165–185.
8. Kyle E. hart, C. M. C. *J. Membr. Sci.*, 2014, **468**, 259–268.
9. Jue, M. L., Lively, R. P. *React. Funct. Polym.*, 2015, **86**, 40–43.
10. McKeown, N. B. *ISRN Mater. Sci.*, 2012, **2012**, 1–16.
11. Freeman, B. D. *Macromolecules*, 1999, **32**, 375–380.
12. Robeson, L. M. *J. Membr. Sci.*, 2008, **320**, 390–400.
13. Sanders, D. F., Smith, Z. P., Guo, R., Robeson, L. M., McGrath, J. E., Paul, D. R., Freeman, B. D. *Polymer*, 2013, 54, 4729–4761.
14. Rose, I., Bezzu, C. G., Carta, M., Comesaña-Gándara, B., Lasseuguette, E., Ferrari, M. C., Bernardo, P., Clarizia, G., Fuoco, A., Jansen, J. C., Hart, K. E., Liyana-Arachchi, T. P., Colina, C. M., McKeown, N. B. *Nat. Mater.*, 2017, **16**, 932–938.
15. McKeown, N. B. *ISRN Mater. Sci.*, 2012, **2012**, 1–16.
16. Kim, S., Lee, Y. M. *Prog. Polym. Sci.*, 2015, **43**, 1–32.
17. Baker, R. W., Low, B. T. *Macromolecules*, 2014, **47**, 6999–7013.
18. Lu, W., Yuan, D., Zhao, D., Schilling, C. I., Plietzsch, O., Krishna, R., Muller, T., Br, S., Guenther, J., Bl, J. *Chem. Mater.*, 2010, **22**, 5964–5972.
19. Lim, H., Cha, M. C., Chang, J. Y. *Polym. Chem.*, 2012, **3**, 868–870.
20. Bera, D., Bandyopadhyay, P., Dasgupta, B., Banerjee, S. *J. Membr. Sci.*, 2012, **407**–**408**, 116–127.
21. Maya, E. M., García-Yoldi, I., Lozano, a. E., de la Campa, J. G., de Abajo, J. *Macromolecules*, 2011, **44**, 2780–2790.
22. Bera, D., Bandyopadhyay, P., Ghosh, S., Banerjee, S. *J. Membr. Sci.*, 2014, **453**, 175–191.
23. Carta, M., Croad, M., Jansen, J. C., Bernardo, P., Clarizia, G., McKeown, N. B. *Polym. Chem.*, 2014, **5**, 5255–5261.
24. McOmie, J. F. W., Watts, M. L., West, D. E. *Tetrahedron*, 1968, **24**, 2289–2292.
25. Apel, S., Nitsche, S., Beketov, K., Seichter, W., Seidel, J., Weber, E. *J. Chem. Soc., Perkin Trans.*, 2001, **2**, 1212–1218.
26. Ma, C., Urban, J. J. *Proc. Nat. Res. Soc.*, 2018, **2**, 2002.
27. Ma, X., Pinnau, I. *Polym. Chem.*, 2016, **7**, 1244–1248.
28. Swaidan, R., Ghanem, B., Litwiller, E., Pinnau, I. *Macromolecules*, 2015, **48**, 6553–6561.
29. Carta, M., Bernardo, P., Clarizia, G., Jansen, J. C., McKeown, N. B. *Macromolecules*, 2014, **47**, 8320–8327.
30. Ma, X., Ghanem, B., Salines, O., Litwiller, E., Pinnau, I. *ACS Macro Lett.*, 2015, **4**, 231–235.
31. Guiver, M. D., Robertson, G. P., Dai, Y., Bilodeau, F., Kang, Y. S., Lee, K. J., Jho, J. Y., Won, J. *J. Polym. Sci. Part A Polym. Chem.*, 2002, **40**, 4193–4204.
32. Aitken, C. L., Koros, W. J., Paul, D. R. *Macromolecules*, 1992, 25, 3424–3434.

Supporting Information

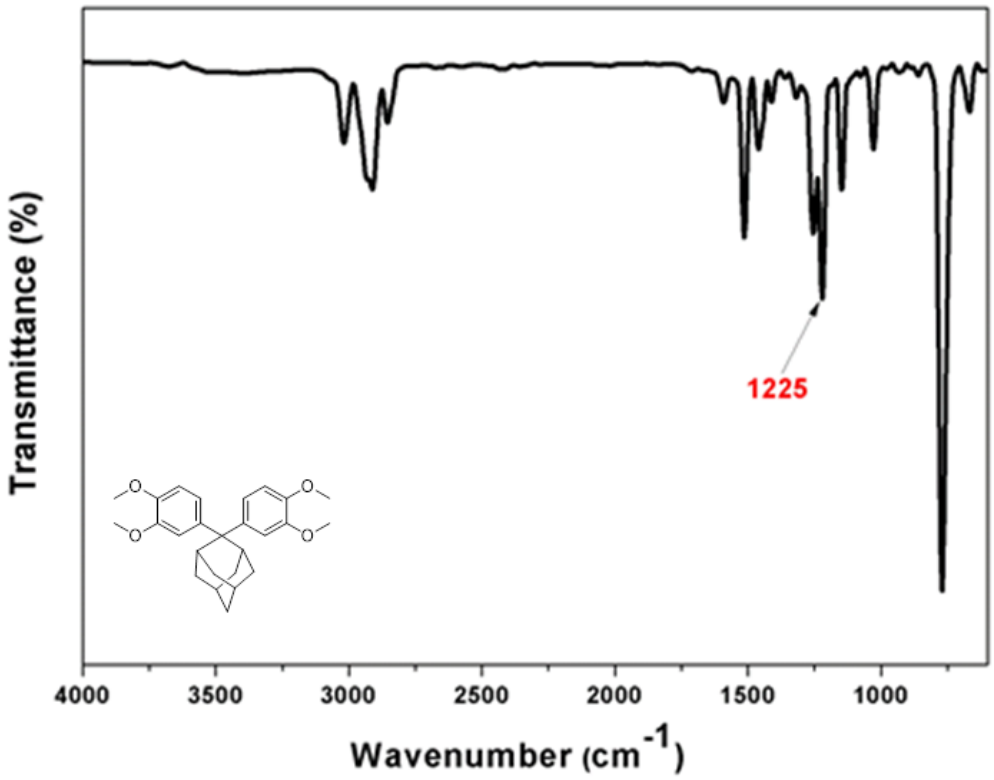

Figure SI 4.1: IR spectrum of (1r,3r)-2,2-bis(3,4-dimethoxyphenyl)adamantane (TMADM)

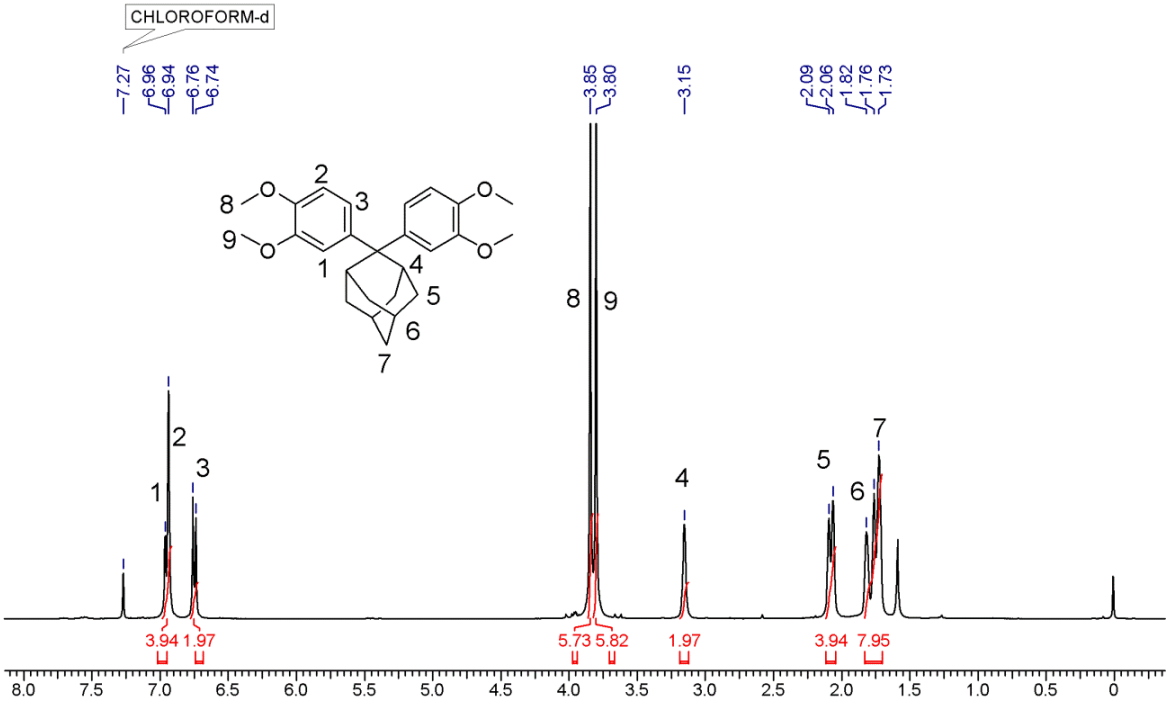

Figure SI 4.2: ^{1}H NMR spectrum (in $CDCl_3$) of (1r,3r)-2,2-bis(3,4-dimethoxyphenyl)adamantane (TMADM)

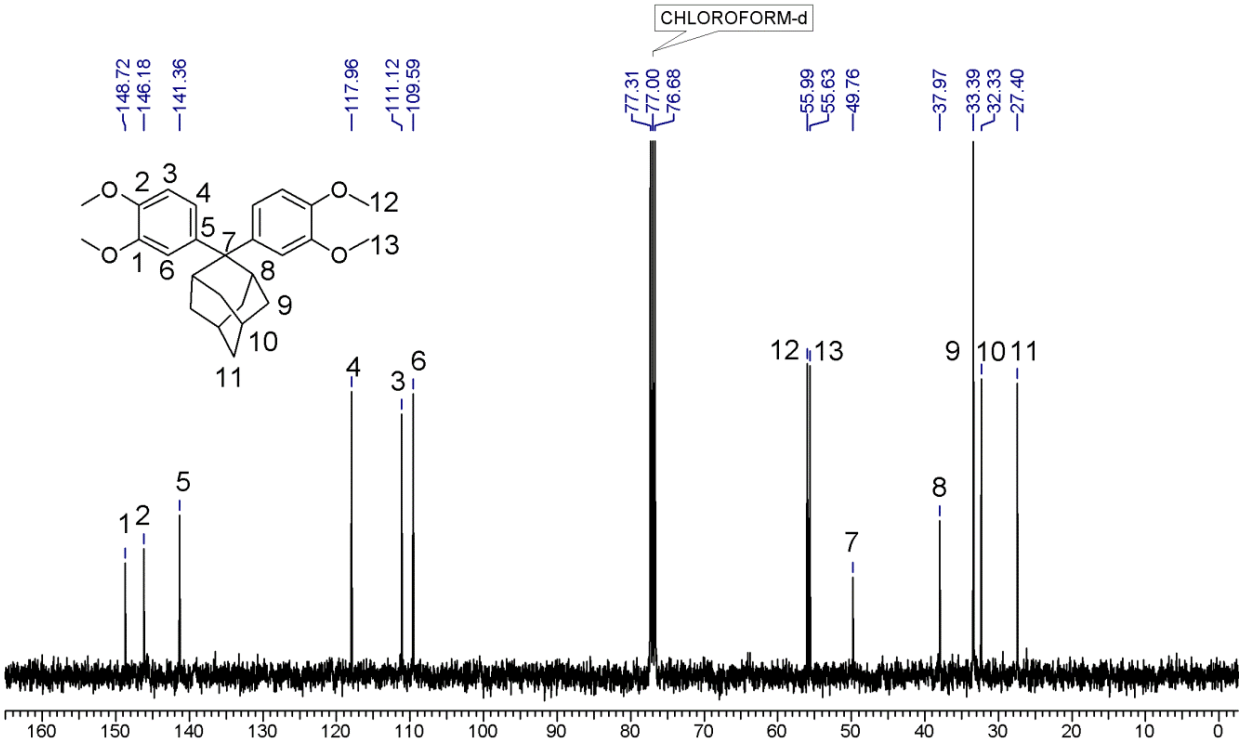

Figure SI 4.3: ^{13}C NMR spectrum (in $CDCl_3$) of (1r,3r)-2,2-bis(3,4-dimethoxyphenyl)adamantane (TMADM)

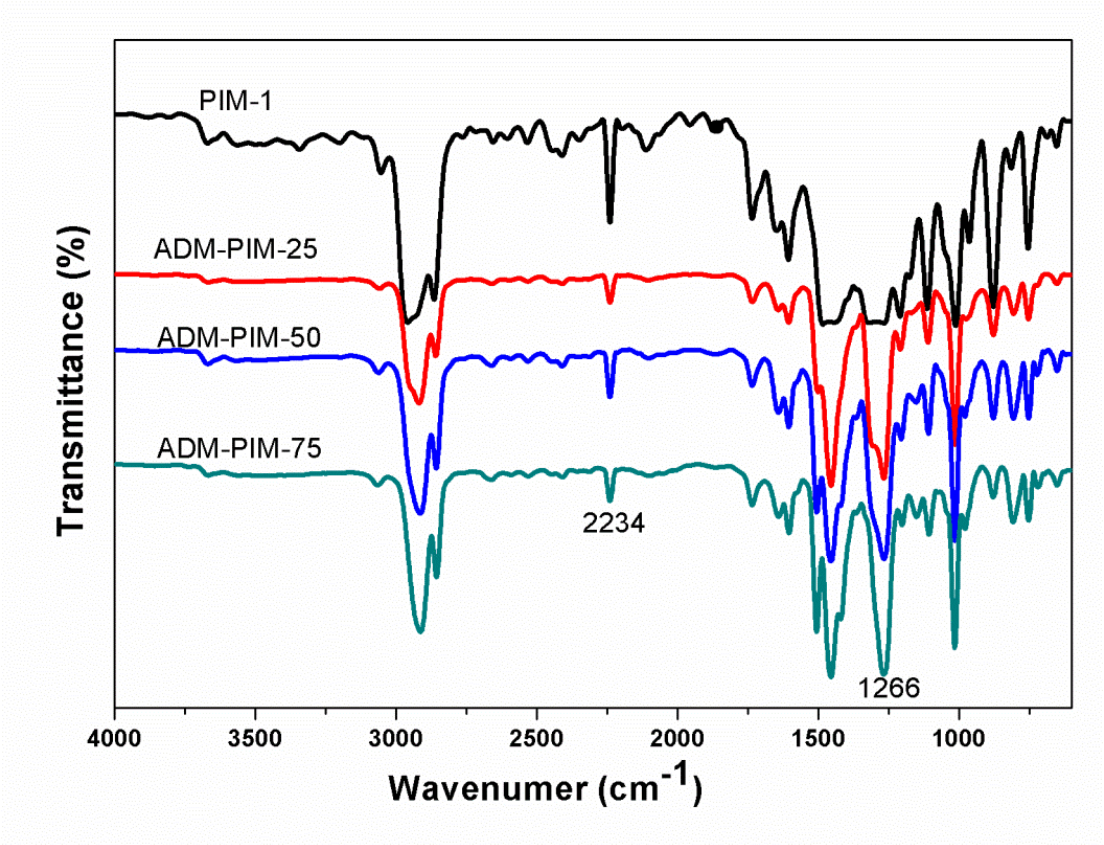

Figure SI 4.4: IR spectra of PIMs

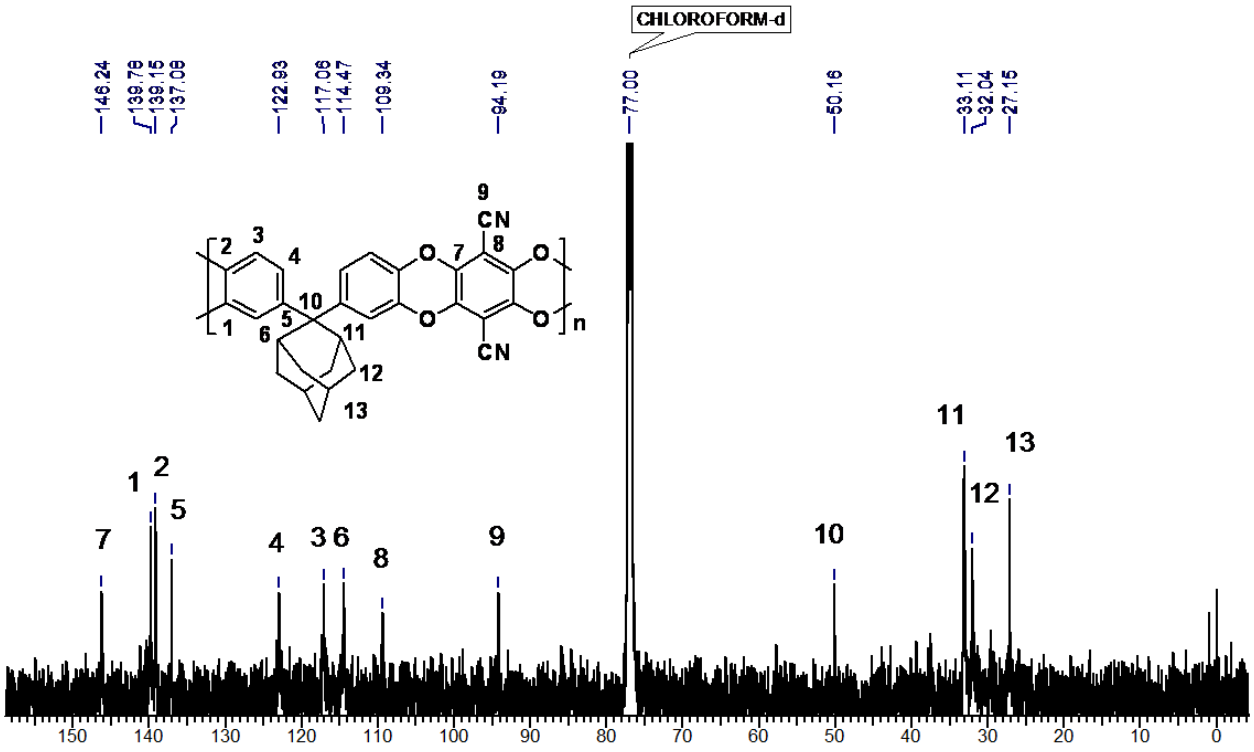

Figure SI 4.5: ^{13}C NMR spectrum (in $CDCl_3$) of ADM-PIM

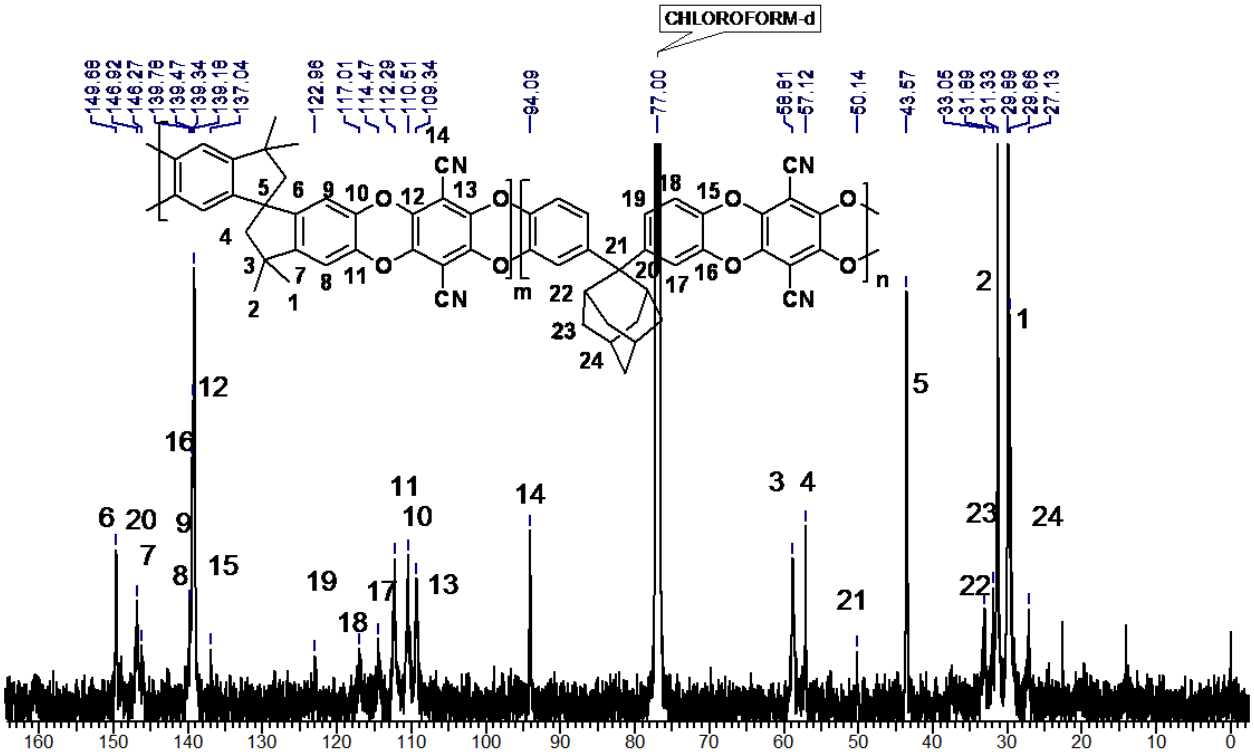

Figure SI 4.6: ^{13}C NMR spectrum (in $CDCl_3$) of ADM-PIM-25

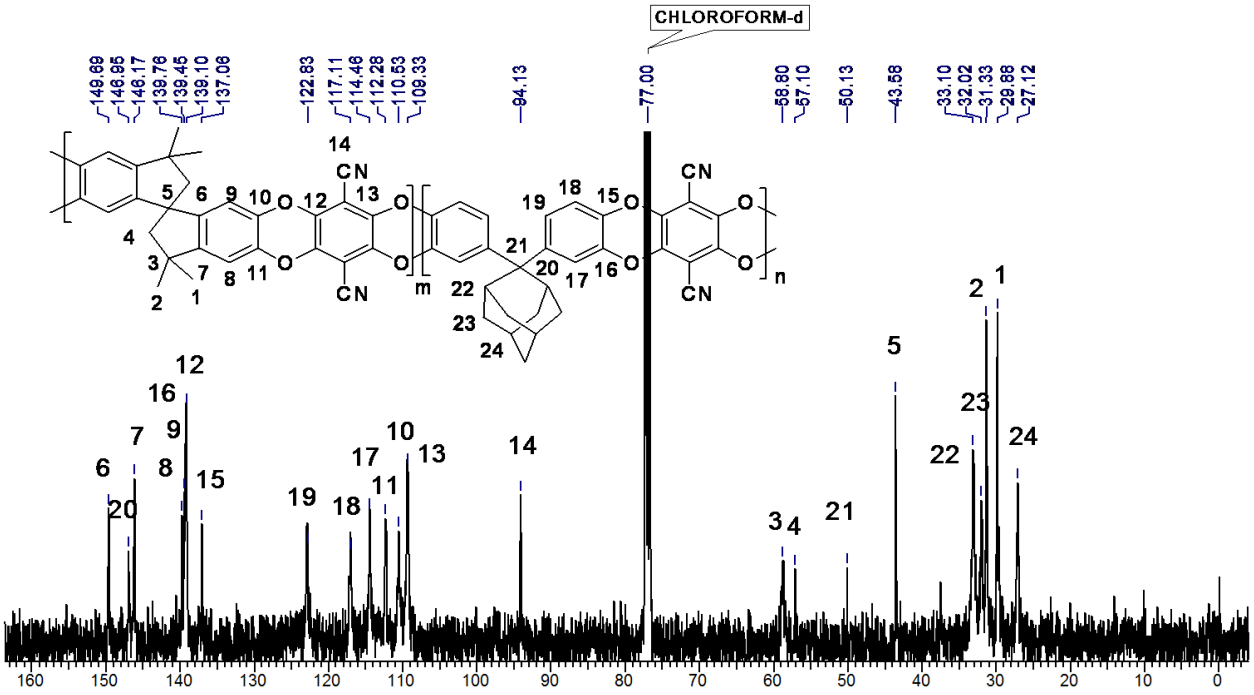

Figure SI 4.7: ^{13}C NMR spectrum (in $CDCl_3$) of ADM-PIM-50

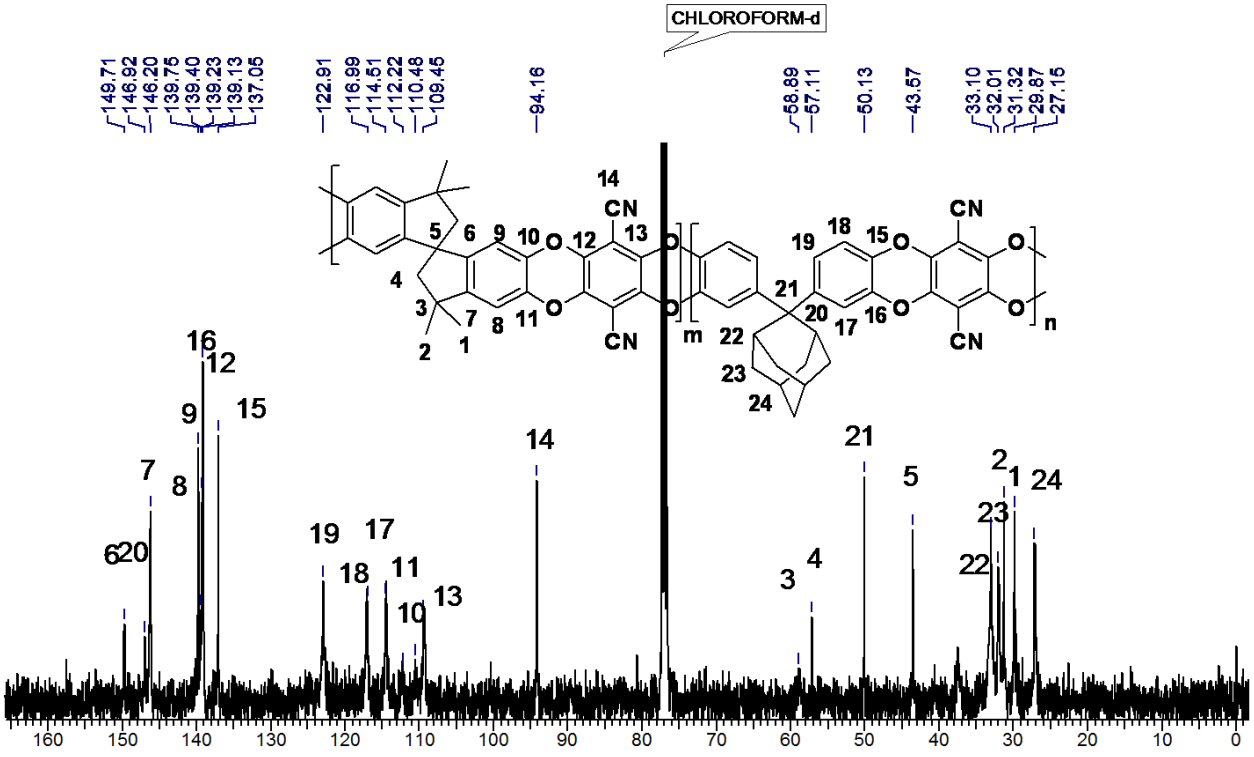

Figure SI 4.8: ^{13}C NMR spectrum (in $CDCl_3$) of ADM-PIM-75

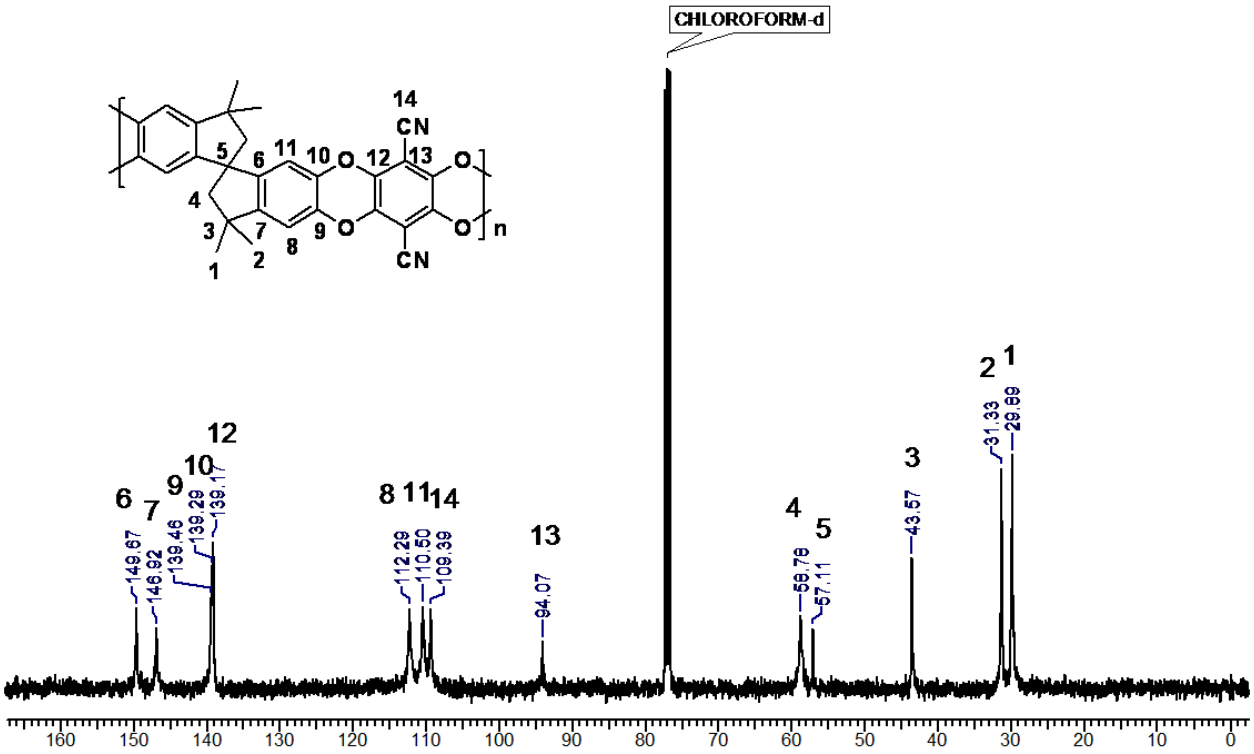

Figure SI 4.9: ^{13}C NMR spectrum (in $CDCl_3$) of PIM-1

Chapter 5

Intrinsically Microporous Polyimides Containing Spirobisindane and Phenazine Units: Synthesis, Characterization and Gas Permeation Properties

A new diamine containing spirobisindane and phenazine units, namely, 3,3,3',3'-tetramethyl-2,2',3,3'-tetrahydro-1,1'-spirobi[cyclopenta[b] phenazine]-7,7'-diamine (TTSBIDA) was designed and synthesized. A series of polyimides of intrinsic microporosity (PIM-PIs) were synthesized by polycondensation of TTSBIDA with commercially available aromatic dianhydrides viz., 1,2,4,5-benzenetetracarboxylic dianhydride (PMDA), 3,3',4,4'-benzophenonetetracarboxylic dianhydride (BTDA), 4,4'-(hexafluoro isopropylidene)diphthalic anhydride (6-FDA), 4,4'-oxydiphthalic anhydride (ODPA) and 4,4-(4,4-isopropylidenediphenoxy)bis(phthalic anhydride) (BPADA). Soluble PIM-PIs exhibited reasonably high molecular weights in the range 40000-42600 g/mol and could be cast into self-standing films. PIM-PIs possessed intrinsic microporosity and displayed BET surface area in the range 59-289 m^2/g. PIM-PIs showed excellent thermal stability with $T_{10\%}$ in the range 488-545 °C. PIM-PIs exhibited appreciable gas permeability and high selectivity. The CO_2 and O_2 permeability of PIM-PIs were in the range 185.4-39.2 and 30.6-6.2 Barrer, respectively. In particular, polyimide derived from TTSBIDA and 4,4'-(hexafluoroisopropylidene)diphthalic anhydride (PIM-PI-6FDA) showed high CO_2 and O_2 permeability of 185.4 and 30.6 Barrer with high CO_2/CH_4 and O_2/N_2 selectivity of 43.1 and 5.1, respectively. The gas permeability data of PIM-PIs was placed above 1991 Robeson upper bound.

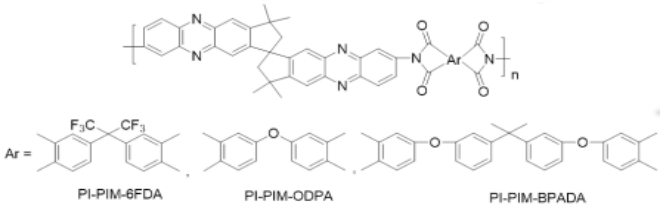

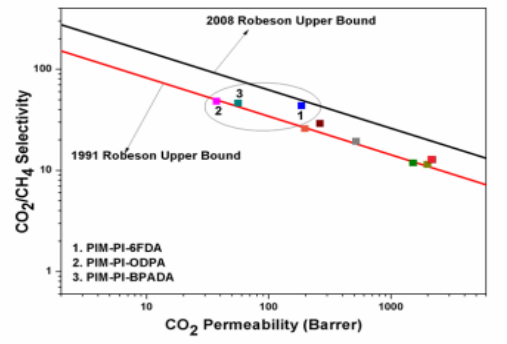

J. Polym. Sci. Part A: Polym. Chem., **2018**, 56, 766-775

5.1 INTRODUCTION

Owing to their high thermo-chemical stability, mechanical stability and structural tunability, aromatic polyimides (PIs) find applications in the fields such as aerospace, opto-electronic devices, memory devices and gas separation.[1] For gas separation applications, PIs possess high selectivity of one gas over other and low permeability.[1] Various strategies have been implemented to improve the gas separation performance of PIs which include the incorporation of bulky and propeller groups, ionic liquids, polar groups and the introduction of microporosity.[2,3] The incorporation of microporosity into PIs is one of the effective strategies to improve gas separation performance and has met with considerable success.[4] The introduction of microporosity into polyimide was first reported by Thomas *et al*. in 2007.[5] Subsequently, McKeown and co-workers in 2008 reported spirobisindane-containing PIM-PIs for gas separation studies and demonstrated that PIM-PIs surpassed 2008 Robeson upper bound.[6] To date, various structural units have been incorporated into polyimides which include triptycene,[7,8] Tröger's base,[9,10] spirobisindane,[11,4,12] spirobifluorene,[13] spirobichromane,[14] binaphthalene,[15] ethanoanthracene,[16] etc. These studies demonstrated that PIM-PIs are of great interest for achieving high separation performance.

Phenazine is a nitrogen containing heterocyclic ring which is known to improve thermal stability and processability.[17] Recently, highly thermally stable ladder type PIMs containing spirobisindane and phenazine units were synthesized.[18] It was demonstrated that PIMs exhibited good combination of gas permeability and selectivity due to the presence of phenazine and spirobisindane units in PIMs.[18] The previous studies suggested that PIM-1 and spirobisindane fused dibenzodioxine based PIM-PIs possessed some flexibility due to the presence of dibenzodioxine units.[4,19,20] In this context, eight membered dihydrooxocine ring was incorporated in PIM to enhance the rigidity of the system resulting into increase in both permeability and selectivity of the modified PIM compared to PIM-1.[21] Taking clues from above mentioned studies, it was considered worthwhile to synthesize polyimides containing both spirobisindane and phenazine units and to study their combined influence on the gas separation properties.

Towards this end, a new diamine containing spirobisindane and phenazine units, namely, 3,3,3',3'-tetramethyl-2,2',3,3'-tetrahydro-1,1'-spirobi[cyclopenta [b]phenazine]-7,7'-diamine (TTSBIDA) was designed and synthesized. TTSBIDA was polycondensed with aromatic dianhydrides to obtain the corresponding PIM-PIs. PIM-PIs were characterized by IR, X-ray diffraction, TGA, DSC, and N_2 adsorption and desorption measurements. The organosoluble PIM-PIs were also characterized by ^1H NMR spectroscopy, inherent viscosity and GPC

measurements. Gas permeation characteristics of selected PIM-PI membranes were evaluated by variable-volume method. The combined influence of spirobisindane and phenazine units on physical and gas permeation properties of PIM-PIs was investigated.

5.2 EXPERIMENTAL

Details of experimental techniques used such as solubility study, IR, ^{1}H and ^{13}C NMR spectroscopy, TGA, DSC, XRD, DFT, mechanical properties (tensile strength, % elongation at break and Young's modulus) and gas permeability analysis have already been given in **Chapter 3**.

5.2.1 Preparations

5.2.1.1 *Synthesis of 3,3,3',3'-tetramethyl-2,2',3,3'-tetrahydro-1,1'-spirobi[indene]-5,5',6,6'-tetraone (TTSBIQ)*

Into a 500 mL two necked round bottom flask equipped with a magnetic stirring bar and a nitrogen inlet were charged glacial acetic acid (75 mL), nitric acid (50 mL), 5,5′,6,6′-tetrahydroxy- 3,3,3′,3′-tetramethyl-1,1′-spiro-bisindane (60 g, 17.6 mmol) and ethanol (100 mL). The reaction mixture was stirred at 0 °C for 2 h and then at room temperature for 24 h. A deep red colored TTSBIQ was collected by filtration, washed with water followed by washing with ethanol. The product was dried under vacuum at 70 °C for 4 days**.**

Yield: 30.9 g, 52 %

Melting point: > 300 °C

IR ($CHCl_3$, cm^{-1}): 1656 (C=O stretching).

^{1}H-NMR (200 MHz, $CDCl_3$, δ/ppm): 6.26 (s, 2H, -CH), 6.16 (s, 2H, -CH), 2.30 (q, 4H, -CH_2), 1.40 (s, 6H, -CH_3), 1.38 (s, 6H, -CH_3).

^{13}C NMR (50 MHz, $CDCl_3$, δ/ppm): 178.8, 168.0, 166.8, 124.9, 121.3, 55.3, 54.3, 42.5, 29.5, 27.9.

HRMS (ESI): calcd. for $C_{21}H_{21}O_4$ ($[M+H]^+$): 337.1434; Found 337.1451.

5.2.1.2 *Synthesis of 3,3,3',3'-tetramethyl-7,7'-dinitro-2,2',3,3'-tetrahydro-1,1'-spirobi [cyclopenta[b]phenazine] (TTSBIDN)*

A 500 mL two-necked round bottom flask equipped with a magnetic stirring bar, a nitrogen inlet and a reflux condenser was charged with TTSBIQ (30 g, 89.2 mmol), 4-nitro-1,2-phenylenediamine (27.3 g, 178.4 mmol) and acetic acid (500 mL). The reaction mixture was refluxed for 24 h, cooled and precipitated into ice-cold water (1500 mL). The crude product was collected by filtration, washed with water (1000 mL) and dried under vacuum. The crude product was purified by column chromatography using pet ether: ethyl acetate (75: 25, v/v) as an eluent to obtain TTSBIDN as a yellow solid.

Yield: 11.2 g, 22 %

Melting point: > 300 °C

IR ($CHCl_3$, cm^{-1}): 1545 (-NO_2 asymmetric stretching) and 1353 (-NO_2 symmetric stretching).

^{1}H-NMR (200 MHz, $CDCl_3$, δ/ppm): 9.15 (d, J = 2.27 Hz, 2H, Ar-H), 8.47 (dd, J = 9.47 Hz, 2.53 Hz, 2H, Ar-H), 8.21 (d, J = 9.47 Hz, 2H, Ar-H), 8.15 (s, 2H, Ar-H), 7.74 (s, 2H, Ar-H), 2.83-2.68 (m, 4H, -CH_2), 1.73 (s, 6H, -CH_3), 1.65 (s, 6H, -CH_3).

^{13}C NMR (50 MHz, $CDCl_3$, δ/ppm): 159.7, 159.3, 147.8, 144.9, 144.9, 144.0, 141.2, 131.3, 126.5, 124.5, 122.8, 121.9, 59.7, 57.5, 44.2, 31.9, 30.1.

HRMS (ESI): Calcd. for $C_{33}H_{27}N_6O_4$ ($[M+H]^+$): 571.2088; Found 571.2089.

5.2.1.3 *Synthesis of 3,3,3',3'-tetramethyl-2,2',3,3'-tetrahydro-1,1'-spirobi[cyclopenta[b] phenazine]-7,7'-diamine (TTSBIDA)*

A 500 mL three-necked round bottom flask equipped with a magnetic stirring bar, a nitrogen inlet and a reflux condenser was charged with TTSBIDN (9 g, 15.8 mmol), 10 wt % Pd/C (1 g) and ethanol (150 mL). To the reaction mixture, hydrazine hydrate (35 mL) was added dropwise over a period of 1 h at room temperature under inert atmosphere and then the reaction mixture was refluxed overnight. After completion of the reaction (monitored by TLC), the reaction mixture was filtered, cooled and poured into water (1000 mL). The solids were collected by filtration, washed with water and dried under vacuum at 80 °C. The product was purified by recrystallization from ethanol to obtain TTSBIDA as a red solid.

Yield: 6.04 g, 75 %

Melting point: > 300 °C

IR ($CHCl_3$, cm^{-1}): 3410 (N–H asymmetric stretching) and 3260 (N-H symmetric stretching)

^{1}H-NMR (200 MHz, DMSO-d_6, δ/ppm): 7.8 (s, 2H, Ar-H), 7.74 (d, J = 9.16 Hz, 2H, Ar-H), 7.41 (s, 2H, Ar-H), 7.36 (dd, J = 9.16 Hz, 1.91 Hz, 2H, Ar-H), 6.92 (d, J = 1.91 Hz, 2H, Ar-H), 6.39 (s, 4H, -NH_2), 2.61-2.50 (m, 4H, -CH_2), 1.60 (s, 6H, -CH_3), 1.50 (s, 6H, -CH_3)

^{13}C NMR (50 MHz, DMSO-d_6, δ/ppm): 156.4, 153.2, 150.6, 145.2, 143.2, 139.8, 138.5, 129.9, 126.0, 123.3, 119.8, 101.4, 59.3, 56.4, 43.2, 31.4, 30.0

HRMS (ESI): Calcd. for $C_{33}H_{31}N_6$ ($[M+H]^+$): 511.2599; Found 511.2605

5.2.1.4 Synthesis of Polyimide

A 100 mL three-necked round bottom flask equipped with a magnetic stirring bar, a nitrogen inlet and a $CaCl_2$ guard tube was charged with TTSBIDA (1 g, 1.95 mmol) and *m*-cresol (12 mL). The reaction mixture was stirred until TTSBIDA dissolved and then 6-FDA (0.87 g, 1.95 mmol) was added at once. The reaction mixture was heated at 90 °C for 6 h and then at 200 ºC for 10 h. The viscous polymer solution was cooled to room temperature, precipitated into methanol, washed with methanol, filtered and dried at 100 ºC for 2 days under vacuum.

The other polyimides were synthesized by the same procedure as used for PIM-PI-6FDA.

5.2.2 Preparation of Dense Membranes

The films of PIM-PI-6FDA, PIM-PI-ODPA and PIM-PI-BPADA were prepared *via* solution casting method. The polymer was dissolved in NMP (~5% w/v), the solution was filtered and was poured onto a clean petridish. The solvent was slowly evaporated at 90 °C for 20 h. The obtained films were treated with methanol for 1 h to remove residual NMP. The methanol-treated films were dried at 120 °C for 4 days under vacuum. The thickness of dried films was measured by digital micrometer (60±5μm).

5.3 RESULTS AND DISCUSSION

5.3.1 Synthesis and Characterization of 3,3,3',3'-Tetramethyl-2,2',3,3'-tetrahydro-1,1'-spirobi[cyclopenta[b]phenazine]-7,7'-diamine (TTSBIDA)

A new diamine containing spirobisindane and phenazine units was designed and synthesized by a three step synthetic route as depicted in **Scheme 5.1**. In the first step, oxidation of commercially available 5,5′,6,6′-tetrahydroxy-3,3,3′,3′-tetramethyl-1,1′-spirobisindane (TTSBI) was carried out using nitric acid to obtain 3,3,3',3'-tetramethyl-2,2',3,3'-tetrahydro-1,1'-spirobi[indene]-5,5',6,6'-tetraone (TTSBIQ) in 52 % yield. TTSBIQ was characterized by IR (**Figure SI 5.1**), ^{1}H (**Figure SI 5.2**) and ^{13}C NMR (**Figure SI 5.3**) spectroscopy and HRMS analysis. Further, TTSBIQ was condensed with 4-nitro-1,2-phenylenediamine in acetic acid to afford 3,3,3',3'-tetramethyl-7,7'-dinitro-2,2',3,3'-tetrahydro-1,1'spirobi[cyclopenta[b] phenazine] (TTSBIDN) in 22 % yield. The structure of TTSBIDN was characterized by IR (**Figure SI 5.4**), ^{1}H (**Figure SI 5.5**) and ^{13}C NMR (**Figure SI 5.6**) spectroscopy and HRMS analysis. Finally, reduction of TTSBIDN was carried out using hydrazine hydrate to obtain 3,3,3',3'-tetramethyl-2,2',3,3'-tetrahydro-1,1'-spirobi[cyclopenta[b]phenazine]-7,7'-diamine (TTSBIDA) using catalytic amount of Pd/C as the catalyst in ethanol.

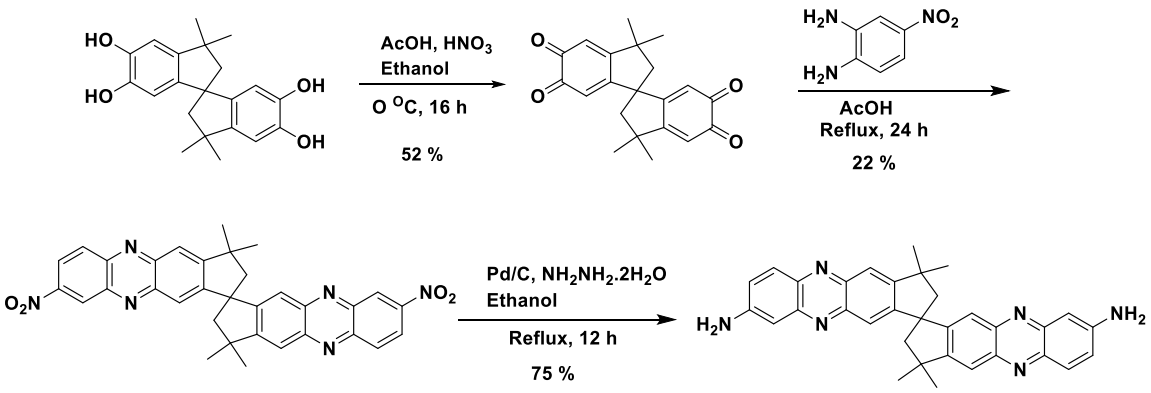

Scheme 5.1: Synthesis of 3,3,3',3'-tetramethyl-2,2',3,3'-tetrahydro-1,1'-spirobi[cyclopenta [b]phenazine]-7,7'-diamine (TTSBIDA).

The product was purified by crystallization from ethanol. The chemical structure of TTSBIDA was confirmed by IR, ^{1}H and ^{13}C NMR spectroscopy and HRMS analysis.

IR spectrum of TTSBIDA (**Figure 5.1**) exhibited bands at 3410 and 3260 cm^{-1} corresponding to asymmetric and symmetric stretching of $–NH_2$ group, respectively.

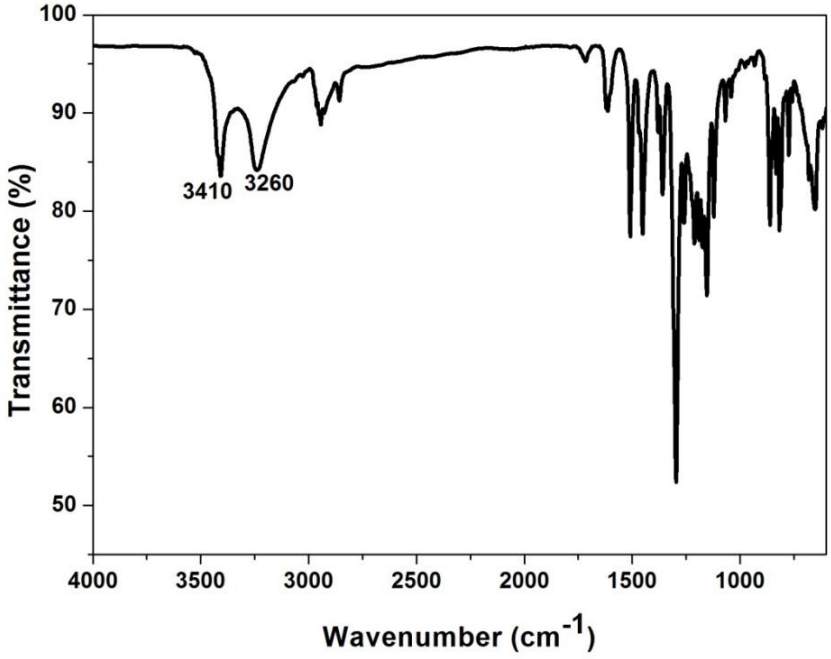

Figure 5.1: IR spectrum of 3,3,3',3'-tetramethyl-2,2',3,3'-tetrahydro-1,1'-spirobi [cyclopenta [b]phenazine]-7,7'-diamine (TTSBIDA).

^{1}H NMR spectrum of TTSBIDA is represented in **Figure 5.2**. In ^{1}H NMR spectrum, the peaks appeared at δ = 1.60 and 1.50 ppm corresponding to the two methyl groups while methylene protons appeared as multiplet in the range δ = 2.61-2.50 ppm and were overlapped with peaks due to DMSO-d_6 solvent. The aromatic protons of TTSBIDA were observed in the range δ = 7.89-6.92 ppm. The protons *ortho* and *meta* to amino group of aromatic ring appeared as two doublets at δ = 6.92 and 7.74 ppm and a doublet of doublet at δ = 7.37-7.35 ppm. It is worth to note that after reduction, the protons of TTSBIDN labelled as 1-3 shifted to upfield region in TTSBIDA spectrum due to shielding effect exerted by amino group. The protons of indane substituted aromatic rings labelled as 4 and 5 appeared as two singlets at δ = 7.89 and 7.41 ppm, respectively. In addition, the signal at δ = 6.39 ppm appeared due to $–NH_2$ groups which confirmed the formation of TTSBIDA.

2D NMR spectrum of TTSBIDA is shown in F**igure 5.3**. In 2D NMR spectrum, the proton labelled as 1 is coupled with 2 due to *meta* coupling, the proton labelled as 2 is coupled with 1 and 3 due to *meta* and *ortho* coupling, respectively and the proton labelled as 3 is coupled with 2 due to *ortho* coupling. It is noted that the coupling intensity of 2 and 3 is higher than that of 1 and 2 due to strong *ortho* coupling.

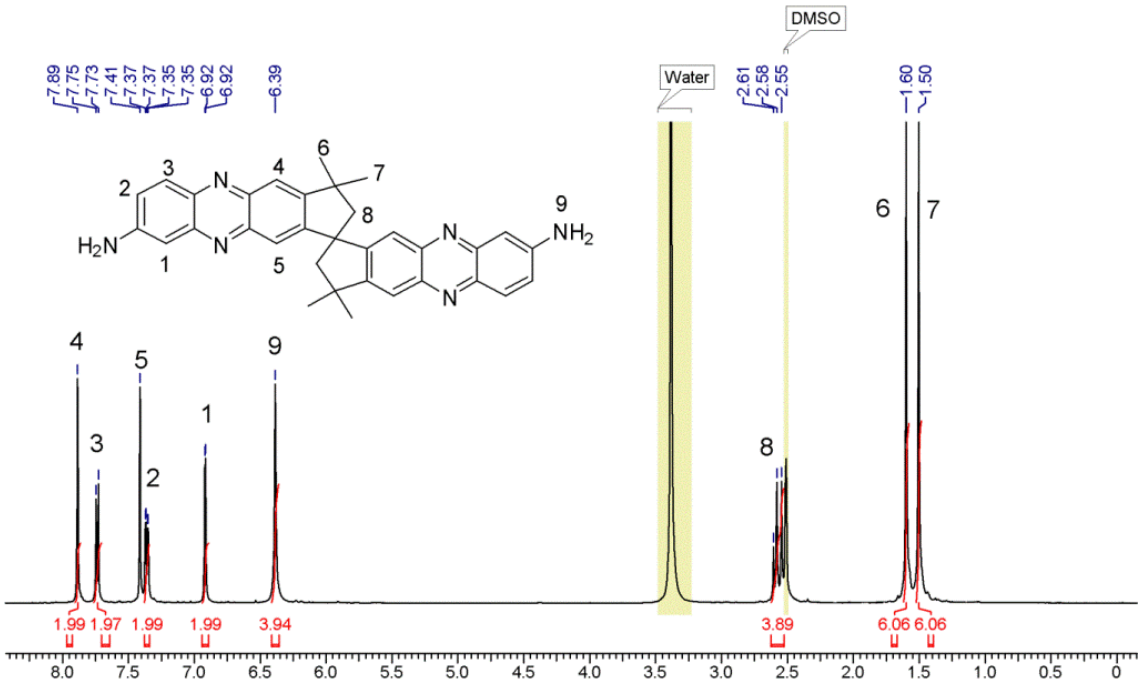

Figure 5.2: ^{1}H NMR spectrum (in DMSO-d_6) of 3,3,3',3'-tetramethyl-2,2',3,3'-tetrahydro-1,1'-spirobi[cyclopenta [b]phenazine]-7,7'-diamine **(**TTSBIDA).

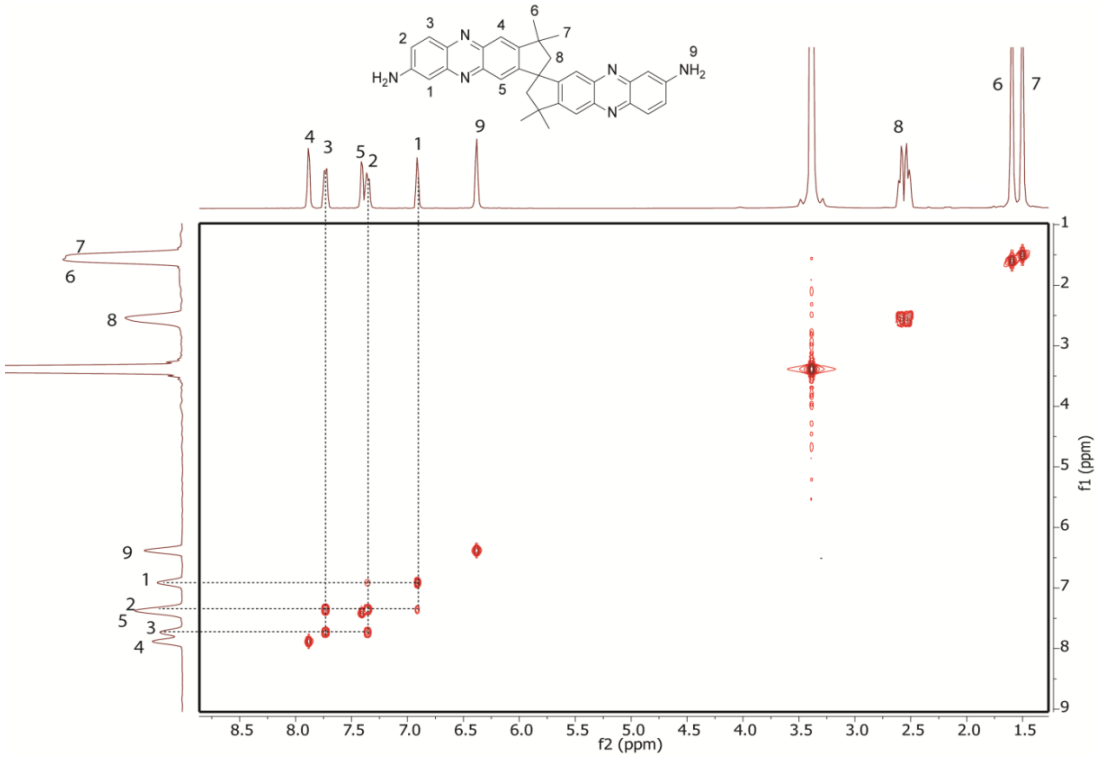

Figure 5.3: ^{1}H-^{1}H 2D NMR spectrum (in DMSO-d_6) of 3,3,3',3'-tetramethyl-2,2',3,3'-tetrahydro-1,1'-spirobi[cyclopenta[b] phenazine]-7,7'-diamine (TTSBIDA)

^{13}C NMR spectrum of TTSBIDA along with assignments is presented in **Figure 5.4.** In ^{13}C NMR spectrum, carbon attached to amino group appeared at δ = 156.4 ppm. The other aromatic carbon peaks appeared in the region δ = 153.2- 101.4 ppm while aliphatic carbons appeared in the region δ = 59.3-30.0 ppm.

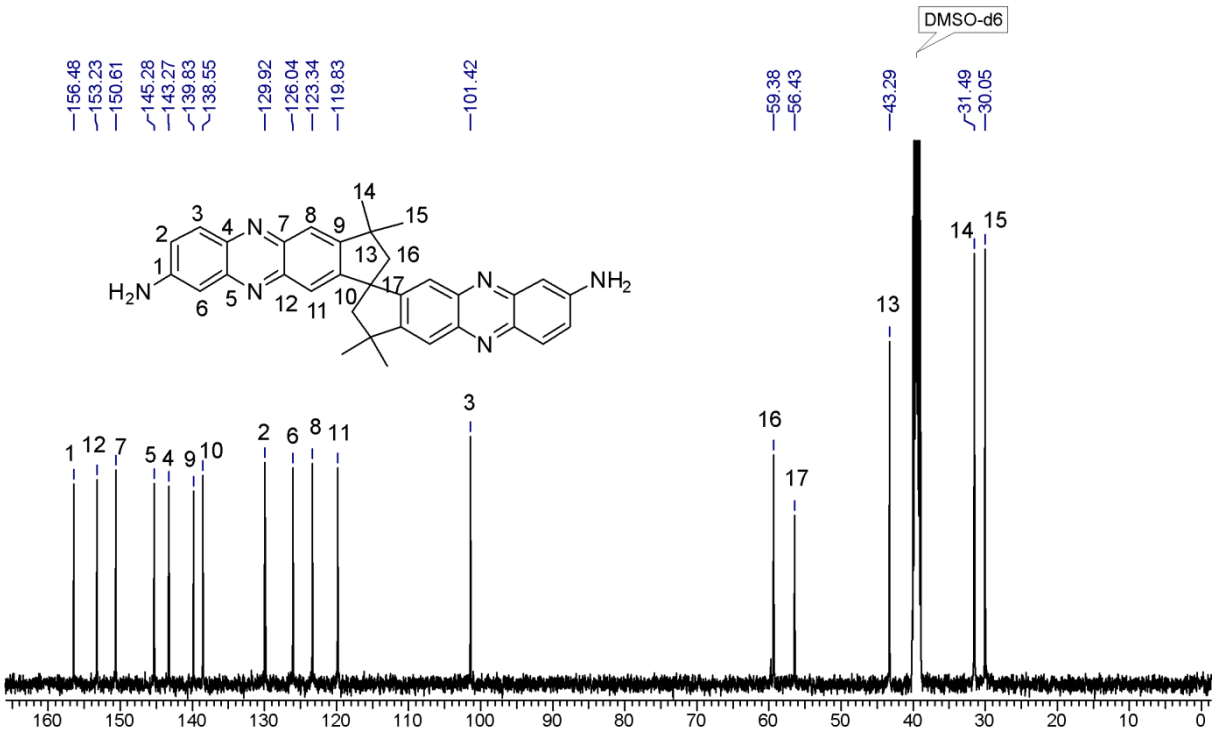

Figure 5.4: ^{13}C NMR spectrum (in DMSO-d_6) of 3,3,3',3'-tetramethyl-2,2',3,3'-tetrahydro-1,1'-spirobi[cyclopenta[b] phenazine]-7,7'-diamine (TTSBIDA)

In HRMS analysis (**Figure 5.5**), the peak appeared at 511.2605 corresponding to ($[M+H]^+$) of TTSBIDA (cald. $[M+H]^+$ for $C_{33}H_{31}N_6$ =511.2599).

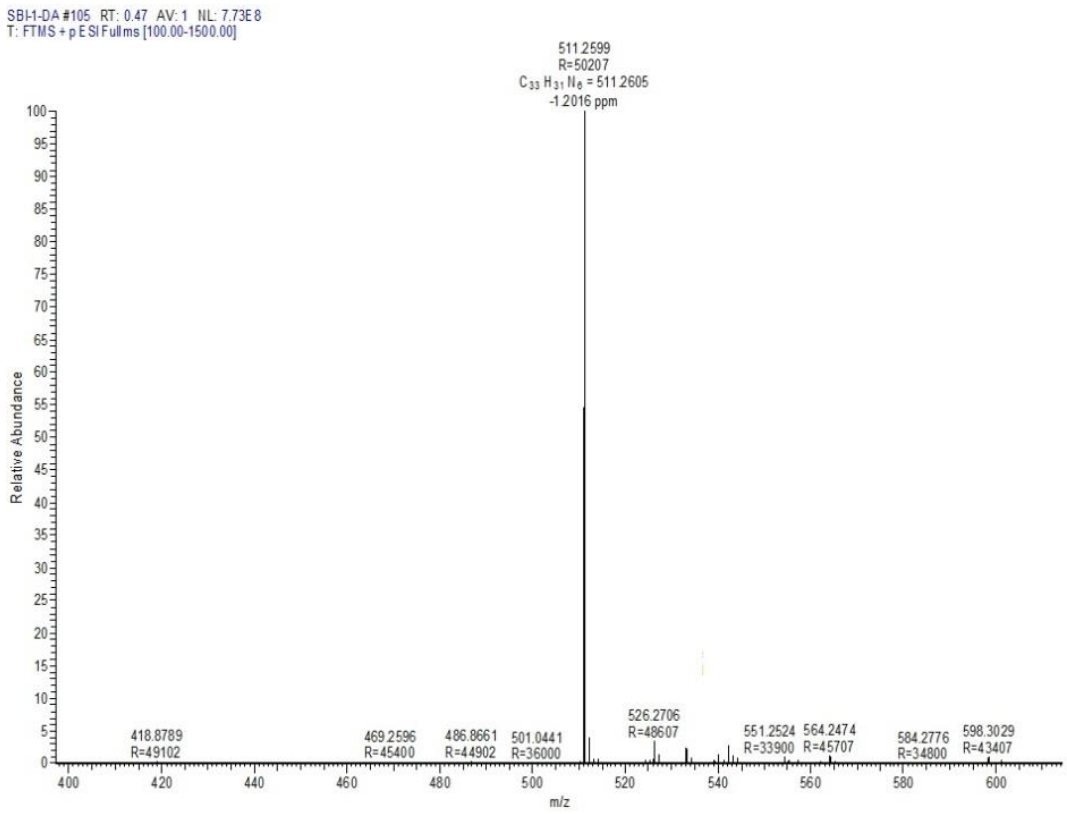

Figure 5.5: HRMS of 3,3,3',3'-tetramethyl-2,2',3,3'-tetrahydro-1,1'-spirobi[cyclopenta[b] phenazine]-7,7'-diamine (TTSBIDA).

5.3.2 Synthesis and Characterization of PIM-PIs Containing Spirobisindane and Phenazine Units

A series of PIM-PIs containing spirobisindane and phenazine units were synthesized from TTSBIDA and commercially available aromatic dianhydrides *viz.* 1,2,4,5-benzenetetracarboxylic dianhydride (PMDA), 3,3',4,4'-benzophenonetetracarboxylic dianhydride (BTDA), 4,4′-(hexafluoroisopropylidene)diphthalic anhydride (6-FDA), 4,4′-oxydiphthalic anhydride (ODPA) and 4,4-(4,4-isopropylidenediphenoxy)bis(phthalic anhydride) (BPADA) as shown in **Scheme 5.2**. The polycondensation was carried out using high temperature method in *m*-cresol by reacting stoichiometric quantities of TTSBIDA and aromatic dianhydride using isoquinoline as the catalyst. The polymerization reactions proceeded in a homogeneous fashion and polyimides were isolated by precipitation into methanol.

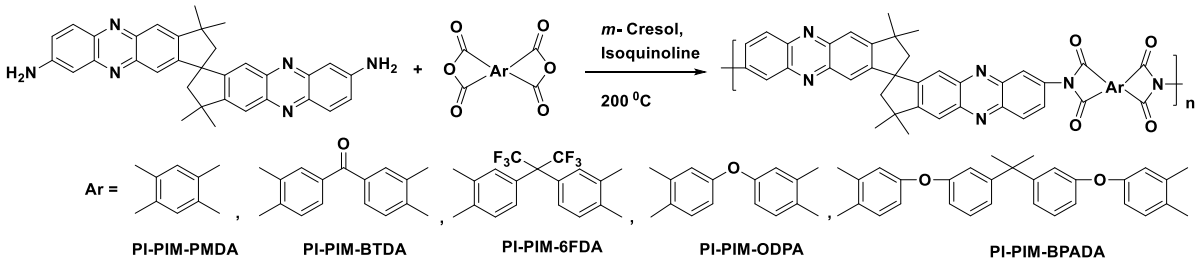

Scheme 5.2: Synthesis of polyimides containing spirobisindane and phenazine units

The formation of PIM-PIs was confirmed by IR, ^{1}H and ^{13}C NMR spectroscopy. A representative IR spectrum of PIM-PI-6FDA (**Figure 5.6**) showed the absorption bands at 1780 and 1722 cm^{-1} corresponding to asymmetric and symmetric stretching of imide, respectively. In addition, absorption bands of C-N and imide ring deformation were observed at 1345 and 824 cm^{-1}, respectively. IR spectra of other PIM-PIs are shown in the supporting information (**Figure SI 5.7).**

In ^{1}H NMR spectra of polyimides (PIM-PI-PMDA and PIM-PI-BTDA), all resonance signals could be assigned to the corresponding protons (**Figure 5.7 and 5.8**). In ^{1}H NMR spectrum, *ortho* protons to the imide ring labelled as 1-3 appeared in the downfield region due to deshielding effect exerted by electron withdrawing imide ring. It can be seen from ^{1}H NMR spectra that no peaks for amic acid of poly(amic acid) were observed, indicating complete conversion of polyamic acid to PI. PIM-PI-PMDA, PIM-PI-BTDA and PIM-PI-ODPA could not be analyzed by NMR spectroscopy as a consequence of their insolubility in $CDCl_3$ and DMSO-d_6.

^{13}C NMR spectra of PIM-PI-6FDA and PIM-PI-BPADA along with assignments are shown in **Figure SI 5.8 and 5.9**. Solid state ^{13}C NMR spectra of PIM-PI-PMDA, PIM-PI-BTDA, and PIM-PIODPA along with assignments of carbon atoms are included in the supporting information (**Figure SI 5.10-5.12**). ^{13}C NMR spectral data were in support of the formation of PIs.

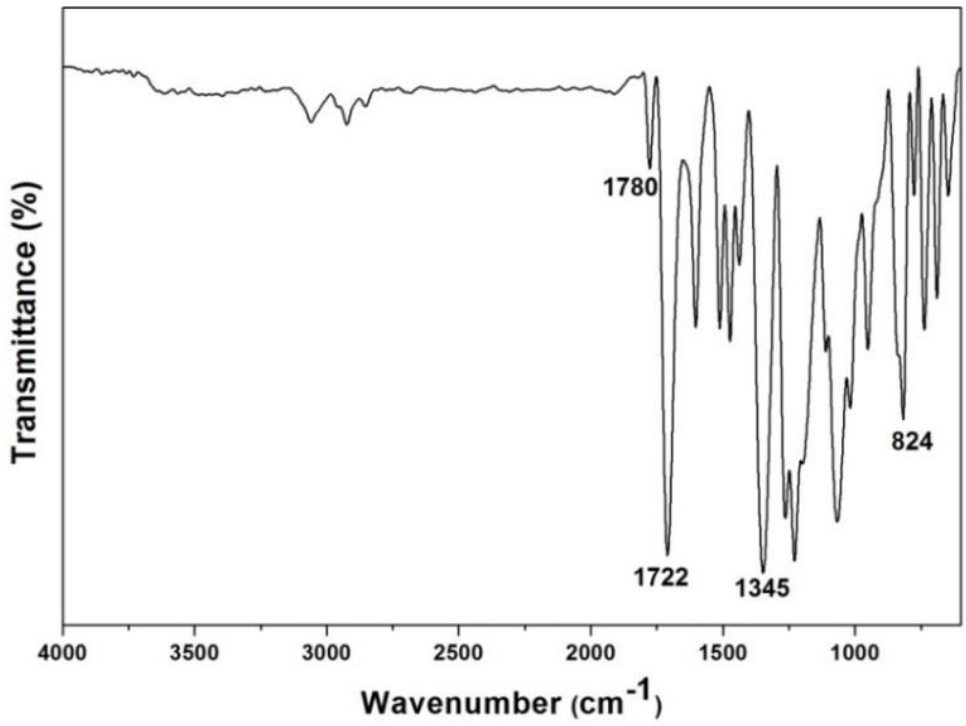

Figure 5.6: IR spectrum of PIM-PI-6FDA

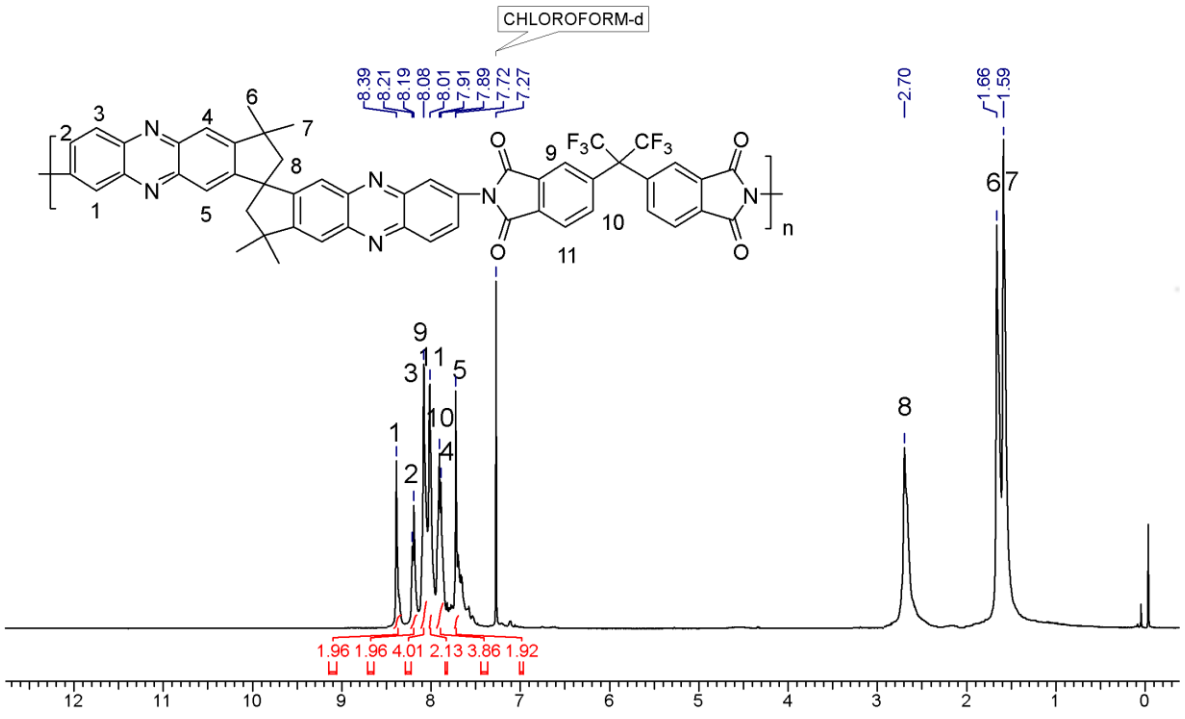

Figure 5.7: ^{1}H NMR spectrum (in $CDCl_3$) of PIM-PI-6FDA.

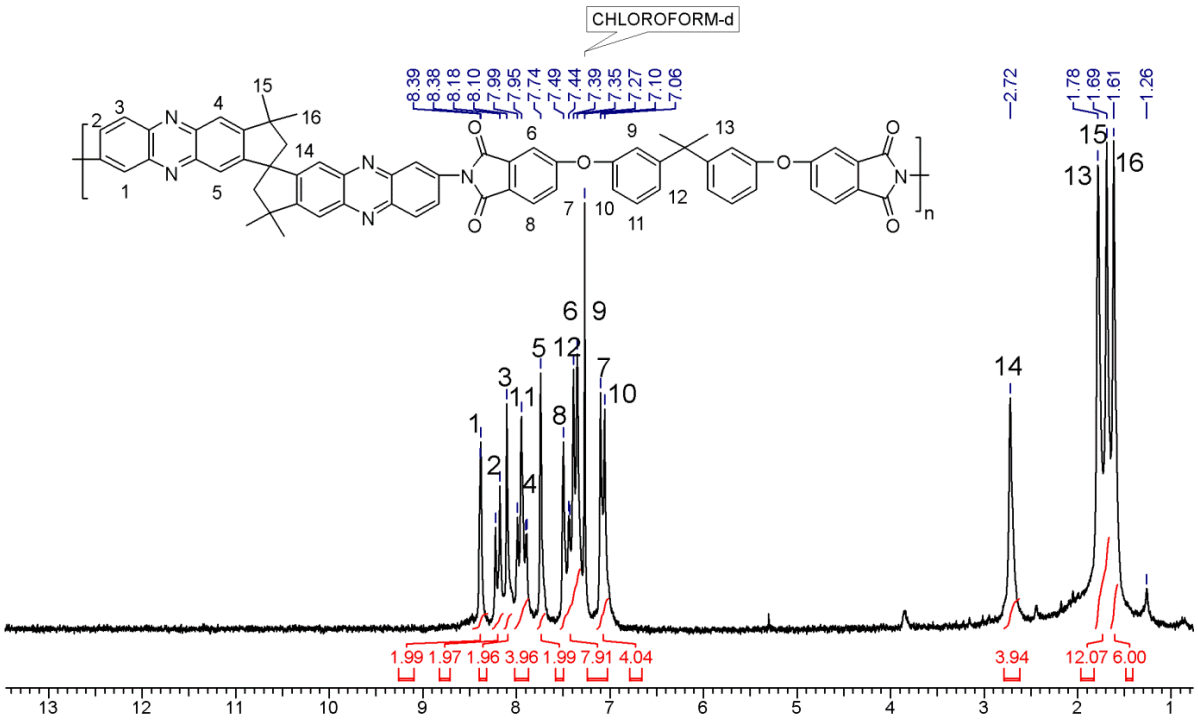

Figure 5.8: ^{1}H NMR spectrum (in $CDCl_3$) of PIM-PI-BPADA.

5.3.3 Solubility of PIM-PIs

The solubility tests of PIM-PIs containing spirobisindane and phenazine units (3 wt %) were carried out at room temperature in various organic solvents such as chlorofrom ($CHCl_3$), dichloromethane (DCM), tetrahydrofuran (THF), *N*,*N*-dimethylacetamide (DMAc), *N*-methyl-2-pyrrolidone (NMP), dimethyl sulfoxide (DMSO), toluene, and acetone (**Table 5.1**). PIM-PI-6FDA and PIM-PI-BPADA were found to be soluble in DCM, $CHCl_3$, DMAC and NMP while PIM-PI-ODPA was found to be soluble only in NMP. PIM-PI-PMDA and PIM-PI-BTDA were insoluble or partially soluble in tested organic solvents and hence their characterization by solution-based techniques was not possible. The lower solubility of PIM-PI-PMDA and PIM-PI-BTDA could be due to the presence of rigid dianhyride moities.

Table 5.1: Solubility data of PIM-PIs[a]

Sr. No.	Polymer	$CHCl_3$	DCM	THF	DMAc	NMP	DMSO	Toluene	Acetone
1	**PIM-PI-PMDA**	--	--	--	--	+-	--	--	--
2	**PIM-PI-BTDA**	--	--	--	--	+-	--	--	--
3	**PIM-PI-6FDA**	++	++	--	++	++	--	--	--
4	**PIM-PI-ODPA**	--	--	--	--	++	--	--	--
5	**PIM-PI-BPADA**	++	++	--	++	++	--	--	--

[a:] Solubility tests of PI-PIMs were carried out at 3 weight % (w/v) concentration at room temperature. ++ : Soluble, +- : Partially soluble, -- :Insoluble

5.3.4 Inherent Viscosity and Molecular Weights of PIM-PIs

Inherent viscosity of PIM-PI-6FDA, PIM-PI-ODPA and PIM-PI-BPADA was determined in NMP and the values were in the range 0.55-0.58 dL/g (**Table 5.2**). GPC analysis of PIM-PI-6FDA and PIM-PI-BPADA, both of which are soluble in $CHCl_3$, was carried out using polystyrene as a standard. Number average molecular weights of PIM-PI-6FDA and PIM-PI-BPADA were 40000 and 42600 g/mol, respectively while dispersity values were 2.1 and 2.6, respectively (**Table 5.2**). Inherent viscosity and GPC analysis indicated that polymers were of reasonably high molecular weights. Self-standing films of PIM-PIs could be cast from their solution in NMP, except for PIM-PI-PMDA and PIM-PI-BTDA. The films of PIM-PI-PMDA and PIM-PI-BTDA were not feasible due to their insolubility in organic solvents such as chloroform, THF, DMF, DMAc and NMP.

Table 5.2: Synthesis and properties of PIM-PIs

Sr. No.	Polymer	η_{inh} (dL/ g)[a]	M_n (g/mol)[b]	M_w (g/mol)[b]	Dispersity[c]	$T_{10\%}$[d] (°C)	Char Yield[e] (%)	T_g[f] (°C)
1	**PIM-PI-PMDA**	ns	ns	ns	ns	545	56	nd
2	**PIM-PI-BTDA**	ns	ns	ns	ns	542	55	nd
3	**PIM-PI-6FDA**	0.56	40000	84100	2.1	540	54	nd
4	**PIM-PI-ODPA**	0.55	ns	ns	ns	490	60	nd
5	**PIM-PI-BPADA**	0.58	42600	110000	2.6	488	48	350

[a:] Inherent viscosity was measured at a polymer concentration of 0.5 g/dL in NMP at 35±0.1 °C. [b:] Molecular weights were obtained from GPC in chloroform (Polystyrene standard). [c:] Dispersity: M_w/M_n. [d:] Temperature at which 10% weight loss was recorded by TGA at a heating rate of 10 °C/min. under N_2 atmosphere. [e:] Percentage char yield under nitrogen atmosphere at 900 °C. [f:] T_g was obtained from second heating scan in DSC. nd: Not detected. ns: Inherent viscosity and GPC measurements could not be carried out due to insolubility of PIM-PIs in $CHCl_3$, THF, DMF and NMP.

Table 5.3: Film density, FFV, *d*-spacing and BET surface area of PIM-PIs

Sr. No.	Polymer	ρ[a] (g/cm^3)	FFV[b] (%)	*d*-Spacing[c] (Å)	S_{BET}[d] (m^2/g)	Total pore volume[e]
1	**PIM-PI-PMDA**	–	–	5.46	59	0.16
2	**PIM-PI-BTDA**	–	–	5.50	65	0.21
3	**PIM- PI-6FDA**	1.17	17.7	5.67	289	0.42
4	**PIM- PI-ODPA**	1.25	13.7	5.53	134	0.26
5	**PIM-PI-BPADA**	1.19	16.3	5.60	143	0.28

[a:] Density was calculated by specific gravity bottle method. [b:] Fractional free volume was calculated from Bondi's equation (FFV= $V-V_o/V$). [c:] *d*-Spacing was calculated from XRD patterns using Bragg's equation. [d:] BET surface area was calculated from N_2 adsorption method. [e:] Pore volume was calculated from nitrogen adsorption at $p/p_o = 0.98$.

5.3.5 X-Ray Diffraction and Fractional Free Volume (FFV) of PIM-PIs

The crystallinity of polymers was determined by X-ray diffraction (XRD) analysis. In XRD patterns (**Figure 5.9**), PIM-PIs exhibited a broad halo over the range 2θ ≈ 10-30° which indicated their amorphous nature. The amorphous nature of these PIM-PIs could be attributed to the presence of rigid and contorted spirobisindane units which decreased inter-chain interaction by creating internal free volume. The *d*-spacing is the inter-chain distance between polymer chains. The *d*-spacing of PIM-PIs was calculated from peak maxima of XRD patterns using Bragg's equation and the values were in the range 5.46-5.67Å **(Table 5.3)**. In this series, the *d*-spacing varied with changing the dianhydride component in polymer. The order of *d*-spacing of PIM-PIs is as follows: PIM-PI-6FDA > PIM-PI-BPADA > PIM-PI-ODPA > PIM-PI-BTDA > PIM-PI-PMDA. PIM-PI-6FDA showed highest *d*-spacing in this series compared to other PIM-PIs. This could be attributed to the presence of bulky $–CF_3$ groups which disturbed polymer chain packing.

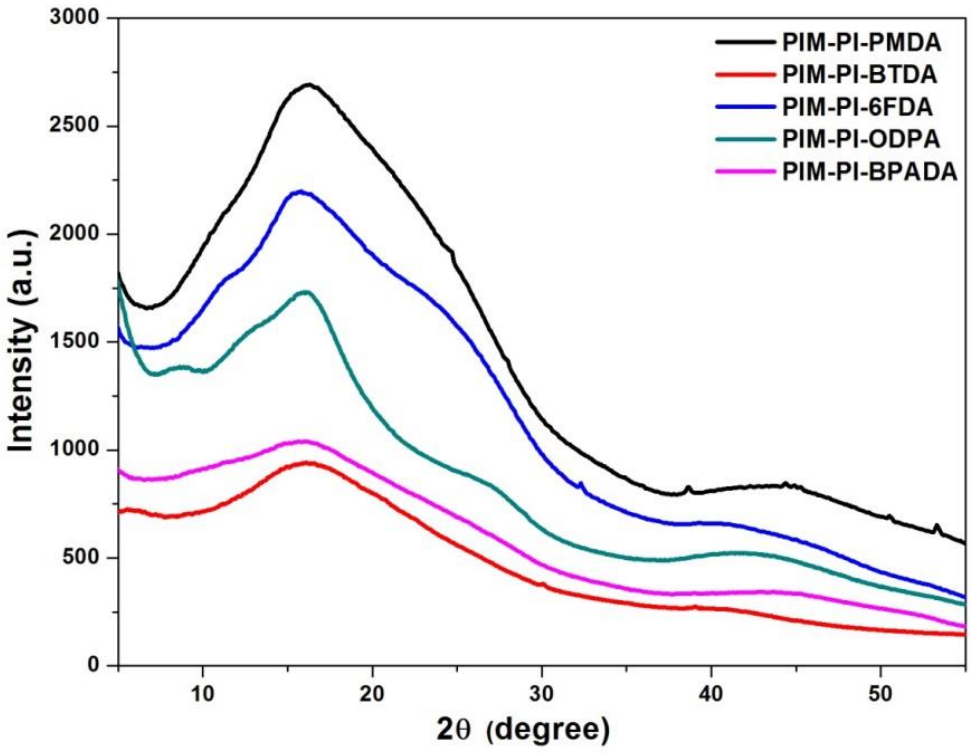

Figure 5.9: X-Ray diffractograms of PIM-PIs.

The density and fractional free volume (FFV) of PIM-PI membranes is given in **Table 5.3**. The density of PIM-PIs was determined by density bottle method and the values were in the range 1.17-1.25 g/cm^3. PIM-PI-6FDA showed lower density than PIM-PI-BPADA and PIM-PI-ODPA which could be due to presence of bulky $–CF_3$ groups which disturb packing of polymer chains. FFV was calculated by Bondi's method and the values are given in **Table 5.3**. The order of FFV is as: PIM-PI-6FDA > PIM-PI-BPADA > PIM-PI-ODPA. PIM-PI-

6FDA showed higher FFV than PIM-PI-BPADA and PIM-PI-ODPA because of the presence of bulky $–CF_3$ groups which hinder polymer chain packing. PIM-PI-BPADA exhibited higher FFV than PIM-PI-ODPA due to the presence of bulky isopropylidene ($C(CH_3)_2$) groups. These results are consistent with the bulkiness of substituent present in the dianhydride component of PIM-PIs which is in the order: (-($C(CF_3)_2$) > ($C(CH_3)_2$) > -O-) **(Table 5.4)**.[22] The higher FFV and lower density of PIM-PI-6FDA possessing $–CF_3$ groups supported loosening of chain packing in polymer matrix. The trends in the results can be further corroborated by taking into consideration van der Waals volume (V_w) of hinge groups present in dianhydride component of PIM-PIs. The V_w values of ($C(CF_3)_2$), ($C(CH_3)_2$) and -O- are 88.5, 44.35 and 5.5 cm^3 mol^{-1}, respectively **(Table 5.4)**.

Table 5.4: The van der Waals volumes of hinge group present in dianhydride moieties [22]

Sr. No.	Polymer code	Repeating unit	Hinge group	Van der walls volume (cm^3 mol^{-1})
1	**PI-6FDA**	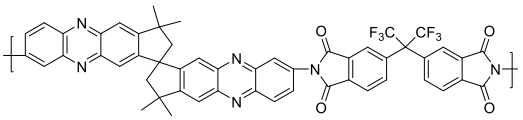	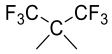	88.5
2	**PI-ODPA**	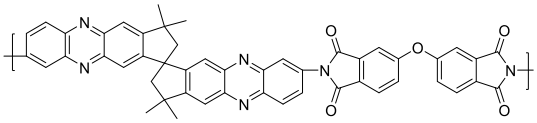		5.5
3	**PI-BPADA**	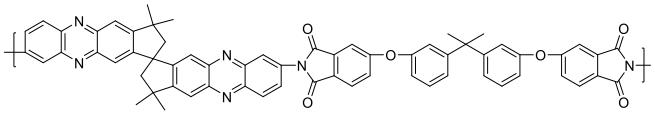	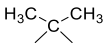	44.35

5.3.6 Thermal Properties of PIM-PIs

The thermal properties of PIM-PIs were analysed by thermogravimetric analysis and results are summarized in **Table 5.2** and **Figure 5.10**. The analysis was carried out under nitrogen at a heating rate of 10 °C / min. The temperature for 10 % weight loss and char yields at 900 °C of these PIM-PIs were observed in the range 488-545 °C and 48-60%, respectively, indicating their excellent thermal stability. In this series, the thermal stability varies with dianhydride component and the decreasing order is as follows: PIM-PI-PMDA > PIM-PI-BTDA > PIM-PI-6FDA> PIM-PI-ODPA > PIM-PI-BPADA. PIM-PI-PMDA showed highest T_{10} value in this series compared to other PIM-PIs. This could be attributed to the rigid structure of PMDA and higher density of imide linkages. As anticipated, PIM-PI-BPADA which contains BPADA exhibited lowest T_{10} value due to the presence of multiple ether linkages and lower percentage of imide linkages in the polymer backbone.

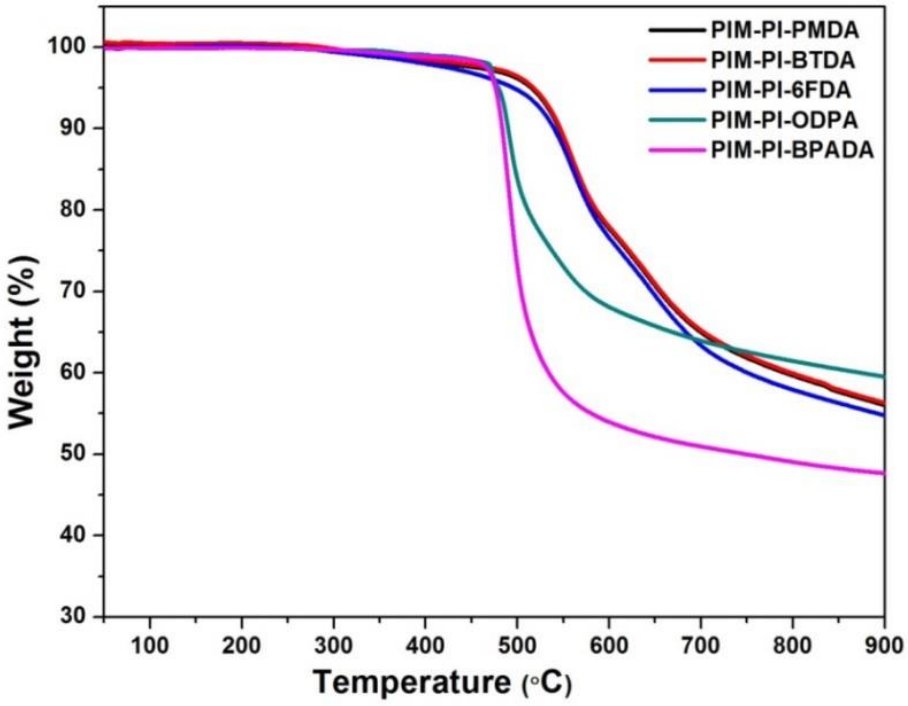

Figure 5.10: TG curves of PIM-PIs

Differential scanning calorimetry (DSC) was used to determine glass transition temperature of PIMs. The experiment was performed in the range 30-390 °C under N_2 atmosphere. Except for PIM-PI-BPADA which exhibited T_g value of 350 °C, T_g was not detected for PIM-PIs in DSC analysis carried out up to 390 °C which could be explained on the basis of highly rigid structure of PIM-PIs. T_g was not detected in DSC measurements for reported spirobisindane-containing PIM-PIs.[12]

5.3.7 Mechanical Properties of PIM-PIs

Mechanical properties of PIM-PIs are included in **Table 5.5**. PIM-PI films exhibited tensile strength, Young's modulus and elongation at break in the range 48.6-60.4 MPa, 1.09-1.47 GPa and 4.5-8.1 %, respectively. These data indicated that PIM-PIs showed good mechanical properties. The lower values of elongation at break of these PIM-PIs could be attributed to their rigid structures.

Table 5.5 Mechanical properties of PIM-PIs

Sr. No.	Polymer	Tensile Strength (MPa)	Young's Modulus (GPa)	Elongation at Break (%)
1	**PIM- PI-6FDA**	48.6±5.2	1.47±0.09	4.5 ±0.4
2	**PIM- PI-ODPA**	60.4±1.5	1.20±0.04	6.4±0.6
3	**PIM-PI-BPADA**	56.6±6.5	1.09±0.04	8.1±2.0

5.3.8 Intrinsic Microporosity of PIM-PIs

The nitrogen adsorption/desorption isotherms of PIM-PIs were measured at 77 K (**Figure 5.11)**. Before analysis, all samples were degassed at 120 °C for 12 h. The N_2 adsorption isotherms showed that the uptake of nitrogen increased with increase in pressure and exhibited characteristics loops similar to that of polymers of intrinsic microporosity (Type I).[23] The intrinsic microporosity of these PIM-PIs could be attributed to the presence of spirobisindane and fused phenazine units which hinder polymer chain packing by creating free volume. From nitrogen isotherms, BET surface area of PIM-PIs was determined and was in the range 59-289 m^2/g (**Table 4.3**). The decreasing order of BET surface area of PIM-PIs is as follows: PIM-PI-6FDA > PIM-PI-BPADA > PIM-PI-ODPA > PIM-PI-BTDA > PIM-PI-PMDA. PIM-PI-6FDA exhibited relatively higher BET surface area compared to other PIM-PIs. This could be attributed to the presence of $–CF_3$ groups which increase the free volume by hindering polymer chain packing. The BET surface area was in good agreement with trends in *d*-spacing and FFV.

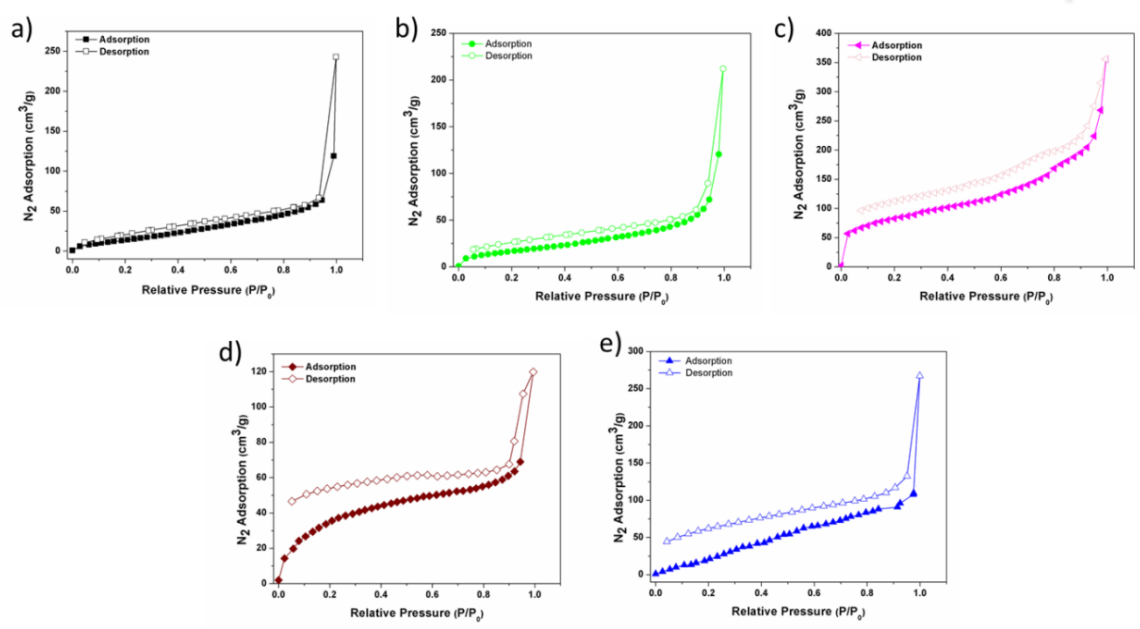

Figure 5.11: Nitrogen adsorption and desorption isotherms of PIM-PIs of a) PIM-PI-PMDA, b) PIM-PI-BTPA, c) PIM-PI-6FDA, d) PIM-PI-ODPA and e) PIM-PI-BPADA

5.4 GAS PERMEABILITY

The gas permeability of films of PIM-PI-6FDA, PIM-PI-ODPA and PIM-PI-BPADA was determined for He, H_2, N_2, O_2, CH_4 and CO_2 by the variable-volume method at 4-5 bar and at room temperature (**Table 5.6 and 5.7**). For all PIMs, the order of gas permeability is as follows: CO_2 > H_2 > He > O_2 > CH_4 > N_2. A similar trend was reported in the literature for spirobisindane-containing PIM-PIs.[20]

5.4.1 Effect of Spirobisindane, Phenazine and Dianhydride on Gas Permeability

The present PIM-PIs showed higher selectivity as compared to spirobisindane-containing PIM-PIs (**Table 5.6** and **5.7**). PIM-PIs exhibited appreciable gas permeability as well as high selectivity due to the introduction of spirobisindane and fused phenazine units. In this series, the gas permeability increased with bulkiness of the hinge groups in dianhydride component and the decrease in the order is as follows: PIM-PI-6FDA > PIM-PI-BPADA > PIM-PI-ODPA. PIM-PI-6FDA derived from TTSBIDA and 6-FDA was found to be comparatively more permeable for all gases than PIM-PIs derived from TTSBI and ODPA or BPADA. For example, the CO_2 permeability of PIM-PI-6FDA was observed to be ~four fold higher than that of PIM-PI-BPADA and PIM-PI-ODPA. These results could be attributed to the presence of bulky $–CF_3$ groups which increased gas permeability due to increased free volume as well as maintained selectivity by hindering chain rotation. PIM-PI-BPADA showed higher permeability and lower selectivity than PIM-PI-ODPA because of the presence of bulky isopropylidene $[C(CH_3)_2]$ linkages in the former. The gas permeability data was in good agreement with *d*-spacing, BET surface area and FFV.

Table 5.6: Gas permeability of PIM-PIs

Sr. No.	Polymer	Permeability (Barrer)[a,b,c]					
		He	**H_2**	**N_2**	**O_2**	**CH_4**	**CO_2**
1	**PIM-PI-6FDA**	119.6	162.0	6.0	30.6	4.3	185.4
		(79.5)	(102.8)	(4)	(21.2)	(3.0)	(132.6)
2	**PIM-PI-ODPA**	30.3	35.1	1.1	6.2	0.8	39.2
		(20.5)	(26.4)	(0.8)	(4.8)	(0.6)	(30.0)
3	**PIM-PI-BPADA**	35.7	50.6	1.8	9.4	1.2	56.3
		(26.7)	(34.1)	(1.0)	(5.8)	(0.7)	(34.1)
4	**PIM-PI-1**[20]	340	750	91	284	175	2000
5	**PIM-PI-3**[20]	190	360	23	85	27	520
6	**PIM-PI-9**[20]	400	840	94	295	170	2180
7	**PIM-PI-10**[20]	300	670	84	270	168	2154
8	**PIM-PI-11**[20]	332	624	65	208	129	1523
9	**PIM-6FDA-OH**[12]	-	259	10.8	45.2	9.1	263
10	**PIM-PMDA-OH**[12]	-	190	6.9	30.5	7.7	198

[a:] Units of permeability (P): 1 Barrer = 10^{-10} cm^3(STP) cm cm^{-2} s cm Hg. [b:] Gas permeability of aged films (260 days) of PIM-PIs are given in parentheses. [c:] Gas permeability data taken from literature (entries 4-10) are marked in red.

Table 5.7: Gas selectivity of PIM-PIs

Sr. No.	Polymer	Selectivity[a,b,c]			
		H_2/N_2	O_2/N_2	CO_2/N_2	CO_2/CH_4
1	**PIM-PI-6FDA**	27.0 (25.7)	5.1 (5.3)	30.9 (33.1)	43.1 (44.2)
2	**PIM-PI-ODPA**	31.9 (35.2)	5.6 (6.0)	35.6 (37.5)	49.0 (50.0)
3	**PIM-PI-BPADA**	28.1 (34.1)	5.2 (5.8)	31.3 (34.1)	46.9 (48.7)
4	**PIM-PI-1**[20]	8.24	3.1	22.0	11.4
5	**PIM-PI-3**[20]	15.7	3.7	22.6	19.3
6	**PIM-PI-9**[20]	8.93	3.1	23.2	12.7
7	**PIM-PI-10**[20]	7.97	3.2	25.6	12.8
8	**PIM-PI-11**[20]	9.6	3.2	23.4	11.8
9	**PIM-6FDA-OH**[12]	24	4.2	24	28.9
10	**PIM-PMDA-OH**[12]	28	4.5	29	25.71

[a:] Selectivity (α) = P_1/P_2. [b:] Gas selectivity of aged films (260 days) of PIM-PIs are given in parentheses. [c:] Gas selectivity data taken from literature (entries 4-10) are marked in red.

5.4.2 Effect of Physical Aging on Gas Permeability

The gas permeability measurements of PIM-PI membranes physically aged at room temperature for 260 days were carried out and the results are included in **Table 5.6** and **5.7**. After physical aging, decrease in gas permeability and increase in selectivity was observed. For instance, CO_2 permeability of PIM-PIs decreased from 39.2-185.4 to 30.0-132.6 Barrer while selectivity for CO_2/CH_4 increased from 43.1-49 to 44.2-50. These results could be attributed to the reduction in free volume with time upon aging of PIM-PIs. Similar observations have been reported in the literature.[24,25]

5.4.3 Comparison of Present PIM-PIs with Reported Spirobisindane-Based Polymers

In gas separation, PIs have been explored more than any other class of glassy polymers.[26] The literature reported data on spirobisindane-containing PIM-PIs are also included in **Table 5.6** and **5.7** (Sr. No. 4–10) for comparison.[4,12,20] It could be seen from **Figure 5.12** that these PIM-PIs exhibited promising results and are positioned near or above 1991 Robeson upper bound. The present PIM-PIs are less permeable, however, the selectivity of present PIM-PIs is higher than reported spirobisindane-containing PIM-PIs. This result could be due to the additional rigidity imposed by the presence of phenazine units in PIM-PIs. In particular, the data of PIM-PI-6FDA for the O_2/N_2 gas pair was located near 1991 Robeson upper bound and for CO_2/CH_4 gas pair, the data was above 1991 Robeson upper bound. The selectivity for

O_2/N_2 and CO_2/CH_4 gas pairs demonstrated that the present PIM-PIs are potentially attractive membrane materials for gas separation especially for CO_2 and O_2.

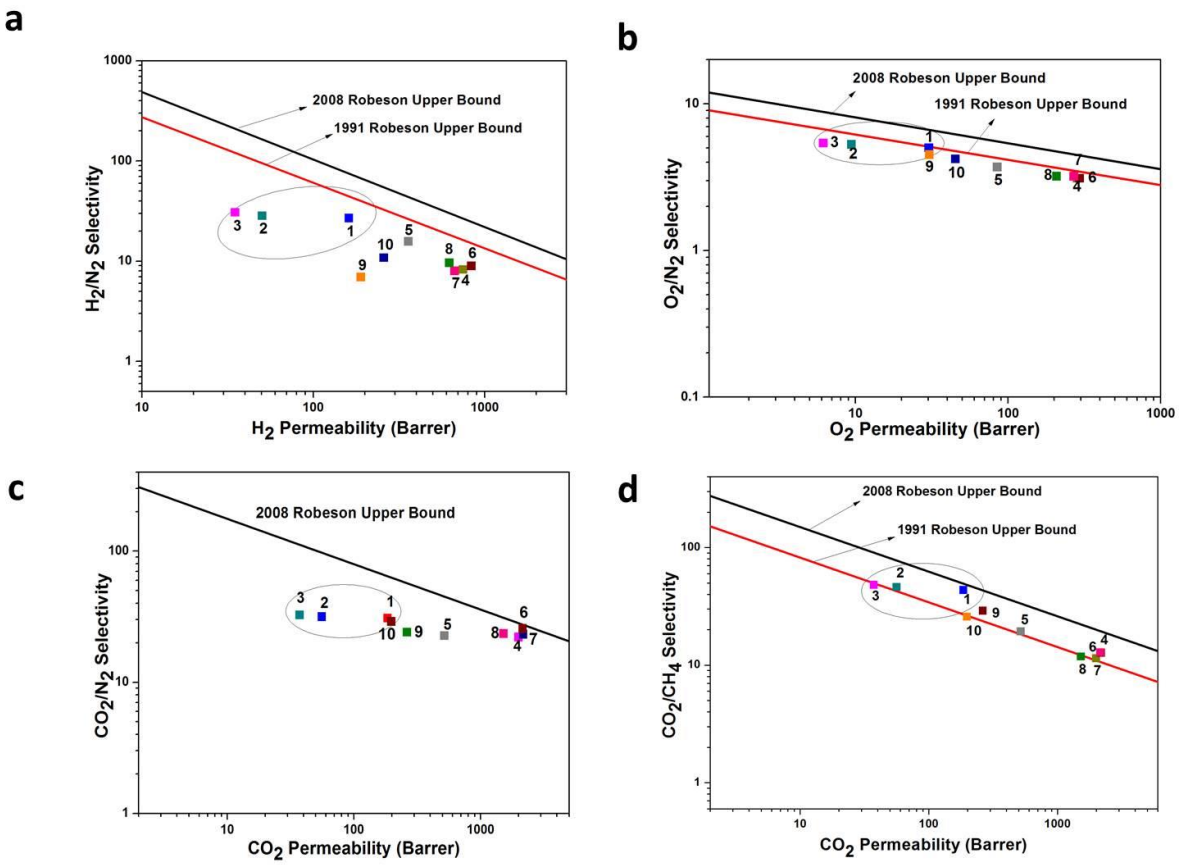

Figure 5.12: Robeson plots of (1) PIM-PI-6FDA, (2) PIM-PI-ODPA, (3) PIM-PI-BPADA and (4) PIM-PI-1 [21], (5) PIM-PI-3 [21], (6) PIM-PI-9 [30], (7) PIM-PI-10 [30], (8) PIM-PI-11 [32], (9) PI-6FDA-OH [22], (10) PI-PMDA-OH [22].

5.4.4 Density Functional Theory (DFT) Analysis

The observed high selectivity of present PIM-PIs could be further explained by DFT calculations. The reported PIM-PI-3 containing spirobisindane fused dibenzodioxane and PIM-PI-6FDA containing spirobisindane fused phenazine were selected for the comparison (**Figure 5.13**). The rigidity parameters of PIMs such as SBF-PIM,[27] PMDA−SBF and PMDA−BSBF,[13] PIM-1 and PIM-C1[21] and TPE-PIM[25] have been calculated and reported in the literature. These results demonstrated that more energy is required for more rigid structure due to more densely packed structure. The dihedral angle potential energy surface for the specified dihedrals were calculated using Density Functional Theory (DFT) with Turbomole 6.0 software package.[28] Dihedrals were constrained and optimized at ten degrees of increment at PBE[29]/TZVP[30] level of theory. The structural rigidity parameters were calculated by fitting a harmonic model to the obtained dihedral angle potential energy surface. Additional details concerning computational studies are included in the supporting information. The rigidity

parameter values of PIM-PI-6FDA and PIM-PI-3 (**Figure 5.13**) were 24.4 Kcal mol^{-1} rad^{-2} and 8.5 Kcal mol^{-1} rad^{-2}, respectively. DFT results indicated that the system containing phenazine fused to spirobisndane is more rigid than the system containing dibenzodioxin fused to spirobisindane which is reflected in the higher selectivity exhibited by PIM-PI-6FDA compared to PIM-PI-3.

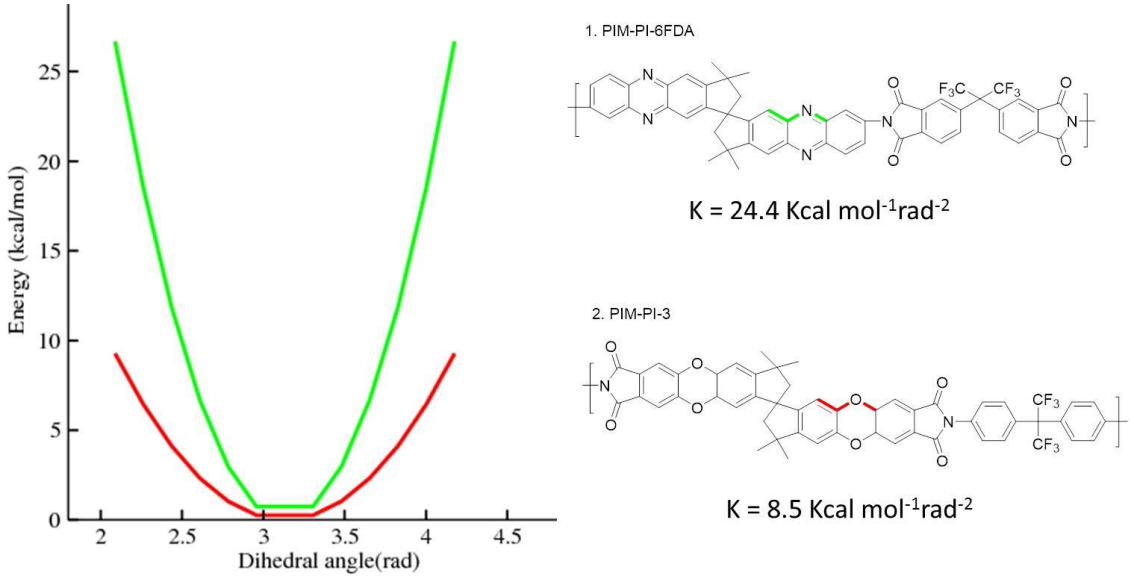

Figure 5.13: Dihedral angle potential energy surfaces calculated at PBE/TZVP level of theory.

5.5 CONCLUSIONS

In conclusion, a new aromatic diamine containing spirobisindane and phenazine units, namely, 3,3,3',3'-tetramethyl-2,2',3,3'-tetrahydro-1,1'-spirobi[cyclopenta[b]phenazine]-7,7'-diamine (TTSBIDA) was designed and successfully synthesized. A new series of PIM-PIs containing spirobisindane and phenazine units were synthesized from TTSBIDA and commercially available aromatic dianhydrides by polycondensation in *m*-cresol using the high-temperature solution method. PIM-PIs exhibited reasonably high molecular weights (40000-42600 g/mol), high BET surface area (59-289 m^2/g) and excellent thermal stability (T_{10} = 488-545 °C). The films of PIM-PI-6FDA, PIM-PI-ODPA and PIM-PI-BPADA could be cast from their NMP solutions. The gas permeation studies of selected PIM-PIs demonstrated appreciable gas permeability and high selectivity. Particularly, PIM-PI-6FDA exhibited high CO_2 permeability of 185.4 Barrer and high CO_2/N_2 and CO_2/CH_4 gas pair selectivity of 30.9 and 43.1, respectively. The gas separation performance of the present PIM-PIs was near or above 1991 Robeson upper bound. These results suggested that PIM-PIs containing spirobisindane and phenazine units are attractive candidates for gas separation applications.

5.6 REFERENCES

1. Liaw, D. J., Wang, K. L., Huang, Y. C., Lee, K. R., Lai, J. Y., Ha, C. S. *Prog. Polym. Sci.*, 2012, **37**, 907–974.
2. Dhara, M. G., Banerjee, S. *Prog. Polym. Sci.*, 2010, **35**, 1022–1077.
3. Shaplov, A. S., Morozova, S. M., Lozinskaya, E. I., Vlasov, P. S., Gouveia, A. S. L., Tomé, L. C., Marrucho, I. M., Vygodskii, Y. S. *Polym. Chem.*, 2016, **7**, 580–591.
4. Ghanem, B. S., McKeown, N. B., Budd, P. M., Al-Harbi, N. M., Fritsch, D., Heinrich, K., Starannikova, L., Tokarev, A., Yampolskii, Y. *Macromolecules*, 2009, **42**, 7881–7888.
5. Weber, J., Su, Q., Antonietti, M., Thomas, A. *Macromol. Rapid Commun.*, 2007, **28**, 1871–1876.
6. Ghanem, B. S., McKeown, N. B., Budd, P. M., Selbie, J. D., Fritsch, D. *Adv. Mater.*, 2008, **20**, 2766–2771.
7. Ghanem, B. S., Swaidan, R., Litwiller, E., Pinnau, I. *Adv. Mater.*, 2014, **26**, 3688–3692.
8. Swaidan, R., Al-Saeedi, M., Ghanem, B., Litwiller, E., Pinnau, I. *Macromolecules*, 2014, **47**, 5104–5114.
9. Wang, Z., Wang, D., Zhang, F., Jin, J. *ACS Macro Lett.*, 2014, **3**, 597–601.
10. Lee, M., Bezzu, C. G., Carta, M., Bernardo, P., Clarizia, G., Jansen, J. C., McKeown, N. B. *Macromolecules*, 2016, **49**, 4147–4154.
11. Wang, Z., Wang, D., Jin, J. *Macromolecules*, 2014, **47**, 7477–7483.
12. Ma, X., Swaidan, R., Belmabkhout, Y., Zhu, Y., Litwiller, E., Jouiad, M., Pinnau, I., Han, Y. *Macromolecules*, 2012, **45**, 3841–3849.
13. Ma, X., Salinas, O., Litwiller, E., Pinnau, I. *Macromolecules*, 2013, **46**, 9618–9624.
14. Zhang, C., Li, P., Cao, B. *J. Membr. Sci.*, 2017, **530**, 176–184.
15. Ritter, N., Senkovska, I., Kaskel, S., Weber, J. *Macromol. Rapid Commun.*, 2011, **32**, 438–443.
16. Rogan, Y., Malpass-Evans, R., Carta, M., Lee, M., Jansen, J. C., Bernardo, P., Clarizia, G., Tocci, E., Friess, K., Lanč, M., McKeown, N. B. *J. Mater. Chem. A*, 2014, **2**, 4874–4877.
17. H.M. Gajiwala, R. Z. *Polymer*, 2006, **94**, 254–260.
18. Ghanem, B., Alghunaimi, F., Alaslai, N., Ma, X., Pinnau, I. *RSC Adv.*, 2016, **6**, 79625–79630.
19. Heuchel, M., Fritsch, D., Budd, P. M., McKeown, N. B., Hofmann, D. *J. Membr. Sci.*, 2008, **318**, 84–99.
20. Rogan, Y., Starannikova, L., Ryzhikh, V., Yampolskii, Y., Bernardo, P., Bazzarelli, F., Jansen, J. C., McKeown, N. B. *Polym. Chem.*, 2013, **4**, 3813–3820.
21. Zhang, J., Kang, H., Martin, J., Zhang, S., Thomas, S., Merkel, T. C., Jin, J. *Chem. Commun.*, 2016, **52**, 6553–6556.
22. Ghosh, S., Banerjee, S. *J. Membr. Sci.*, 2016, **497**, 172–182.
23. McKeown, N. B. *ISRN Mater. Sci.*, 2012, **2012**, 1–16.
24. Ghanem, B., Alghunaimi, F., Ma, X., Alaslai, N., Pinnau, I. *Polymer*, 2016, **101**, 225–232.
25. Ma, X., Pinnau, I. *Polym. Chem.*, 2016, **7**, 1244–1248.
26. Sanders, D. F., Smith, Z. P., Guo, R., Robeson, L. M., McGrath, J. E., Paul, D. R., Freeman, B. D. *Polymer*, 2013, 54, 4729–4761.
27. Bezzu, C. G., Carta, M., Tonkins, A., Jansen, J. C., Bernardo, P., Bazzarelli, F., Mckeown, N. B. *Adv. Mater.*, 2012, **24**, 5930–5933.
28. Ahlrichs, R., Bar, M., Marco, H., Horn, H., Kolmel, C. *Chem. Phys. Lett.*, 1989, **162**, 165–169.
29. Perdew, J. P., Burke, K., Ernzerhof, M. *Phys. Rev. Lett.*, 1997, **78**, 1396–1396.
30. Schäfer, A., Huber, C., Ahlrichs, R., Schafer, A., Huber, C., Ahlrichs, R. *J. Chem. Phys.*, 1994, **8**, 5829–5835.

31. Eichkorn, K., Treutler, O., Ohm, H., Marco, H., Ahlrichs, R. *Chem. Phys. Lett.*, 1995, **4**, 283–290.
32. Sierka, M., Hogekamp, A., Ahlrichs, R. *J. Chem. Phys.*, 2003, **9136**, 9136–9148.

Supporting Information

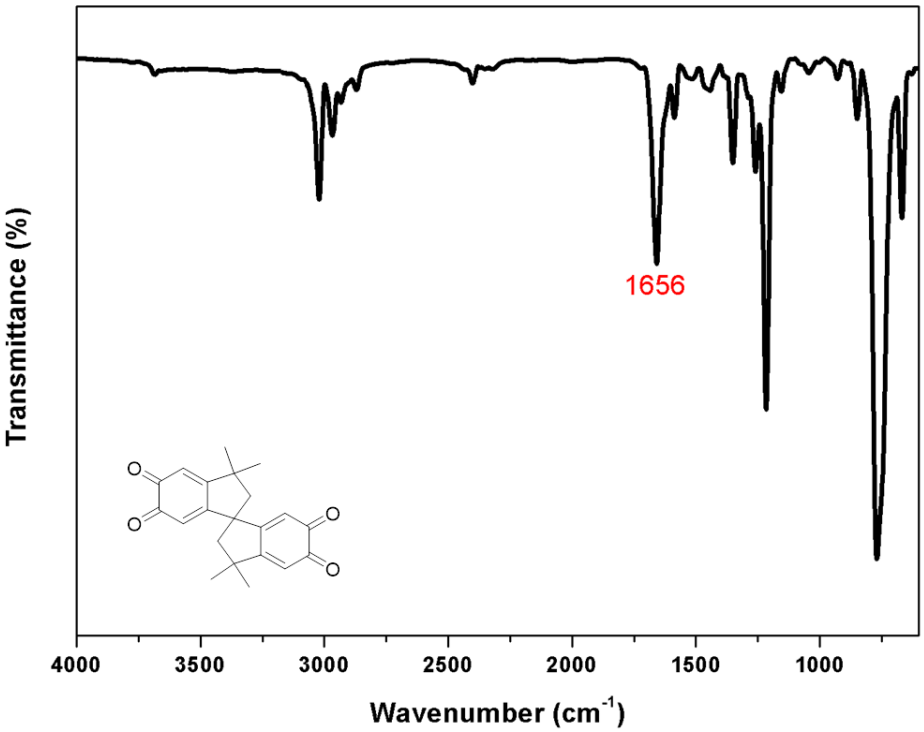

Figure SI 5.1: IR spectrum of 3,3,3',3'-tetramethyl-2,2',3,3'-tetrahydro-1,1'-spirobi[indene]-5,5',6,6'-tetraone (TTSBIQ)

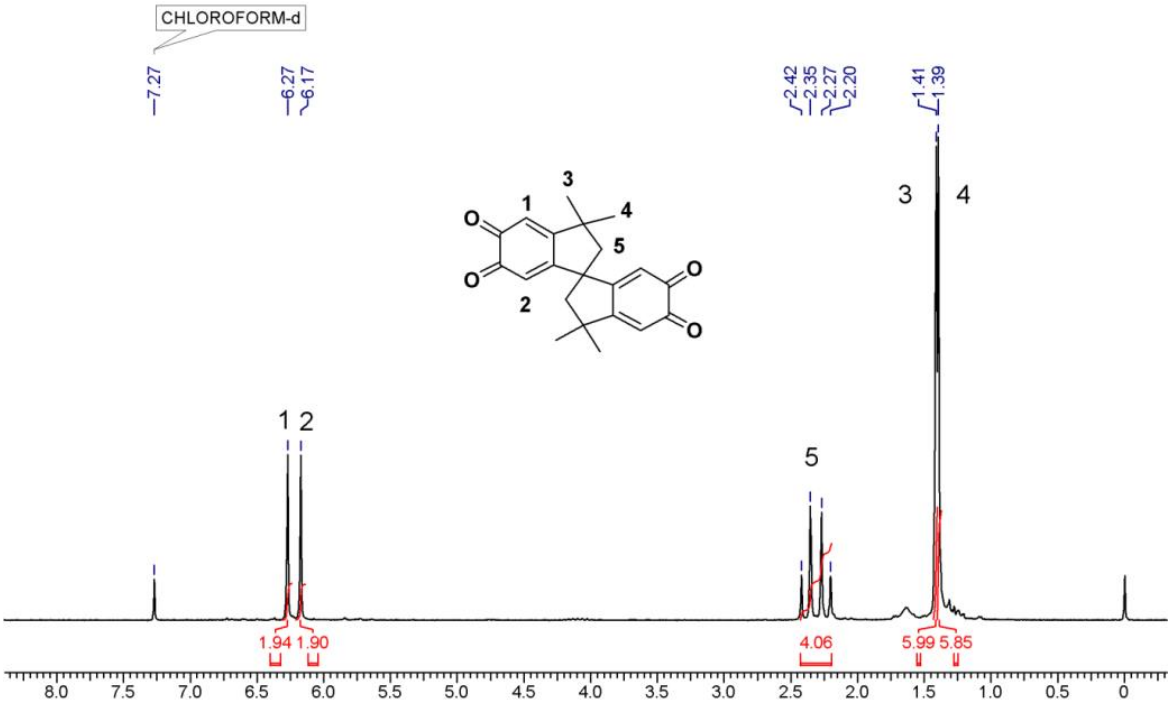

Figure SI 5.2: ^{1}H NMR spectrum (in $CDCl_3$) of 3,3,3',3'-tetramethyl-2,2',3,3'-tetrahydro-1,1'-spirobi[indene]-5,5',6,6'-tetraone (TTSBIQ).

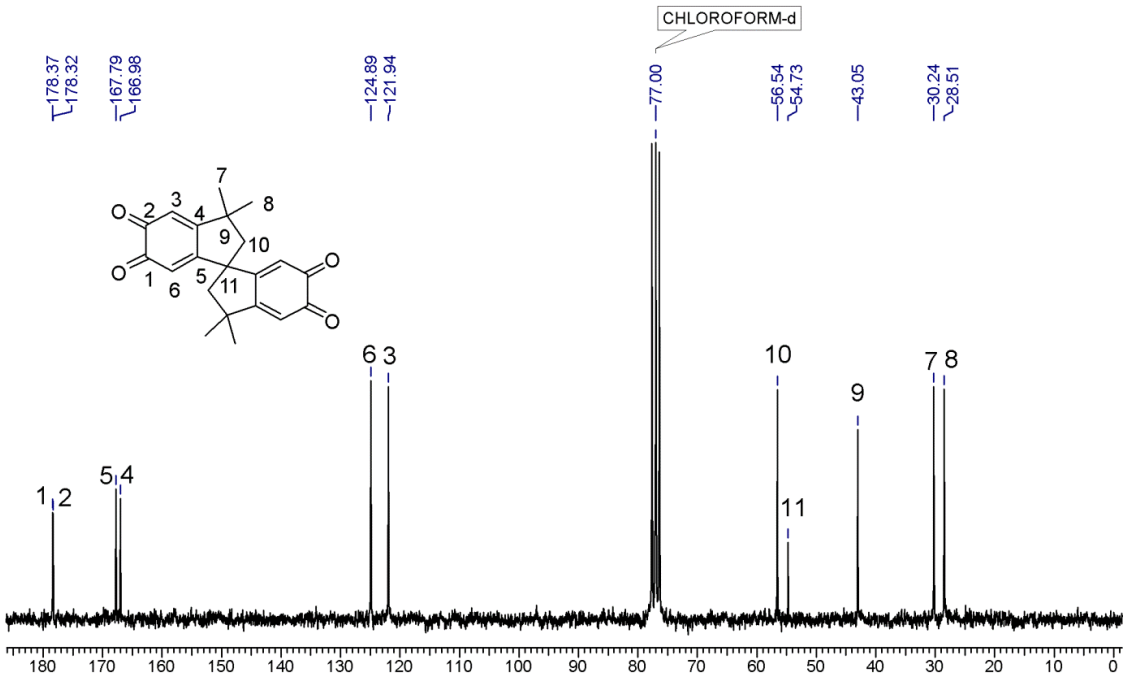

Figure SI 5.3: ^{13}C NMR spectrum (in $CDCl_3$) of 3,3,3',3'-tetramethyl-2,2',3,3'-tetrahydro-1,1'-spirobi[indene]-5,5',6,6'-tetraone (TTSBIQ).

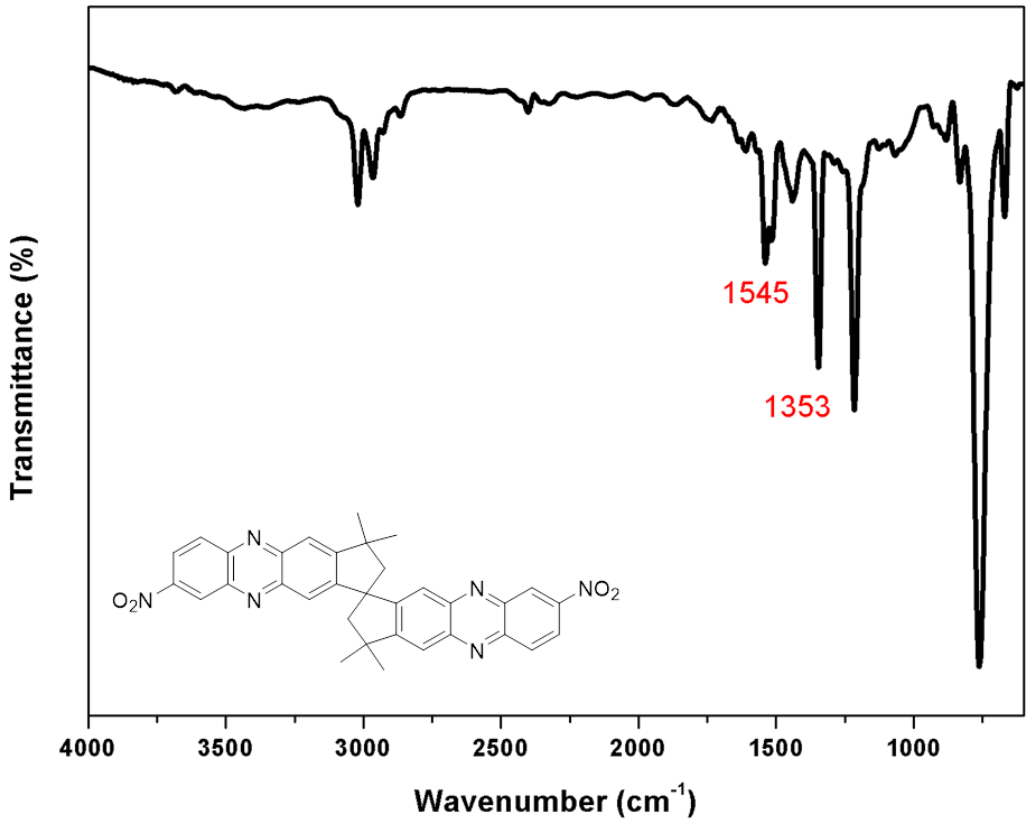

Figure SI 5.4: IR spectrum of 3,3,3',3'-tetramethyl-7,7'-dinitro-2,2',3,3'-tetrahydro-1,1'-spirobi[cyclopenta[b]phenazine] (TTSBIDN)

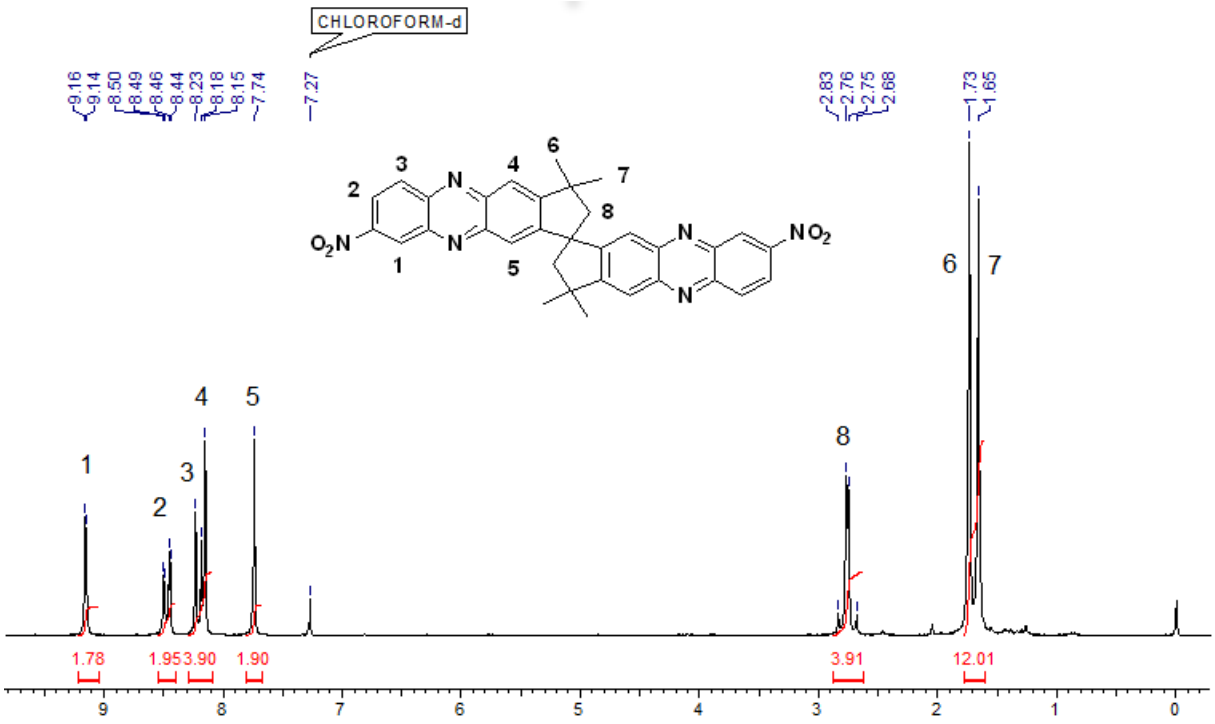

Figure SI 5.5: ^{1}H NMR spectrum (in $CDCl_3$) of 3,3,3',3'-tetramethyl-7,7'-dinitro-2,2',3,3'-tetrahydro-1,1'-spirobi[cyclopenta[b]phenazine] (TTSBIDN)

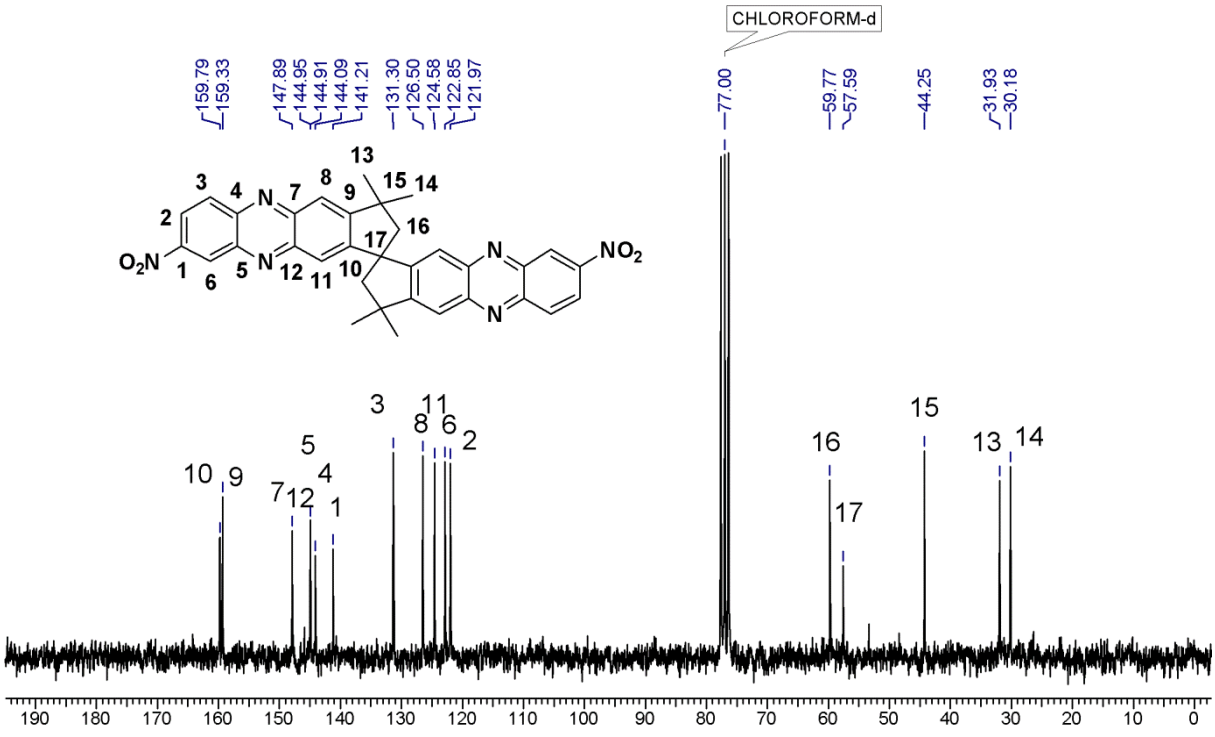

Figure SI 5.6: ^{13}C NMR spectrum (in $CDCl_3$) of 3,3,3',3'-tetramethyl-7,7'-dinitro-2,2',3,3'-tetrahydro-1,1'-spirobi[cyclopenta[b]phenazine] (TTSBIDN)

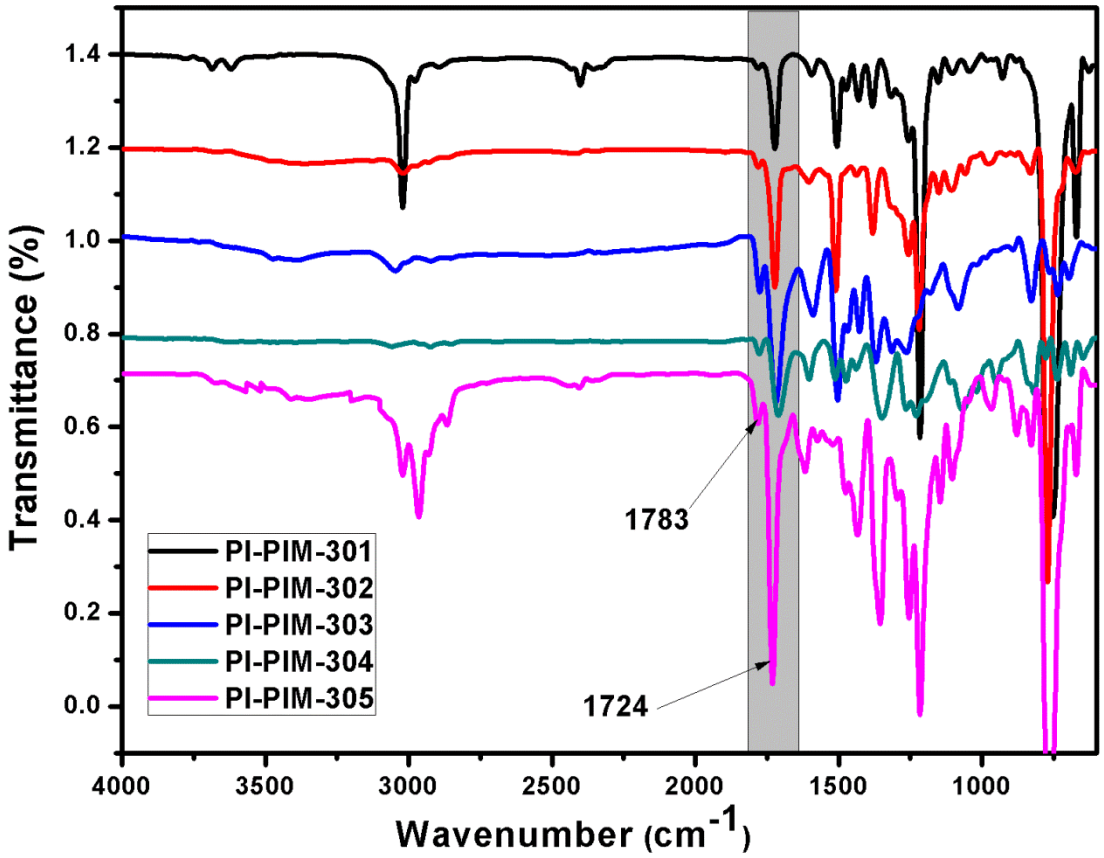

Figure SI 5.7: IR spectra of PIM-PIs

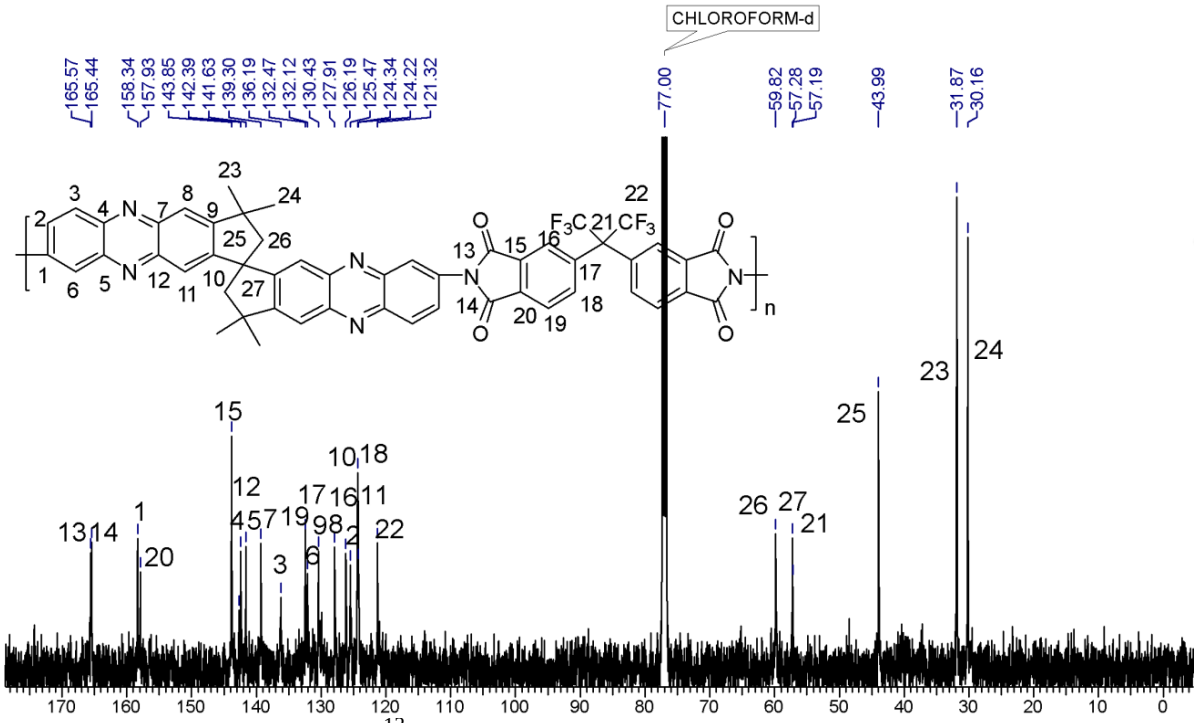

Figure SI 5.8: ^{13}C NMR spectrum (in $CDCl_3$) of PIM-PI-6FDA

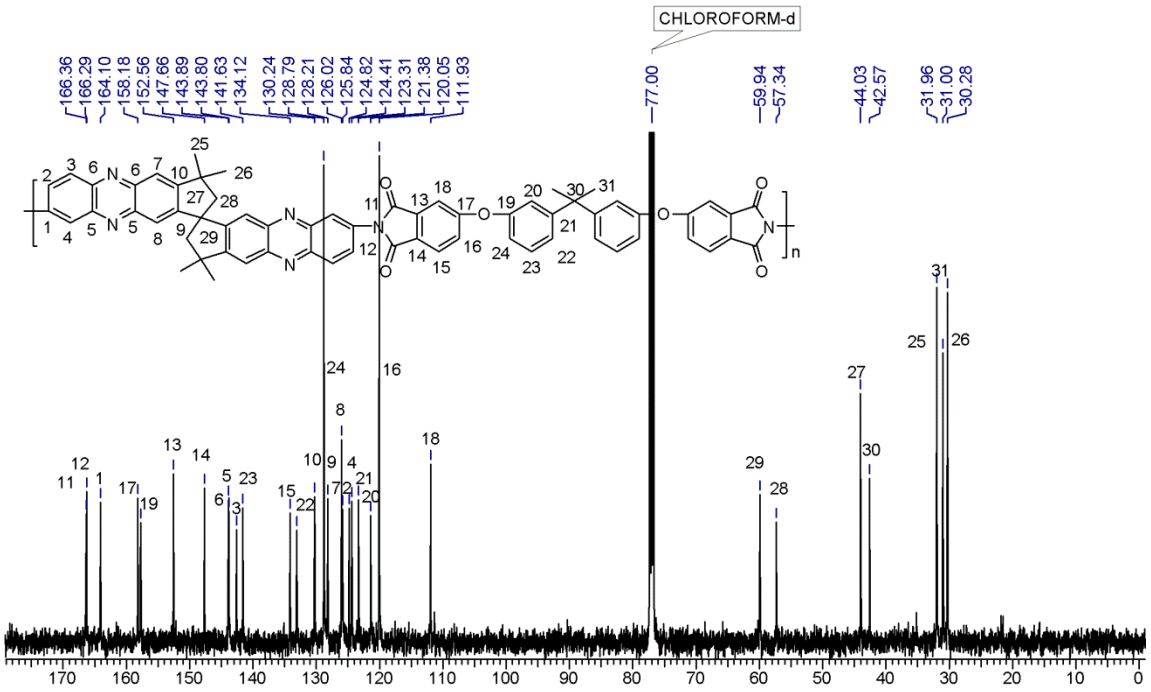

Figure SI 5.9: ^{13}C NMR spectrum (in $CDCl_3$) of PIM-PI-BPADA

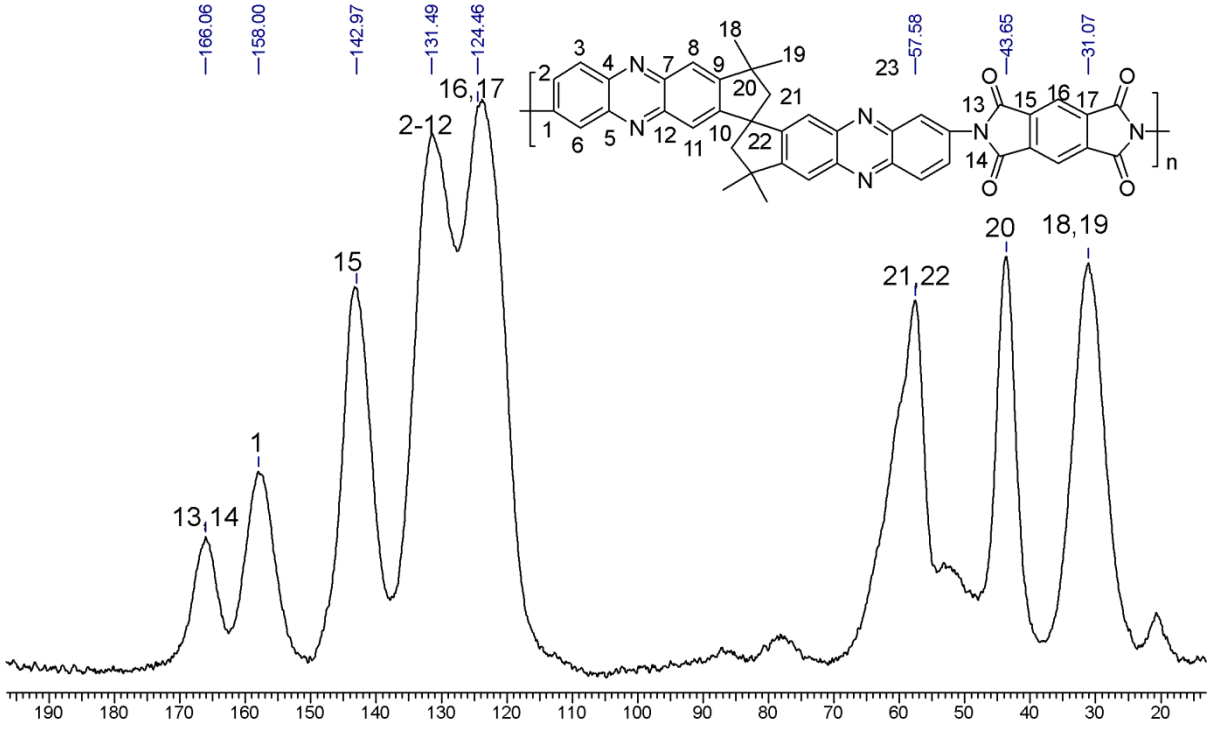

Figure SI 5.10: Solid state ^{13}C NMR spectrum of PIM-PI-PMDA.

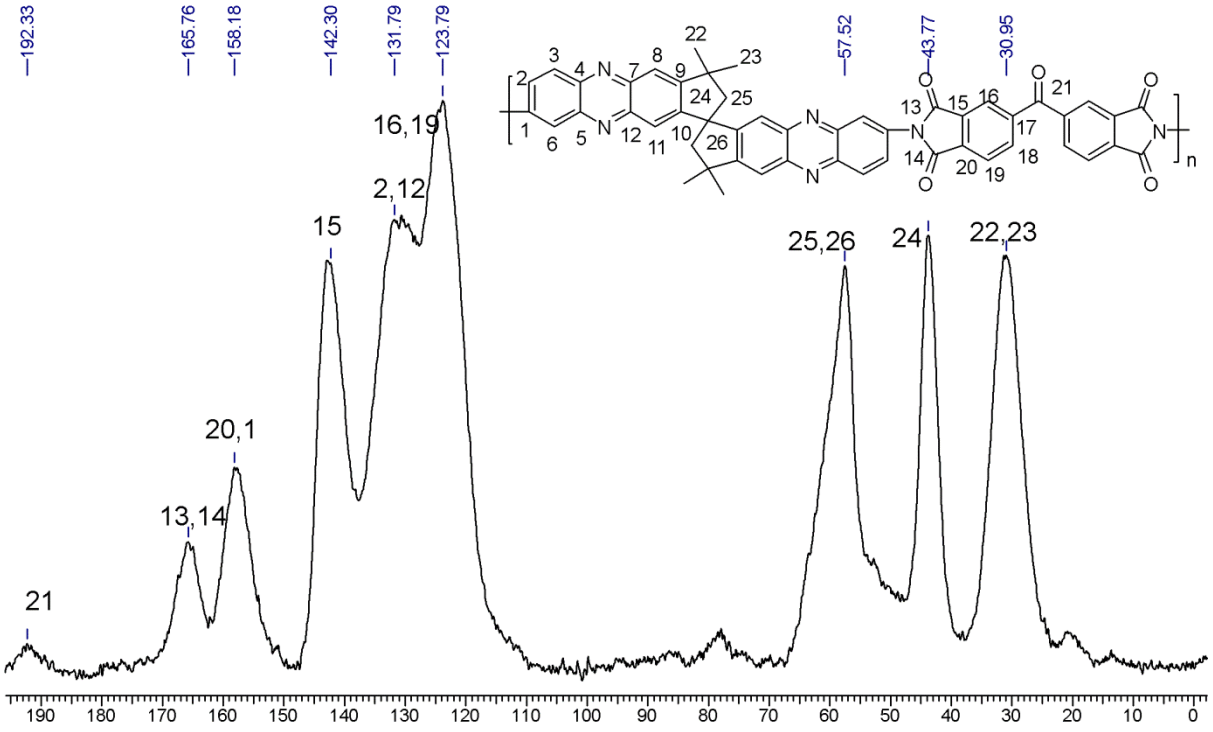

Figure SI 5.11: Solid state ^{13}C NMR spectrum of PIM-PI-BTDA

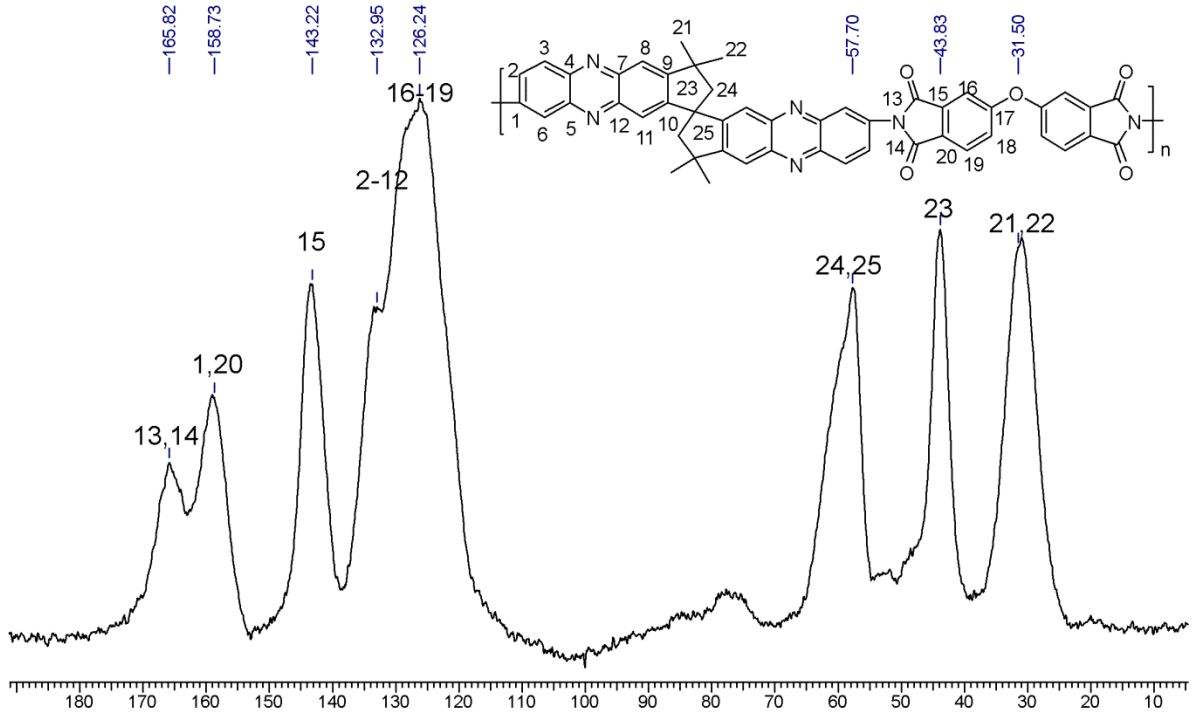

Figure SI 5.12: Solid state ^{13}C NMR spectrum of PIM-PI-ODPA

Computational Study

All the DFT calculations were carried out using the Turbomole 6.0 suite of programs[28]. Geometry optimizations were performed using the dispersion corrected Perdew, Burke, and Erzenhof density functional (PBE) [29]. The electronic configuration of the atoms was described by a triple-ζ basis set augmented by a polarization function (Turbomole basis set TZVP) [30]. The resolution of identity (ri) [31], along with the multipole accelerated resolution of identity (marij)[32] approximations were employed for an accurate and efficient treatment of the electronic Coulomb term in the density functional calculations. The dihedral were constrained and optimized at ten degree of increment starting from the DFT optimized structure. The structural rigidity parameter was calculated by fitting a harmonic model in the best approximation of $V_D=(\phi_{ijkl}-\phi_0)^2$ with k_{ijkl} as a spring constant. The spring constant of harmonic model is considered as a rigidity parameter.

Table SI 5.1. Harmonic model fitting data for **PI-PIM-6FDA.**

K_{ijkl} = 24.48 Kcal $mol^{-1}rad^{-2}$

Dihedral angle (°)	Dihedral angle(rad)	Energy (Kcal/mol) from DFT	$\phi_{ijkl}-\phi_0$	$(\phi_{ijkl}-\phi_0)^2$	$V_D=k_{ijkl}(\phi_{ijkl}-\phi_0)^2$ (Kcal/mol)	$Error^2$ $<r^2>$
120	2.088	26.393287	1.044	1.089936	26.68163	0.083144
130	2.262	18.229037	0.87	0.7569	18.52891	0.089925
140	2.436	11.92482	0.696	0.484416	11.8585	0.004398
150	2.61	6.4598082	0.522	0.272484	6.670408	0.044352
160	2.784	2.8976118	0.348	0.121104	2.964626	0.004491
170	2.958	0.8704931	0.174	0.030276	0.741156	0.016728
180	3.132	0	0	0	0	0
190	3.306	0.837875	-0.174	0.030276	0.741156	0.009354
200	3.48	2.9535659	-0.348	0.121104	2.964626	0.000122
210	3.654	6.707734	-0.522	0.272484	6.670408	0.001393
220	3.828	11.686807	-0.696	0.484416	11.8585	0.02948
230	4.002	18.828798	-0.87	0.7569	18.52891	0.089931
240	4.176	27.071138	-1.044	1.089936	26.68163	0.151714
					Sum of $error^2$	0.52

Table SI 5.2. Harmonic model fitting data for **PI-PIM-3**.

K_{ijkl} = 8.51 Kcal $mol^{-1}rad^{-2}$

Dihedral angle (°)	Dihedral angle(rad)	Energy (Kcal/mol) from DFT	$\phi_{ijkl}-\phi_0$	$(\phi_{ijkl}-\phi_0)^2$	$V_D=k_{ijkl}(\phi_{ijkl}-\phi_0)^2$ (Kcal/mol)	Error^2 <r^2>
120	2.088	9.5953623	1.044	1.089936	9.276565	0.101632
130	2.262	6.1284367	0.87	0.7569	6.442059	0.098359
140	2.436	3.4941748	0.696	0.484416	4.122918	0.395318
150	2.61	1.4526004	0.522	0.272484	2.319141	0.750893
160	2.784	1.0133981	0.348	0.121104	1.030729	0.0003
170	2.958	0.1193386	0.174	0.030276	0.257682	0.019139
180	3.132	0	0	0	0	0
190	3.306	0.1444982	-0.174	0.030276	0.257682	0.012811
200	3.48	0.4723036	-0.348	0.121104	1.030729	0.311839
210	3.654	1.8710243	-0.522	0.272484	2.319141	0.200809
220	3.828	3.9046313	-0.696	0.484416	4.122918	0.047649
230	4.002	6.3860135	-0.87	0.7569	6.442059	0.003141
240	4.176	9.9927229	-1.044	1.089936	9.276565	0.512882
					Sum of error^2	2.45

Cartisian coordinates of PI-PIM-6FDA

C	-6.603	0.381	-10.007
C	-6.548	-0.726	-9.075
N	-5.375	-1.270	-8.698
C	-4.258	-0.739	-9.231
C	-4.315	0.370	-10.169
N	-5.489	0.915	-10.542
C	-2.988	-1.275	-8.864
C	-1.844	-0.742	-9.405
C	-1.898	0.348	-10.329
C	-3.102	0.896	-10.703
C	-7.879	0.912	-10.360
C	-9.024	0.379	-9.823
C	-8.986	-0.718	-8.900
C	-7.765	-1.248	-8.545
C	-0.408	-1.186	-9.163
C	0.401	0.015	-9.755
C	-0.503	0.737	-10.797
C	-0.097	-2.568	-9.829
C	0.930	-3.315	-8.928
C	0.700	-2.663	-7.574
C	-0.055	-1.454	-7.707
C	1.135	-3.092	-6.343
C	0.841	-2.319	-5.181
C	0.080	-1.085	-5.319
C	-0.362	-0.681	-6.614
N	1.273	-2.747	-3.980
C	0.974	-1.978	-2.918
C	0.223	-0.747	-3.055
N	-0.215	-0.318	-4.255
C	1.400	-2.378	-1.616
C	1.111	-1.610	-0.518
C	0.383	-0.387	-0.662
C	-0.050	0.037	-1.900
C	-0.271	2.256	-10.778
C	0.659	-4.828	-8.914
C	2.383	-3.064	-9.386
C	-0.264	0.206	-12.228
N	0.085	0.374	0.502
C	1.000	0.603	1.570
C	0.254	1.425	2.567
C	-1.028	1.667	2.081
C	-1.174	1.000	0.755
O	-2.147	0.971	0.029
O	2.149	0.208	1.627
C	0.659	1.937	3.792
C	-0.269	2.692	4.517
C	-1.570	2.944	4.032
C	-1.954	2.427	2.782
C	-2.486	3.858	4.878
C	-2.418	3.498	6.380
C	-2.430	2.133	6.729
C	-2.442	1.708	8.063
C	-2.441	2.684	9.049
C	-2.432	4.039	8.713

C	-2.429	4.473	7.396
C	-2.456	2.566	10.541
N	-2.462	3.891	11.019
C	-2.444	4.840	9.977
O	-2.436	6.050	10.122
O	-2.461	1.565	11.234
C	-2.497	4.239	12.427
C	-10.276	-1.256	-8.343
C	-2.010	5.327	4.589
F	-0.806	5.558	5.175
F	-2.874	6.264	5.053
F	-1.859	5.545	3.264
C	-3.998	3.739	4.472
F	-4.380	2.436	4.448
F	-4.799	4.375	5.356
F	-4.259	4.263	3.247
H	-2.972	-2.097	-8.144
H	-3.179	1.733	-11.400
H	-7.906	1.747	-11.063
H	-9.996	0.795	-10.100
H	-7.688	-2.083	-7.845
H	0.631	0.715	-8.938
H	1.357	-0.303	-10.193
H	-1.028	-3.152	-9.867
H	0.265	-2.460	-10.861
H	1.706	-4.013	-6.206
H	-0.950	0.235	-6.688
H	1.957	-3.312	-1.528
H	1.440	-1.920	0.472
H	-0.615	0.958	-2.031
H	-0.919	2.767	-11.506
H	0.771	2.490	-11.042
H	-0.477	2.677	-9.783
H	1.380	-5.356	-8.272
H	0.752	-5.244	-9.929
H	-0.351	-5.047	-8.544
H	2.541	-3.470	-10.398
H	3.093	-3.556	-8.706
H	2.627	-1.992	-9.404
H	-0.436	-0.877	-12.296
H	0.769	0.412	-12.544
H	-0.945	0.695	-12.940
H	1.663	1.756	4.176
H	0.024	3.100	5.484
H	-2.936	2.604	2.346
H	-2.432	1.383	5.938
H	-2.456	0.647	8.317
H	-2.443	5.541	7.186
H	-1.906	3.507	12.992
H	-3.528	4.233	12.810
H	-2.078	5.245	12.544
H	-10.100	-2.105	-7.670
H	-10.817	-0.479	-7.779
H	-10.948	-1.590	-9.149

Cartisian coordinates of PI-PIM-3

C	-2.686	2.579	-12.453
C	-3.013	1.461	-11.522
C	-1.817	0.863	-11.111
C	-0.682	1.587	-11.752
N	-1.279	2.595	-12.540
C	-4.245	0.997	-11.081
C	-4.249	-0.082	-10.194
C	-3.043	-0.692	-9.785
C	-1.809	-0.212	-10.233
O	-5.474	-0.532	-9.753
C	-5.465	-1.637	-8.910
C	-4.268	-2.238	-8.496
O	-3.030	-1.762	-8.917
C	-4.288	-3.350	-7.660
C	-5.521	-3.855	-7.235
C	-6.717	-3.253	-7.644
C	-6.693	-2.136	-8.484
C	-5.771	-5.034	-6.309
C	-7.305	-5.271	-6.522
C	-7.932	-3.942	-7.042
C	-5.363	-4.743	-4.827
C	-4.869	-6.079	-4.192
C	-4.474	-6.873	-5.428
C	-4.951	-6.281	-6.602
C	-3.752	-8.068	-5.485
C	-3.505	-8.649	-6.725
C	-3.955	-8.037	-7.903
C	-4.690	-6.857	-7.849
O	-2.793	-9.844	-6.750
C	-2.494	-10.359	-7.990
C	-2.918	-9.725	-9.180
O	-3.680	-8.579	-9.156
C	-1.760	-11.547	-8.031
C	-1.436	-12.058	-9.281
C	-1.824	-11.414	-10.458
C	-2.570	-10.242	-10.432
C	-1.300	-12.182	-11.620
N	-0.618	-13.303	-11.058
C	-0.670	-13.282	-9.631
C	0.061	-14.297	-11.812
C	0.934	-13.928	-12.843
C	1.627	-14.908	-13.547

C	1.471	-16.272	-13.247
C	0.574	-16.626	-12.230
C	-0.119	-15.650	-11.514
C	2.266	-17.294	-14.090
O	-0.172	-14.107	-8.889
O	-1.407	-11.938	-12.807
C	-5.994	-6.804	-3.423
C	-3.683	-5.838	-3.243
C	-9.037	-4.214	-8.074
C	-8.511	-3.091	-5.890
O	0.516	1.392	-11.647
C	-0.534	3.534	-13.354
O	-3.434	3.347	-13.036
H	-3.341	-3.808	-7.366
H	-7.604	-1.644	-8.828
H	-7.435	-6.049	-7.290
H	-7.799	-5.630	-5.608
H	-6.183	-4.292	-4.252
H	-4.530	-4.022	-4.830
H	-3.371	-8.566	-4.590
H	-5.030	-6.402	-8.782
H	-1.451	-12.033	-7.105
H	-2.889	-9.733	-11.342
H	-5.185	1.453	-11.392
H	-0.884	-0.688	-9.903
H	-0.586	3.264	-14.419
H	0.511	3.507	-13.026
H	-0.948	4.542	-13.226
H	-9.473	-3.276	-8.450
H	-9.853	-4.797	-7.620
H	-8.648	-4.779	-8.934
H	-8.893	-2.131	-6.269
H	-7.752	-2.871	-5.127
H	-9.347	-3.620	-5.405
H	-5.641	-7.772	-3.039
H	-6.324	-6.199	-2.564
H	-6.864	-6.998	-4.064
H	-3.984	-5.182	-2.411
H	-3.321	-6.781	-2.807
H	-2.843	-5.361	-3.769
C	2.261	-18.731	-13.460
C	1.546	-17.370	-15.484
C	3.750	-16.880	-14.210
C	4.520	-17.091	-15.363
C	5.870	-16.738	-15.392
C	6.508	-16.183	-14.275
C	5.737	-15.990	-13.119
C	4.386	-16.330	-13.085
H	4.080	-17.534	-16.255
H	6.440	-16.901	-16.310
C	7.973	-15.835	-14.303
H	6.199	-15.561	-12.226
H	3.816	-16.159	-12.171
F	3.111	-19.564	-14.102
F	2.655	-18.688	-12.161
F	1.034	-19.320	-13.491
F	1.948	-18.429	-16.239
F	0.205	-17.477	-15.345
F	1.786	-16.249	-16.213
H	-0.798	-15.946	-10.715
H	0.396	-17.668	-11.971
H	2.318	-14.602	-14.332
H	1.073	-12.877	-13.093
H	8.184	-14.936	-13.706
H	8.580	-16.654	-13.883
H	8.325	-15.658	-15.328

Chapter 6

Spiro[fluorene-9,9'-xanthene]-Based Copolymers of Intrinsic Microporosity: Synthesis, Characterization and Gas Permeation Properties

In the recent years, polymers containing spirocyclic units have gained great attention as membrane materials for gas separation and are often used for the synthesis of polymers of intrinsic microporosity (PIMs) due to their contorted and rigid structure. In this context, in the present work, a new spiro[fluorene-9,9'-xanthene]-containing bis(catechol), namely, 4,4'-(spiro[fluorene-9,9'-xanthene]-2',7'-diyl)bis (benzene-1,2-diol) (THSFX) was designed and synthesized. Polycondenstaion of THSFX and varying compositions of THSFX and 5,5',6,6'-tetrahydroxy-3,3,3',3'-tetramethyl-1,1'-spirobisindane (TTSBI) was carried with 2,3,5,6-tetrafluoroterephthalonitrile (TFTPN)to obtain homopolymer and copolymers. These polymers exhibited amorphous nature, excellent thermal properties (T_{10} = 490-510 °C) and possessed intrinsic microporosity with high BET surface area (360-796 m^2/g). The selected PIMs exhibited high gas permeability and appreciable selectivity. The gas permeability of PIMs were located near 1991 Robeson upper bound.

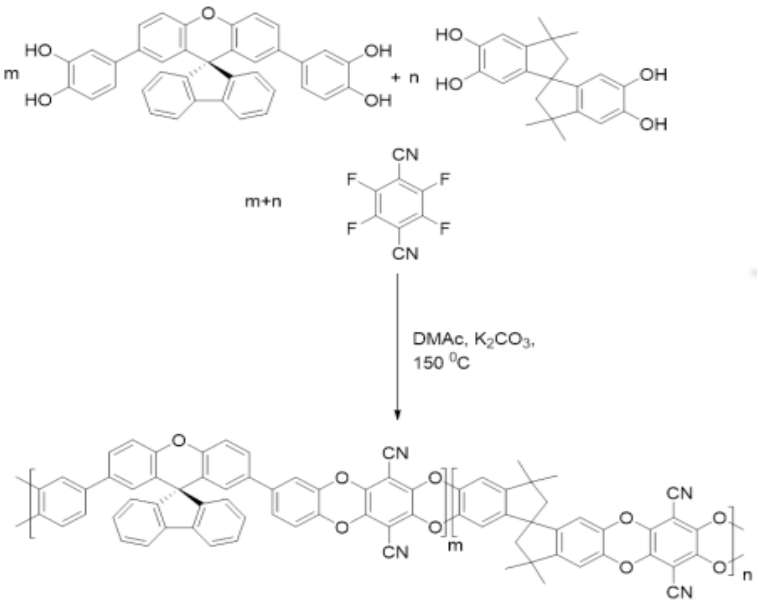

m/n = 0/1 (PIM-1); 1/3 (SFX-PIM-25); 1/2 (SFX-PIM-33); 2/3 (SFX-PIM-40); 1/1 (SFX-PIM-50); 1/0 (SFX-PIM)

6.1 INTRODUCTION

In the recent years, polymers of intrinsic microporosity (PIMs) have emerged as the next generation membrane materials with extraordinary gas separation performance.[1–7] In this context, polymers containing spirocyclic units have gained considerable attention due to their contorted structure which creates microporosity in polymers and results into improved gas separation performance.[4,8–18] To date, spirobisindane, spirobifluorene and spirobischromane units have been used as a building block to induce microporosity.[1,4–6,19–22]

Recently, spiro[fluorene-9,9'-xanthene] (SFX) unit containing polymers have been investigated for different applications such as solar cells,[23] OLEDs,[9] hydrogen uptake,[24] and gas separation[8] due to their excellent thermo-chemical and physical properties. SFX unit is a spirocyclic moiety containing oxygen atom present in the spiro-skeleton in which fluorene and xanthene moieties are connected through a quaternary carbon atom.[25] To the best of our knowledge, SFX unit has not yet been explored as an alternative building block for the synthesis of PIMs.

In this work, a new bis(catechol), namely, 4,4'-(spiro[fluorene-9,9'-xanthene]-2',7'-diyl)bis(benzene-1,2-diol) (THSFX) was designed and synthesized. Homopolymer was synthesized by polycondensation of THSFX with 2,3,5,6-tetrafluoroterephthalonitrile (TFTPN) *via* double aromatic nucleophilic substitution reaction. In addition, copolymers with intrinsic microporosity were synthesized by polycondenstaion of varying compositions of THSFX and 5,5′,6,6′-tetrahydroxy-3,3,3′,3′-tetramethyl-1,1′-spirobisindane (TTSBI) with TFTPN. PIMs were characterized by IR, ^{1}H and ^{13}C NMR spectroscopy, GPC, XRD, TGA, and N_2 adsorption and desorption. Furthermore, the gas permeation properties of PIMs were investigated. The influence of SFX units on physical and gas permeation properties was investigated.

6.2 EXPERIMENTAL

Details about materials used in the study and experimental techniques such as solubility study, IR, ^{1}H and ^{13}C NMR spectroscopy, GPC, TGA, DSC, XRD, N_2 adsorption method and gas permeability analysis have been given in **Chapter 3**.

6.2.1 Preparations

6.2.1.1 Synthesis of 2',7'-dibromospiro[fluorene-9,9'-xanthene] (DBSFX)

Into a two-necked round-bottom flask equipped with a magnetic stirring bar and a nitrogen inlet were charged 4-bromophenol (17.3 g, 100 mmol), 9-fluorenone (3.38 g, 10 mmol) and

methanesulfonic acid (2.6 ml, 3.84 g, 40 mmol). The reaction mixture was heated at 150 °C for 30 h, cooled and precipitated into methanol. The crude product was then extracted with ethyl acetate, washed with brine and was concentrated on a rotary evaporator. The crude product was purified by column chromatography on silica gel using pet ether and ethyl acetate (98: 2, v/v) as eluent to obtain DBSFX as a white solid.

Yield: 14.8 g, 30%

Melting Point: 218 °C

IR: 1260 (C-O-C) and 1095 (Ar-Br)

^{1}H NMR (200 MHz, DMSO-d_6,), δ(ppm): 8.0 (d, J = 10 Hz, 2H, Ar-H), 7.45-7.41 (m, 4H, Ar-H), 7.30-7.27 (m, 4H, Ar-H), 7.13 (d, 2H, Ar-H), 6.23 (s, 2H, Ar-H).).

^{13}C-NMR (50 MHz, DMSO-d_6, δ/ppm): 153.3, 149.7, 138.9, 131.7, 129.1, 129.0, 128.8, 126.4, 125.2, 120.9, 119.4, 115.1, 53.2:

HRMS: calcd for $C_{25}H_{14}Br_2O$: 487.9406, found: 487.9397.

6.2.1.2 Synthesis of tetramethoxyxanthene2',7'-bis(3,4-dimethoxyphenyl)spiro[fluorene-9,9'-xanthene] (TMSFX)

Into a Schlenk tube were charged DBSFX (5 g, 10.2 mmol), 2,4-dimethoxyphenylboronic acid (4.08 g, 22.4), potassium carbonate (8.28g) and toluene (40 mL) and the reaction mixture was degassed for 30 minutes. Tetrakis(triphenylphosphine)palladium (0) (0.58 g, 0.5 mmol) was added and the reaction mixture was degassed for 10 minutes. The reaction mixture was heated at 100 °C for 20 h. After completion of reaction (monitored by TLC), the reaction mixture was cooled to room temperature and extracted with ethyl acetate. The ethyl acetate solution was washed with brine and was evaporated on a rotary evaporator. The crude product was purified by column chromatography on silica gel using pet ether: ethyl acetate (70:30, v/v) as eluent to obtain TMSFX as a white solid.

Yield: 4.1 g, 66%

Melting Point: 254 °C

IR: 1248 (C-O-C)

^{1}H NMR (200 MHz, DMSO-d_6, δ/ppm): 7.81 (d, 2H, Ar-H), 7.41-7.38 (m, 4H, Ar-H), 7.31 (d, 2H, Ar-H), 7.27 (d, 2H, Ar-H), 7.25 (d, 2H, Ar-H), 6.76 (d, 6H, Ar-H), 6.57 (dd, 2H, Ar-H), 6.59 (d, 2H, Ar-H), 3.84 (s, 6H, -CH_3), 3.81 (s, 6H, -CH_3);

^{13}C-NMR (50 MHz, $CDCl_3$, δ/ppm): 154.5, 150.7, 148.9, 148.2, 139.7, 136.2, 133.4, 128.3, 127.8, 126.6, 126.0, 125.6, 125.3, 120.0, 118.9, 117.0, 111.2, 110.2, 55.9, 55.8, 54.8.;

HRMS: calcd. for $C_{41}H_{32}O_5$: 604.2244, found: 604.2239

6.2.1.3 Synthesis of tetrahydroxyxanthene4,4'-(spiro[fluorene-9,9'-xanthene]-2',7'-diyl)bis (benzene-1,2-diol) (THSFX)

Into a two necked round bottom flask equipped with a magnetic stirrer bar, a nitrogen inlet and an addition funnel were charged TMSFX (4g, 6.6 mml) and dichloromethane. To the reaction mixture, BBr_3 in dichloromethane (10.2 ml, 26.4 mmol) was added dropwise over a period of 15 minutes at 0 °C and then stirred at room temperature for another 12 h. The reaction mixture was quenched by water and was extracted with ethyl acetate. The ethyl acetate solution was washed with brine and the ethyl acetate was evaporated on rotary evaporator. The crude product was purified by column chromatography on silica gel using pet ether: ethyl acetate (50:50, v/v) as eluent to obtain THSFX as a colourless solid.

Yield: 3.2 g, 88%

Melting Point: 264 °C

IR: 3428 and 3260 cm^{-1} (-OH)

^{1}H NMR (200 MHz, DMSO-d_6, δ/ppm): 8.96 (s, 2H, Ar-H), 8.94 (s, 2H), 8.04 (d, 2H, Ar-H), 7.48-7.43 (t, 2H, Ar-H), 7.41 (dd, 2H, Ar-H), 7.34 (d, 2H, Ar-H), 7.29 (t, 2H, Ar-H), 7.18 (d, 2H, Ar-H), 6.65 (d, 2H, Ar-H). 6.53 (d, 2H, Ar-H), 6.49 (dd, 2H, Ar-H), 6.34 (d, 2H, Ar-H);

^{13}C-NMR (50 MHz, $CDCl_3$, δ/ppm): 154.4, 149.6, 145.4, 144.9, 139.1, 135.8, 130.4, 128.7, 128.3, 126.3, 125.2, 124.6, 124.2, 120.6, 117.2, 117.0, 116.0, 113.1, 53.9.;

HRMS: calcd. for $C_{37}H_{25}O_5$: 549.1697, found: 549.1686

6.2.1.4 Polymerization

Into a 100 mL three-necked round-bottom flask equipped with a magnetic bar and a nitrogen inlet were charged THSFX (1.5 g, 4.256 mmol), TFTPN (0.8516 g, 4.25mmol) and DMAc (15 mL). The reaction mixture was heated at 120 °C for 5 minutes and then potassium carbonate (3.5g, 25.53 mmol) was added in one portion (color changed from orange-red to orange- yellow). Then the reaction mixture was heated at 150 °C for 5 minutes; 2 mL toluene was added and stirred at same temperature until the solution became viscous (10-20 minutes). The resulting viscous solution was precipitated into methanol; yellow powder was collected by filtration, washed with hot water and methanol and dried at 100 °C for four days.

Copolymers were synthesized by polycondensation of varying compositions of THSFX and TTSBI with TFTPN using the similar procedure. PIMs were designated as SFX-PIM-25, SFX-PIM-33, SFX-PIM-40 and SFX-PIM-50 wherein the feed molar composition of THSFX was 25, 33, 40 and 50 mol%, respectively.

6.2.2 Preparation of Dense Membrane

Dense polymer films for gas permeability measurements were prepared from ~ 5 wt % polymer solutions in chloroform. Polymer solution was cast onto a clean levelled petridish and solvent was evaporated slowly at room temperature. The thickness of membrane was in the range 75±5 μm as measured by digital micrometer.

6.3 RESULTS AND DISCUSSION

6.3.1 Synthesis and Characterization of 4,4'-(Spiro[fluorene-9,9'-xanthene]-2',7'-diyl)bis(benzene-1,2-diol) (THSFX)

The synthesis of a new bis(catechol) containing spiro[fluorene-9,9'-xanthene] (SFX) unit viz., 4,4'-(spiro[fluorene-9,9'-xanthene]-2',7'-diyl)bis(benzene-1,2-diol) (THSFX) was carried out in three steps as shown in **Scheme 6.1**. Firstly, the synthesis of 2',7'-dibromospiro[fluorene-9,9'-xanthene] (DBSFX) was carried out by condensation of 9-fluorenone with 4-bromophenol in the presence of methanesulfonic acid using the reported procedure.[26] The chemical structure of DBSFX was characterized by IR (**Figure SI 6.1**), ^{1}H (**Figure SI 6.2**), ^{13}C NMR (**Figure SI 6.3**) spectroscopy and HRMS.

DBSFX was converted into 2',7'-bis(3,4-dimethoxyphenyl)spiro[fluorene-9,9'-xanthene] (TMSFX) *via* Suzuki coupling reaction of DBSFX with 3,4-dimethoxyphenylboronic acid in the presence of tetrakis(triphenylphosphine)palladium(0) as a catalyst. The chemical structure of DBSFX was characterized by IR (**Figure SI 6.4**), ^{1}H (**Figure SI 6.5**) and ^{13}C NMR (**Figure SI 6.6**) spectroscopy and HRMS.

Finally, the demethylation of TMSFX was carried out using BBr_3 to afford 4,4'-(spiro[fluorene-9,9'-xanthene]-2',7'-diyl)bis(benzene-1,2-diol) (THSFX). The chemical structure of THSFX was confirmed by IR, ^{1}H and ^{13}C NMR spectroscopy and HRMS.

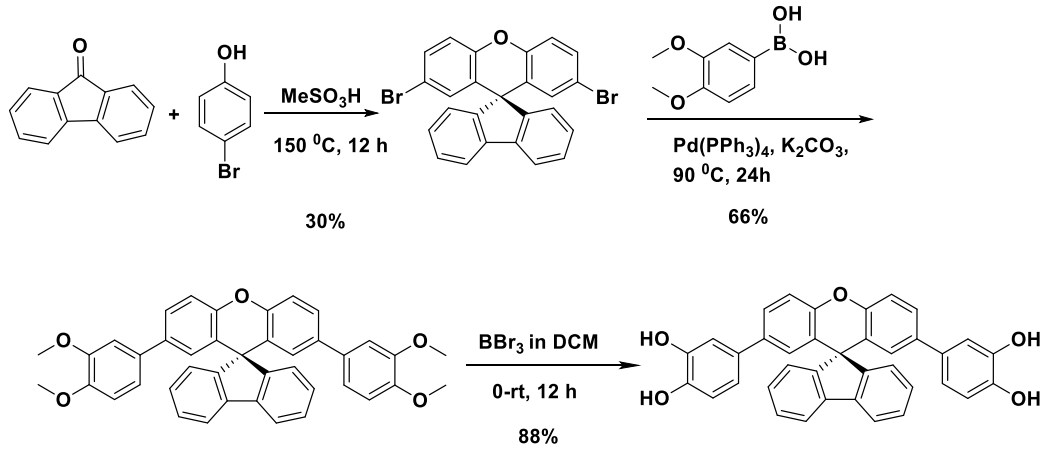

Scheme 6.1: Synthesis of 4,4'-(spiro[fluorene-9,9'-xanthene]-2',7'-diyl)bis(benzene-1,2-diol) (THSFX).

IR spectrum of THSFX is shown in **Figure 6.1**.The bands observed at 3428 and 3260 cm^{-1} could be attributed to the phenolic -OH groups.

^{1}H NMR spectrum of THSFX along with assignments is shown in **Figure 6.2**. The phenolic hydroxyl protons appeared as two separate singlets at δ = 8.96 and 8.94 ppm. The aromatic protons appeared in the region δ = 8.05-6.34 ppm and integrated intensity ratios of the peaks was consistent with the assignments.

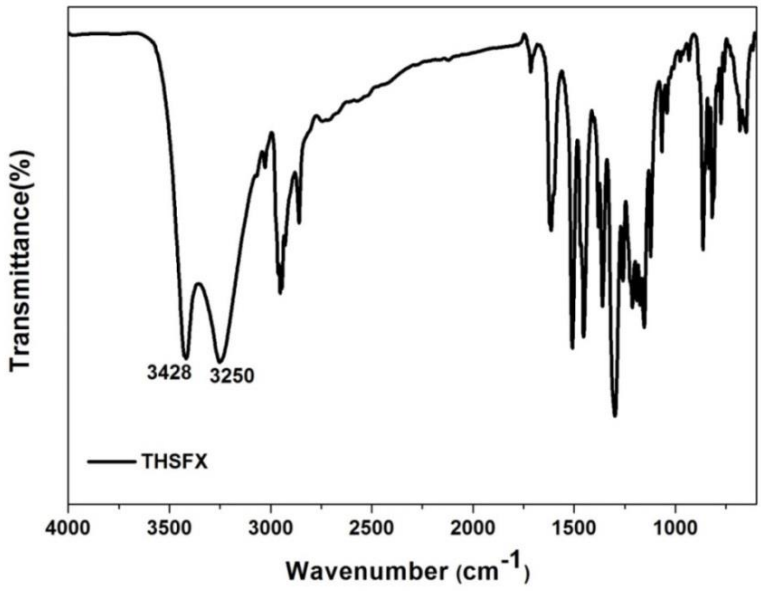

Figure 6.1: IR spectrum of 4,4'-(spiro[fluorene-9,9'-xanthene]-2',7'-diyl)bis(benzene-1,2-diol) (THSFX).

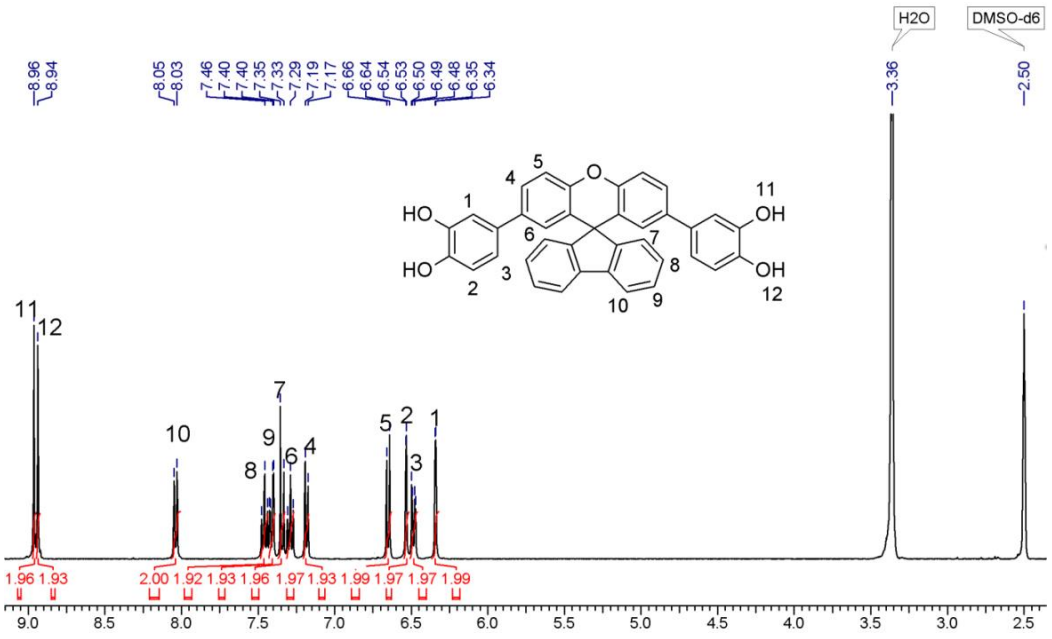

Figure 6.2: ^{1}H NMR spectrum (in DMSO-d_6) of 4,4'-(spiro[fluorene-9,9'-xanthene]-2',7'-diyl)bis(benzene-1,2-diol) (THSFX).

^{13}C NMR spectrum of THSFX along with assignments is shown in **Figure 6.3**. The carbon atoms attached to phenolic groups showed two peaks at δ = 149.6 and 145.4 ppm while the carbon attached to ether linkage labelled as 10 appeared at δ = 154.4 ppm. The other aromatic carbons appeared in the range δ = 144.9-113.6 ppm.

Furthermore, HR-MS (**Figure 6.4**) analysis of THSFX showed peak at 549.1697 corresponding to ($[M+H]^+$) of THSFX (calcd. ($[M+H]^+$) for $C_{37}H_{25}O_5$ = 549.1686).

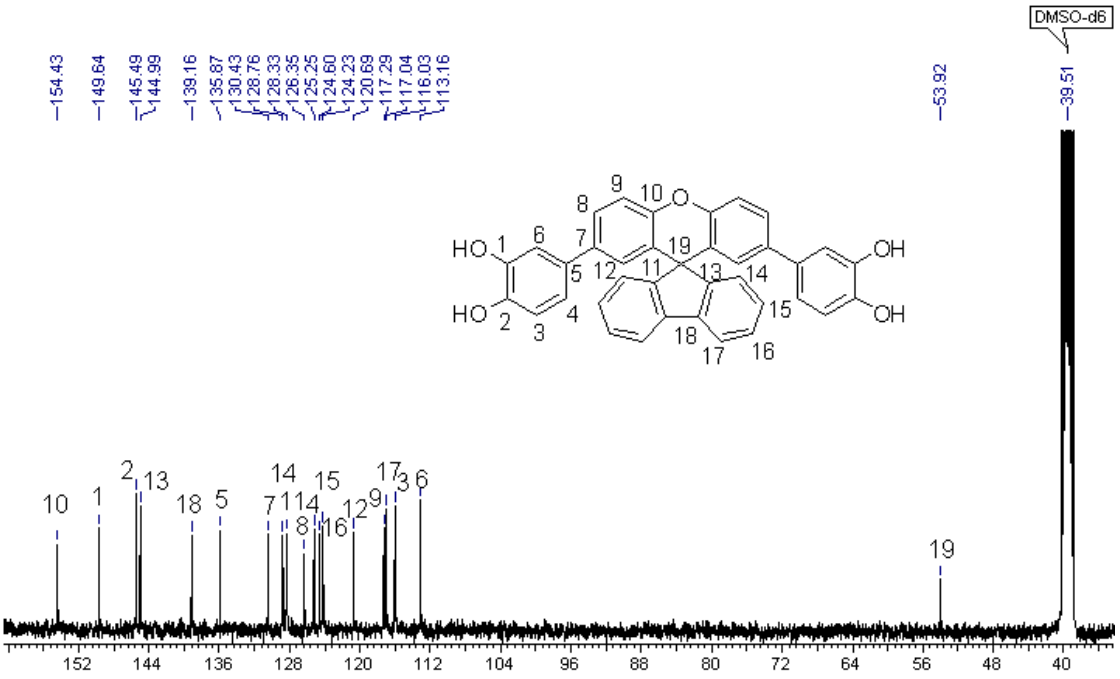

Figure 6.3: ^{13}C NMR spectrum (in DMSO-d_6) of 4,4'-(spiro[fluorene-9,9'-xanthene]-2',7'-diyl)bis(benzene-1,2-diol) (THSFX)

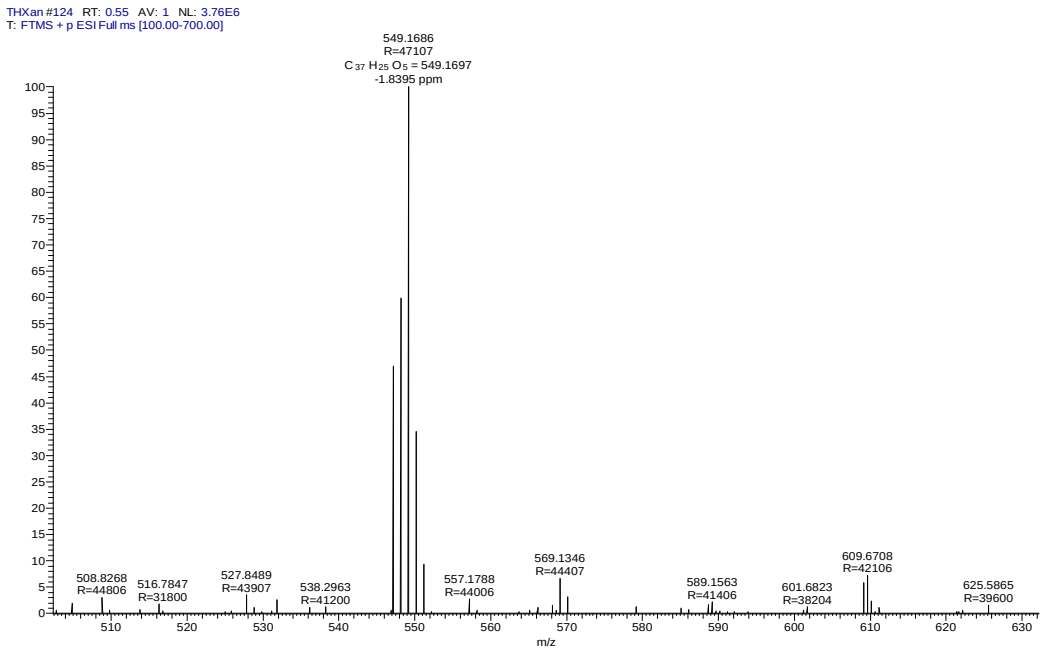

Figure 6.4: HR-MS of 4,4'-(spiro[fluorene-9,9'-xanthene]-2',7'-diyl)bis(benzene-1,2-diol) (THSFX)

6.3.2 Synthesis and Characterization of PIMs Containing SFX Units

Scheme 6.2 illustrates synthesis of homopolymer and copolymers from THSFX. Homopolymer containing spiro[fluorene-9,9'-xanthene] units was synthesized by polycondensation of THSFX with TFTPN to obtain SFX-PIM. The polycondensation reaction was carried out in DMAc at 150 °C using potassium carbonate as a base *via* double aromatic nucleophilic substitution polymerization reaction to form polymer containing dibenzodioxine ring. In addition, copolymers were prepared by the similar procedure using various feed ratios of THSFX and 5,5,6',6'-tetrahydroxy-3,3,3',3'-tetramethylspirobisindane (TTSBI). The compositions of THSFX were varied such as 25, 33, 40 and 50 mol % and the corresponding copolymers were designated as SFX-PIM-25, SFX-PIM-33, SFX-PIM-40 and SFX-PIM-50. PIM-1 was synthesized as a reference polymer using the similar reaction conditions by reaction of TTSBI with TFTPN.

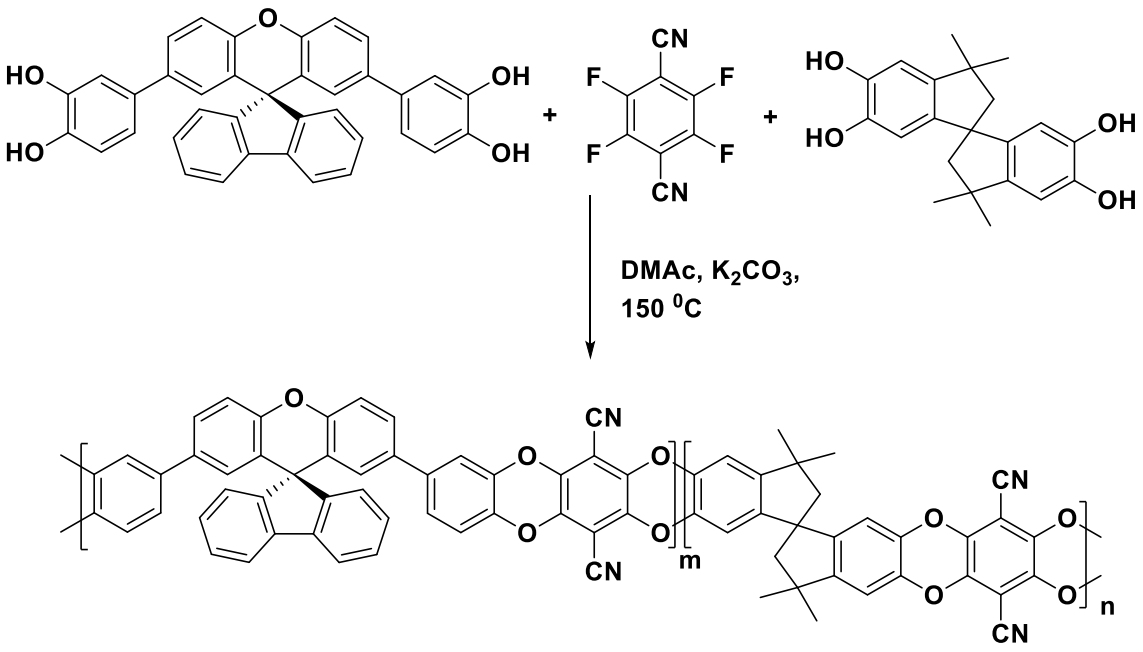

m/n = 0/1 (PIM-1); 1/3 (SFX-PIM-25); 1/2 (SFX-PIM-33); 2/3 (SFX-PIM-40); 1/1 (SFX-PIM-50); 1/0 (SFX-PIM)

Scheme 6.2: Synthesis of of homopolymer and copolymers containing SFX units

The molecular structures of PIM-1, SFX-PIM-25 and SFX-PIM-33 were characterized by IR and ^{1}H NMR spectroscopy.

In IR spectrum (**Figure 6.5**), the characteristics band of –CN appeared at 2240 cm^{-1} while band of Ar-O-Ar was observed at 1260 cm^{-1}.

^{1}H NMR spectra of SFX-PIM-25, SFX-PIM-33 and PIM-1 are shown in **Figure 6.6**. In ^{1}H NMR spectra (**Figure 6.6**), the protons of spiro[fluorene-9,9'-xanthene] units are labeled as 1-10. The copolymer compositions (**Table 6.1**) of these PIMs were calculated by comparing

the integrated intensity ratios of protons of spirobisindane unit (labeled as 13) with aromatic protons of SFX unit (labeled as 10). The data in **Table 6.1** indicated that there was good agreement between observed and feed compositions.

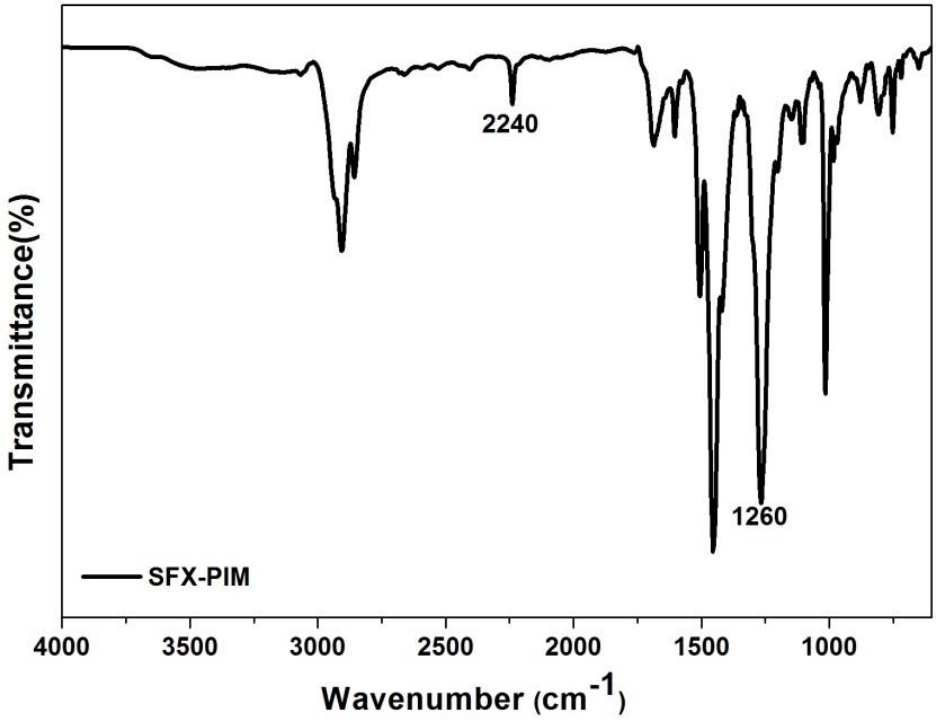

Figure 6.5: IR spectrum of SFX-PIM

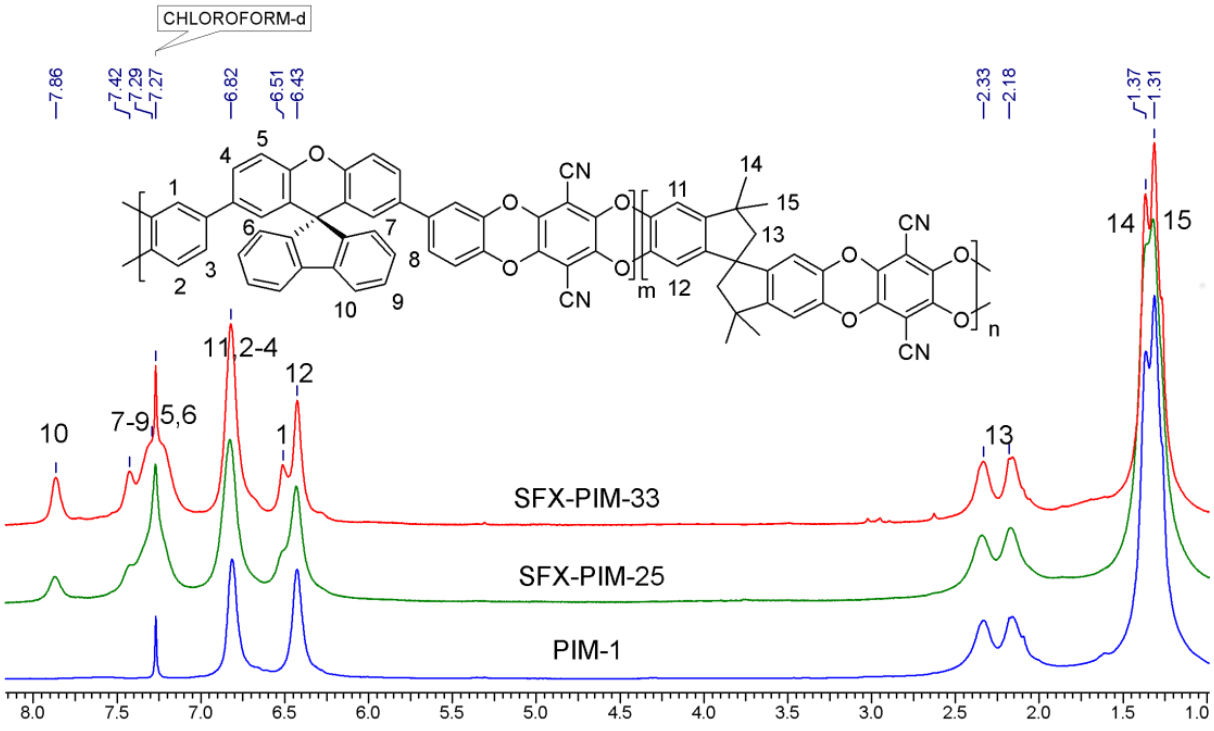

Figure 6.6: ^{1}H NMR spectra (in $CDCl_3$) of PIM-1, SFX-PIM-25 and SFX-PIM-33.

Table 6.1: Copolymer composition of PIMs from ^{1}H NMR spectra

Sr. No.	Polymer	Feed THSFX (mol %)	Observed THSFX (mol %)
1	**SFX-PIM-25**	25	24.3 ± 0.4
2	**SFX-PIM-33**	33	32.4 ± 0.3

6.3.3 Solubility of PIMs

The solubility of PIMs was tested at room temperature in organic solvents and the results are summarized in **Table 6.2**. SFX-PIM-25 and SFX-PIM-33 were found to be soluble in dichloromethane (DCM), chloroform ($CHCl_3$), tetrahydrofuran (THF), and *N*,*N*-dimethylacetamide (DMAc) whereas SFX-PIM-40, SFX-PIM-50, and SFX-PIM were found to be partially soluble or insoluble in organic solvents. The solution-based characterization such as GPC, NMR spectroscopy and film-fabrication of SFX-PIM-40, SFX-PIM-50, and SFX-PIM was not feasible due to the insolubility.

Table 6.2: Solubility data of PIMs.

Sr. No.	Polymer	$CHCl_3$	DCM	THF	DMAc	DMF	DMSO	Toluene	Acetone
1	**SFX-PIM-25**	++	++	++	++	--	--	+-	--
2	**SFX-PIM-33**	++	++	++	++	--	--	+-	--
3	**SFX-PIM-40**	+-	+-	+-	+-	--	--	--	--
4	**SFX-PIM-50**	--	--	--	--	--	--	--	--
5	**SFX-PIM**	--	--	--	--	--	--	--	--

[a:] Solubility tests of PI-PIMs were carried out 3 weight % (w/v) at room temperature. ++ : Soluble, +- : Partially Soluble, -- :Insoluble

6.3.4 Molecular Weights of PIMs

The molecular weights and dispersity values were determined by GPC analysis and the data are given in **Table 6.3**. Number average molecular weight (M_n) and dispersity values of SFX-PIM-25, SFX-PIM-33 and PIM-1 were in the range 23300-34100 g/mol and 2.1-2.8, respectively.

Table 6.3: Molecular weight data of SFX-PIMs and PIM-1

Sr. No.	Polymer	THSFX (mol %)	TTSBI (mol %)	TFTPN (mol %)	M_n (g/mol)[a]	M_w (g/mol)[a]	Dispersity[b]
1	**SFX-PIM**	100	0	100	ns	ns	ns
2	**SFX-PIM-50**	50	50	100	ns	ns	ns
3	**SFX-PIM-40**	40	60	100	ns	ns	ns
4	**SFX-PIM-33**	33	67	100	23300	65200	2.8
5	**SFX-PIM-25**	25	75	100	28900	83000	2.8
6	**PIM-1**	0	100	100	34100	71100	2.1

[a:] Molecular weights were obtained from GPC in chloroform (polystyrene standard). [b:] dispersity = Mw/Mn. ns: Inherent viscosity and GPC measurements could not be carried out due to insolubility in organic solvents such as $CHCl_3$, DMF and THF.

SFX-PIM-25 and SFX-PIM-33 could be cast into self-standing films by solution-casting method in chloroform and the photographs of films are shown in **Figure 6.7**.

Figure 6.7: Films of SFX-PIM-25 and SFX-PIM-33.

Table 6.4: Thermal properties, *d*-spacing, BET surface area, density and FFV of PIMs

Sr. No.	Polymer	$T_{10\%}$[a] (°C)	*d*-Spacing[b]	S_{BET} (m^2/g)[c]	Pore Volume[d]	Density[e] ($g\ cm^{-3}$)	FFV[f] (%)
1	**SFX-PIM**	480	6.65	366	0.37	-	-
2	**SFX-PIM-50**	505	7.07	596	0.45	-	-
3	**SFX-PIM-40**	504	7.55	661	0.47	-	-
4	**SFX-PIM-33**	508	7.62	682	0.50	1.20	18
5	**SFX-PIM-25**	512	7.82	731	0.56	1.15	19
6	**PIM-1**	490	7.96	796	0.62	1.12	22

[a:] Temperature at which 10% weight loss was recorded by TGA at a heating rate of 10 °C/min. under N_2 atmosphere. [b:] *d*-Spacing was calculated from XRD patterns using Bragg's equation. [c:] BET surface area obtained from N_2 adsorption method. [d:] Pore volume was calculated from nitrogen adsorption at $p/p_o = 0.98$. [e:] Density was calculated by specific gravity bottle method. [f:] Fractional free volume was calculated from Bondi's equation ($FFV= V-V_o/V$).

6.3.5 X-Ray Diffraction of PIMs

X-Ray diffraction study was used to determine the crystallinity of polymers (**Figure 6.8**). The broad halo around 2θ = 10-25° in X-ray diffraction patterns indicated amorphous nature of SFX-PIMs. The inter-segmental distance (*d*-spacing) is considered as the distance between polymer chains and was calculated by Bragg's equation from peak maxima of X-ray diffractograms (**Table 6.4**). The *d*-spacing of PIMs were in the range 6.65-7.96 Å. The high *d*-spacing in PIMs is likely due to the poor chain packing efficiency by the incorporation of the SFX and TTSBI units in the polymer backbone. The order of *d*-spacing is as: PIM-1 > SFX-PIM-25 > SFX-PIM-33 > SFX-PIM-40 > SFX-PIM-50 > SFX-PIM. SFX-PIMs showed lower *d*-spacing than PIM-1 which indicated that spirobisindane unit is more effective than SFX unit in disturbing polymer chain packing.

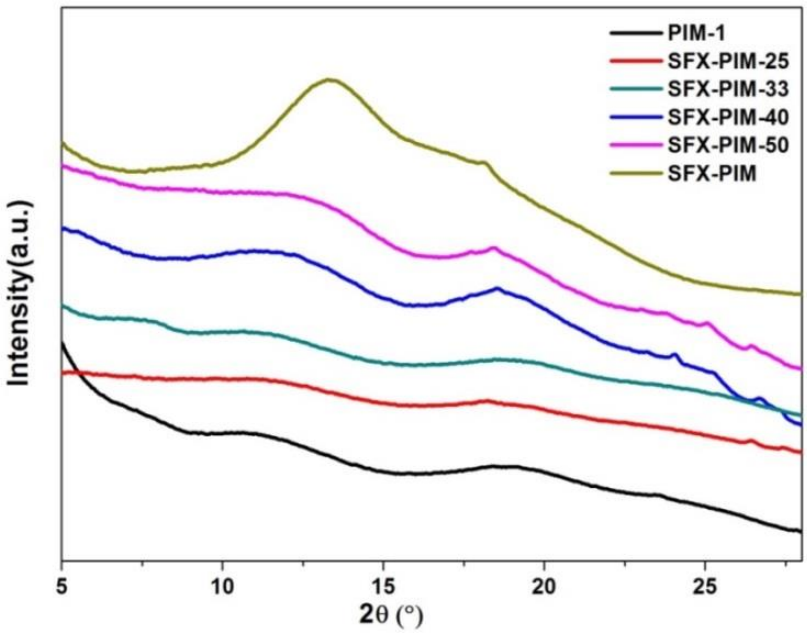

Figure 6.8: X-Ray diffractograms of PIM-1 and SFX-PIMs

6.3.6 Density and Fractional Free Volume (FFV) of PIMs

The data on density and fractional free volume (FFV) of films of SFX-PIM-25, SFX-PIM-33 and PIM-1 are given in **Table 6.4**. The density of PIM films was calculated by density bottle method and was in the range 1.12-1.20 g cm^{-3}. The density of SFX-PIMs was higher than that of PIM-1 which indicated relatively closer chain packing in the former systems. The FFV values of SFX-PIM-25, SFX-PIM-33 and PIM-1 were calculated using Bondi's method and the values were in the range 18-22 %. The FFV values of SFX-PIM-25 and SFX-PIM-33 were lower than that of PIM-1. These data indicated that SFX unit is less effective as compared to spirobisindane unit in disturbing polymer chain packing.

6.3.7 Thermal Properties of PIMs

The thermal stability of PIMs was determined by TGA measurements under nitrogen carried out upto 800 °C. TG curves of these PIMs are shown in **Figure 6.9**. SFX-PIMs showed excellent thermal stability with T_{10} values in the range 480-512 °C (**Table 6.4**). DSC measurements were carried out on PIMs to determine glass transition temperature (T_g). No T_g was detected in DSC measurement carried out up to 390 °C. Similar observations concerning T_g were reported for hexaphenylbenzene and spirobifluorene-based PIMs.[27,28]

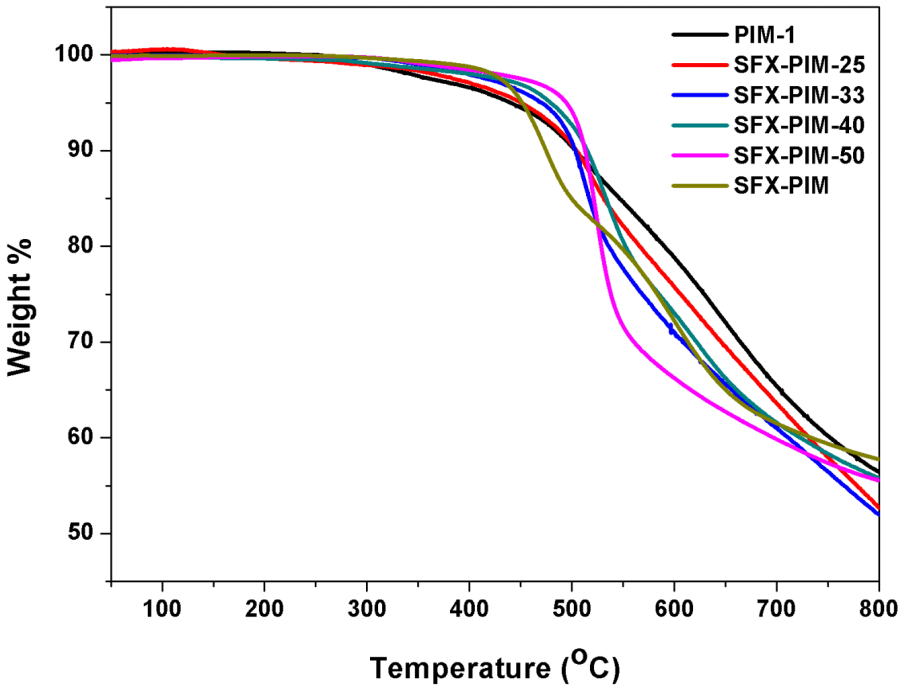

Figure 6.9: TG curves of PIM-1 and SFX-PIMs.

6.3.8 Intrinsic Microporosity of PIMs

Adsorption/desorption isotherms of SFX-PIMs were recorded at 77 K using nitrogen. Adsorption/desorption isotherms (**Figure 6.10**) of PIMs demonstrated high nitrogen uptake at low pressure and characteristics loops for microporosity were observed (Type I). This indicated that PIMs possessed intrinsic microporosity due to the presence of ladder spirocyclic units such as SFX and spirobisindane units. The N_2 adsorption isotherms provided high apparent BET surface area and the values were in the range 366-796 m^2/g (**Table 6.4**). The order of BET surface area is as: PIM-1 > SFX-PIM-25 > SFX-PIM-33 > SFX-PIM-40 > SFX-PIM-50 > SFX-PIM. These results are in accordance with the trends observed in d-spacing and FFV values.

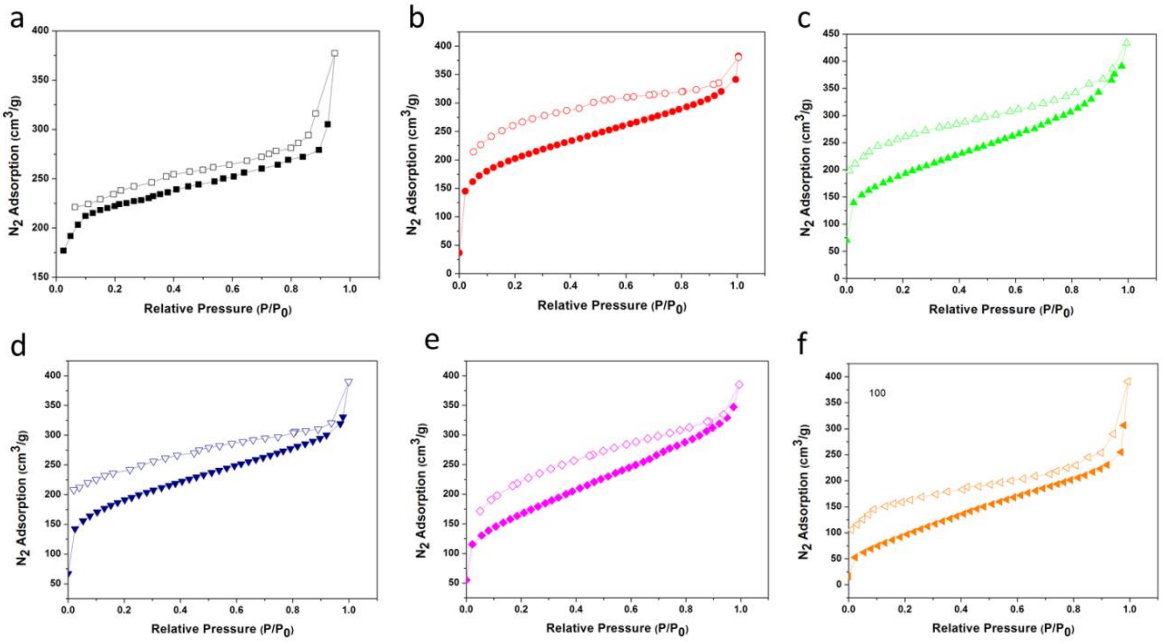

Figure 6.10: Nitrogen adsorption (filled) and desorption (empty) isotherms at 77 K of a) PIM-1, b) SFX-PIM-25, b) SFX-PIM-33, b) SFX-PIM-40, e) SFX-PIM-50 and f) SFX-PIM.

6.3.9 Density Functional Theory (DFT) Analysis

DFT analysis was performed to elucidate the effect of SFX unit on polymer chain packing. The energy optimization of two repeating units structures of SFX-PIM and PIM-1 were carried out using DFT (**Figure 6.11)**. In PIM-1, the angle at spirobisindane spiro center was 114° while in SFX-PIM, the angle at SFX-PIM spiro-center was 111°. These results indicated that SFX-PIM is relatively compact than PIM-1 due to its lower angle at spiro-center. This explains lower *d*-spacing, FFV and BET surface area values of SFX-PIMs as compared to PIM-1.

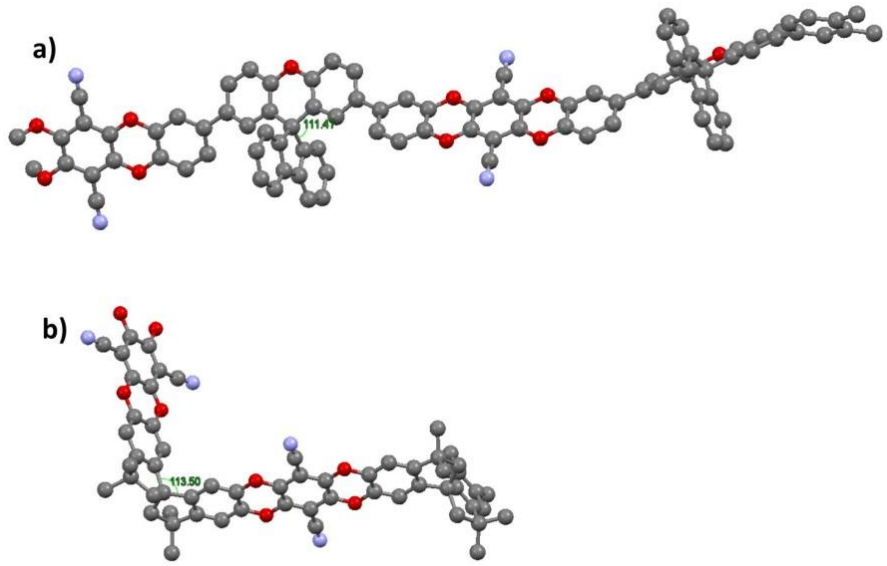

Figure 6.11: Two repeating units of a) SFX-PIM and b) PIM-1.

6.4 GAS PERMEABILITY

The pure gas permeability of films of SFX-PIM-25 and SFX-PIM-33 was determined using variable-volume method for He, H_2, N_2, O_2, CH_4 and CO_2 gases with feed pressure ranging from 28-32 psi. SFX-PIM-40, SFX-PIM-50 and SFX-PIM were partially soluble or insoluble in organic solvents and, therefore, films of these polymers could not be made to measure the gas permeability. Considerable variations in the gas permeability of PIMs with the variation in contents of SFX units were observed and the results are discussed below.

6.4.1 Effect of SFX and SBI Units on Gas Permeation properties

The gas permeability studies on methanol-treated PIMs and that of PIMs films aged for 130 days were carried out. Methanol treatment is known to remove any residual casting solvent which induces additional free volume by increasing inter-chain distances.

The order of gas permeability for SFX-PIM-25, SFX-PIM-33 and PIM-1 is as: $PN_2 < PCH_4 < PO_2 < PHe < PH_2 < PCO_2$. Similar trends were observed for PIMs in the literature.[28] The gas permeability and selectivity data of methanol-treated films of SFX-PIM-25, SFX-PIM-33 and PIM-1 are presented in **Table 6.5** and **6.6**. SFX-PIM-25 and SFX-PIM-33 exhibited high permeability and appreciable selectivity of one gas over other. Under the similar conditions of measurements, SFX-PIMs are more selective for all gas pairs and less permeable as compared to PIM-1. For instance, methanol-treated film of SFX-PIM-33 exhibited CO_2 permeability of 3595 Barrer with selectivity for CO_2/N_2 gas pair was 23.5 whereas methanol-treated film of PIM-1 exhibited CO_2 permeability of 4644 Barrer with selectivity for CO_2/N_2 gas pair was 14.7. These results implied that SFX unit disturbed polymer chain packing less effectively as compared to spirobisindane unit. This trend is also consistent with *d*-spacing, BET surface area and FFV (**Table 6. 4**).

6.4.2 Effect of Physical Aging on Gas Permeation properties

Physical aging is a process in which polymer chains undergo relaxation resulting into decrease in permeability over time due to reduction of free volume.[29] The gas permeability and selectivity data of SFX-PIM-25, SFX-PIM-33 and PIM-1 for the methanol-treated films which were physically aged at 130 days are shown in **Table 6.4** and **6.5.** It was observed that there was decrease in permeability with increase in selectivity for all gases. For instance, the CO_2 permeability of SFM-PIM-33 decreased from 3595 to 1848 Barrer with increase in selectivity for CO_2/N_2 and CO_2/CH_4 gas pairs from 23.5 to 30.8 and from 8.7 to 11.9, respectively. Thus, films of SFX-PIMs after aging demonstrated further enhancement in gas selectivity.

Table 6.5: Gas permeability of SFX-PIMs and reported PIMs and SFX-based polymers

Sr. No.	Polymer	Permeability (Barrer)[a,b,c]					
		He	H_2	N_2	O_2	CH_4	CO_2
1	**SFX-PIM-33**	637	1284	153	489	413	3595
		(318)	(749)	(60)	(289)	(155)	(1848)
2	**SFX-PIM-25**	793	1522	208	606	500	4034
		(496)	(1018)	(105)	(411)	(200)	(2120)
3	**PIM-1**	992	2152	316	822	618	4644
		(595)	(1432)	(154)	(510)	(308)	(2526)
4	**SBF-PIM**[6]	2200	6320	786	2640	1100	13900
5	**PIM-1**[6]	1950	5010	823	2270	1360	13600
6	**PA S1**[8]	-	-	1.88	14	1.5	48
7	**PA S2**[8]	-	-	1.50	11	1.27	45

[a:] Units of permeability (P): 1 Barrer = 10^{-10} cm^3 (STP)cm /cm^2 s cm Hg. [b:] Gas permeability of aged films (130 days) of PIMs are given in parentheses. [c:] Gas permeability data taken from literature (4-7) are marked in red.

Table 6.6: Gas selectivity of SFX-PIMs and reported PIMs and SFX-based polymers

Sr. No.	Polymer	Selectivity (α)[a,b,c]			
		H_2/N_2	O_2/N_2	CO_2/N_2	CO_2/CH_4
1	**SFX-PIM-33**[d]	8.4 (12.5)	3.2 (4.8)	23.5 (30.8)	8.7 (11.9)
2	**SFX-PIM-25**[d]	7.3 (9.7)	2.9 (3.9)	19.4 (20.2)	8.0 (10.6)
3	**PIM-1**[d]	6.8 (9.3)	2.6 (3.3)	14.7 (16.4)	7.5 (8.2)
4	**SBF-PIM**[6]	8.04	3.35	17.7	12.63
5	**PIM-1**[6]	6.08	2.8	16.6	10
6	**PA S1**[8]	-	7.45	25.53	32
7	**PA S2**[8]	-	7.80	30	35.43

[a:] Selectivity (α) = P_1/P_2. [b:] Gas selectivity of aged films (130 days) of PIMs are given in parentheses. [c:] Gas selectivity data taken from literature (4-7) are marked in red.

6.4.3 Comparison of SFX-PIMs with Reported PIMs and SFX-based Polymers

In order to understand efficacy of SFX-PIMs, it is worth to compare the gas permeability data of SFX-PIMs with reported PIMs and SFX-based polymers. The gas permeation properties of previously reported SBF-PIM and SFX-based polymers are also included in **Table 6.5** and **6.6** for comparison. It is worth to note that the present PIMs showed higher permeability than

SFX-based polymers and higher selectivity than PIMs containing spirobisindane and spirobifluorene units.[6] In the Robeson plots (**Figure 6.12**), the present PIMs films followed the usual trade-off relationship between permeability and selectivity and the gas permeability data of SFX-PIM-25 and SFX-PIM-33 for CO_2/N_2, CO_2/CH_4, H_2/N_2 and O_2/N_2 was located close to 1991 Robeson upper bound.

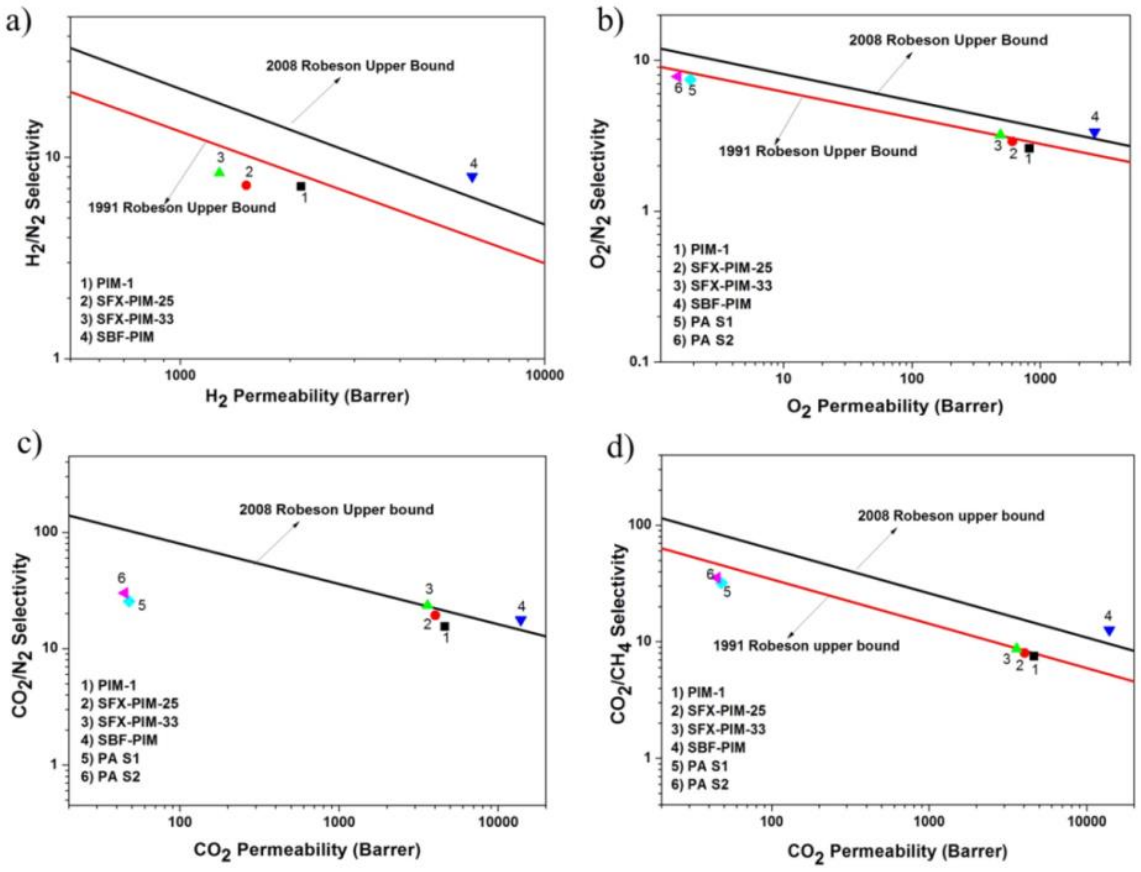

Figure 6.12: Robeson plots for (a) H_2/N_2; (b) O_2/N_2; (c) CO_2/N_2; and (d) CO_2/CH_4 gas pairs.

6.5 CONCLUSIONS

In this work, a new bis(catechol) containing spiro[fluorene-9,9'-xanthene] unit, namely, 4,4'-(spiro[fluorene-9,9'-xanthene]-2',7'-diyl)bis (benzene-1,2-diol) (THSFX) was designed and synthesized. Polycondensation of THSFX and varying compositions of THSFX and TTSBI with TFTPN was carried out to afford homo and copolymers with intrinsic microporosity. The soluble PIMs showed reasonably high molecular weights and could be cast into thin films. The resulting polymers exhibited excellent thermal stability (T_{10} = 490-510 °C), amorphous nature and high FFV (17-20%). These PIMs possessed intrinsic microporosity as indicated by N_2 adsorption method and showed high BET surface area in the range 360-796 m^2/g. Gas permeability analysis showed that methanol-treated films of SFX-PIM-25 and SFX-PIM-33 are highly permeable with appreciable selectivity. The gas permeability of methanol-treated films of SFX-PIMs for CO_2/N_2 and O_2/N_2 gas pairs was close to 1991

Robeson upper bound. Overall, the results indicated that SFX unit is an interesting building block to introduce intrinsic microporosity in PIMs and SFX-containing PIMs exhibited attractive gas permeability characteristics.

6.6 REFERENCES

1. McKeown, N. B., Budd, P. M. *Chem. Soc. Rev.*, 2006, **35**, 675–683.
2. Kim, S., Lee, Y. M. *Prog. Polym. Sci.*, 2015, **43**, 1–32.
3. McKeown, N. B. *ISRN Mater. Sci.*, 2012, **2012**, 1–16.
4. Du, N., Park, H. B., Dal-Cin, M. M., Guiver, M. D. *Energy Environ. Sci.*, 2012, **5**, 7306–7322.
5. Budd, P. M., Elabas, E. S., Ghanem, B. S., Makhseed, S., McKeown, N. B., Msayib, K. J., Tattershall, C. E., Wang, D. *Adv. Mater.*, 2004, **16**, 456–459.
6. Bezzu, C. G., Carta, M., Tonkins, A., Jansen, J. C., Bernardo, P., Bazzarelli, F., Mckeown, N. B. *Adv. Mater.*, 2012, **24**, 5930–5933.
7. McKeown, N. B., Gahnem, B., Msayib, K. J., Budd, P. M., Tattershall, C. E., Mahmood, K., Tan, S., Book, D., Langmi, H. W., Walton, A. *Angew. Chem. Int. Ed.*, 2006, **45**, 1804–1807.
8. Bandyopadhyay, P., Banerjee, S. *Eur. Polym. J.*, 2015, **69**, 140–155.
9. Jiang, H., Sun, J., Yuan, K., Zhang, Q. *Synth. Met.*, 2014, **197**, 217–224.
10. Ma, X., Ghanem, B., Salines, O., Litwiller, E., Pinnau, I. *ACS Macro Lett.*, 2015, **4**, 231–235.
11. Ghanem, B. S., McKeown, N. B., Budd, P. M., Selbie, J. D., Fritsch, D. *Adv. Mater.*, 2008, **20**, 2766–2771.
12. Budd, P. M., Elabas, E. S., Ghanem, B. S., Makhseed, S., McKeown, N. B., Msayib, K. J., Tattershall, C. E., Wang, D. *Adv. Mater.*, 2004, **16**, 456–459.
13. Bezzu, C. G., Carta, M., Tonkins, A., Jansen, J. C., Bernardo, P., Bazzarelli, F., Mckeown, N. B. *Adv. Mater.*, 2012, **24**, 5930–5933.
14. Du, N., Park, H. B., Dal-Cin, M. M., Guiver, M. D. *Energy Environ. Sci.*, 2012, **5**, 7306–7322.
15. Sen, S. K., Banerjee, S. *J. Membr. Sci.*, 2010, **365**, 329–340.
16. Weber, J., Su, Q., Antonietti, M., Thomas, A. *Macromol. Rapid Commun.*, 2007, **28**, 1871–1876.
17. Wang, Z., Wang, D., Jin, J. *Macromolecules*, 2014, **47**, 7477–7483.
18. Ma, X., Salinas, O., Litwiller, E., Pinnau, I. *Macromolecules*, 2013, **46**, 9618–9624.
19. Du, N., Robertson, G. P., Pinnau, I., Thomas, S., Guiver, M. D. *Macromol. Rapid Commun.*, 2009, **30**, 584–588.
20. McKeown, N. B., Budd, P. M. *Chem. Soc. Rev.*, 2006, **35**, 675–683.
21. Xu, Z. K., Dannenberg, C., Springer, J., Banerjee, S., Maier, G. *Chem. Mater.*, 2002, **14**, 3271–3276.
22. Ghosh, S., Banerjee, S. *J. Membr. Sci.*, 2016, **497**, 172–182.
23. Maciejczyk, M., Ivaturi, A., Robertson, N. *J. Mater. Chem. A*, 2016, **4**, 4855–4863.
24. Chen, Q., Wang, J., Wang, Q., Bian, N., Li, Z., Yan, C., Han, B. *Macromolecules*, 2011, **44**, 7987–7993.
25. Zhang, S., Li, Y., Ma, T., Zhao, J., Xu, X., Yang, F., Xiang, X. *Polym. Chem.*, 2010, **1**, 485–493.
26. Zhao, J., Xie, G. H., Yin, C. R., Xie, L. H., Han, C. M., Chen, R. F., Xu, H., Yi, M. D., Deng, Z. P., Chen, S. F., Zhao, Y., Liu, S. Y., Huang, W. *Chem. Mater.*, 2011, **23**, 5331–5339.
27. Bezzu, C. G., Carta, M., Tonkins, A., Jansen, J. C., Bernardo, P., Bazzarelli, F., McKeown, N. B. *Adv. Mater.*, 2012, **24**, 5930–5933.
28. Carta, M., Bernardo, P., Clarizia, G., Jansen, J. C., Mckeown, N. B. *Macromolecules*, 2014, **47**, 8320–8327.
29. Swaidan, R., Ghanem, B., Litwiller, E., Pinnau, I. *Macromolecules*, 2015, **48**, 6553–6561.

Supporting Information

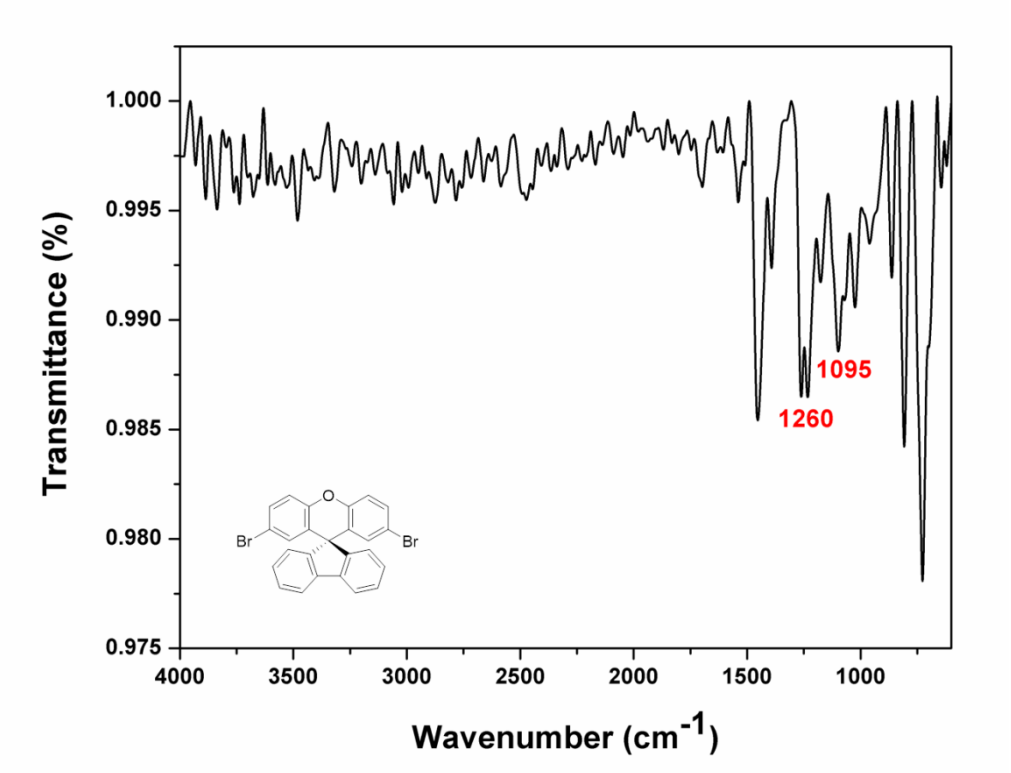

Figure SI 6.1: IR spectrum of 2',7'-dibromospiro[fluorene-9,9'-xanthene] (DBSFX).

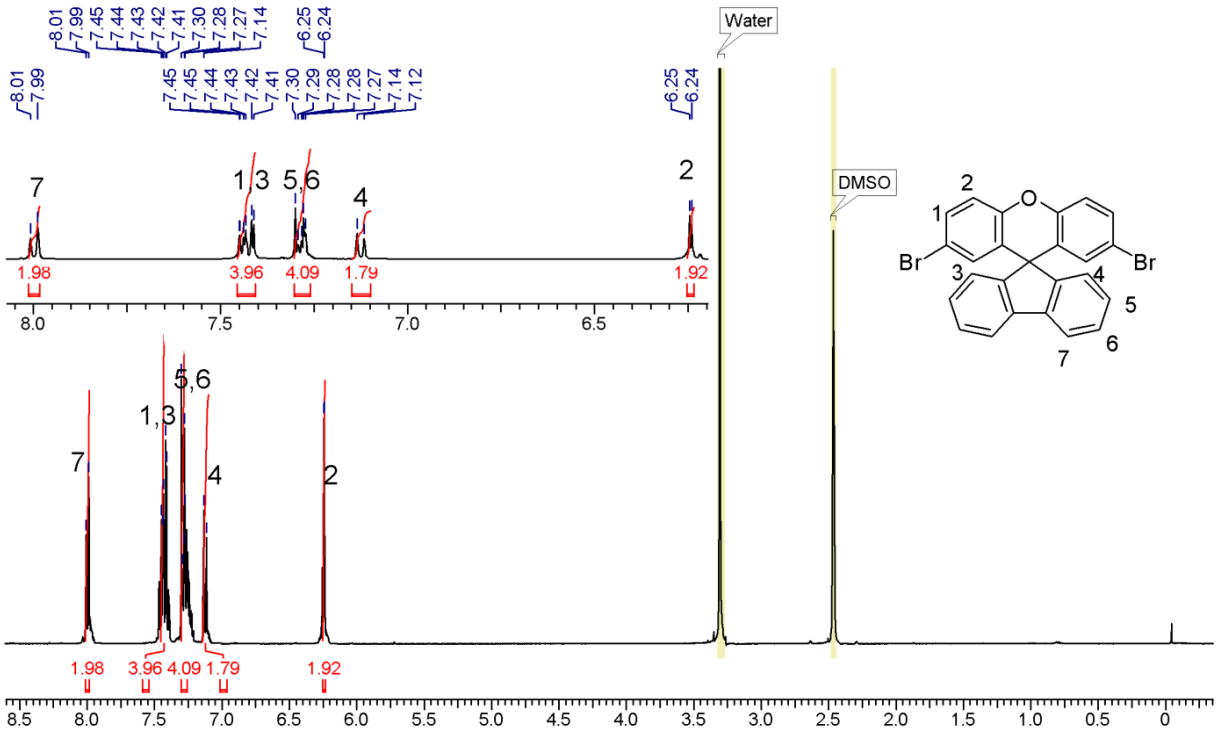

Figure SI 6.2: ^{1}H NMR spectrum (in DMSO-d_6) of 2',7'-dibromospiro[fluorene-9,9'-xanthene] (DBSFX).

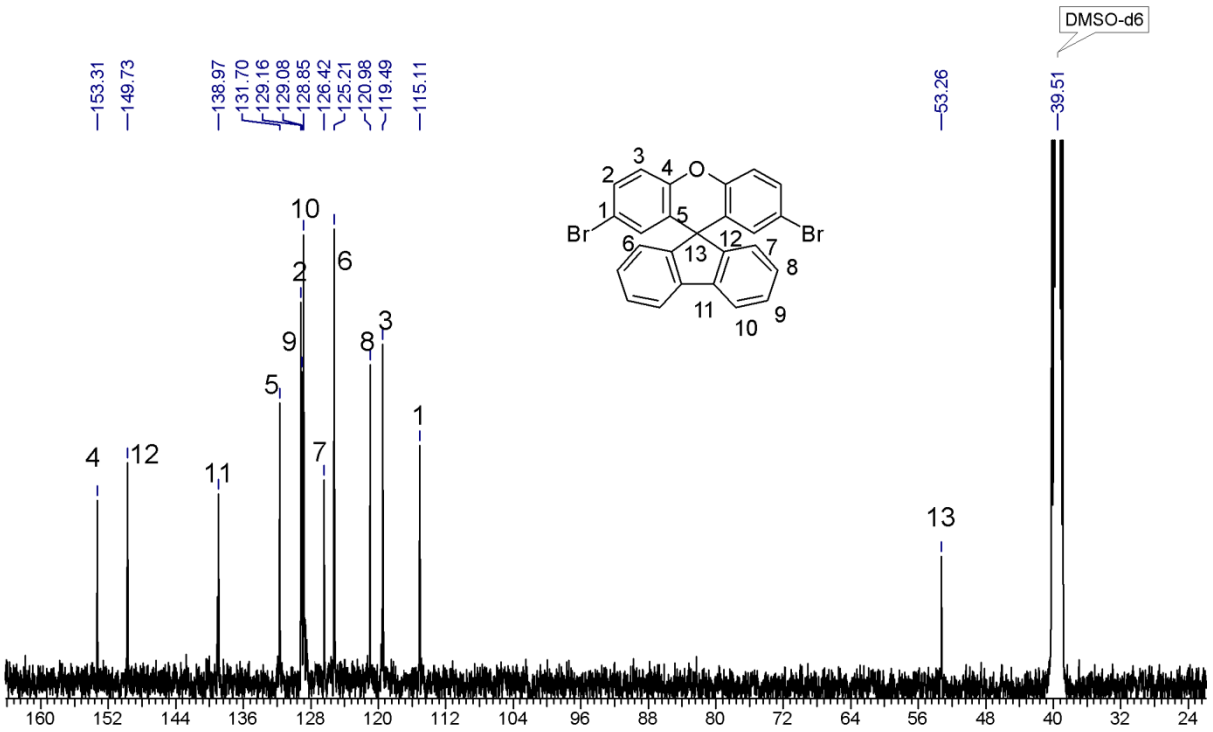

Figure SI 63: ^{13}C NMR spectrum (in DMSO-d_6) of 2',7'-dibromospiro[fluorene-9,9'-xanthene] (DBSFX).

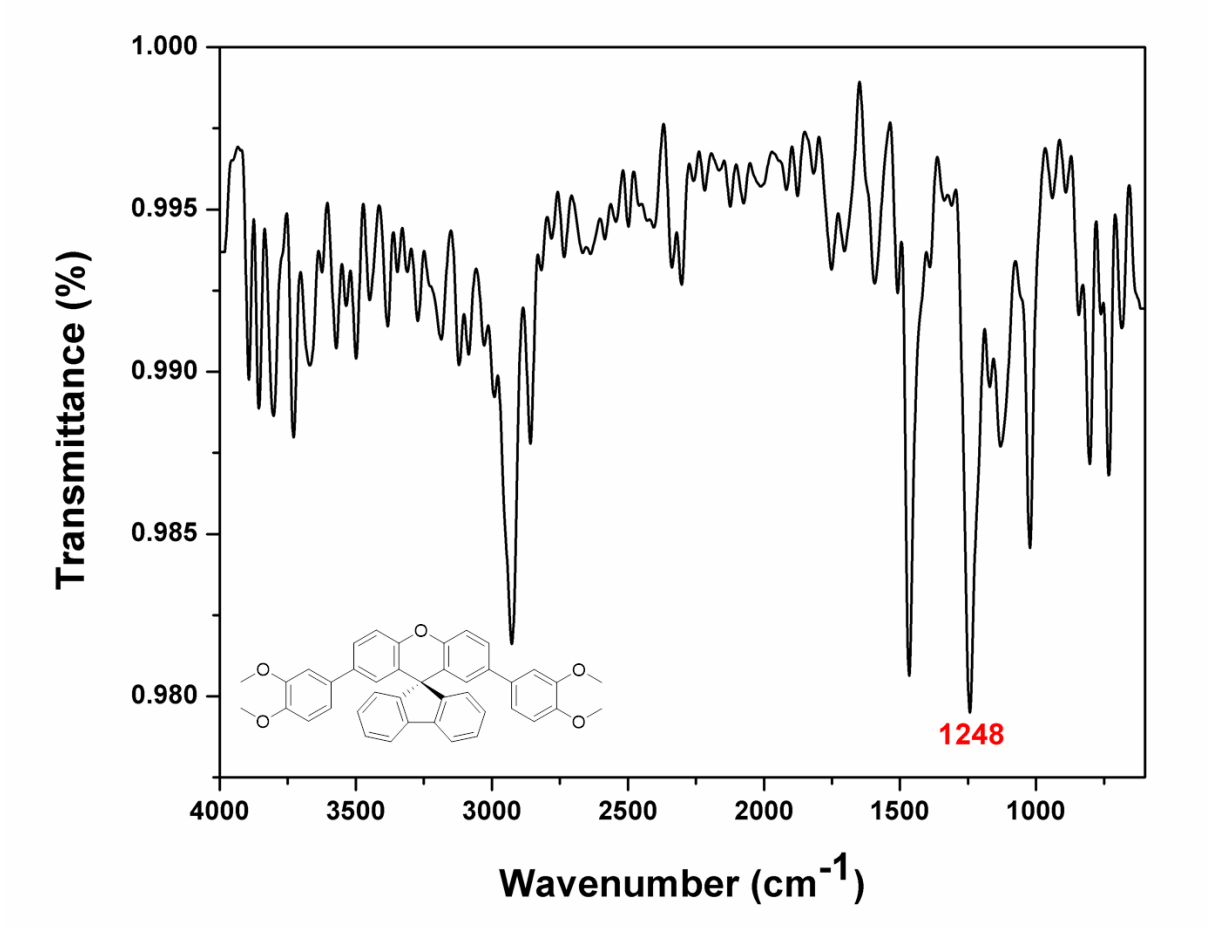

Figure SI 6.4: IR spectrum of tetramethoxyxanthene2',7'-bis(3,4-dimethoxyphenyl)spiro [fluorene-9,9'-xanthene] (TMSFX).

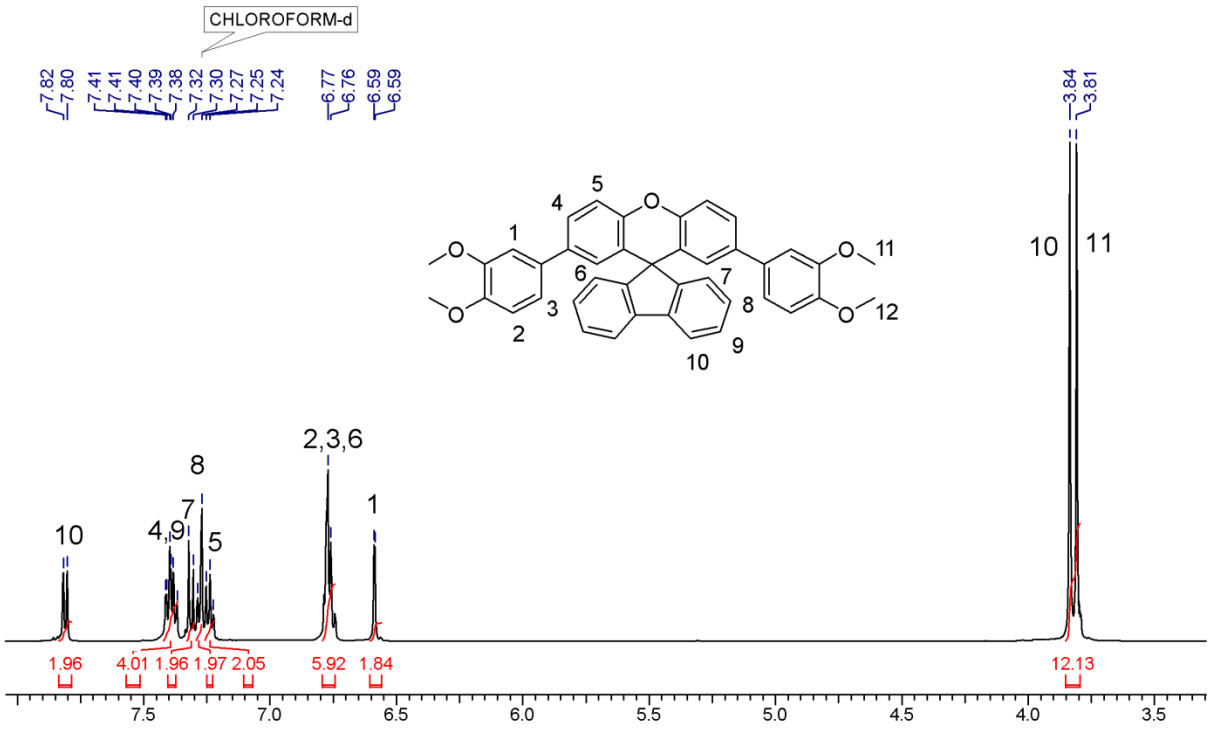

Figure SI 6.5: ^{1}H NMR spectrum (in $CDCl_3$) of tetramethoxyxanthene2',7'-bis(3,4-dimethoxyphenyl)spiro [fluorene-9,9'-xanthene] (TMSFX).

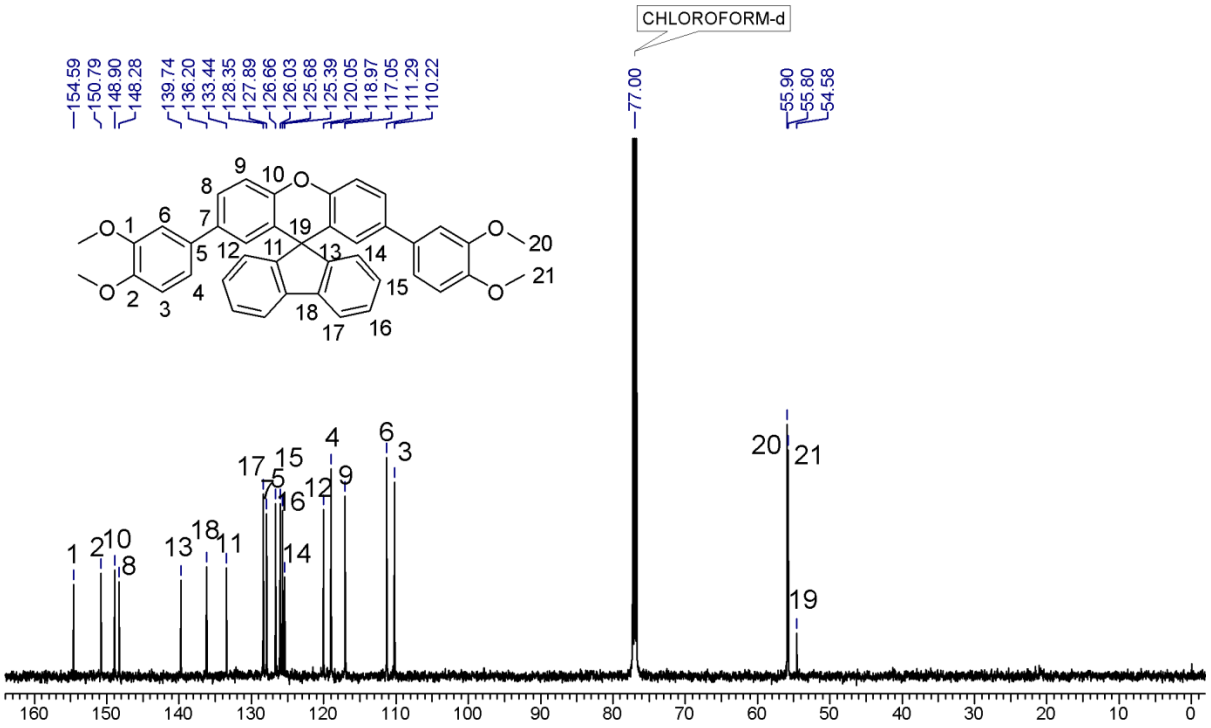

Figure SI 6.6: ^{13}C NMR spectrum (in $CDCl_3$) of tetramethoxyxanthene2',7'-bis(3,4-dimethoxyphenyl)spiro [fluorene-9,9'-xanthene] (TMSFX).

Chapter 7

Design, Synthesis and Gas Permeation Properties of Polyimide-Based Poly(ionic liquid)s

In the recent years, film-forming poly(ionic liquid)s (PILs) have gained significant attention as emerging materials for gas separation applications. The aim of the present work was to synthesize new film-forming polyimide-based poly(ionic liquid)s (PI-PILs) and evaluate their performance as membrane materials for gas separation applications. In this context, a new aromatic diamine, namely, N^1-(4-aminophenyl)-N^1-(4-(2-phenyl-1H-imidazol-1-yl)phenyl)benzene-1,4-diamine (ImTPADA) was designed and synthesized. ImTPADA was polycondensed with three aromatic dianhydrides to form corresponding polyimides (PIs). Further, PI-PILs were prepared by N-quaternization of PI-6FDA with methyl iodide followed by anion exchange reaction with bis(trifluoromethane)sulfonimide lithium salt ($LiTf_2N$). PIs and PI-PILs exhibited reasonably high molecular weights (79200-35000 g/mol) and amorphous nature. PI-PILs showed good solubility in polar organic solvents and could be cast into self-standing films from their DMAc solutions. TGA indicated that T_{10} values of PIs and PI-PILs were in the range 545-475 °C and 303-306 °C, respectively. Gas permeability analysis demonstrated that incorporation of ionic groups into PI-6FDA resulted in increased permeability while maintaining selectivity. In particular, PI-PIL bearing Tf_2N^- anion exhibited high CO_2 permeability (33.3 Barrer) and high selectivity for CO_2/CH_4 (41.1) and CO_2/N_2 (35.4).

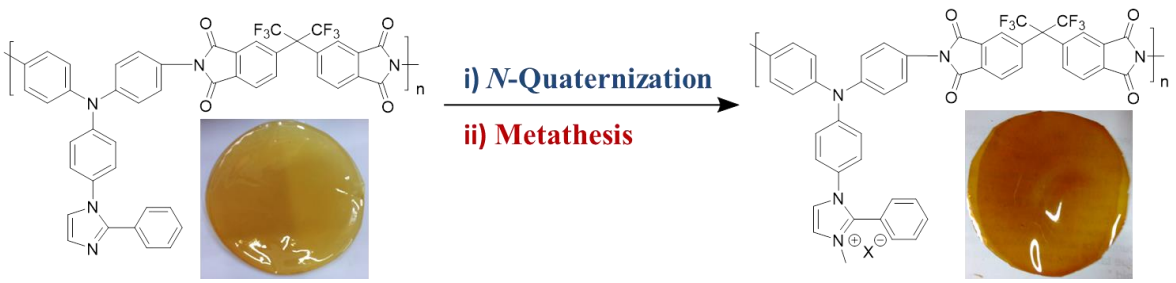

J. Polym. Sci. Part A: Polym. Chem., (***Manuscript Accepted***)

7.1 INTRODUCTION

Polymeric ionic liquids (PILs) have gained considerable attention in recent years for various applications including lithium-ion batteries, PEMFC, super-capacitors, gas separation, etc.[1–6] PILs contains ionic groups either in the backbone or as pendant and their physical properties can be tuned by varying the contents and compositions of ionic groups.[7] For gas separation, PILs exhibited excellent gas permeation properties particularly for CO_2 separation because of the interaction of ionic counterpart with CO_2.[1,7–11] Till date, various classes of polymers containing ionic liquids have been reported including polybenzimidazole, polyethers, polyimides, etc.[1,4,7,11–16] Taking into consideration the attractive performance of PILs, it is of interest to synthesize new film-forming PILs and improve the understanding of structure-property relationships.

Polyimides (PIs) are widely studied polymers for gas separation applications due to their highly rigid structure, high thermo-chemical stability, and possibilities of structural variation *via* appropriate choice of monomers.[17–23] The incorporation of ionic groups into PIs is one of the promising strategies to improve both permeability and selectivity. The incorporation of ionic groups into PIs was first reported by Li and co-workers in 2010 and they found increase in CO_2-based selectivity.[13] The post-modification of polyimides to polyimide-based PILs was firstly reported by Shaplov and coworkers.[15] Compared to parent polyimides, PI-PILs exhibited an improvement in gas separation performance. These results suggested that incorporation of ionic groups into polymers is of great interest for obtaining both high permeability and selectivity.

In this work, a new aromatic diamine *viz*. N^1-(4-aminophenyl)-N^1-(4-(2-phenyl-1H-imidazol-1-yl) phenyl)benzene-1,4-diamine (ImTPADA) was synthesized and polycondensed with three commercially available aromatic dianhydrides *viz.*, 4,4′-(hexafluoro isopropylidene)diphthalic anhydride (6-FDA), 4,4’-(4,4’-isopropylidenediphenoxy)bis (phthalic anhydride) (BPADA) and 4,4′-oxydiphthalic anhydride (ODPA) to obtain PIs. The *N*-quaternization of polyimide-based on 6FDA (PI-6FDA) and its anion exchange reaction was performed to afford polyimide-based poly(ionic liquid)s (PI-PILs). PIs and PI-PILs were characterized by IR and ^{1}H NMR spectroscopy, GPC, XRD, TGA, and DSC. The effects of dianhydrides and anion variation on physical and gas permeation properties were investigated.

7.2 EXPERIMENTAL

Details about materials used in the study and experimental techniques such as solubility study, IR, ^{1}H and ^{13}C NMR spectroscopy, TGA, DSC, XRD and gas permeability analysis have been given in **Chapter 3**.

7.2.1 Preparations

7.2.1.1 Synthesis of 1-(4-nitrophenyl)-2-phenyl-1H-imidazole (ImN)

Into a 500 mL two-necked round-bottom flask equipped with a magnetic stirring bar, a reflux condenser and a nitrogen inlet were charged dry dimethyl sulfoxide (250 mL), sodium hydride (5 g, 208 mmol) and 2-phenylimidazole (20 g, 138.7 mmol). The reaction mixture was stirred under nitrogen at room temperature for 1 h and then 1-fluoro-4-nitrobenzene (17.67 mL, 166.4 mmol) in dimethyl sulfoxide (30 mL) was added dropwise over a period of 30 minutes. The reaction mixture was heated at 140 °C for 48 h under nitrogen, cooled to room temperature and precipitated into ice-cold water (1000 mL). The solids were collected by filtration, washed several times with water and dried under vacuum at 70 °C. ImN was purified by recrystallization from methanol.

Yield: (28 g, 76 %)

Melting point: 110 °C.

IR ($CHCl_3$, cm^{-1}): 1597 (-NO_2 asymmetric stretching) and 1345 (-NO_2 symmetric stretching).

^{1}H NMR (200 MHz, $CDCl_3$, δ/ppm): 8.23 (d, 2H, Ar-H), 7.42-7.33 (m, 8H, Ar-H), 7.26 (d, 1H, Ar-H).

^{13}C NMR (50 MHz, $CDCl_3$, δ/ppm): 146.8, 146.6, 143.4, 129.8, 129.4, 129.0, 128.7, 128.4, 126.0, 124.8, 122.0.

HRMS (ESI): calcd. for $C_{15}H_{12}N_3O_2$ ($[M+H]^+$): 266.0924; found 266.0922.

7.2.1.2 Synthesis of 4-(2-phenyl-1H-imidazol-1-yl) aniline (ImA)

Into a 500 mL three-necked round-bottom flask equipped with a magnetic stirring bar, a nitrogen inlet and a reflux condenser were charged ImN (26 g, 98 mmol), 10 wt% Pd/C (1 g) and ethanol (200 mL). To the reaction mixture, hydrazine hydrate (10 mL) was added dropwise at room temperature over a period of 30 minutes under nitrogen atmosphere and then refluxed overnight. After completion of reaction (monitored by TLC), the reaction mixture was filtered, cooled and precipitated into ice-cold water (1000 mL). The solids were collected by filtration and dried under vacuum at 70 °C. The crude product was recrystallized from ethanol to afford 4-(2-phenyl-1H-imidazol-1-yl) aniline as colorless crystals.

Yield: (18 g, 78 %)

Melting Point: 170 °C.

IR ($CHCl_3$, cm^{-1}): 3463 (N–H asymmetric stretching) and 3387 (N–H symmetric stretching).

^1H NMR (200 MHz, $CDCl_3$, δ/ppm): 7.46 (d, 2H, Ar-H), 7.28-7.24 (m, 4H, Ar-H), 7.11 (s, 1H) (d, 2H, Ar-H), 6.67 (d, 2H, Ar-H). 3.71 (s, 2H, $-NH_2$)

^{13}C NMR (50 MHz, $CDCl_3$, δ/ppm): 146.5, 146.4, 129.9, 129.0, 128.4, 128.3, 128.1, 127.8, 126.9, 123.3, 115.2.

HRMS (ESI): calcd. for $C_{15}H_{14}N_3$ ($[M+H]^+$) : 236.1182; found 236.1181.

7.2.1.3 Synthesis of 4-nitro-N-(4-nitrophenyl)-N-(4-(2-phenyl-1H-imidazol-1-yl)phenyl) aniline (ImTPADN)

Into a 500 mL two-necked round-bottom flask equipped with a magnetic stirring bar, a reflux condenser and a nitrogen inlet were charged ImA (16 g, 68 mmol), sodium hydride (4.9 g, 204 mmol) and dry dimethyl sulfoxide (150 mL). The reaction mixture was stirred under nitrogen atmosphere at room temperature for 1 h and then 1-fluoro-4-nitrobenzene (17.34 mL, 163.2 mmol) in dimethyl sulfoxide (30 mL) was added dropwise. The reaction mixture was heated at 140 °C for 72 h, cooled to room temperature and precipitated into ice-cold water (1000 mL). The solids were collected by filtration, washed several times with water and dried under vacuum at 70 °C. The product was dissolved in ethyl acetate. The ethyl acetate solution was washed with brine, water, dried over sodium sulfate and filtered. Ethyl acetate was evaporated on a rotary evaporator. The crude product was purified by silica gel column chromatography using pet ether: ethyl acetate (50:50, v/v) as an eluent to afford ImTPADN as a faint yellow solid.

Yield: (15 g, 46 %)

Melting point: above 300 °C.

IR ($CHCl_3$, cm^{-1}): 1580 ($-NO_2$ asymmetric stretching) and 1312 ($-NO_2$ symmetric stretching);

^1H NMR (200 MHz, $CDCl_3$, δ/ppm): 8.21 (d, 4H, Ar-H), 7.40 (d, 2H, Ar-H), 7.31-7.27 (m, 7H, Ar-H), 7.24-7.19 (m. 6H, Ar-H).

^{13}C NMR (50 MHz, $CDCl_3$, δ/ppm): 151.2, 146.0, 145.4, 143.4, 135.1, 129.9, 129.0, 128.6, 127.8, 127.2, 126.7, 125.7, 123.1, 122.7.

HRMS (ESI): calcd. for $C_{27}H_{20}N_5O_4$ ($[M+H]^+$) : 478.1510; found 478.1511.

7.2.1.4 Synthesis of N^1-(4-aminophenyl)-N^1-(4-(2-phenyl-1H-imidazol-1-yl)phenyl)benzene-1,4-diamine (ImTPADA)

Into a 500 mL three-necked round-bottom flask equipped with a magnetic stirring bar, a nitrogen inlet and a reflux condenser were charged ImTPADN (14 g, 29.3 mmol), 10 wt% Pd/C (1 g) and ethanol (150 mL). To the reaction mixture, hydrazine hydrate (30 mL) was

added dropwise over a period of 1 h at room temperature under nitrogen atmosphere and then refluxed overnight. After completion of reaction (monitored by TLC), the reaction mixture was filtered while hot, cooled and precipitated into ice-cold water (800 mL). The crude product was collected by filtration, washed with water and dried under vacuum at 70 °C. The product was purified by recrystallization from ethanol to afford ImTPADA as colorless crystals.

Yield: (9 g, 74%)

Melting point: 204 °C

IR ($CHCl_3$, cm^{-1}): 3463 (N–H asymmetric stretching) and 3400 (N–H symmetric stretching);

^1H NMR (200 MHz, $CDCl_3$, δ/ppm): 7.52 (d, 2H, Ar-H), 7.32-7.27 (m, 4H, Ar-H), 7.27 (d, 2H, Ar-H), 7.11 (d, 1H, Ar-H), 6.99-6.93 (m, 6H, Ar-H), 6.83 (d, 2H, Ar-H), 6.64 (d, 4H, Ar-H), 3.38 (s, 4H, 2-NH_2)

^{13}C NMR (50 MHz, $CDCl_3$, δ/ppm): 149.4, 146.1, 143.1, 138.1, 128.9, 128.8, 128.6, 128.5, 128.2, 127.4, 126.8, 126.4, 123.3, 118.2, 116.1.

HRMS (ESI): calcd. for $C_{27}H_{23}N_5$ ($[M+H]^+$): 417.1948; found 417.1945.

7.2.2 Synthesis of Polyimides

Into a 100 mL three-necked round-bottom flask equipped with a magnetic stirring bar, a nitrogen inlet and a calcium chloride guard tube were charged ImTPADA (2.5 g, 5.98 mmol) and freshly distilled *m*-cresol (35 mL). After complete dissolution of ImTPADA, 6-FDA (2.66 g, 5.98 mmol) and isoquinoline (1 mL) were added. The reaction mixture was stirred at room temperature for 4 h, at 140 °C for overnight and at 200 °C for 8 h. The viscous polymer solution was poured into methanol (1000 mL), filtered, washed with methanol and dried at 80 °C for two days under vacuum.

IR (Film, cm^{-1}): 1784 (asymmetric stretching) and 1722 (symmetric stretching).

^1H-NMR (200 MHz, $CDCl_3$, δ/ppm): 8.06 (d, 2H, Ar-H), 7.92 (d, 4H, Ar-H), 7.38-7.16 (m, 19H, Ar-H).

The other PIs namely PI-BPADA and PI-ODPA were synthesized following the similar procedure by polycondesation of ImTPADA with aromatic dianhydrides namely BPADA and ODPA, respectively.

7.2.3 Post-modification of polyimides

7.2.3.1 N-Quaternization of PI-6FDA

Into a 250 mL two-necked round-bottom flask equipped with a magnetic stirring bar and a nitrogen inlet were charged [PI-6FDA] [I] (2.9 g, 3.5 mmol) and DMSO (30 mL). To the

reaction mixture, methyl iodide (0.16 mL, 2.5 mmol) was added dropwise and stirred at room temperature for 48 h. The polymer solution was precipitated into methanol, filtered, washed with methanol (2 × 500 mL) and dried at 100 °C for four days under vacuum.

IR (Film, cm^{-1}): 1784 (asymmetric stretching) and 1722 (symmetric stretching)

^{1}H-NMR (200 MHz, DMSO-d_6, δ/ppm): 8.21-8.12 (m, 4H), 7.95 (s, 2H), 7.78 (s, 2H), 7.62-7.44 (m, 6H), 7.37-7.09 (m, 13H), 3.8 (s, 3H).

7.2.3.2 Anion exchange of [PI-6FDA] [I]

Into a 250 mL two-necked round-bottom flask equipped with a magnetic stirring bar and a nitrogen inlet were charged [PI-6FDA] [I] (1.5 g, 1.5 mmol) and DMF (20 mL). To the reaction mixture, LiTFSI (0.89 g, 3.1 mmol) in DMF (5 mL) was added and stirred at room temperature for 48 h. The polymer solution was precipitated into water, washed thoroughly with methanol and dried at 100 °C for four days.

IR (Film, cm^{-1}): 1784 (asymmetric stretching) and 1722 (symmetric stretching).

^{1}H-NMR (200 MHz, DMSO-d_6, δ/ppm): 8.20-8.09 (m, 4H), 7.76 (s, 2H), 7.60 (s, 2H), 7.47-7.08 (m, 19H), 3.79 (s, 3H).

The degree of *N*-quaternization was determined by both ^{1}H NMR spectroscopy and Volhard's method. Volhard's method was used to determine the percent of the iodide exchanged with Tf_2N^- anion.[16] 0.1 g of PI-PIL powder was added into 0.01 M $AgNO_3$ solution (10 mL) and stirred at room temperature for 30 h. An excess of $AgNO_3$ was titrated with 0.01 M KSCN, from which the extent of anion exchange in the PIL was estimated.

7.2.4 Preparation of Dense Membranes

The dense membranes were prepared *via* solution casting method (~5 wt %, w/v). The polymer was dissolved in DMAc, the solution was filtered, and poured onto a leveled glass surface, which was then kept in a vacuum oven at 90 °C for 20 h. Further, these films were dried at 100 °C in a vacuum oven for one week. The average membrane thickness was in the range 65-70 microns.

7.3 RESULTS AND DISCUSSION

7.3.1 Synthesis and Characterization of N^1-(4-Aminophenyl)-N^1-(4-(2-phenyl-1H-imidazol-1-yl)phenyl) benzene-1,4-diamine (ImTPADA)

The four step route for the synthesis of N^1-(4-aminophenyl)-N^1-(4-(2-phenyl-1H-imidazol-1-yl)phenyl) benzene-1,4-diamine (ImTPADA) is depicted in **Scheme 7.1**. *N*-Arylation of 2-phenylimidazole was carried out with 4-nitro-1-fluorobenzene in the presence of sodium

hydride as the base in DMSO solvent to form 1-(4-nitrophenyl)-2-phenyl-1H-imidazole (ImN). The structure of ImN was characterized by IR (**Figure SI 7.1**), ^{1}H (**Figure SI 7.2**), ^{13}C NMR (**Figure SI 7.1**) spectroscopy and HRMS analysis.

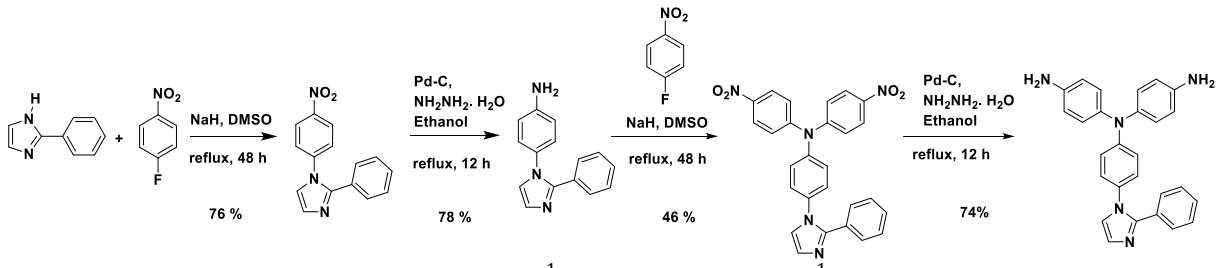

Scheme 7.1: Synthesis of N^1-(4-aminophenyl)-N^1-(4-(2-phenyl-1H-imidazol-1-yl)phenyl)benzene-1,4-diamine (ImTPADA).

Further, ImN was subjected to reduction with hydrazine hydrate in ethanol using Pd/C as the catalyst to obtain 4-(2-phenyl-1H-imidazol-1-yl) aniline (ImA). The structure of ImA was characterized by IR (**Figure SI 7.4**), ^{1}H (**Figure SI 7.5**) and ^{13}C NMR (**Figure SI 7.6**) spectroscopy and HRMS analysis. ImA was reacted with 4-nitro-1-fluorobenzene *via* double aromatic nucleophilic substitution reaction (S_NAr) to afford intermediate 4-nitro-N-(4-nitrophenyl)-N-(4-(2-phenyl-1H-imidazol-1-yl) phenyl)aniline (ImTPADN). The S_NAr reaction was carried out in the presence of sodium hydride in DMSO solvent. This reaction is facilitated if electron withdrawing group (such as $–NO_2$, -CHO, etc) is present at *para* position of the leaving group. The chemical structure of ImTPADN was confirmed by IR (**Figure SI 7.7**), ^{1}H (**Figure SI 7.8**) ^{13}C NMR (**Figure SI 7.9**) spectroscopy and HRMS analysis. Finally, ImTPADN was converted into ImTPADA by reduction of nitro groups with hydrazine hydrate in the presence of Pd/C as the catalyst in ethanol. The overall yield of 20 % was obtained in the four step synthesis of ImTPADA. The structure of ImTPADA was characterized by IR, ^{1}H and ^{13}C NMR spectroscopy and HR-MS analysis. IR spectrum of ImTPADA (**Figure 7.1**) showed absorption bands of N-H stretching of amino group in the range 3463-3400 cm^{-1}.

In ^{1}H NMR spectrum of ImTPADA **(Figure 7.2)**, the broad peak appeared at δ = 3.58 ppm corresponding to protons of amino group. The protons *ortho* to amino groups (labelled as 1) appeared in the upfield region as a doublet at δ = 6.65 ppm due to shielding effect of amino groups. The peaks due to aromatic protons of ImTPADA appeared in the range δ = 6.83-7.53 ppm.

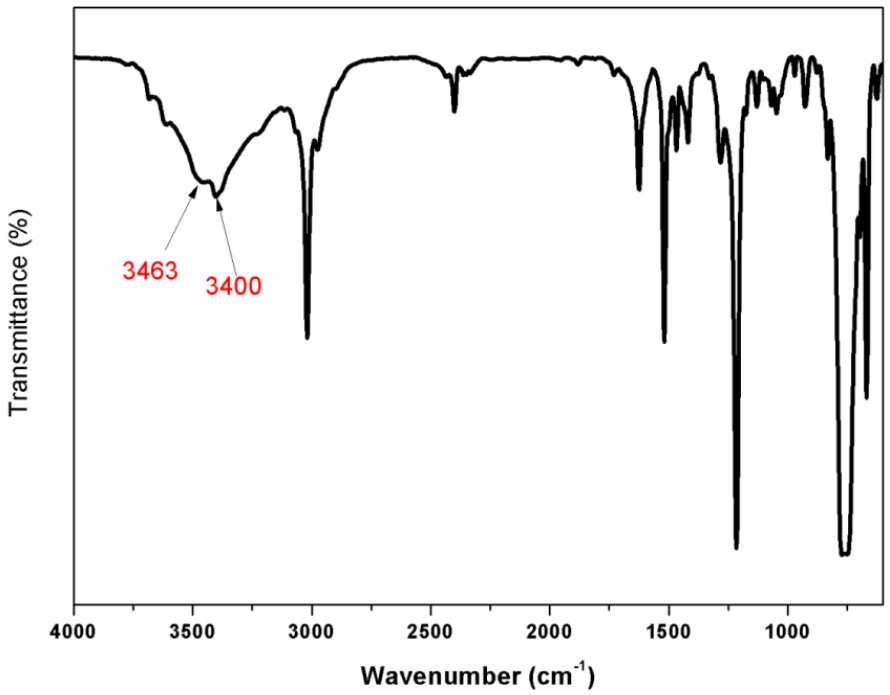

Figure 7.1: IR spectrum of N^1-(4-aminophenyl)-N^1-(4-(2-phenyl-1H-imidazol-1-yl)phenyl)benzene-1,4-diamine (ImTPADA)

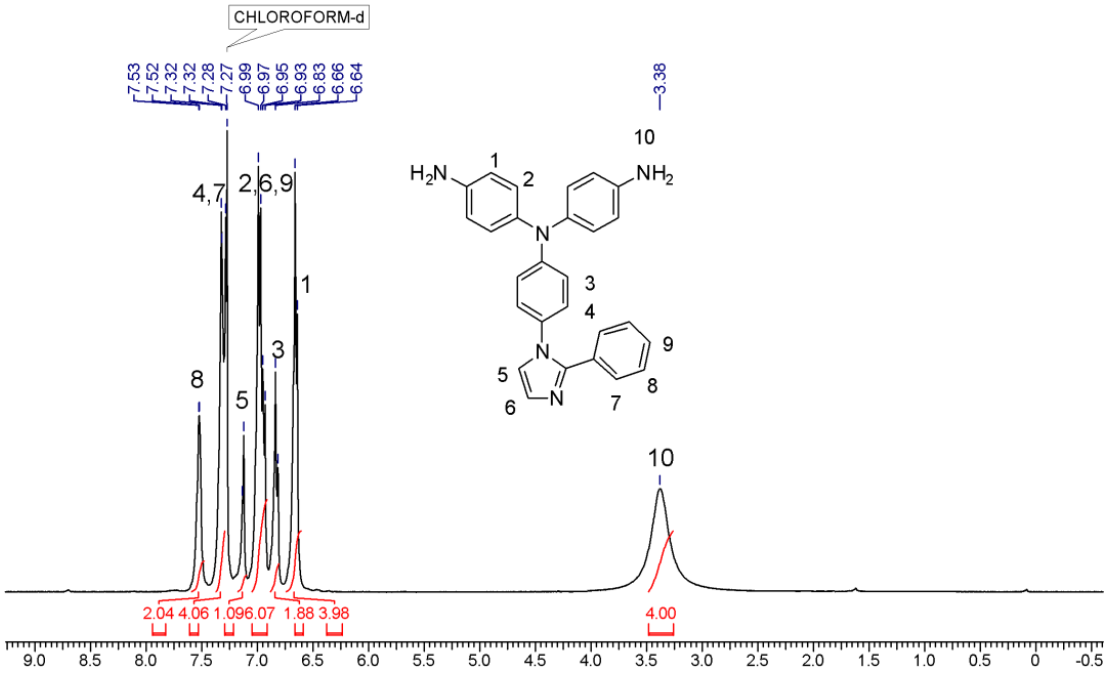

Figure 7.2: ^{1}H NMR spectrum (in $CDCl_3$) of N^1-(4-aminophenyl)-N^1-(4-(2-phenyl-1H-imidazol-1-yl)phenyl)benzene-1,4-diamine (ImTPADA).

^{13}C NMR spectrum of ImTPADA along with assignments is shown in **Figure 7.3**. In ^{13}C NMR spectrum, the peak of carbon attached to amino group appeared δ = 149.4 ppm. The other aromatic carbons appeared in the range at δ = 146.1 – 116.1ppm.

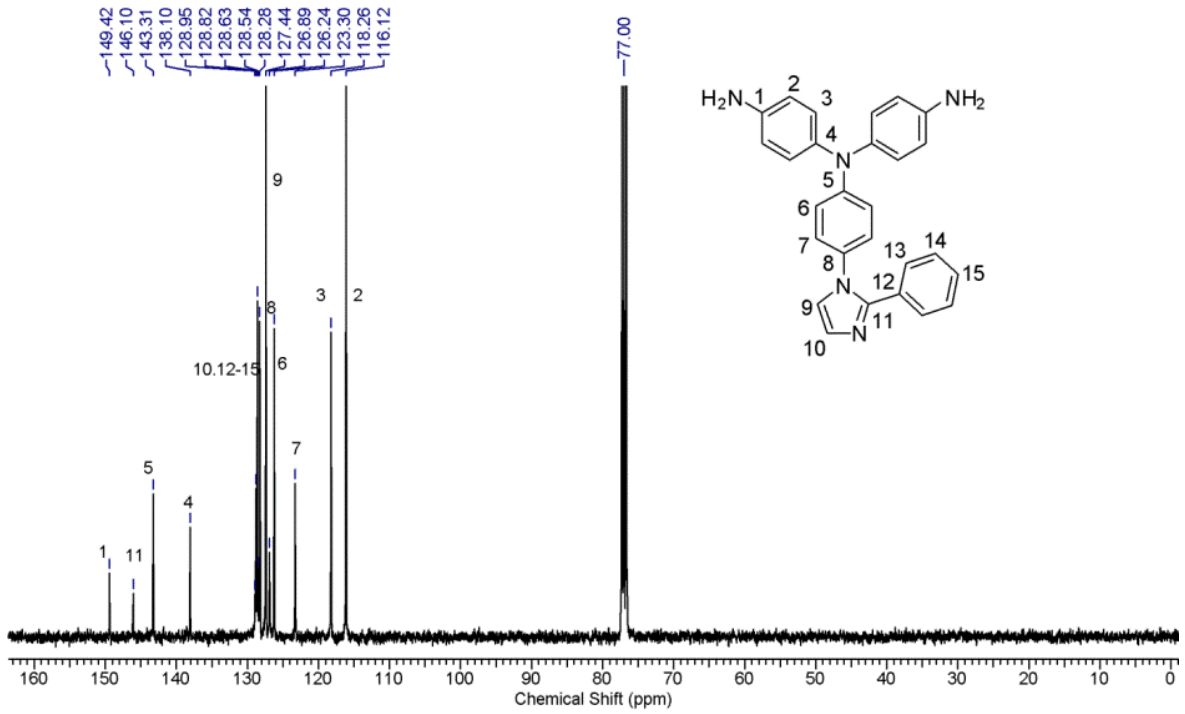

Figure 7.3: ^{13}C NMR spectrum (in $CDCl_3$) of N^1-(4-aminophenyl)-N^1-(4-(2-phenyl-1H-imidazol-1-yl)phenyl)benzene-1,4-diamine (ImTPADA).

HRMS of ImTPADA is shown in **Figure 7.4**. HRMS showed peak at 417.1945 corresponding to ($[M+H]^+$) of ImTPADA **(**Calcd. ($[M+H]^+$) for $C_{27}H_{23}N_5$=417.1948).

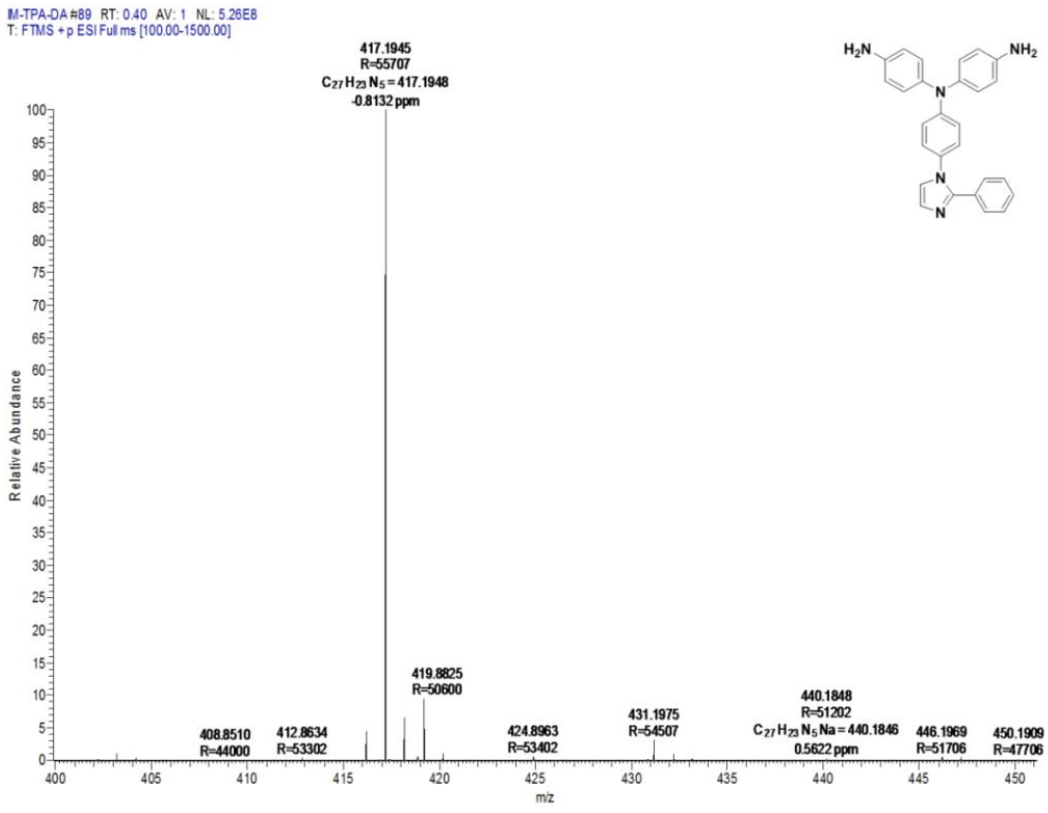

Figure 7.4: HR-MS of N^1-(4-aminophenyl)-N^1-(4-(2-phenyl-1H-imidazol-1-yl)phenyl)benzene-1,4-diamine (ImTPADA).

7.3.2 Synthesis and Characterization of PIs and PI-PILs

Polyimides containing triphenylamine and pendant 2-phenylimidazole units were synthesized by polycondensation of ImTPADA with three commercially available aromatic dianhydrides namely, 4,4′-(hexafluoro isopropylidene)diphthalic anhydride (6-FDA), 4,4'-(4,4'-isopropylidenediphenoxy)bis (phthalic anhydride) (BPADA) and 4,4′-oxydiphthalic anhydride (ODPA) to form corresponding PIs *viz.*, PI-6FDA, PI-BPADA and PI-ODPA, respectively. Polycondensation was performed in *m*-cresol in the presence of isoquinoline as the catalyst at room temperature for 4 h, at 140 °C for overnight and at 200 °C for 8 h by one-step high temperature method (**Scheme 7.2**).

Further, polyimide-based poly(ionic liquid)s (PI-PILs) were synthesized from PI-6FDA by N-quaternization followed by anion exchange reaction (**Scheme 7.3**). The *N*-quaternization reaction of PI-FDA containing pendant 2-phenylimidazole was performed with methyl iodide in DMSO at room temperature to afford [PI-6FDA] [I]. In order to synthesize film-forming PI-PILs with the optimum content of ionic moieties, PI-6FDA was reacted with various equivalent quantities such as 0.5, 0.7 and 1 equivalents of methyl iodide. PI-PILs prepared using 0.5 and 0.7 equivalents of methyl iodide could be cast into self-standing films while the film was brittle in case of PI-PILs prepared using 1 equivalent of methyl iodide. The anion exchange reaction of iodide anion in [PI-6FDA] [I] was performed using bis(trifluoromethane) sulfonimidelithium salt ($LiNTf_2$) in DMF at room temperature to form [PI-6FDA] [Tf_2N]. The degree of *N*-quaternization was measured by ^1H NMR spectroscopy and Volhard's method and the results of both these methods were in good agreement. The extent of anion exchange was determined by Volhard's method and the results indicated that nearly quantitative anion exchange was observed. The chemical structure of PIs and PILs were characterized by IR and ^1H and ^{13}C NMR spectroscopy.

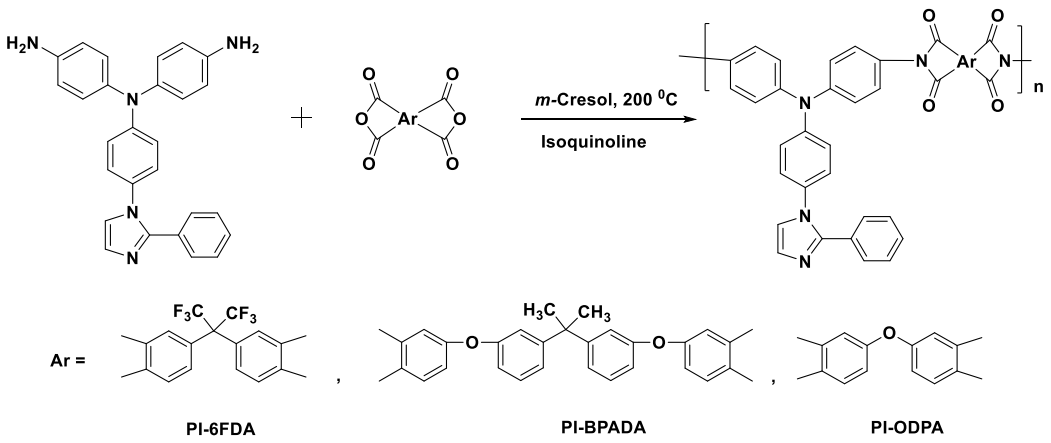

Scheme 7.2: Synthesis of polyimides containing triphenylamine and 2-phenyl imidazole units

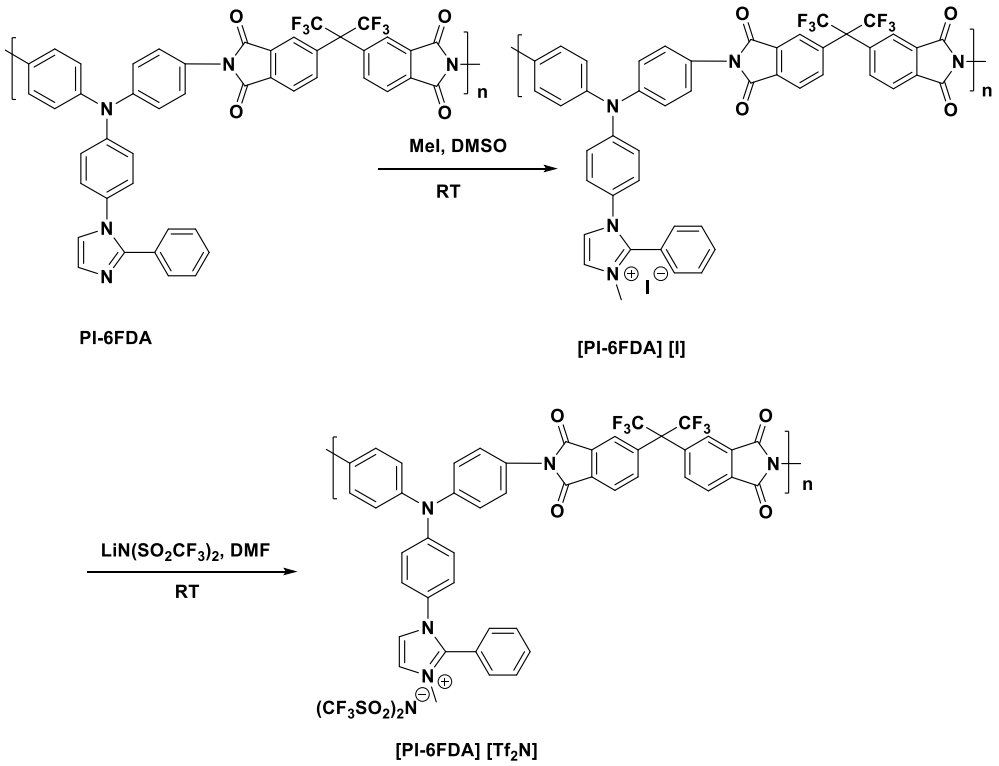

Scheme 7.3: Synthesis of polyimide-based poly(ionic liquid)s

IR spectra of PIs and PI-PILs are shown in **Figure 7.5**. In IR spectra, PIs and PI-PILs exhibited characteristics bands of imide at 1784 and 1722 cm $^{-1}$. In addition, bands of C-N and imide ring deformation were observed at 1364 and 820 cm $^{-1}$, respectively. The bands for amino group and acid of poly(amic acid) were not observed in the IR spectra, which indicated complete conversion of poly(amic acid) into PI.

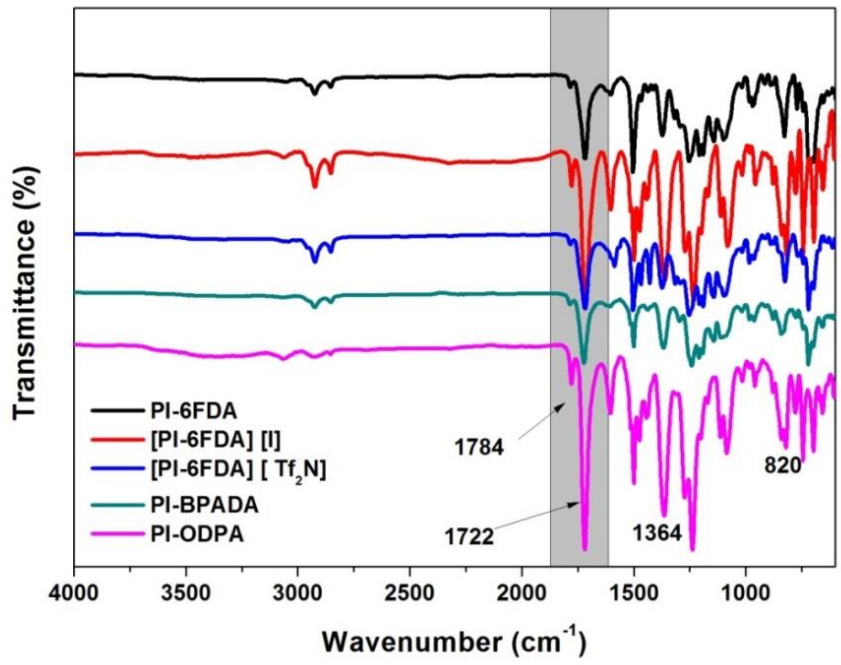

Figure 7.5: IR spectra of PIs and PI-PILs

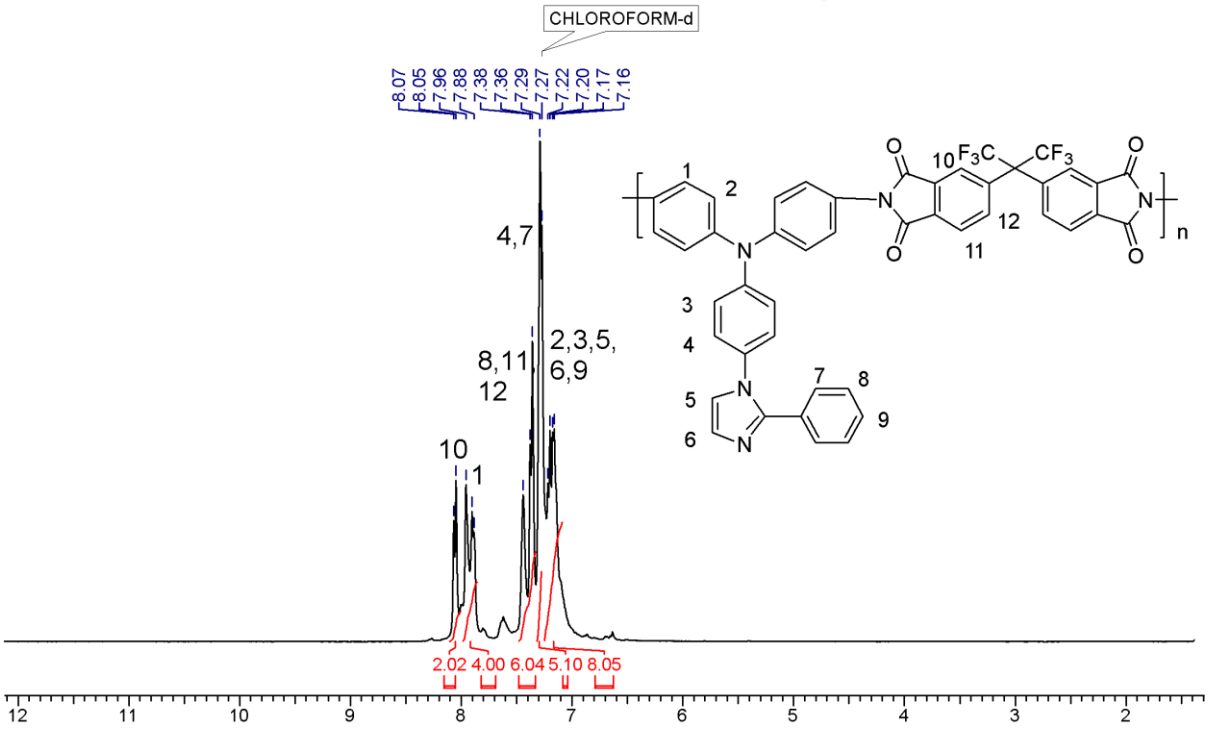

Figure 7.6: ^{1}H NMR spectrum (in $CDCl_3$) of PI-6FDA.

^{1}H NMR spectra of PIs and PI-PILs along with assignments are presented in **Figure 7.6** to **7.10**. In ^{1}H NMR spectrum of PI-6FDA (**Figure 7.6**), the protons of ImTPADA moiety labelled as 1 appeared as a doublet at δ = 7.96 ppm while the protons of 6FDA moiety labelled as 10 appeared as a doublet at δ = 8.06 ppm. The rest of aromatic protons of ImTPADA and 6FDA moieties appeared in the region δ = 7.88-7.16 ppm.

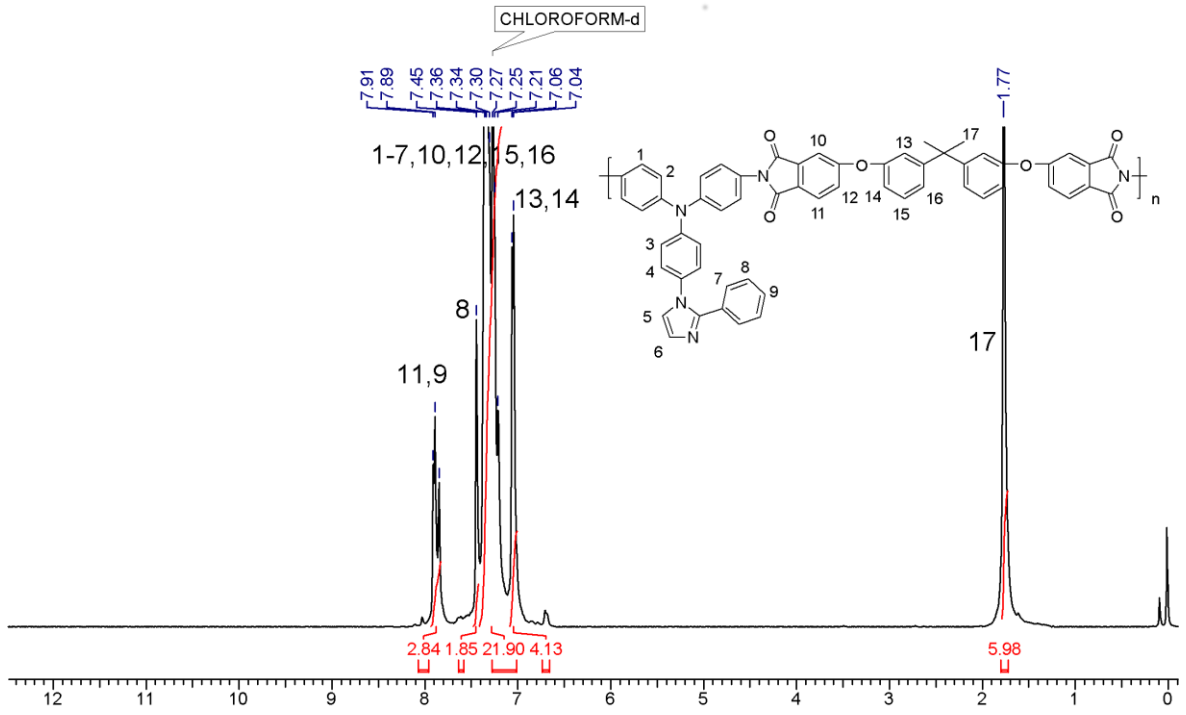

Figure 7.7: ^{1}H NMR spectrum (in $CDCl_3$) of PI-BPADA.

^{1}H NMR spectrum of PI-BPADA is reproduced in **Figure 7.7**. In ^{1}H NMR spectrum of PI-BPADA, the protons of BPADA moiety labelled as 13 and 14 appeared in the upfield region as a doublet at δ = 7.04 ppm due to shielding effect of ether linkage. The rest of aromatic protons of ImTPADA and BPADA moieties appeared in the region δ = 7.91-7.21 ppm. The methyl protons exhibited a singlet at δ = 1.77 ppm.

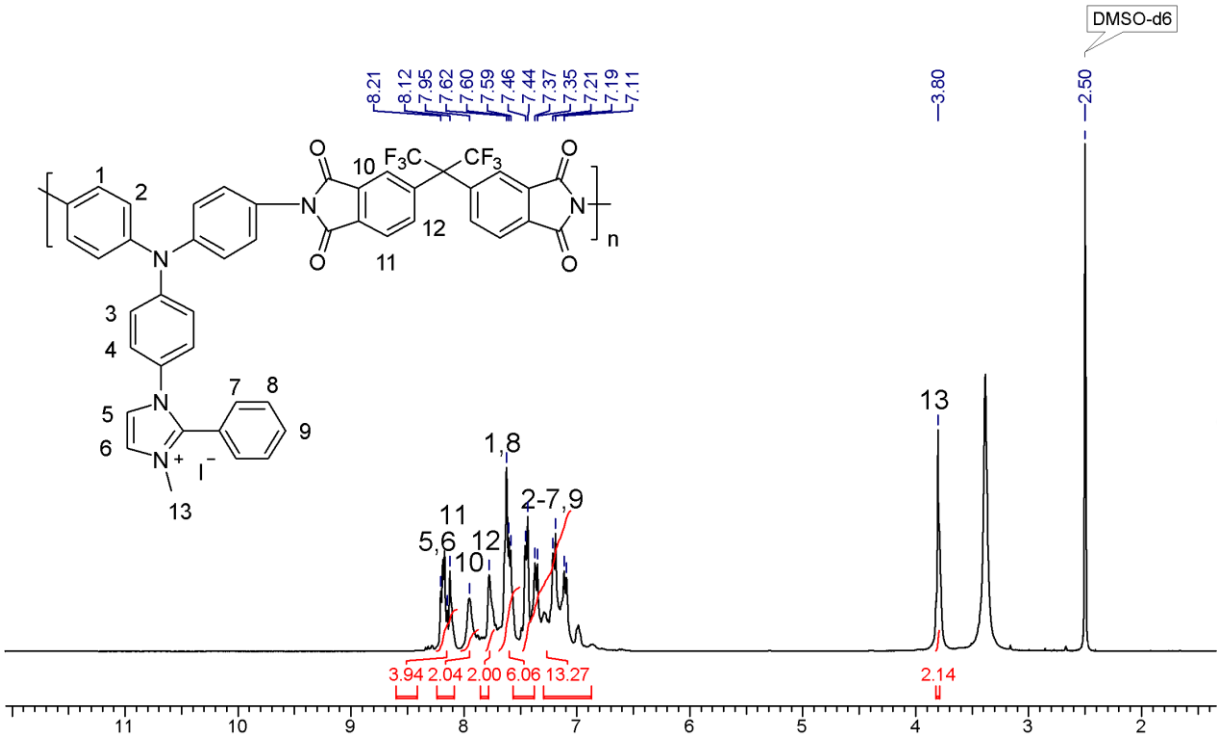

Figure 7.8: ^{1}H NMR spectrum (in DMSO-d_6) of [PI-6FDA] [I].

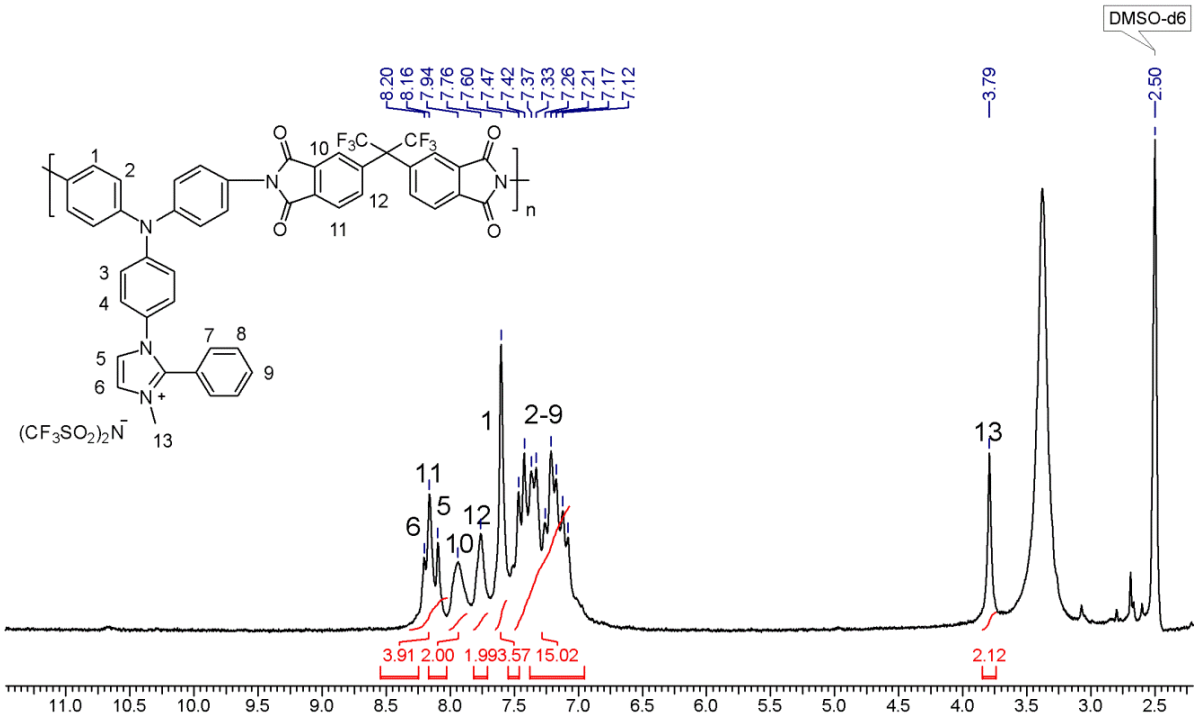

Figure 7.9: ^{1}H NMR spectrum (in DMSO-d_6) of [PI-6FDA] [Tf_2N].

^{1}H NMR spectrum of [PI-6FDA] [I] along with assignments is shown in **Figure 7.8.** The aromatic protons appeared in the region δ = 8.21-7.09 ppm. After *N*-quaternization of 2-phenylimidazole of [PI-6FDA], a new peak for *N*-quaternized methyl group appeared at 3.80 ppm which indicated *N*-quaternization reaction was successful.

^{1}H NMR spectrum of [PI-6FDA] [Tf_2N] is presented in **Figure 7.9.** In ^{1}H NMR of [PI-6FDA] [Tf_2N], the aromatic protons appeared in the region δ = 8.20-7.08 ppm. The peak due to *N*-quaternized methyl group appeared at δ = 3.79 ppm. ^{13}C NMR spectra of PIs and PI-PILs are shown in the supporting information (**Figure SI 7.10-7.13**).

The degree of *N*-quaternization was measured by ^{1}H NMR spectroscopy and Volhard's method and the results of both these methods were in good agreement. The extent of anion exchange was determined by Volhard's method and the results indicated that nearly quantitative anion exchange was observed.

7.3.3 Solubility of PIs and PI-PILs

The solubility tests of PIs and PI-PILs were carried out at 3 wt % concentration in various organic solvents at room temperature and the results are summarized in **Table 7.1**. PI-6FDA and PI-BPADA were found to be soluble in various organic solvents such as chloroform ($CHCl_3$), dichloromethane (DCM), *N*,*N*-dimethylacetamide (DMAc), *N*,*N*-dimethylformamide (DMF), *N*-methylpyrrolidone (NMP) and dimethyl sulfoxide (DMSO) while PI-ODPA was insoluble in these organic solvents. Thus, the solution-based characterization of PI-ODPA by GPC and NMR spectroscopy was not feasible**.** PI-PILs were found to be soluble in polar solvents such as DMAc, DMF, NMP and DMSO. The good solubility of PIs and PI-PILs could be attributed to the presence of propeller-shaped triphenylamine and (N-quaternized) 2-phenylimidazole units. The self-standing films of PIs and PI-PILs could be cast from their DMAc solution, except for PI-ODPA.

Table 7.1: Solubility data of PIs and PI-PILs[a]

Sr. No.	Polymer	$CHCl_3$	DCM	THF	DMAc	DMF	NMP	DMSO
1	**PI-6FDA**	++	++	++	++	++	++	++
2	**[PI-6FDA] [I]**	--	--	--	++	++	++	++
3	**[PI-6FDA] [Tf_2N]**	--	--	--	++	++	++	++
4	**PI-BPADA**	++	++	++	++	++	++	++
5	**PI-ODPA**	--	--	--	+-	+-	+-	+-

[a] Solubility tests of PI-PIMs were carried out at 3 wt % (w/v) concentration at room temperature. ++ : Soluble, +- : Partially Soluble, -- :Insoluble

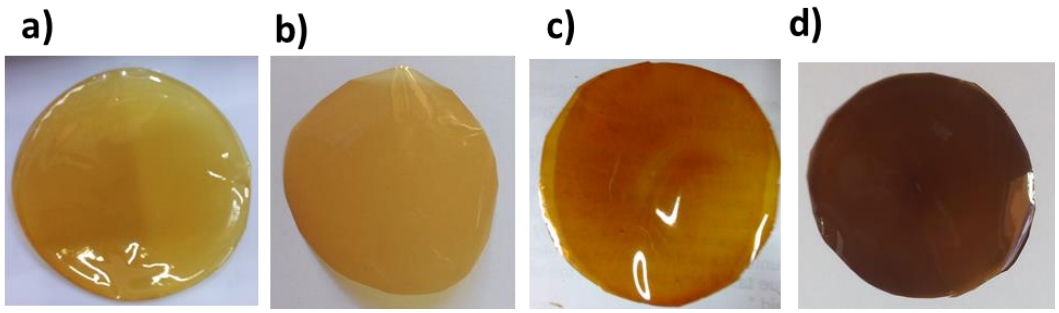

Figure 7.10: Films of a) PI-6FDA, b) [PI-6FDA] [I], c) PI-6FDA] [Tf_2N] and d) PI-BPADA

7.3.4 Inherent Viscosity and Molecular Weights of PIs and PI-PILs

PIs and PI-PILs were obtained in almost quantitative yields and their inherent viscosity values were in the range 0.62-0.72 dL/g **(Table 7.2).** Molecular weights of PIs and PI-PILs were obtained by GPC in DMF using polystyrene as a standard. PIs and PI-PILs exhibited number average molecular weight and dispersity values in the range 79200-35000 g/mol and 2.1-1.6, respectively (**Table 7.2**). Inherent viscosity and GPC measurements indicated that polymers were of reasonably high molecular weights. The measured GPC molecular weights of PI-PILs were lower than that of corresponding parent PI which could be attributed to the differences in solubility parameters and hydrodynamic volume due to variation in their chemical structures. Similar observations have been reported in the literature for PILs.[15]

Table 7.2: Synthesis of PIs and PI-PILs

Sr. No.	Polymer	η_{inh} (dL/ g)[a]	M_n[b]	M_w[b]	Dispersity[c]
1	**PI-6FDA**	0.72	79200	128000	1.6
2	**[PI-6FDA] [I]**	0.65	40200	85000	2.1
3	**[PI-6FDA] [Tf_2N]**	0.62	35000	60000	1.7
4	**PI-BPADA**	0.70	73000	117000	1.6
5	**PI-ODPA**	ns	ns	ns	ns

[a:] Inherent viscosity was measured at a polymer concentration of 0.5 g/dL in DMAc at 35±0.1 °C. [b:] Molecular weights were obtained from GPC in DMF (Polystyrene standard). [c:] Dispersity = M_w/M_n. ns: Not soluble in organic solvents. ns: Inherent viscosity and GPC measurements could not be carried out due to insolubility in organic solvents such as $CHCl_3$, DMF and THF.

7.3.5 X-Ray Diffraction of PIs and PI-PILs

X-Ray diffraction patterns of PIs and PI-PILs are shown in **Figure 7.11**. The broad halo around 2θ = 10-30° in wide angle XRD patterns indicated that PIs and PI-PILs were amorphous in nature. The amorphous nature could be attributed to the presence of bulky triphenylamine and (*N*-quaternized) 2-phenylimidazole units in the polymer which disturbed polymer chain packing *via* creating free volume.

Table 7.3: Physical properties of PIs and PI-PILs

Sr. No.	Polymer	*d*-Spacing (Å)[a]	$T_{10\%}$[b] (°C)	Char Yield[c] (%)	T_g[d] (°C)
1	**PI-6FDA**	5.49	545	55	303
2	**[PI-6FDA] [I]**	5.63	303	38	nd
3	**[PI-6FDA] [Tf_2N]**	5.67	306	49	nd
4	**PI-BPADA**	5.46	475	56	248
5	**PI-ODPA**	5.43	508	60	298

[a:] *d*-Spacing was calculated from XRD patterns using Bragg's equation. [b:] Temperature at which 10 weight % loss was observed recorded by TGA at a heating rate of 10 °C/min. under N_2 atmosphere. [c:] Percentage char yield under nitrogen atmosphere at 900 °C. [d:] Glass transition temperature (T_g) recorded by DSC.

The inter-chain distance (*d*-spacing) of polymers was calculated from peak maxima of X-ray diffractograms using Bragg's equation. The *d*-spacing values of PIs and PI-PILs were in the range 5.43-5.67 Å (**Table 7.3**). The order of *d*-spacing is as follows: PI-ODPA < PI-BPADA < PI-6FDA < [PI-6FDA] [I] < [PI-6FDA] [Tf_2N]. The variations in the *d*-spacing of PIs and PI-PILs were correlated to both the substituent bulk and nature of the anion. For example, PI-6FDA showed higher *d*-spacing as compared to PI-ODPA and PI-BPADA. This could be due to the bulky hexafluoroisopropylidene linkages which disturbed polymer chain packing more effectively as compared to PI-ODPA and PI-BPADA which contain isopropylidene and ether linkages, respectively (**Table 7.4**).[22,24]

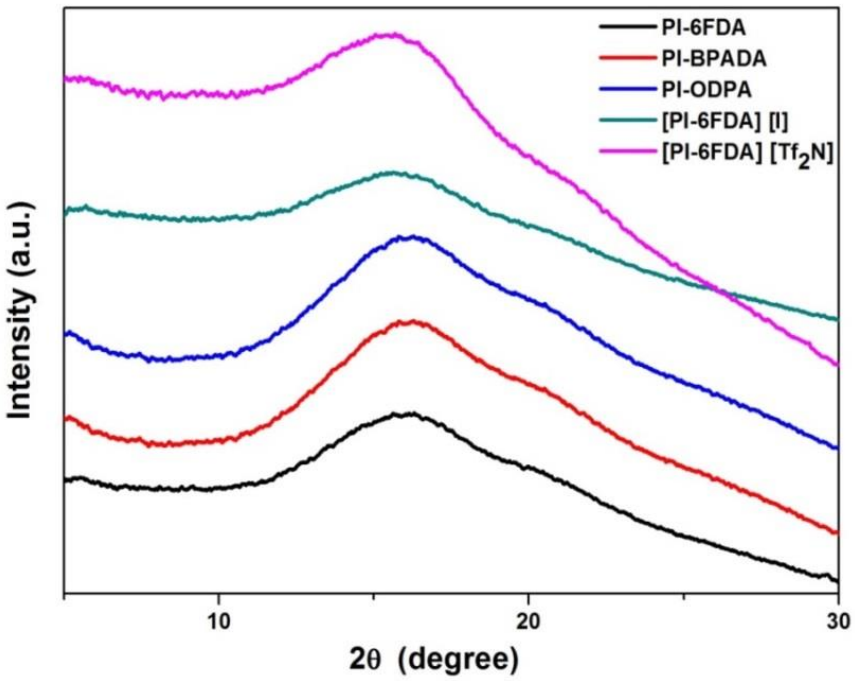

Figure 7.11: X-Ray diffractrograms of PIs and PI-PILs.

These results are in good agreement with the van der Waals volume (V_w). The van der Waals volumes of hexafluoroisopropylidene, isopropylidene and ether linkages are 88.5, 44.35 and 5.5 cm^3 mol^{-1}, respectively, which indicated that hexafluoroisopropylidene occupied more space followed by isopropylidene linkages as shown in **Table 7.4**. PI-PILs exhibited higher *d*-spacing as compared to PIs which could be due to the presence of bulky ionic groups. In the case of PI-PILs, PI-6FDA [TF_2N] showed higher *d*-spacing compared to [PI-6FDA] [I], which indicated more disturbed chain packing due to the bulkier nature of anion in the former. These results implied that both bulk of hinge groups present in the dianhydride and bulk of anion play an important role in governing the polymer chain packing.

Table 7.4: The van der Waals volumes of hinge group present in dianhydride moities[22,24]

Sr. No.	Polymer code	Repeating unit	Hinge group	Van der Waals volume (cm^3 mol^{-1})
1	**PI-6FDA**	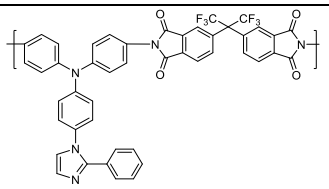	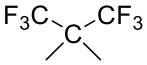	88.5
2	**PI-ODPA**	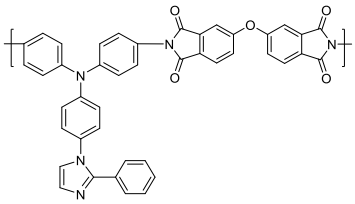		5.5
3	**PI-BPADA**	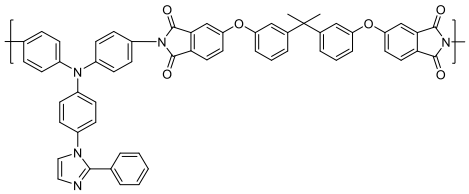	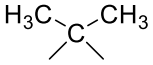	44.35

7.3.6 Thermal Properties of PIs and PI-PILs

The thermal properties of PIs and PI-PILs were determined by TGA and DSC and the results are summarized in **Table 7.3** and **Figure 7.12**. The temperature for 10 % weight loss and % char yield at 900 °C of PIs were in the range 475-545 °C and 55-60 %, respectively, which indicated their good thermal stability. The 10 % weight loss temperature of PI-PILs was in the range 303-306 °C. PI-PILs exhibited lower T_{10} values as compared to the corresponding PIs. This could be due to decreased rigidity of polymer chains and higher propensity of ionic

moieties to degrade as compared to the parent heterocyclic moiety.[25] Glass transition temperature (T_g) of PIs were measured by DSC and the values were in the range 248-303 °C **(Table 7.3).** In case of PIs with varying dianhydrides, T_g was in accordance with the order of rigidity of dianhydrides: 6FDA > ODPA > BPADA.[21] No T_g was detected in DSC analysis of PI-PILs carried out up to their degradation temperature. Similar observations have been reported in earlier study of PILs based on PIs in the literature.[15]

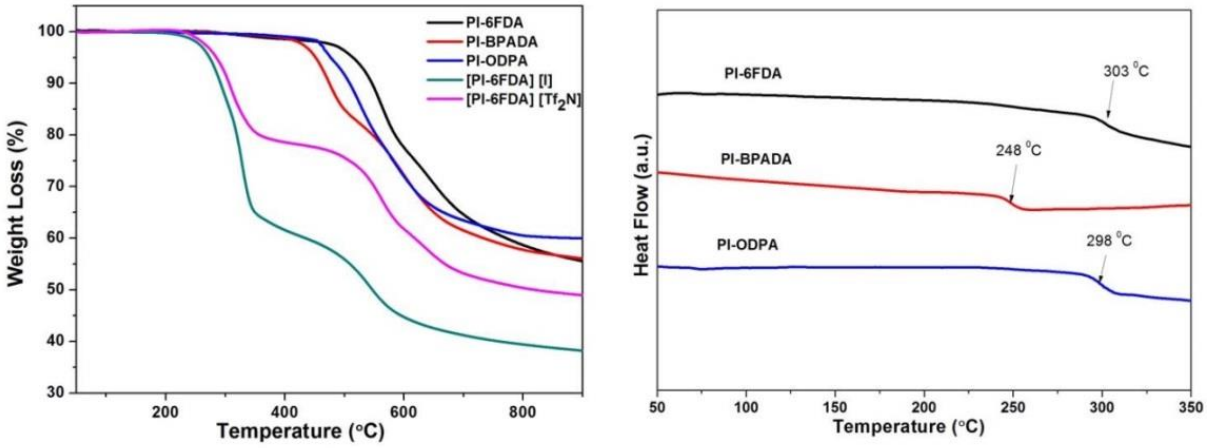

Figure 7.12: a) TG curves of PIs and PI-PILs and b) DSC curves of PIs

7.3.7 Mechanical Properties of PIs and PI-PILs

For gas separation applications, membrane should possess good mechanical properties and sustain pressure. The present polymers sustained pressure of 5-6 bar during gas permeability measurement experiments. The mechanical properties of polymers such as tensile strength, Young's modulus and elongation at break are shown in **Table 7.5 and Figure 7.13**. PIs and PI-PILs exhibited tensile strength, Young's modulus and elongation at break in the range of 43.5–49.3 MPa, 0.91–1.38 GPa and 7.9–31.5 %, respectively. It was observed that the mechanical properties of PI-PILs were inferior than that of parent polyimide. This could be attributed to the weaker inter-chain interactions between polymer chains in PI-PILs as compared to parent polyimide.[16]

Table 7.5: Mechanical properties of PIs and PI-PILs

Sr. No.	Polymer	Tensile Strength (MPa)	Young's Modulus (GPa)	Elongation at Break (%)
1	**PI-6FDA**	47.1±2.6	1.34±0.07	31.5±1.9
2	**[PI-6FDA] [I]**	43.5±4.5	0.91±0.01	9.2±0.6
3	**[PI-6FDA] [Tf_2N]**	44.6±1.5	1.0±0.03	7.9±0.8
4	**PI-BPADA**	49.3±0.3	1.38±0.04	22.7±0.9

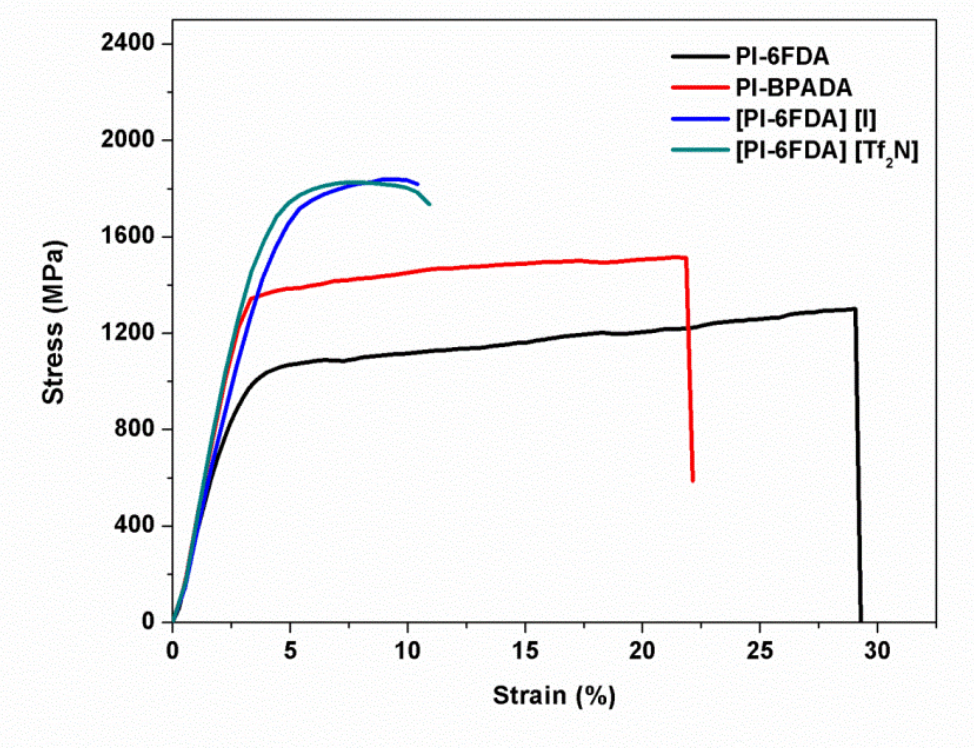

Figure 7.13: Stress and strain curves of PIs and PI-PILs

7.4 GAS PERMEABILITY

The gas permeability studies of PI-6FDA, PI-BPADA, [PI-6FDA] [I] and [PI-6FDA] [Tf_2N] films were carried out at room temperature and at 5-6 bar using variable-volume method.[26,27] The gas permeability data of PIs and PI-PILs are summarized in **Table 7.6 and 7.7**. The order of gases studied is as follows: He, H_2, N_2, O_2, CH_4 and CO_2. A large variation in the gas permeability of PIs and PI-PILs with variation in PI backbone and anion variation was observed which is discussed below.

7.4.1 Effect of Dianhydride on Gas Permeation Properties

In this series, the gas permeability changes with dianhydrides and anion and the order is as: PI-BPADA < PI-6FDA < [PI-6FDA] [I] < [PI-6FDA] [Tf_2N]. PIs exhibited CO_2 permeability in the range 11.9-19.7 Barrer and selectivity for CO_2/CH_4 and CO_2/N_2 gas pairs was in the range 35.2-42.5 and 27-34, respectively. It was observed that PI-6FDA possessing 6FDA moiety exhibited relatively higher permeability than that of PI-BPADA possessing BPADA moiety. This could be attributed to the presence of bulky hexafluoroisopropylidene linkages in PI-6FDA which disturbed polymer chain packing more effectively compared to isopropylidene linkages in PI-BPADA. Further, this could be correlated to the size of hinge group, which governs the chain packing of polymers. The van der Waals volume of hexafluoroisopropylidene (88.5) is higher than that of isopropylidene (44.35) linkages which

results into higher free volume in the case of PI-6FDA as compared to PI-BPADA. These results are supported by *d*-spacing values. The higher *d*-spacing and higher V_w of PI-6FDA was an indication of loosening of polymer chain packing as compared to PI-BPADA.

Table 7.6: Gas permeability of PIs and PI-PILs and commercially available polymers

Sr. No.	Polymer	Permeability[a,b]					
		He	**H_2**	**N_2**	**O_2**	**CH_4**	**CO_2**
1	**PI-6FDA**	31.1	23.0	0.73	3.5	0.56	19.7
2	**PI-BPADA**	14.5	9.9	0.35	1.8	0.28	11.9
3	**[PI-6FDA] [I]**	33.1	24.8	0.78	3.9	0.65	26.2
4	**[PI-6FDA] [Tf_2N]**	44.3	29.6	0.94	4.6	0.81	33.3
5	**Matrimid**[28]	-	18.0	0.32	2.1	0.28	10.0
6	**Polysulfone**[29]	-	14.0	0.25	1.40	0.25	5.6

[a:] Units of permeability (P): 1 Barrer = 10^{-10} cm3 (STP) cm /cm^2 s cm Hg. [b:] Gas permeability data taken from literature (entries 5 and 6) are marked in red.

Table 7.7: Gas selectivity of PIs and PI-PILs and commercially available polymers

Sr. No.	Polymer	Selectivity[a,b]			
		H_2/N_2	**O_2/N_2**	**CO_2/N_2**	**CO_2/CH_4**
1	**PI-6FDA**	31.5	4.8	27.0	35.2
2	**PI-BPADA**	28.3	5.1	34.0	42.5
3	**[PI-6FDA] [I]**	31.8	5.0	33.6	40.3
4	**[PI-6FDA] [Tf_2N]**	31.5	4.9	35.4	41.1
5	**Matrimid**[28]	56.0	6.6	31.2	36.0
6	**Polysulfone**[29]	56.0	5.6	22.4	22.0

[a:] Selectivity (α) = P_1/P_2. [b:] Gas selectivity data taken from literature (entries 5 and 6) are marked in red.

7.4.2 Effect of Anion Variation on Gas Permeation Properties

PI-6FDA was selected for the synthesis of PI-PILs due to its higher permeability than PI-BPADA. In addition to the dianhydride, anion of PI-PILs also plays a crucial role in governing its gas permeability. It can be seen from data in **Table 7.6 and 7.7** that the incorporation of ionic groups into PI resulted in increased permeability while maintaining

selectivity. PI-6FDA] [Tf_2N] showed higher permeability compared to [PI-6FDA] [I]. For instance, [PI-6FDA] [Tf_2N] exhibited CO_2 permeability of 33.3 Barrer and selectivity for CO_2/N_2 and CO_2/CH_4 was 35.4 and 41.1, respectively. The improvement of gas permeation properties of PI-PILs could be attributed to the presence of ionic moieties which are known to interact with carbon dioxide and loosening of packing of polymer chains.[30] The gas permeability for CO_2 was increased with the variation of anion as $I^- < Tf_2N^-$, indicating bulk of the anion contributed in governing the gas permeability in PILs. This trend was in good agreement with the *d*-spacing values. Overall, these results indicated that permeability of PIs and PI-PILs increased with the bulkiness of hinge groups, ionic character and bulk of anion.

7.4.3 Comparison of present PI-PILs with reported PI-PILs

It would be worth to compare gas permeation properties of present polymers with reported PI based PILs and commercial polymers. The gas permeability data of commercially available polymers such as Matrimid[28] and polysulfone[29] which are widely studied for gas separation applications are also included in **Table 7.6 and 7.7** for comparison. Notably, the present PI-PILs exhibited higher permeability than Matrimid and polysulfone. This is due to the presence of bulky anion in PI-PILs, which not only disturb polymer chain packing but also interact with CO_2 by Lewis acid-base interaction.

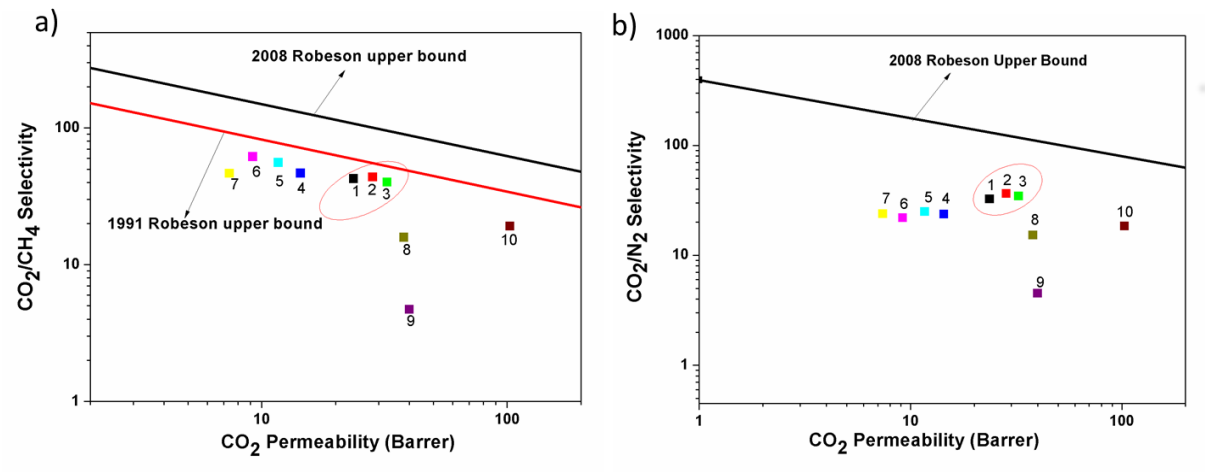

Figure 7.14: Robeson plots of (1) PI-6FDA, (2) [PI-6FDA] [I], (3) [PI-6FDA] [Tf_2N] and (4) 6.5 mol % mRTIL,[13] (5) 14.8 mol % mRTIL,[13] (6) 25.8 mol % mRTIL,[13] (7) 8 mol % diRTIL,[13] (8) PI-1-50IL,[15] (9) PI-1.TFSI[15] and (10) PI-1.TFSI-50IL[15] for a) CO_2/CH_4 and (b) CO_2/N_2 gas pairs.

Robeson plots (**Figure 7.14**) were used to compare the performance of present PI s and PI-PILs with reported PI-PILs.[13,15] It can be seen from **Figure 7.14** that the present PI-PILs were placed above 1991 Robeson upper bound compared to reported PI-PILs specifically for the

CO_2/CH_4 gas pair. Overall, PIs and PI-PILs are good candidates for gas separations, especially for CO_2-based separation. The present methodology of PI-based polymeric ionic liquids provides the possibility of tuning not only physical properties, but also the gas permeability of CO_2 due to the presence of ionic character.

7.5 CONCLUSIONS

In this work, a new aromatic diamine, namely, N^1-(4-aminophenyl)-N^1-(4-(2-phenyl-1H-imidazol-1-yl)phenyl)benzene-1,4-diamine (ImTPADA) was designed and successfully synthesized. ImTPADA was polycondensed with commercially available aromatic dianhydrides to obtain corresponding PIs containing triphenylamine and 2-phenylimidazole groups. PI-PILs were synthesized by *N*-quaternization of 2-phenylimidazole groups in [PI-6FDA] with methyl iodide followed by anion exchange with bis(trifluoromethane)sulfonimide lithium salt ($LiTf_2N$). PIs and PI-PILs were of reasonably high molecular weights (79200-35000 g/mol). The self-standing films of PI-PILs prepared using 0.5 and 0.7 equivalents of methyl iodide could be cast from DMAc solutions. T_{10} values of PIs and PI-PILs were in the range 545-475 °C and 303-306 °C, respectively. The gas permeability increased due to the presence of ionic moieties in PI-PILs. Gas permeability data of PI-PILs were located near 1991 Robeson upper bound. Overall, the gas permeability data demonstrated that the present PI-PILs are attractive candidates for gas separation applications, particularly for CO_2 separation.

7.6 REFERENCES

1. Cowan, M. G., Gin, D. L., Noble, R. D. *Acc. Chem. Res.*, 2016, **49**, 724–732.
2. Tome, L. C., Marrucho, I. M. *Chem. Soc. Rev.*, 2016, **45**, 2785–2824.
3. Mittenthal, M. S., Flowers, B. S., Bara, J. E., Whitley, J. W., Spear, S. K., Roveda, J. D., Wallace, D. A., Shannon, M. S., Holler, R., Martens, R., Daly, D. T. *Ind. Eng. Chem. Res.*, 2017, acs.iecr.7b00462.
4. Qin, J., Guo, J., Xu, Q., Zheng, Z., Mao, H., Yan, F. *ACS Appl. Mater. Interfaces*, 2017, **9**, 10504–10511.
5. Yuan, J., Mecerreyes, D., Antonietti, M. *Prog. Polym. Sci.*, 2013, **38**, 1009–1036.
6. Chen, H., Elabd, Y. A. *Macromolecules*, 2009, **42**, 3368–3373.
7. Yuan, J., Antonietti, M. *Polymer*, 2011, **52**, 1469–1482.
8. Liu, J., Hou, X., Park, H. B., Lin, H. *Chem. Eur. J.*, 2016, **22**, 15980–15990.
9. Kumbharkar, S. C., Bhavsar, R. S., Kharul, U. K. *RSC Adv.*, 2014, **4**, 4500–4503.
10. Zulfiqar, S., Sarwar, M. I., Mecerreyes, D. *Polym. Chem.*, 2015, **6**, 6435–6451.
11. Morozova, S. M., Shaplov, A. S., Lozinskaya, E. I., Mecerreyes, D., Sardon, H., Zulfiqar, S., Suárez-García, F., Vygodskii, Y. S. *Macromolecules*, 2017, **50**, 2814–2824.
12. Zhou, X., Obadia, M. M., Venna, S. R., Roth, E. A., Serghei, A., Luebke, D. R., Myers, C., Chang, Z., Enick, R., Drockenmuller, E., Nulwala, H. B. *Eur. Polym. J.*, 2016, **84**, 65–76.
13. Li, P., Zhao, Q., Anderson, J. L., Varanasi, S., Coleman, M. R. *J. Polym. Sci. Part A Polym. Chem.*, 2010, **48**, 4036–4046.
14. Cowan, M. G., Masuda, M., McDanel, W. M., Kohno, Y., Gin, D. L., Noble, R. D. *J. Membr. Sci.*, 2016, **498**, 408–413.
15. Shaplov, A. S., Morozova, S. M., Lozinskaya, E. I., Vlasov, P. S., Gouveia, A. S. L., Tomé, L. C., Marrucho, I. M., Vygodskii, Y. S. *Polym. Chem.*, 2016, **7**, 580–591.
16. Bhavsar, R. S. Kumbharkar S. C. Rewar, A. S. and Kharul, U. K. *Polym. Chem.*, 2014, **5**, 4083–4096.
17. Liaw, D. J., Wang, K. L., Huang, Y. C., Lee, K. R., Lai, J. Y., Ha, C. S. *Prog. Polym. Sci.*, 2012, **37**, 907–974.
18. Dhara, M. G., Banerjee, S. *Prog. Polym. Sci.*, 2010, **35**, 1022–1077.
19. White, L. S., Blinka, T. A., Kloczewski, H. A., Wang, I. fan *J. Membr. Sci.*, 1995, **103**, 73–82.
20. Du, N., Park, H. B., Dal-Cin, M. M., Guiver, M. D. *Energy Environ. Sci.*, 2012, **5**, 7306–7322.
21. Ghosh, S., Banerjee, S. *J. Membr. Sci.*, 2016, **497**, 172–182.
22. Coleman, M. R., Koros, W. J. *Macromolecules*, 1997, **30**, 6899–6905.
23. Lau, C. H., Li, P., Li, F., Chung, T. S., Paul, D. R. *Prog. Polym. Sci.*, 2013, 38, 740–766.
24. Matsumoto, K., Xu, P. *J. Membr. Sci.*, 1993, **81**, 23–30.
25. Nagase, Y., Suleimenova, B., Umeda, C., Taira, K., Oda, T., Suzuki, S., Okamura, Y., Koguchi, S. *Polymer*, 2018, **135**, 142–153.
26. Sava, I., Chisca, S., Wolinska-grabczyk, A., Jankowski, A., Sava, M., Bruma, M. *Polym. Int.*, 2014, **64**, 154–164.
27. Rewar, A. S., Shaligram, S. V., Kharul, U. K. *J. Membr. Sci.*, 2016, **497**, 282–288.
28. Sanders, D. F., Smith, Z. P., Guo, R., Robeson, L. M., McGrath, J. E., Paul, D. R., Freeman, B. D. *Polymer*, 2013, **54**, 4729–4761.
29. Aitken, C. L., Koros, W. J., Paul, D. R. *Macromolecules*, 1992, 25, 3424–3434.
30. Tang, J., Tang, H., Sun, W., Radosz, M., Shen, Y. *J. Polym. Sci. Part A Polym. Chem.*, 2005, **43**, 5477–5489.

Supporting Information

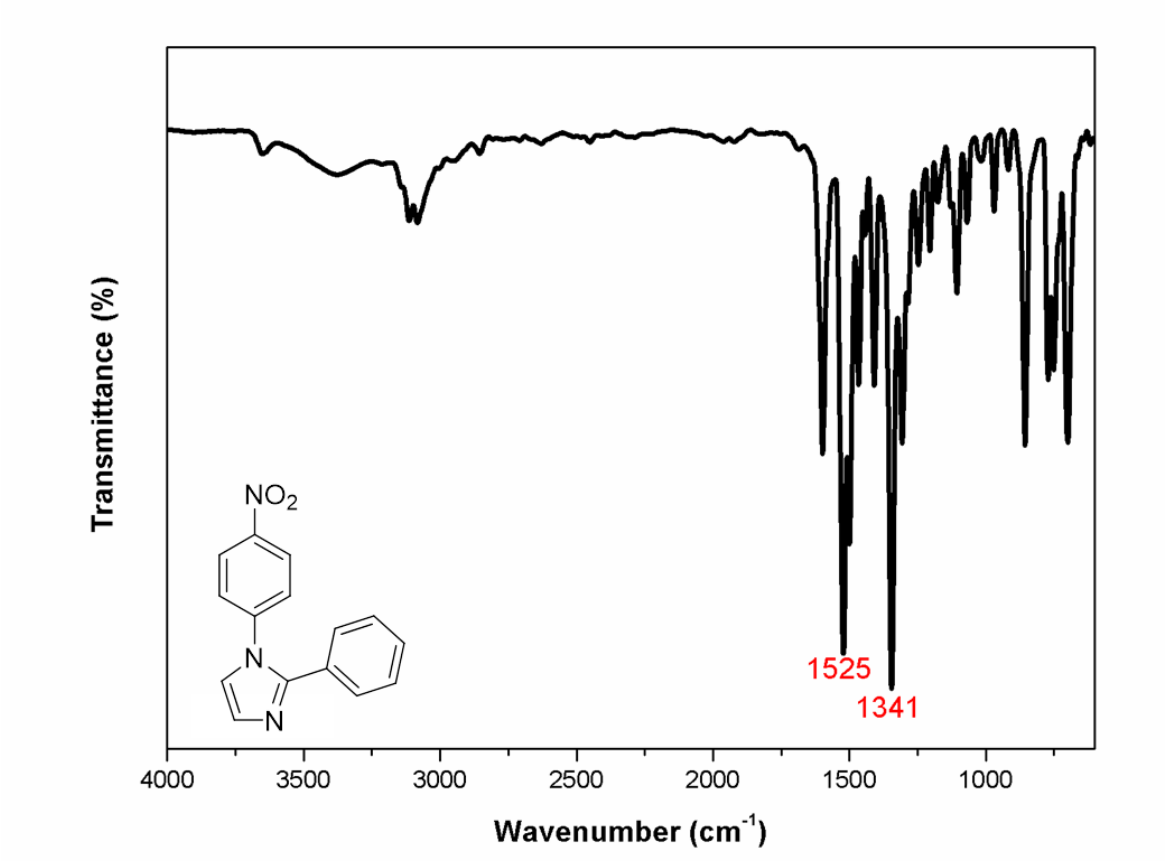

Figure SI 7.1: IR spectrum of 1-(4-nitrophenyl)-2-phenyl-1H-imidazole (ImN)

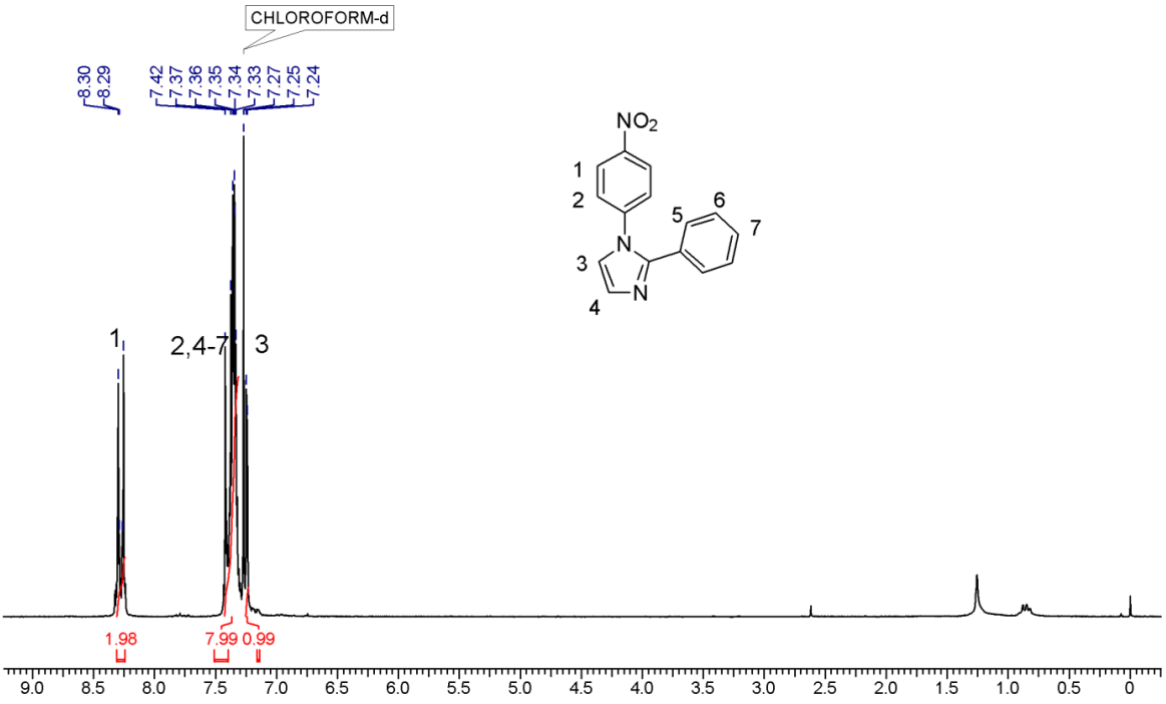

Figure SI 7.2: ^{1}H NMR spectrum (in $CDCl_3$) of 1-(4-nitrophenyl)-2-phenyl-1H-imidazole (ImN).

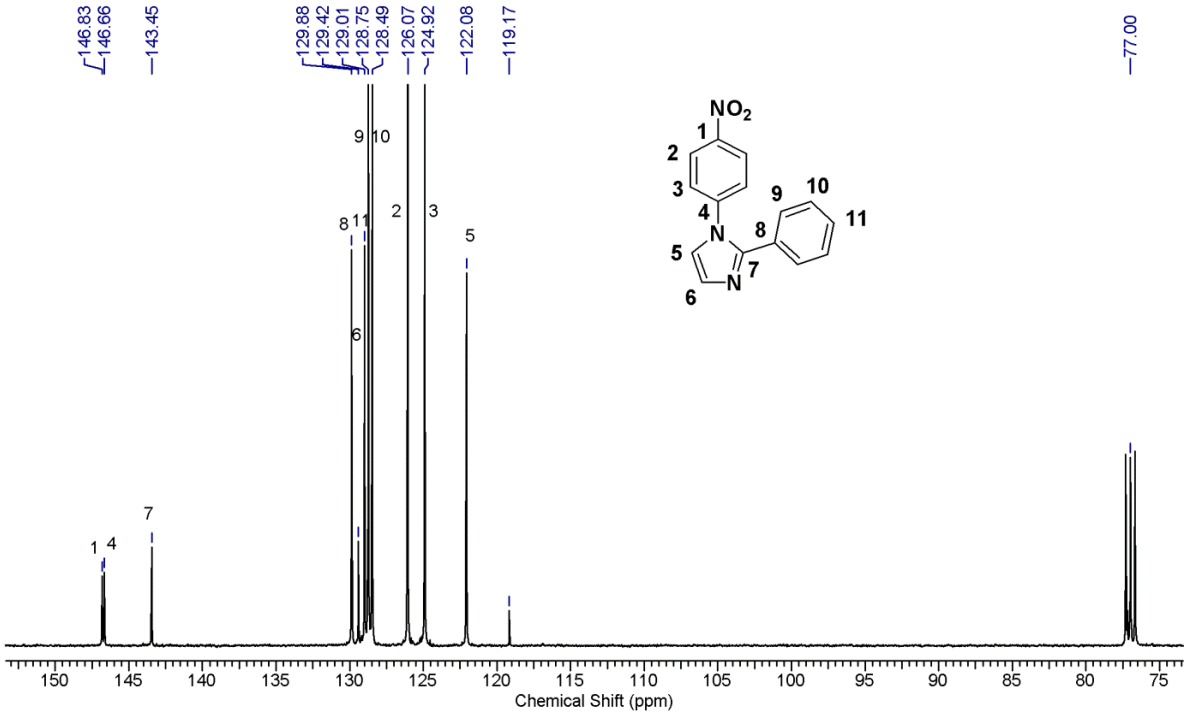

Figure SI 7.3: ^{13}C NMR spectrum (in $CDCl_3$) of 1-(4-nitrophenyl)-2-phenyl-1H-imidazole (ImN).

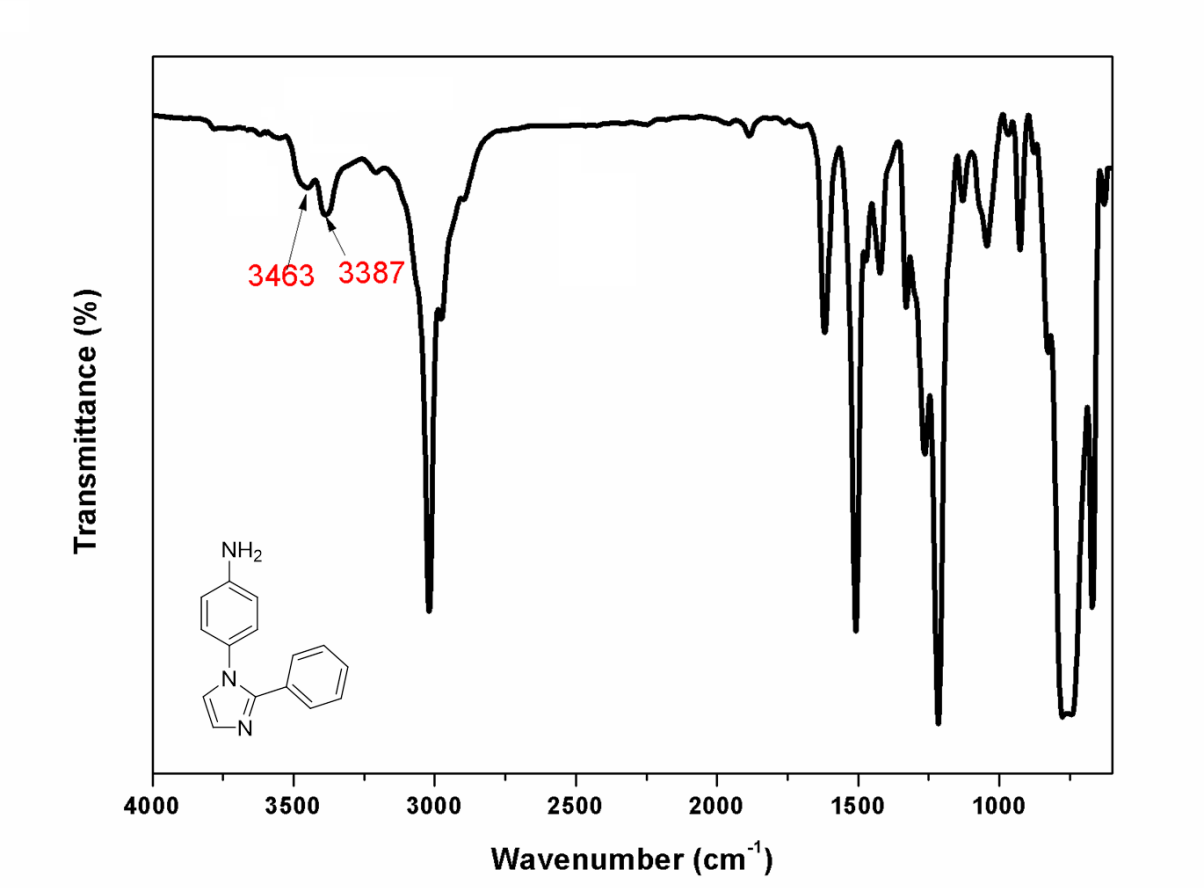

Figure SI 7.4: IR spectrum of 4-(2-phenyl-1H-imidazol-1-yl) aniline (ImA)

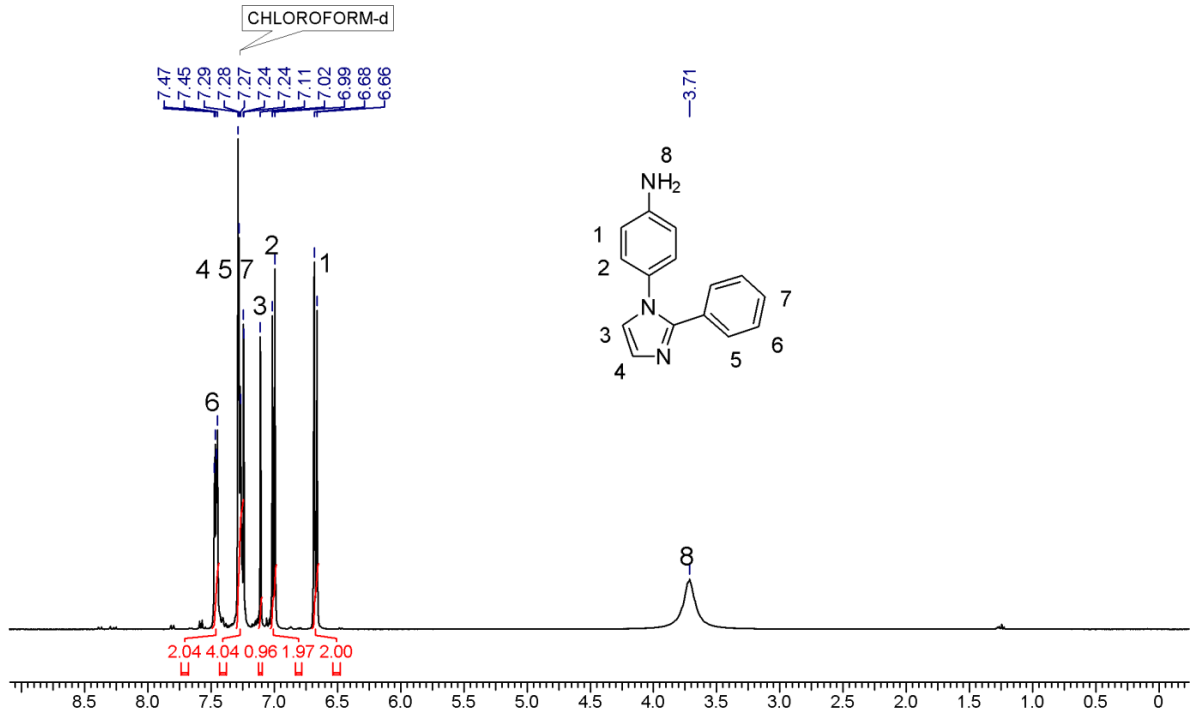

Figure SI 7.5: ^{1}H NMR spectrum (in $CDCl_3$) of 4-(2-phenyl-1H-imidazol-1-yl) aniline (ImA).

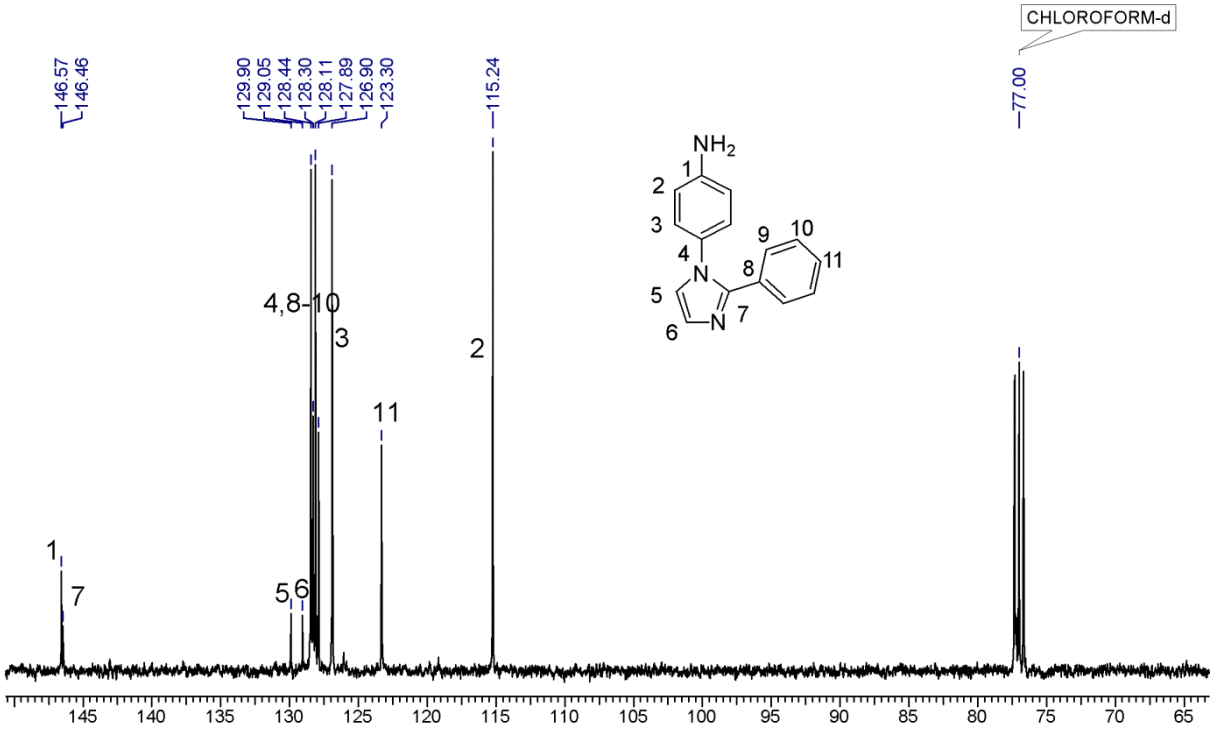

Figure SI 7.6: ^{1}H NMR spectrum (in $CDCl_3$) of 4-(2-phenyl-1H-imidazol-1-yl) aniline (ImA).

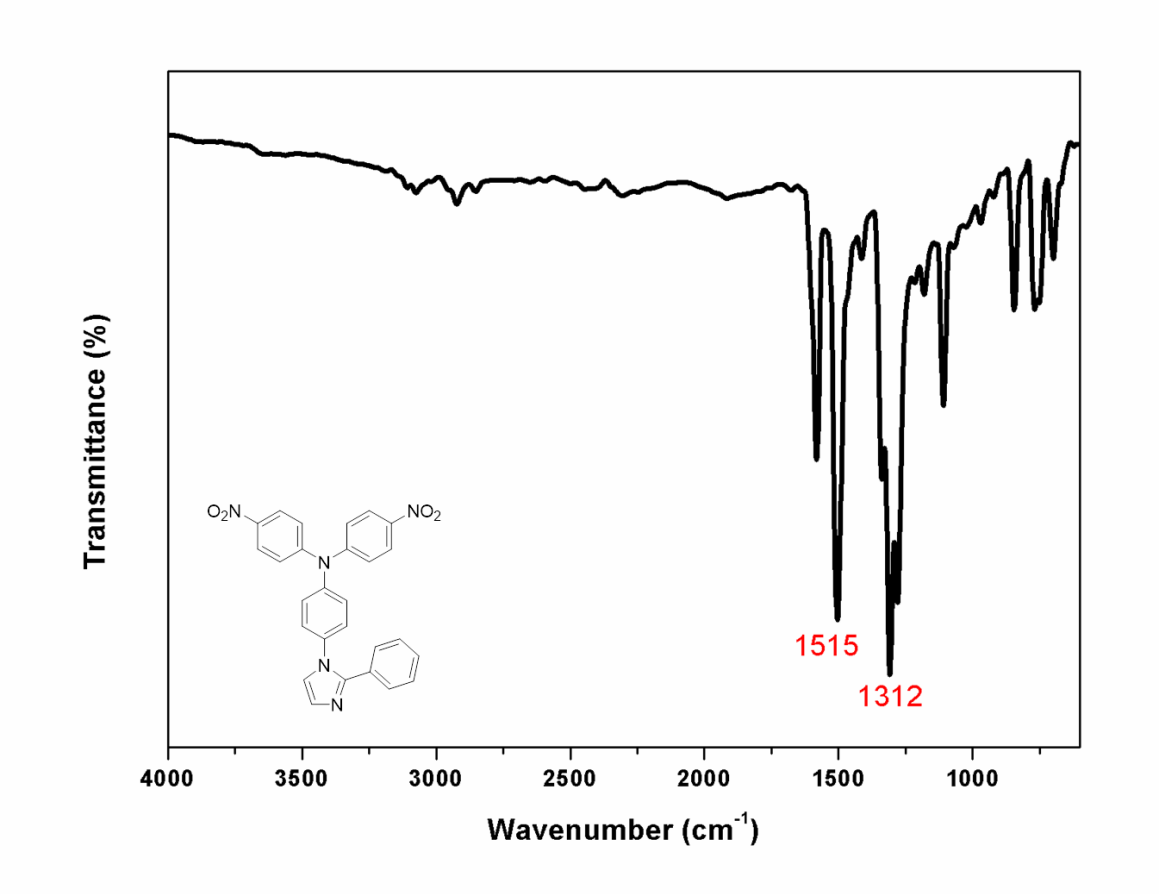

Figure SI 7.7: IR spectrum of 4-nitro-N-(4-nitrophenyl)-N-(4-(2-phenyl-1H-imidazol-1-yl) phenyl)aniline (ImTPADN)

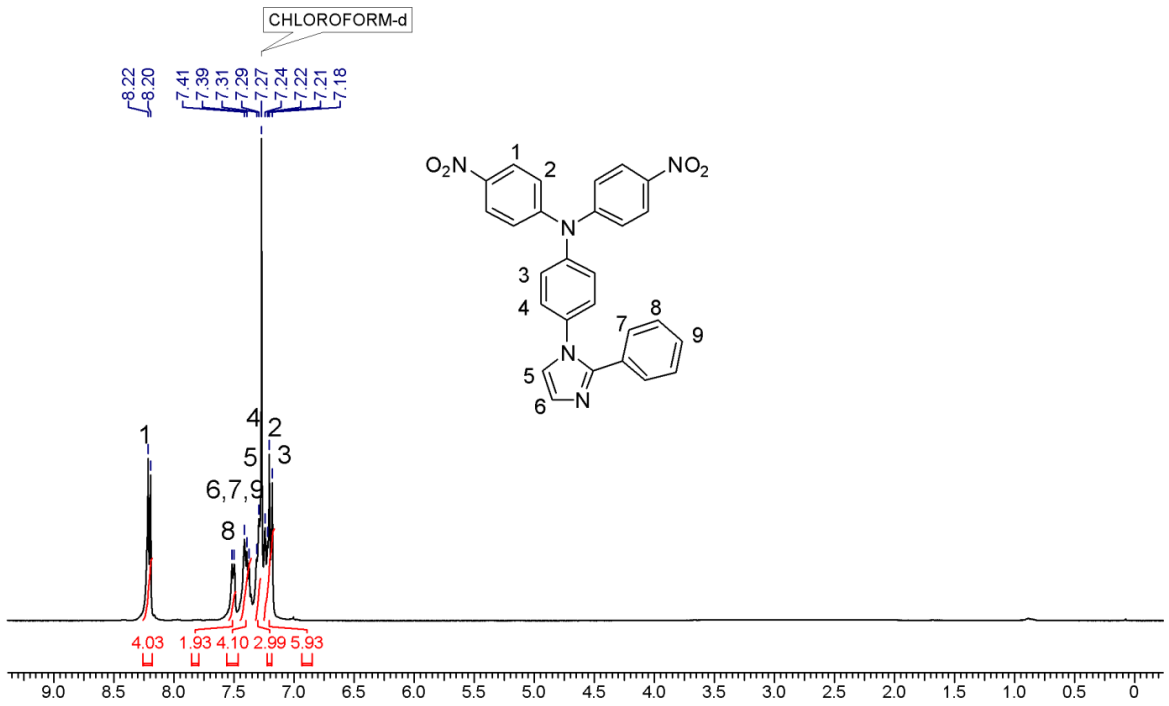

Figure SI 7.8: ^{1}H NMR spectrum (in $CDCl_3$) of 4-nitro-N-(4-nitrophenyl)-N-(4-(2-phenyl-1H-imidazol-1-yl) phenyl)aniline (ImTPADN).

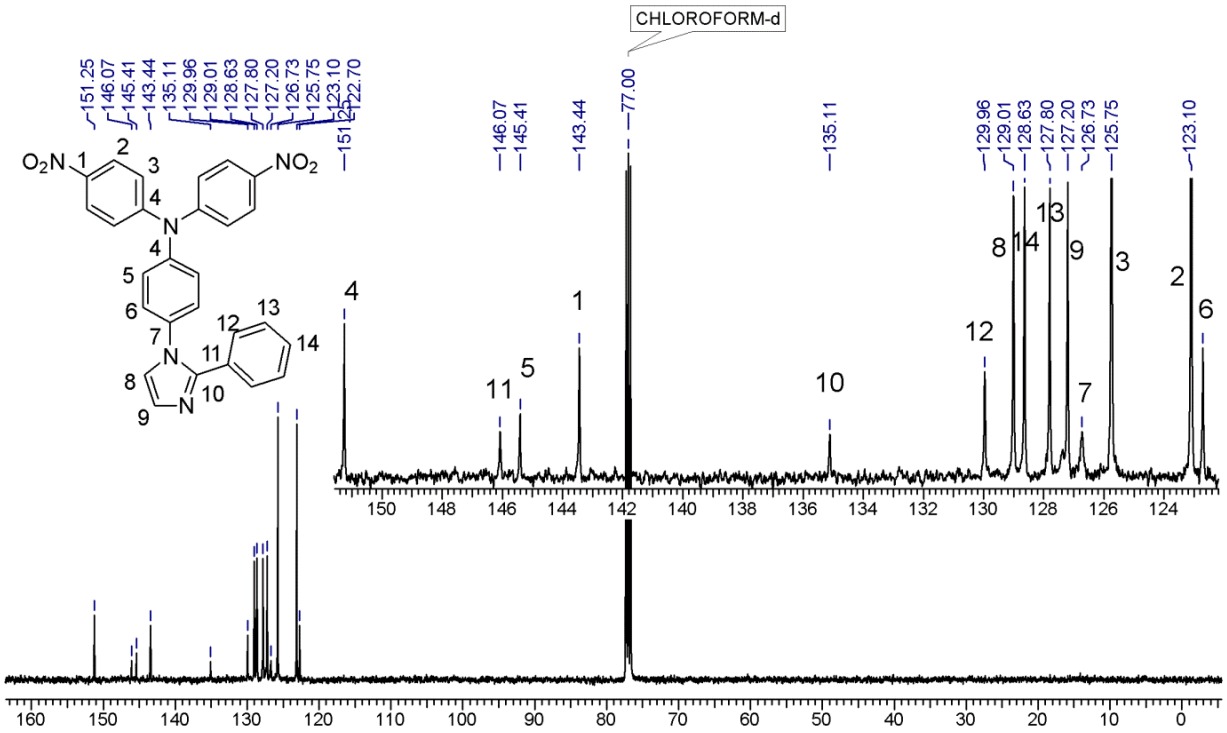

Figure SI 7.9: ^{13}C NMR spectrum (in $CDCl_3$) of 4-nitro-N-(4-nitrophenyl)-N-(4-(2-phenyl-1H-imidazol-1-yl) phenyl)aniline (ImTPADN).

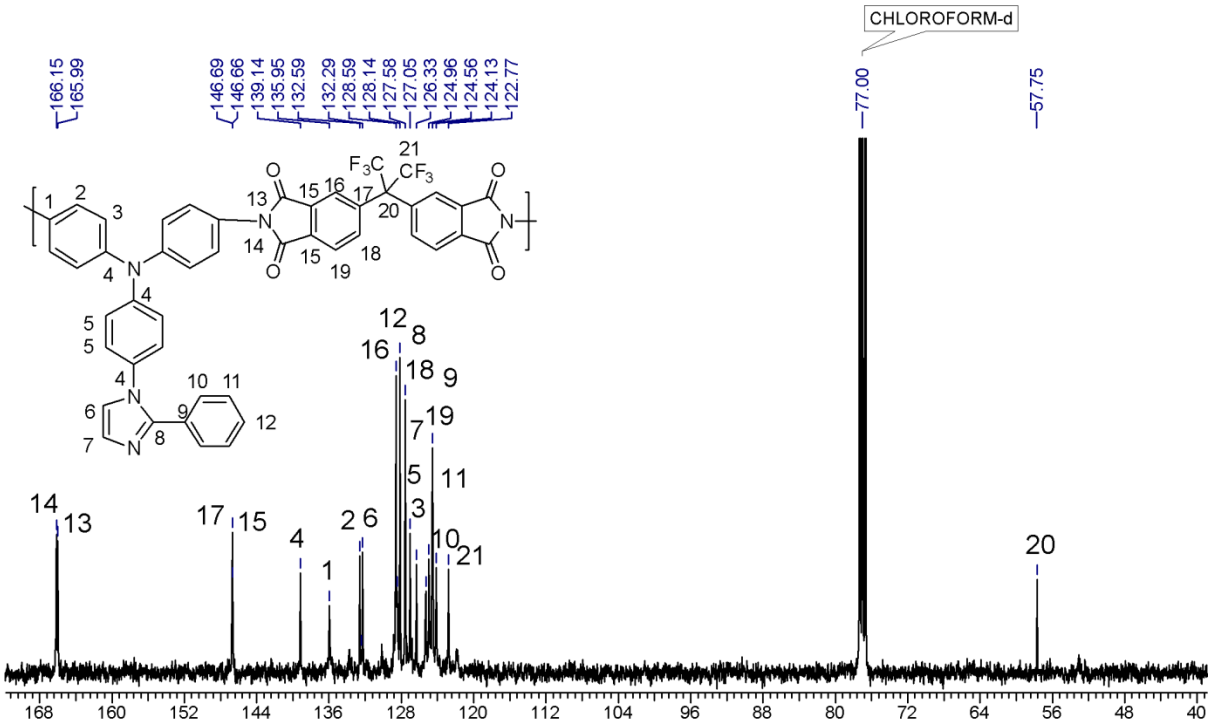

Figure SI 7.10: ^{1}H NMR spectrum (in $CDCl_3$) of PI-6FDA

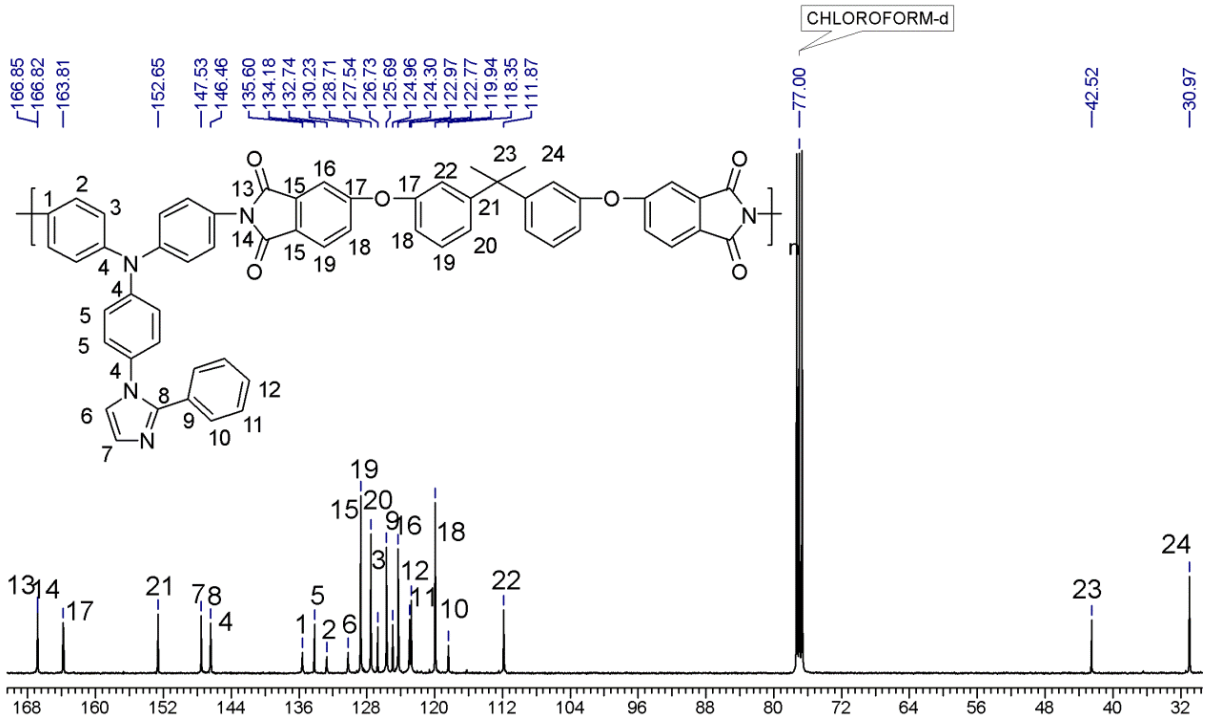

Figure SI 7.11: ^{1}H NMR spectrum (in $CDCl_3$) of PI-BPADA

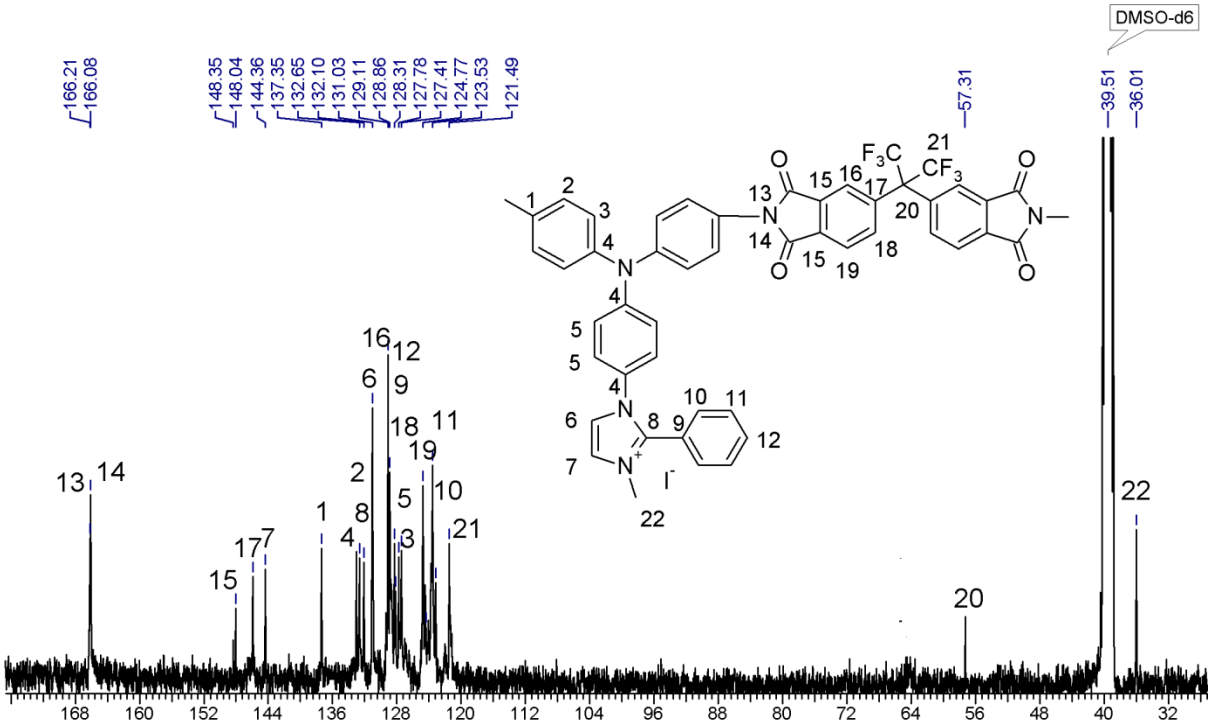

Figure SI 7.12: ^{1}H NMR spectrum (in DMSO-d_6) of [PI-6FDA] [I]

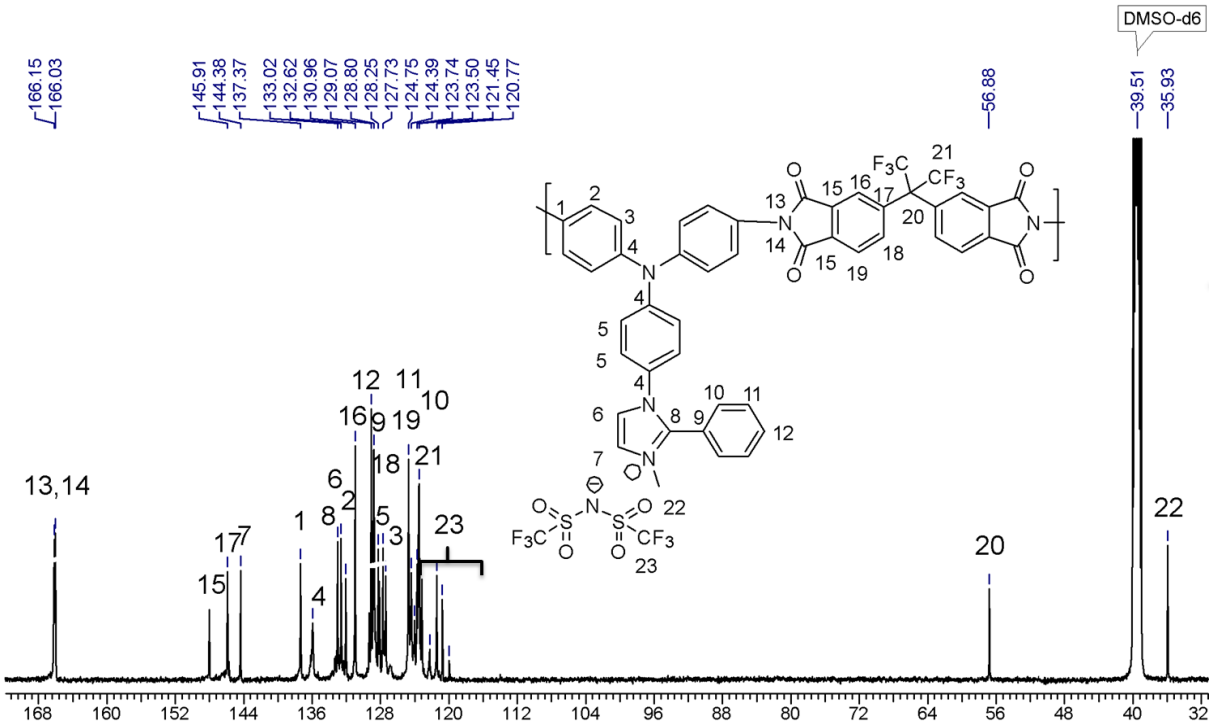

Figure SI 7.13: ^{1}H NMR spectrum (in DMSO-d_6) of [PI-6FDA] [Tf_2N]

Chapter 8

Summary, Conclusions and Future Perspectives

8.1 SUMMARY AND CONCLUSIONS

The overall objective of the work was to develop understanding of structure-property-performance relationships in PIMs and PILs with respect to their gas permeation characteristics.

The work involved design and synthesis of four new monomers containing special structural features. The following four monomers were synthesized:

1. 4,4'-((1r,3r)-Adamantane -2,2-diyl)bis(benzene-1,2diol) (THADM)
2. 3,3,3',3'-Tetramethyl-2,2',3,3'-tetrahydro-1,1'-spirobi[cyclopenta[b]phenazine]-7,7'-diamine (TTSBIDA)
3. 4,4'-(Spiro[fluorene-9,9'-xanthene]-2',7'-diyl)bis(benzene-1,2-diol) (THSFX)
4. N^1-(4-Aminophenyl)-N^1-(4-(2-phenyl-1H-imidazol-1-yl)phenyl)benzene-1,4-diamine (ImTPADA)

With an objective to tune the permeability and selectivity of PIMs, bulky adamanatane unit was chosen with an anticipation that it would result in loosening of polymer chain packing. A new bis(catechol) viz., 4,4'-((1r,3r)-adamantane -2,2-diyl)bis(benzene-1,2diol) (THADM) was synthesized in two steps involving condensation of 2-adamantanone with veratrole followed by demethylation of the intermediate (1r,3r)-2,2-bis(3,4-dimethoxyphenyl)adamantane (TMADM). Homopolymer and copolymers were synthesized by polycondensation of THADM or various compositions of THADM and 5,5′,6,6′-tetrahydroxy-3,3,3′,3′-tetramethyl-1,1′-spirobisindane (TTSBI) with 2,3,5,6-tetrafluoroterephthalonitrile (TFTPN). PIMs showed good solubility in organic solvents and self-standing films could be cast from their solutions in $CHCl_3$. GPC analysis indicated that PIMs exhibited reasonably high molecular weights (38,100–61,700 g/mol). X-Ray diffraction analysis revealed that PIMs were amorphous in nature. The N_2 absorption/desorption studies indicated that PIMs possessed intrinsic microporosity with high BET surface area (703–741 m^2/g). PIMs showed excellent thermal stability with T_{10} values in the range 513–518 °C. Gas permeability analysis demonstrated that PIMs exhibited high permeability and appreciable selectivity. In this series, gas permeability decreased and selectivity increased with increase in content of adamantane units. The gas permeability data of PIMs were located close to 2008 Robeson upper bound for gas pairs such as CO_2/CH_4, CO_2/N_2, H_2/N_2, and O_2/N_2. Results of DFT analysis showed that adamantane containing PIMs are more compact than PIM-1 which was used as reference polymer. The gas permeability studies of physically aged films of PIMs over 150 days were carried out. After aging, there was a significant decrease in gas permeability for all the gases *viz*. He, H_2, N_2, O_2, CH_4 and CO_2 and increase in selectivity for all gas pairs. For instance, the CO_2 permeability of ADM-PIM decreased from 1080 to 720

Barrer with increase in selectivity of CO_2/N_2 and CO_2/CH_4 from 26.7 to 30 and 22.6 to 24, respectively. Overall, the incorporation of cardo adamantane units alone or in combination with contorted spirobisindane units in PIMs was demonstrated as an efficient strategy to tune their physical and gas permeation properties.

It is generally recognised that selectivity can be improved by increasing rigidity of polymers. Taking a clue from this, a new rigid aromatic diamine containing spirobisindane and phenazine units, namely, 3,3,3',3'-tetramethyl-2,2',3,3'-tetrahydro-1,1'-spirobi[cyclopenta[b]phenazine]-7,7'-diamine (TTSBIDA) was designed and synthesized. A series of new polyimides of intrinsic microporosity (PIM-PIs) were synthesized by polycondensation of TTSBIDA with commercially available aromatic dianhydrides. Soluble PIM-PIs exhibited reasonably high molecular weights (40000-42600 g/mol), as measured by GPC (polystyrene as a standard), and could be cast into self-standing films. PIM-PIs possessed intrinsic microporosity and displayed BET surface area in the range 59-289 m^2/g. TGA analysis indicated that PIM-PIs showed excellent thermal stability with T_{10} values in the range 488-545 °C. The gas permeability of films of selected PIM-PIs were evaluated and they exhibited appreciable gas permeability as well as high selectivity. In particular, polyimide obtained by polycondensation of TTSBIDA with 4,4'-(hexafluoroisopropylidene)diphthalic anhydride (PIM-PI-6FDA) exhibited high CO_2 and O_2 permeability of 185.4 and 30.6 Barrer with CO_2/CH_4 and O_2/N_2 selectivity of 43.1 and 5.1, respectively. Interestingly, these PIM-PIs exhibited higher selectivity than that of reported spirobisindane-containing PIM-PIs. These results suggested that PIM-PIs containing spirobisindane and phenazine units are attractive candidates for membrane-based gas separations.

Recently, spirocyclic units have been evaluated as a building block to introduce microporosity into polymers because of their twisted structure which helps to increase inter-chain distance between polymer chains by creating free volume. Moreover, these spirocyclic unit containing polymers have been used for gas separations due to improved permeability characteristics. Encouraged by the attractive results of PIMs containing spirocyclic units, current research efforts were directed towards design and synthesis of a monomer containing spirocyclic unit. Towards this end, a new bis(catechol) containing spiro[fluorene-9,9'-xanthene] (SFX), namely, 4,4'- (spiro[fluorene-9,9'-xanthene]-2',7'-diyl)bis(benzene-1,2-diol) (THSFX) was synthesized and utilized to prepare homo and copolymers possessing intrinsic microporosity (SFX-PIMs). Soluble PIMs exhibited number average molecular weight in the range 34100–23300 g/mol and could be cast into self-standing films. These polymers exhibited amorphous nature, excellent thermal properties ($T_{10\%}$ = 490-510 °C), possessed intrinsic microporosity with high BET surface area (360-796 m^2/g) and high FFV (17-22%)

as determined by XRD, TGA, N_2 absorption method and Bondi's method, respectively. The gas permeability characteristics of methanol-treated and 130 days aged films of SFX-PIM-25 and SFX-PIM-33 were investigated. SFX-PIM-25 and SFX-PIM-33 exhibited high gas permeability and moderate selectivity. The gas permeability data of methanol-treated SFX-PIM-25 and SFX-PIM-33 was close to 1991 Robson upper bound for CO_2/CH_4 and O_2/N_2 gas pairs. Overall, SFX unit was incorporated into PIMs for the first time and encouraging results were obtained in gas permeation studies.

The film-forming PILs are of great interest for gas separation due to their improved properties especially for CO_2 separation. In this context, a new aromatic diamine containing 2-phenylimidazole substituted triphenylamine, namely, N1-(4-aminophenyl)-N1-(4-(2-phenyl-1H-imidazol-1-yl)phenyl)benzene-1,4-diamine (ImTPADA) was synthesized. Polycondensation of ImTPADA with commercially available aromatic dianhydrides *viz*., 4,4′-(hexafluoroisopropylidene) diphthalic anhydride (6FDA), 4,4'-(4,4'-isopropylidenediphenoxy)bis-(phthalicanhydride) (BPADA) and 4,4′-oxydiphthalic anhydride (OPDA) was carried out to obtain a series of new polyimides. The *N*-quaternization of polyimide-based on 6-FDA (PI-6FDA) by methyl iodide followed by anion exchange with bis(trifluoromethane)sulfonimide lithium salt ($LiTf_2N$) was carried out to obtain corresponding PI-PILs. PIs and PI-PILs exhibited number average molecular weights in the range 79200-35000 g/mol as determined by GPC analysis. XRD analysis revealed that PIs and PI-PILs were amorphous in nature. The selected PIs and PI-PILs exhibited good solubility in polar organic solvents and could be cast into self-standing films from their DMAc solutions. TGA indicated that T_{10} values of PIs and PI-PILs were in the range 545-475 °C and 303-306 °C, respectively. The effects of anion variation in PI-PILs on physical and gas permeation properties were studied. Gas permeability data demonstrated that incorporation of ionic groups into PIs resulted in increased permeability as well as selectivity. In particular, PI-PILs bearing Tf_2N^- anion exhibited high CO_2 permeability of 33.3 Barrer as well high selectivity for CO_2/CH_4 (41.1) and CO_2/N_2 (35.4). A comparison was made of gas permeability data of present PI-PILs with PILs reported in the literature by plotting data on Robeson plots. For CO_2/CH_4 gas pair, [PI-6FDA] [I] containing I^- anion was placed near 1991 Robeson upper bound while [PI-6FDA] [Tf_2N] containing Tf_2N^- anion surpassed 1991 Robeson upper bound. Overall, the gas permeability data demonstrated that the present PI-PILs are attractive candidates for gas separation applications, particularly for CO_2 separation

The gas permeability data generated using newly synthesized PIMs and PILs further demonstrated the critical role of tuning the chain packing and chain rigidity in polymers to achieve the improved performance.

8.2 FUTURE PERSPECTIVES

The work embodied in the thesis was focused on design and synthesis of new step-growth monomers for preparation of polymers with improved gas permeability characteristics and has opened many new avenues for the future work.

- The diamines viz., 3,3,3',3'-tetramethyl-2,2',3,3'-tetrahydro-1,1'-spirobi[cyclopenta[b]phenazine]-7,7'-diamine (TTSBIDA) and N1-(4-aminophenyl)-N1-(4-(2-phenyl-1H-imidazol-1-yl)phenyl)benzene-1,4-diamine (ImTPADA) synthesized in the present work are potentially useful monomers for synthesis of Tröger's base containing polymers.
- PIMs synthesized in this work (Chapter 4 and 6) contain cyano groups. The cyano groups present in PIMs could be converted into polar groups such as acid, amino, etc. *via* post-modification. The gas separation applications of modified PIMs especially for CO_2 would be worth exploring.
- The petrochemical industry is waiting for availability of polymeric membranes to separate mixtures of hydrocarbons. It would be worthwhile to evaluate the potential of PIMs synthesized in the present study for separation of hydrocarbons.
- The combination of solution processability, porosity, and optical clarity makes PIMs potentially useful for sensor applications and therefore such studies would be worthwhile.
- The metathesis reaction of PILs containing iodide anion could be further utilized to introduce anions such as BF_4^-, Ac^- and Bz^- by making use of appropriate reagents.
- PI-PILs can be used in fuel cell applications on account of their ionic character.

List of Publications

1. *Synthesis, Characterization, and Gas Permeation Properties of Adamantane-Containing Polymers of Intrinsic Microporosity*
   Bharat Shrimant, Sayali Shaligram, Ulhas K. Kharul and Prakash P. Wadgaonkar
   J. Polym. Sci. Part A: Polym. Chem, 2018, 56, 16-24

2. *Intrinsically Microporous Polyimides Containing Spirobisindane and Phenazine Units: Synthesis, Characterization and Gas Permeation Properties*
Bharat Shrimant, Yuvraj Dangat, Ulhas K. Kharul and Prakash Wadgaonkar,
J. Polym. Sci. Part A: Polym. Chem, 2018, 56, 766-775

3. *Design, Synthesis and Gas Permeation Properties of Polyimide-Based Poly(ionic liquid)s*
Bharat Shrimant, Ulhas K. Kharul and Prakash P. Wadgaonkar
J. Polym. Sci. Part A: Polym. Chem (Manuscript Accepted)

4. *Spiro[fluorene-9,9'-xanthene]-Based Copolymers of Intrinsic Microporosity: Synthesis, Characterization and Gas Permeation Properties*
Bharat Shrimant, Ulhas K. Kharul and Prakash P. Wadgaonkar
Manuscript under preparation

AcSIR	Synopsis of the Thesis Submitted to Academy of Scientific and Innovative Research for the Award of Doctor of Philosophy in Chemistry
Name of the Candidate	Bharat Shrimant
Degree Enrolment No. and Date	Ph.D in Chemical Sciences (10CC12A26049); July 2012
Title of the Thesis	Polymers of Intrinsic Microporosity and Poly(ionic liquid)s: Synthesis, Characterization and Gas Permeation Studies
Research Supervisor	Dr. Prakash P. Wadgaonkar
Research Co-supervisor	Dr. Ulhas K. Kharul

Introduction

Gas separation membranes find applications in hydrogen recovery, natural gas purification, purification of nitrogen from air and purification as well as carbon dioxide capture/separation due to their potential cost effectiveness and environmental benefits.[1] Polymeric membranes for industrial separations should possess both, high permeability as well as selectivity. High permeability is required for reducing membrane area and high selectivity is needed for higher product recovery of the desired product purity.[2] However, a trade-off relationship between permeability and selectivity is generally observed for polymeric membranes as illustrated by the Robeson.[3] A logical approach to surpass limit of the Robeson upper bound is to develop new polymeric materials with high permeability and selectivity.

Statement of Problem

It has been demonstrated that to surpass the Robeson upper bound, it is desirable to prepare polymers with enhanced backbone rigidity and high internal free volume. The permeability can be increased by disturbing polymer chain packing *via* incorporation of bulky groups or contortion sites in the main chain to create highly contorted polymer backbone. The selectivity can be increased by increasing polymer backbone rigidity and/or by incorporation of ionic or polar groups into polymers.[4,5] In this context, polymers of intrinsic microporosity (PIMs) have attracted increased attention in recent years as they contain contorted structure and rigid backbone which restrict conformational freedom and disturb close polymer chain packing. PIMs have been demonstrated to exhibit high permeability and moderate selectivity.[6] Poly(ionic liquids) (PILs) are a new class of functional materials which combine the characteristics of ionic liquids (ILs) and macromolecular structure.[7] They have been reported to exhibit high CO_2 permeability as well high selectivity for CO_2/CH_4 and CO_2/N_2 gas pairs. Most of the reported PILs are brittle in nature, unable to form films and thus cannot be converted into membranes for practical applications.[8] Therefore, there is a need to design new PIMs and PILs with improved performance in gas separation applications.

Dr. Prakash P. Wadgaonkar (Supervisor)	Dr. Ulhas K. Kharul (Co-supervisor)	Bharat Shrimant (Candidate)

Aims and Objectives

The overall aim of the present work was to tune the properties of polymeric membranes by structural variations and develop understanding of structure-gas permeation properties in PIMs and PILs. The following specific objectives were chosen for the work.

1. To synthesize monomers containing bulky and spirocyclic units.
2. To synthesize polymers of intrinsic microporosity (PIMs) and polyimide-based poly(ionic liquid)s (PI-PILs).
3. To investigate the gas permeation characteristics of PIMs and PILs and establish structure-properties-performance relationship.

Methodology Used

1. Synthesized a new bis(catechol) containing adamantane unit and PIMs therefrom; investigated the effects of adamantane and/or spirobisindane units on physical and gas permeation properties of PIMs.
2. Synthesized polyimides of intrinsic microporosity (PIM-PIs) containing spirobisindane and phenazine units; investigated the influence of spirobisindane and phenazine units on their physical and gas permeation properties.
3. Demonstrated spiro[fluorene-9,9'-xanthene] as a new building block to induce microporosity and investigated the effects of spiro[fluorene-9,9'-xanthene] units on physical and gas permeation properties.
4. With chosen polyimide backbone and methyl group as the *N*-substituent, developed a family of film-forming PI-PILs and investigated the effects of PI-PILs and anion variations on gas permeation properties.

Sample Results

Scheme 1: *Synthesis, Characterization and Gas Permeation Properties of Adamantane-Containing Polymers of Intrinsic Microporosity*

A new adamantane-containing bis(catechol), namely, 4,4'-((1r,3r)-adamantane -2,2-diyl)bis(benzene-1,2diol) (THADM) was synthesized and utilized for the preparation of polymers of intrinsic microporosity (ADM-PIMs). The ADM-PIMs exhibited good solubility in organic solvents, amorphous nature and high thermal stability. The physical properties influencing polymer chain packing such as *d*-spacing and microporosity were evaluated and discussed. The gas permeability measurements were carried out by the variable volume method for pure gas, viz.; He, H_2, N_2, O_2, CH_4 and CO_2. The gas permeability measurements demonstrated that with increase in the content of adamantane units in PIMs, selectivity increased and permeability decreased. The Robeson upper bound was plotted to compare the gas permeation properties of obtained ADM-PIMs with reported adamantane containing polymers. The gas separation properties of ADM-PIMs were located close to 2008 Robeson

upper bound for gas pairs such as CO_2/CH_4, CO_2/N_2, H_2/N_2 and O_2/N_2, depicting significance of the performed study.[9]

Scheme 2: *Intrinsically Microporous Polyimides Containing Spirobisindane and Phenazine Units: Synthesis, Characterization and Gas Permeation Properties*

A new series of polyimides of intrinsic microporosity (PIM-PIs) was synthesized by polycondensation of aromatic diamine containing spirobisindane and phenazine units, namely, 3,3,3',3'-tetramethyl-2,2',3,3'-tetrahydro-1,1'-spirobi[cyclopenta [b]phenazine]-7,7'-diamine (TTSBIDA) with commercially available aromatic dianhydrides. The PIM-PIs exhibited amorphous nature, high thermal stability and intrinsic microporosity. The gas permeability characteristics of selected PIM-PIs were studied. They possessed appreciable permeability and high selectivity. In particular, polyimide (PIM-PI-6FDA) derived from TTSBIDA and 4,4'-(hexafluoroisopropylidene)diphthalic anhydride exhibited high CO_2 and O_2 permeability of 185.3 and 30.3 Barrer with CO_2/CH_4 and O_2/N_2 selectivity of 43.09 and 5.05, respectively. The effects of phenazine and spirobisindane units on physical and gas permeability properties of PIM-PIs were evaluated. The present PIM-PIs exhibited higher selectivity than reported spirobisindane-containing PIM-PIs.

Scheme 3: *Spiro[fluorene-9,9'-xanthene]-containing copolymers of Intrinsic Microporosity: Synthesis, Characterization and Gas Permeation Properties*

A new bis(catechol) containing spiro[fluorene-9,9'-xanthene] (SFX), namely, 4,4'-(spiro[fluorene-9,9'-xanthene]-2',7'-diyl)bis(benzene-1,2-diol) (THSFX) was synthesized and utilized to prepare homo and copolymers possessing intrinsic microporosity (SFX-PIMs). The gas permeability characteristics of as-cast, methanol-treated and 130 days aged films of SFX-PIM-25 and SFX-PIM-33 were investigated. SFX-PIM-25 and SFX-PIM-33 exhibited high gas permeability with moderate selectivity.

Scheme 4: *Design, Synthesis and Gas Permeation Properties of Polyimide-Based Poly(ionic liquid)s*

A new aromatic diamine containing 2-phenylimidazole substituted triphenylamine, namely, N^1-(4-aminophenyl)-N^1-(4-(2-phenyl-1H-imidazol-1-yl)phenyl)benzene-1,4-diamine (ImTPADA) was synthesized and was polycondensed with commercially available aromatic dianhydrides *viz.*, 4,4′-(hexafluoroisopropylidene) diphthalic anhydride (6FDA), 4,4'-(4,4'-isopropylidenediphenoxy)bis-(phthalicanhydride) (BPADA) and 4,4′-oxydiphthalic anhydride (OPDA) to obtain a series of polyimides. The *N*-quaternization of polyimide-based on 6-FDA (PI-6FDA) by methyl iodide followed by anion exchange with bis(trifluoromethane)sulfonimide lithium salt ($LiTf_2N$) was carried out. The PIs and PI-PILs exhibited reasonably high molecular weights, amorphous nature and high thermal stability. The effects of anion variation in PI-PILs on physical and gas permeation properties were studied. The gas permeability data demonstrated that incorporation of ionic groups into PIs resulted in increased permeability as well as selectivity. In particular, PI-PILs bearing Tf_2N^- anion exhibited high CO_2 permeability of 41 Barrer as well high selectivity for CO_2/CH_4

(50.61) and CO_2/N_2 (47.12). A comparison was made of gas permeability data of present PI-PILs with PILs reported in the literature by plotting Robeson upper bound. For CO_2/CH_4 gas pair, PI-[PI-6FDA] [I] containing I^- anion was placed near 1991 Robeson upper bound whereas [PI-6FDA] [Tf_2N] containing Tf_2N^- anion surpassed 1991 Robeson upper bound.

References

(1) Sanders, D. F.; Smith, Z. P.; Guo, R.; Robeson, L. M.; McGrath, J. E.; Paul, D. R.; Freeman, B. D. *Polymer.* **2013**, *54* (18), 4729–4761.

(2) Baker, R. W.; Low, B. T. *Macromolecules* **2014**, *47* (20), 6999–7013.

(3) Robeson, L. M. *J. Membr. Sci.* **2008**, *320*, 390–400.

(4) Kim, S.; Lee, Y. M. *Prog. Polym. Sci.* **2015**, *43*, 1–32.

(5) Rose, I.; Bezzu, C. G.; Carta, M.; Comesaña-Gándara, B.; Lasseuguette, E.; Ferrari, M. C.; Bernardo, P.; Clarizia, G.; Fuoco, A.; Jansen, J. C.; Hart, K. E.; Liyana-Arachchi, T. P.; Colina, C. M.; McKeown, N. B. *Nat. Mater.* **2017**, *16* (9), 932–938.

(6) McKeown, N. B. *ISRN Mater. Sci.* **2012**, *2012* (7), 1–16.

(7) Yuan, J.; Antonietti, M. *Polymer.* **2011**, *52* (7), 1469–1482.

(8) Du, N.; Park, H. B.; Dal-Cin, M. M.; Guiver, M. D. *Energy Environ. Sci.* **2012**, *5* (6), 7306–7322.

(9) Shrimant, B.; Shaligram, S. V.; Kharul, U. K.; Wadgaonkar, P. P. *J. Polym. Sci. Part A Polym. Chem.* **2017** (55), 1–9.

Dr. Prakash P. Wadgaonkar (Supervisor)

Dr. Ulhas K. Kharul (Co-supervisor)

Bharat Shrimant (Candidate)